Mathematical modelling of cell cycle network motifs controlling M-Phase progression

Michael Hopkins

A thesis presented for the degree of
Doctor of Philosophy

Merton College
University of Oxford

Michaelmas 2018

Mathematical modelling of cell cycle network motifs controlling M-Phase progression

Michael Hopkins Merton College Michaelmas 2018

A thesis presented for the degree of Doctor of Philosophy.

Abstract

Eukaryotic cells must coordinate growth, replication of their genetic material, and cell division in order to generate two progeny cells from a single progenitor. M-phase is a critical phase of this process during which newly replicated DNA is precisely segregated into two distinct fractions, followed by cell division to produce two new daughter cells. M-phase is a component of both the mitotic cell cycle, during which each daughter cell should inherit an exact copy of the genetic material from the parent cell, and of meiosis, during which each daughter should receive only half of the genetic material from the parent cell to generate a haploid gamete. Despite these differences, both mitotic and meiotic M-phases share many of the same regulatory components.

In this thesis we present work from four different studies in which mathematical modelling is used to analyse the behaviour of the biochemical reaction networks controlling M-phase progression in mitosis and meiosis. We firstly present a theoretical analysis of a conserved network motif (termed here the Feedback-amplified Domineering Substrate or FADS motif), which is responsible for creating bistable switches controlling cell cycle progression at multiple points, including progression through and exit from mitotic M-phase.

We then present three sets of work using mathematical models in combination with data provided by experimental collaborators to examine the regulation of M-phase progression in mitosis and meiosis. We present evidence for how variations on common regulatory themes can generate the distinct outcomes required in each case.

Acknowledgements

I would like to thank my supervisor **Béla Novák** for his invaluable support and guidance over the past 3 years, as well as for originally taking me on as a Part II student way back in 2013, giving me an insight into the possibilities of mathematical modelling which helped me choose to pursue a DPhil in this area. His willingness to have me back as a DPhil student two years later when other projects had fallen through helped me out immensely at a time of great uncertainty, and was likely the difference between me staying and leaving academia at that point. I will always be grateful for it.

Thanks also to other members of the group: **Stefan Heldt**, **Lukas Hutter**, **Scott Rata**, **Paul Lang** and **Reece Lunstone** for interesting discussions, practical support, and chats over coffee.

This project would not have been possible without the essential contributions of experimental collaborators. **Ulrike Gruneberg**, **Flavia Scialpi**, **Dan Hayward**, **Francis Barr**, **Ahmed Rattani** and **Martin Anger** have all been extremely generous in providing the data necessary for the mathematical modelling in this project, as well as for engaging in fruitful scientific discussions. Thanks also to **John Tyson** for his help and expertise which greatly contributed to developing the FADS story into a publication, and to **Marina Martinic**, **Antonio Politi** and **Jan-Michael Peters**, with whom we developed an interesting collaboration which I was unfortunately unable to include in this thesis.

Finally, many thanks go to my family and friends, for countless examples of friendship, support and advice to get me through these 4 years. There are too many examples to name, but you know who you are.

Preface

This thesis comprises six chapters. The first introductory chapter provides relevant background on the eukaryotic cell cycle and meiosis, on the biochemical regulatory networks controlling these processes, and on the mathematical modelling approaches which are used throughout the thesis.

Chapter 2 is a purely theoretical project, introducing a simple network motif responsible for generating a bistable switch at multiple cell cycle transitions. Chapters 3, 4 and 5 detail projects in which modelling work is combined with data provided by experimental collaborators. These explore respectively: the CDK-dependence of APC/C^{Cdc20} activity in mitosis (Chapter 3); the role of APC/C^{Cdh1} in regulating Germinal Vesicle arrest and meiotic resumption during meiosis I (Chapter 4); and the regulation of APC/C^{Cdc20} activity by the spindle assembly checkpoint in Meiosis I (Chapter 5). Each of these projects is largely self-contained and includes its own sections for model description and discussion; further concluding discussion bringing together common themes across Chapters, and an evaluation of the techniques and approaches used, is provided in Chapter 6. A brief overview of the experimental collaboration and of any resulting publications is included at the beginning of each chapter.

A general description of the modelling approaches used is provided in the introduction. This is supplemented by detailed model descriptions in each of the project chapters, which should stand alone to describe the methods used within that chapter. Finally, code and instructions for running each of the models used in the thesis is provided in Appendix A.

Contents

List of Figures

List of Abbreviations

a.a.	Amino acids
APC/C	Anaphase-promoting Complex or Cyclosome
AurB	Aurora B
BEG	B55/ENSA/Gwl
cAMP	cyclic AMP
CAPP	Counter-acting Protein Phosphatase
CCAN	Constitutive Centromere-Associated Network
CCS	Cell Cycle Signal
CCT	Cell Cycle Transition
$Cdc20_A$	Co-activator Cdc20 within APC/C^{Cdc20} complex
$Cdc20_M$	Inhibitory Cdc20 within MCC
CDK	Cyclin-dependent Kinase
CENP	Centromeric Protein
CKI	Cyclin-dependent Kinase Inhibitor
CPC	Chromosome Passenger Complex
CSF	Cytostatic Factor
CycA	Cyclin A
CycB	Cyclin B
EC	Error Correction
ENSA	α-Endosulfine
FADS	Feedback-Amplified Domineering Substrate
GV	Germinal Vesicle
GVBD	Germinal Vesicle Breakdown
Gwl	Greatwall
KT	Kinetochore
LH	Luteinizing Hormone
M/A	Metaphase-Anaphase

MC	Mitotic Checkpoint
MCC	Mitotic Checkpoint Complex
MPF	Maturation/M-Phase–Promoting Factor
MPS1	Monopolar Spindle-1
MS	Mass Spectrometry
MT	Microtubule
NEBD	Nuclear Envelope Breakdown
Noc	Nocodazole
ODE	Ordinary Differential Equation
PIP	PP1-interacting Protein
PKA	Protein Kinase A
Plk1	Polo-like kinase 1
PP1	Protein Phosphatase 1
PP2A	Protein Phosphatase 2A
SAC	Spindle Assembly Checkpoint
SCF	Skp1–Cullin–F-box
Sgol2	Shugoshin-like Protein 2
SIMM	Substrate-Inhibitor-Multiply-Modified
uKT	Unattached Kinetochores

Chapter 1

Introduction

In this introductory chapter we describe the eukaryotic cell cycle, its events, important components, and the mechanisms of control. We will also introduce key concepts necessary for understanding how these components fit together at a systems level, and introduce the modelling tools used here to study them. The aim of this systems-level approach is to enable us to explain complex biochemical reaction networks in a rigorous and precise manner, identifying key network motifs and emergent properties which are necessary for function.

1.1 The Eukaryotic Cell Cycle

The eukaryotic cell cycle is the process by which cells coordinate the events required for growth, DNA replication, chromosome segregation and cell division to produce two new daughter cells. During the normal mitotic cell cycle, it is essential that DNA replication and chromosome segregation are strictly alternated, so that each daughter receives a complete and accurate copy of the genomic information of the parent cell [1].

Precise control of this process is therefore essential to ensure that cell cycle events are accurately completed and occur in the correct sequence. Failure to do so can lead to problems with processes such as DNA replication, chromosome segregation or cytokinesis, leading to deleterious consequences for the cell. On an organism-level scale, cell cycle controls are closely linked to developmental pathways, so their failure can lead to severe developmental defects in the early embryo [2, 3]. Similarly, both dis-regulation of cell division and loss of genomic stability due to aberrant chromosome segregation are important steps on the pathway to cancer [4, 5, 6].

1.1.1 The cell cycle is subdivided into phases

The cell cycle comprises a series of discrete phases associated with specific cellular events (Figure 1.1). The most significant events of the cell cycle are **DNA Replication**, occurring in **S-phase**, and **Chromosome Segregation** and **Cell Division**, occurring during **M-phase**. These phases are separated by the intervening 'gap' phases **G1** and **G2** during which the cell undergoes growth and prepares the necessary resources for the subsequent cell cycle phases [1].

At a molecular level, cell cycle phases are defined by the activity of specific **Cell Cycle Regulators** (usually regulatory proteins or enzymes). We will discuss individual cell cycle regulators in more detail in later sections. In general, cell cycle regulators both initiate the cellular events associated with their specific cell cycle phase, and promote activation of cell cycle regulators associated with the next cell cycle phase. They may also inhibit the activity of cell cycle regulators associated with previous cell cycle phases. By doing so they drive sequential progression through the cell cycle.

1.1.2 M-phase comprises a series of intermediate steps associated with chromosome segregation and cell division

Mitotic chromosomes comprise two identical DNA copies (**Sister Chromatids**) produced during S-phase. Chromosome segregation requires careful control to ensure that each daughter cell receives a single sister chromatid from each replicated chromosome. Central to this process is formation of the **Mitotic Spindle**, a network of tubulin **Microtubules** arising from two **Spindle Poles** at either side of the cell. These are captured by spindle microtubules emanating from both spindle poles (biorientation), and align at the midpoint of the spindle prior to chromosome segregation (See Section 1.4.2).

M-phase is further subdivided into a series of intermediate steps (Figure 1.1). During **Prophase**, chromatin condenses to form discrete mitotic chromosomes and spindle assembly begins. **Nuclear Envelope Breakdown (NEBD)** marks the beginning of **Prometaphase**, during which chromosomes are captured by spindle microtubules, causing them to biorient and align on the mitotic spindle. **Metaphase** occurs once all chromosomes are correctly bioriented and aligned along the midpoint of the spindle, form-

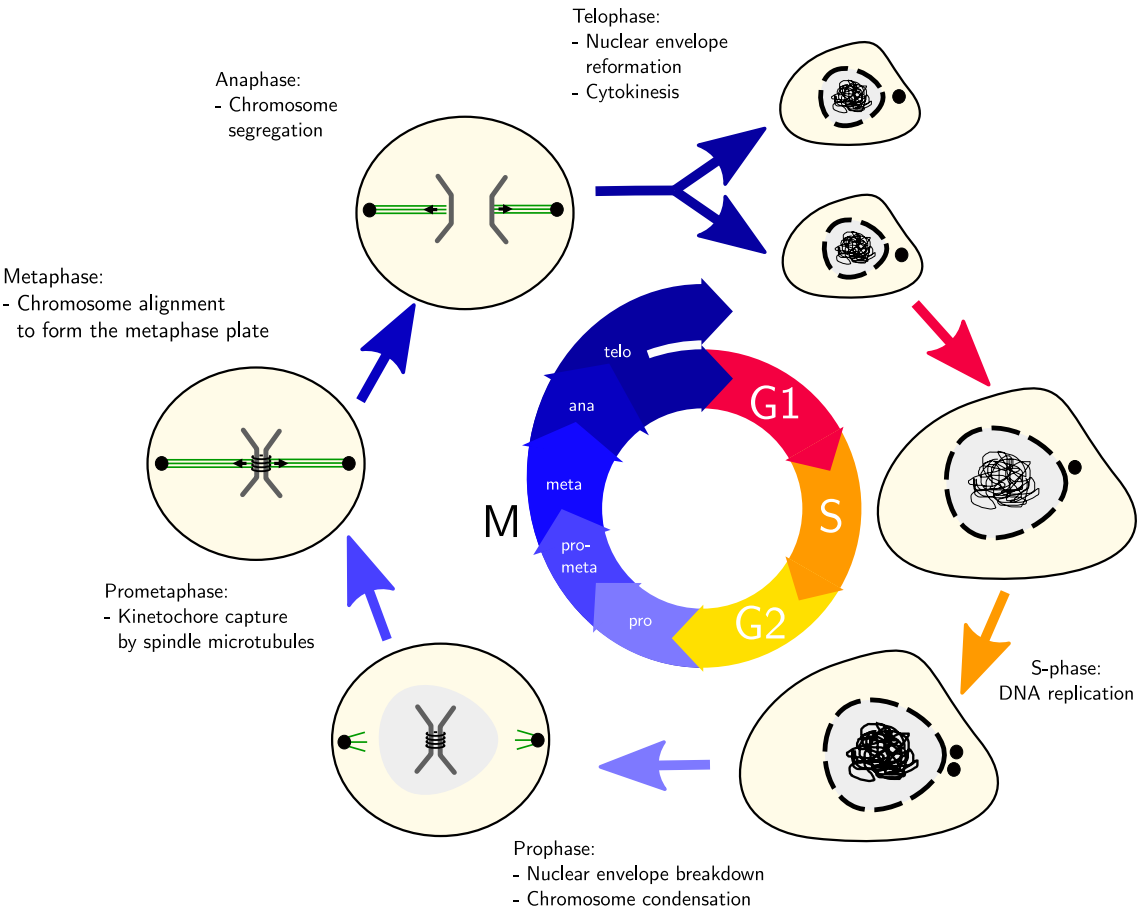

Figure 1.1: Cell cycle stages and associated cellular events. Adapted from [1].

ing the metaphase plate. Once this state has been achieved, sister chromatids separate and the resulting chromosomes are pulled towards the spindle poles during **Anaphase**. This Metaphase-Anaphase (M/A) transition is an important point of regulation which will be discussed in greater detail later. Finally, nuclear envelope reformation, spindle disassembly and cytokinesis occur during **Telophase**, resulting in formation of two new daughter cells, each with one copy of the DNA content of the parent cell [1].

Note that the description above and Figure 1.1 refer to mitotic M-phase in a typical animal cell. Minor differences exist in other eukaryotes, for example some cells (e.g. yeasts) undergo a 'closed' mitosis where NEBD does not occur [7]. Differences also exist between the mitotic cell cycle discussed here, and meiosis (see Section 1.5). While much of the terminology is the same, there is a crucial difference in that rather than alternating, a single meiotic S-phase is followed by two sequential M-phases.

1.1.3 Checkpoints regulate passage between cell cycle phases

As discussed above, progression between cell cycle phases is driven by the activity of cell cycle regulators, which sequentially activate each other to drive progression from one phase of the cell cycle to the next [8]. In the simplest cell cycles (typically those of early embryos) [9], this process occurs without significant external regulation and functions entirely as a free-running **Oscillator** (see Section 1.3.3). However, this has the distinct drawback that progression between cell cycle phases is not strictly linked to completion of the essential cellular processes associated with each phase (growth, DNA replication, chromosome segregation etc.). In order to ensure tight coupling between successful completion of these events and cell cycle progression, in the vast majority of cells the underlying oscillatory mechanism is kept in check by **Cell Cycle Checkpoints** [9, 10].

Multiple examples of checkpoints exist in the eukaryotic cell cycle [10]:

- Start/Restriction Point (G1/S) - *Regulates entry into the cell cycle in response to nutrient availability (yeast) or growth factor signalling (mammals).*
- Cell Size Checkpoint - *Coordinates cell size (growth) with cell division in order to maintain constant cell size between generations. The cell cycle transition at which this acts varies between species.*
- DNA Damage Checkpoint (G2/M) - *Unreplicated DNA or unrepaired DNA damage activates this checkpoint to prevent entry into mitosis. This ensures that DNA replication is completed prior to the onset of chromosome segregation. DNA damage during G1 is also able to block the G1/S transition to prevent replication of damaged DNA.*
- Spindle Assembly Checkpoint or SAC (M/A) - *Blocks chromosome segregation until all chromosomes are correctly bioriented on the mitotic spindle.*

Each of these checkpoints monitors a cellular event necessary for successful cell cycle progression, and delays the relevant cell cycle transition until the checkpoint is satisfied. While most of these checkpoints are common to many species, the significance of each checkpoint for overall control of the cell cycle varies depending on species-specific requirements.

Cyclin Class	CDK	Cyclin
G1	Cdk4, Cdk6	Cyclin D
G1/S	Cdk2	Cyclin E
S	Cdk2, Cdk1	Cyclin A
M	Cdk1	Cyclin B

Table 1.1: Table showing the major mammalian CDKs and their associated cyclins [1].

1.2 Cell Cycle Regulators

As mentioned above, progression through the cell cycle is driven by the activity of cell cycle regulators. In this section we introduce two of the 'master regulators' of cell cycle progression, namely **Cyclin-dependent Kinases (CDKs)** and the **Anaphase-promoting Complex or Cyclosome (APC/C)**. These two regulators constitute the major driving forces promoting progression into and exit from M-phase respectively [11, 12].

1.2.1 Cyclin-dependent Kinases

CDKs are a family of related enzymes which are responsible for driving cell cycle progression from G1 through to metaphase [8, 13, 14]. They do so by phosphorylating a wide range of target proteins to initiate specific cell cycle events [15]. In yeast, a single CDK (Cdk1) is responsible for the entire cell cycle, while multiple homologues of Cdk1 have been identified in mammalian cells [13]. CDK activity is dependent on the availability of a regulatory **Cyclin** subunit, the availability of which varies throughout the cell cycle in response to protein synthesis and degradation. [16, 11].

CDK activity drives progression through the cell cycle

Specific **CDK:Cyclin Complexes** are associated with particular cell cycle phases or transitions. Cyclins can be categorised accordingly as **G1**-, **G1/S**-, **S**- or **M-Cyclins**, aiding comparison between species and providing useful simplification when considering cyclins or CDKs with overlapping function within the same organism. A summary of

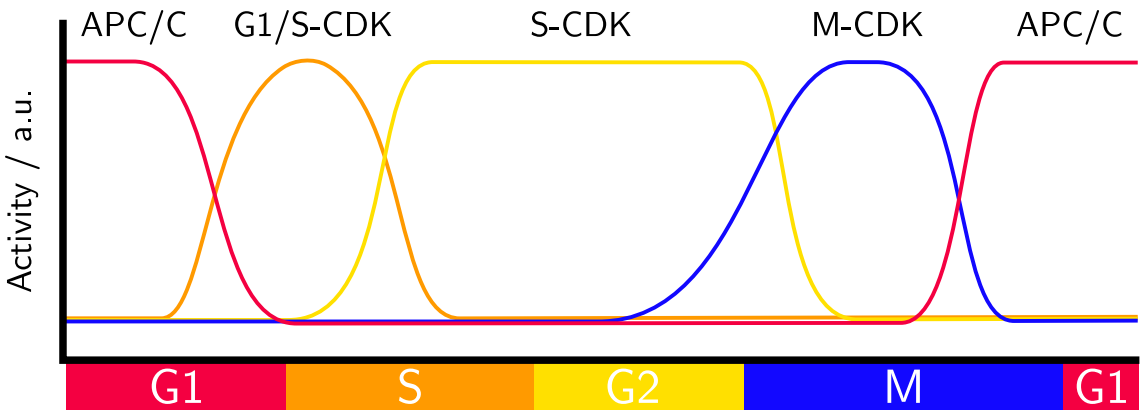

Figure 1.2: Sequential activation and inactivation of CDK:Cyclin complexes drives progression through the cell cycle. Adapted from [1].

the major mammalian CDKs and their associated cyclins is given in Table 1.1. While sufficient for this discussion, this classification is a necessary simplification. Loss of a single CDK or cyclin is rarely lethal at a cellular level due to redundancy in function between cyclins and CDKs associated with different cell cycle phases [14].

Progression through interphase and entry into M-phase is driven by sequential activation of CDKs associated with each cyclin type (Figure 1.2). The activity of each CDK:Cyclin complex promotes accumulation of the next cyclin in the sequence, while turning off the activity of preceding cyclins. Ultimately, Cdk1 in complex with Cyclin B (Cdk1:CycB) promotes activation of APC/C, promoting cyclin degradation and resetting the system for transition into G1.

Inhibitory phosphorylation regulates CDK activity and contributes to positive feedback loops

In addition to regulation by cyclin availability, Cdk1 itself is regulated directly by inhibitory phosphorylation of specific tyrosine and threonine residues [17, 18]. This inhibitory phosphorylation contributes to maintaining the cell in G2 until its removal triggers the G2/M transition and mitotic entry [17], though other factors may also contribute [18]. Phosphorylation is catalysed by the Wee1 and Myt1 kinases, and dephosphorylation by the Cdc25 phosphatase [18].

Release from G2 arrest is initiated following successful completion of DNA replication and loss of signalling associated with DNA damage response pathways which are beyond the scope of this thesis [19]. Crucially however, this kinase/phosphatase pair are also

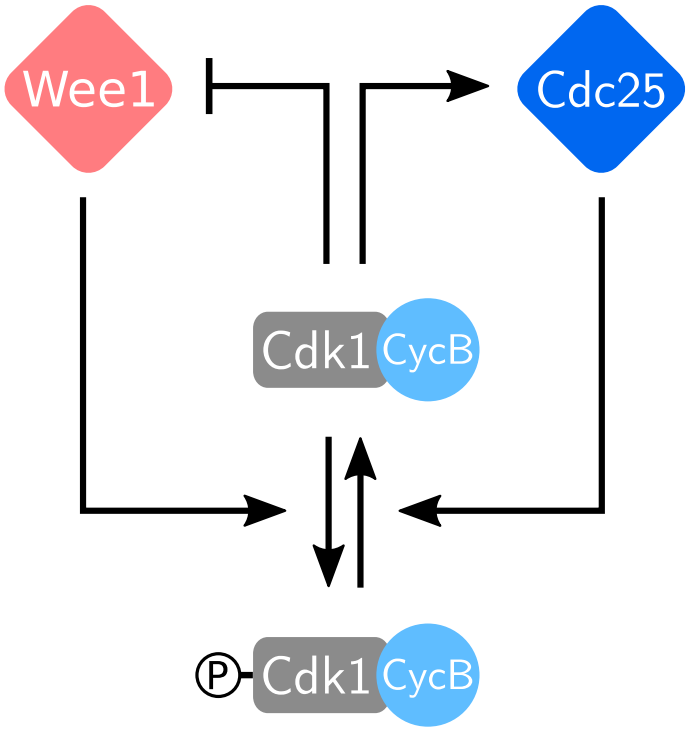

Figure 1.3: Wiring/influence diagram showing the regulation of inhibitory phosphorylation of Cdk1. Active (unphosphorylated) Cdk1 catalyses activatory and inhibitory phosphorylation of Cdc25 and Wee1 respectively.

subject to direct regulation by CDK-dependent phosphorylation. Phosphorylation of Cdc25 is required for its activation, while phosphorylation of Wee1 is inhibitory [17, 19]. This results in two positive feedback loops (one positive-positive and one double-negative) between CDK and the enzymes responsible for its phosphorylation state (Figure 1.3). The existence of these feedback loops contributes to switch-like activation of CDK at mitotic entry [18].

Cyclin-dependent Kinase Inhibitors (CKIs) block CDK activation

CDK activity is also regulated by specific stoichiometric inhibitors **(CKIs)**, which bind and inhibit CDK:Cyclin complexes [20, 21]. A major role of CKIs is to inhibit CDK activity during G1. For example, in budding yeast the CKI Sic1 inhibits S-phase and M-phase CDK:Cyclin complexes (Clb1:6) [22].

1.2.2 Protein Phosphatases

The stability of protein phosphorylation to spontaneous hydrolysis means that regulated dephosphorylation by protein phosphatase enzymes is essential to consider alongside

CDK-dependent phosphorylation. This is particularly relevant during late mitosis, where reversal of mitotic phosphorylation events is required in order to 'reset' the cell for entry into G1. Here we discuss two of the major mitotic exit phosphatases, **PP1** and **PP2A**.

Protein Phosphatase 1 (PP1)

PP1 is a serine/threonine phosphatase responsible for dephosphorylation of proteins implicated in diverse cellular pathways including glycogen metabolism, protein synthesis, cytoskeletal organisation, and ion channel function [23]. Of most relevance here is its role in dephosphorylation during mitotic exit, discussed in more detail in Section 1.4.7. It performs its diversity of functions via association with specific PP1-interacting Proteins (PIPs). These bind to PP1 and restrict its activity to a specific subset of substrates [24].

In addition to restrictions on its activity imposed by PIP binding, PP1 is also regulated by a stoichiometric inhibitor (Inhibitor-1) and by CDK-dependent phosphorylation [25, 26]. PP1 activity is responsible both for the auto-dephosphorylation of CDK target sites on PP1, and for dephosphorylation and inactivation of Inhibitor-1, so that PP1 is self-activating once CDK activity drops below the level needed to maintain inhibition [26].

Protein Phosphatase 2A (PP2A)

Protein Phosphatase 2A (PP2A) is a serine/threonine phosphatase responsible for dephosphorylation of a wide range of cell cycle targets [27]. Its catalytic subunit has an intrinsic substrate specificity for phospho-threonine over phospho-serine, providing a potential mechanism for ordered dephosphorylation of substrates based on their phosphosite [28, 29, 30].

PP2A is a heterotrimeric complex comprising structural and catalytic subunits ($PP2A_A$ and $PP2A_C$), in association with a regulatory $PP2A_B$ subunit which provides substrate specificity. $PP2A_B$ also determines the temporal and spatial pattern of PP2A activity via interaction with specific regulators. **B55** and **B56** are two of the most significant regulatory 'B' subunits involved in reversal of mitotic phosphorylation events following anaphase, and this is discussed in more detail in Section 1.4.7.

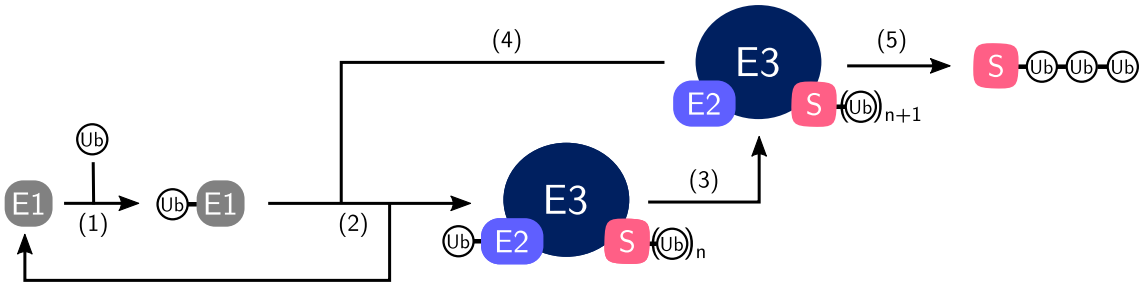

Figure 1.4: Diagram showing role of E1, E2 and E3 enzymes in substrate (S) ubiquitination. $(Ub)_n$ refers to a poly-ubiquitin chain of length n. As a starting point n = 0, in which case ubiquitin is ligated directly to a lysine residue on the substrate. See text for further details. Adapted from [34].

1.2.3 Anaphase-promoting complex or Cyclosome

While CDK activity promotes progression through interphase and into mitosis, the main driver of chromosome segregation and exit from mitosis is APC/C activity. The APC/C is a large protein complex which catalyses **Ubiquitination** of specific target proteins [31]. Its initial activation drives the M/A transition, leading it to be referred to as the 'Anaphase-Promoting Complex' [32]. Control of APC/C activation at M/A is the responsibility of the **Spindle Assembly Checkpoint (SAC)**, which inhibits APC/C until all chromosomes are correctly aligned on the mitotic spindle [33] (See Section 1.4.3). Following mitotic exit, APC/C activity remains high during G1 until it is inactivated by rising CDK activity at the G1/S transition.

APC/C targets its substrates for proteasomal degradation

APC/C is part of the **Ubiquitin Proteasome System**, responsible for regulated degradation and turnover of cellular proteins [35]. Central to this system is the **Proteasome**, a large multi-subunit particle which catalyses the ATP-dependent unfolding and proteolysis of substrate proteins identified by post-translational ubiquitination [36].

APC/C is not unique in targeting proteins to the proteasome: around 600 putative RING-family ubiquitin ligases may be responsible for ubiquitination reactions in human cells, many of which are involved in proteasomal targeting [37]. Nevertheless, APC/C is essential for cell-cycle specific degradation of its target proteins [31]. The other major cell cycle-specific ubiquitin ligase is the **Skp1–Cullin–F-box (SCF) complex**, responsible for ubiquitination of phosphorylated target proteins between G1 and early M-phase [34].

Ubiquitination reactions involve 3 separate enzymes: a **Ubiquitin Activating En-**

zyme (E1), which uses ATP hydrolysis to covalently attach ubiquitin to itself (Reaction 1 in Figure 1.4); a **Ubiquitin Conjugating Enzyme (E2)** which transfers the activated ubiquitin from the E1 enzyme to itself and presents it to the ligase (Reaction 2); and the **Ubiquitin Ligase (E3)** which transfers the ubiquitin from E2 to a lysine residue on the target protein (Reaction 3) [34, 38]. It is this 3rd class of enzymes, of which APC/C and SCF are members, which is mainly responsible for conferring substrate specificity on the reaction [38].

The presence of lysine residues on the ubiquitin molecule which can themselves act as E3 targets provides additional signalling complexity by allowing for creation of poly-ubiquitin chains (Reaction 4) prior to substrate release (Reaction 5). Addition of up to four ubiquitin molecules greatly enhances proteasomal degradation of the target [38]. Polyubiquitination also provides capacity for further regulation via the action of deubiquitinating enzymes in reducing chain length [39].

In most cases in this thesis we assume that APC/C-dependent ubiquitination is synonymous with degradation of the target protein. This is a useful simplification, and under normal conditions should provide a reasonable approximation of the true situation. However, it is worth noting that while much progress has been made in mapping out the landscape of ubiquitin signalling, defining how a specific ubiquitin signal ultimately relates to target degradation (the so-called 'ubiquitin code') remains highly complex [36, 38].

APC/C-dependent degradation of Securin and CycB drives chromosome segregation and mitotic exit

Cyclins are an important target of the APC/C, hence its alternative designation as the 'Cyclosome' [40]. In particular, destruction of the M-phase **Cyclin B (CycB)** during late mitosis drives mitotic exit [41]. The other major APC/C target is **Securin**, a stoichiometric inhibitor of the enzyme **Separase**, which is responsible for cleaving the **Cohesin** proteins maintaining cohesion between sister chromatids (see Section 1.4.2) [42]. By destroying securin and thereby activating separase, APC/C activity initiates chromosome segregation at M/A. Similarly, APC/C-dependent cyclin degradation leads to loss of CDK activity and mitosis-specific phosphorylation. Together, these two effects

of APC/C are responsible for driving the events of mitotic exit [43, 44].

APC/C co-activators are required for substrate recognition

Apo-APC/C is not active in isolation, requiring one of two co-activators for substrate recognition [45]. The major mitotic APC/C co-activators are **Cdc20** and **Cdh1** (also called Fzr1) [31]. While similar in structure and function, these co-activators differ in their regulation and the timing of their activity during the cell cycle. APC/C^{Cdc20} is responsible for initial APC/C activation at the M/A transition, while APC/C^{Cdh1} replaces it during late mitosis and into the subsequent G1-phase [46].

APC/C:co-activator complexes recognise substrates via specific amino acid sequences in the target protein known as **Degrons**. Important degron sequences include the **KEN-box** [47], **D-box** [48], and **ABBA motif** [49]. Despite their role in substrate recognition, addition of a degron sequence alone is insufficient to target a protein to the APC/C, suggesting that additional sequence elements are also required [50].

While CycB and Securin are the major APC/C substrates involved in bringing about the M/A transition, other cell cycle-related substrates are also recognised and targeted for degradation. These include the S-phase **Cyclin A (CycA)**, which is recognised by APC/C^{Cdc20} [49], and Cdc20 itself, which is targeted for degradation by APC/C^{Cdh1}[47].

APC/C^{Cdc20} is active during early mitosis and is subject to checkpoint inhibition

APC/C^{Cdc20} substrates can be divided into two categories: early substrates which are degraded during prometaphase (following NEBD) in a SAC-independent manner, and late substrates which are degraded during metaphase and anaphase only after termination of SAC signalling. Examples of the early substrates include Nek2A and CycA [51, 52]. Securin and CycB are both late substrates, and are the only substrates for which APC/C-dependent degradation is essential for normal cell cycle progression [53].

The factors which determine the ability of Cdc20 to promote degradation of early substrates (in particular CycA) but not late substrates during a SAC arrest are of considerable interest in understanding the mechanism of SAC action. CycA binds Cdc20 during G2-phase, prior to APC/C activation [54]. Binding of the CDK accessory subunit Cks to this complex is also required to target CycA to the APC/C [54, 55].

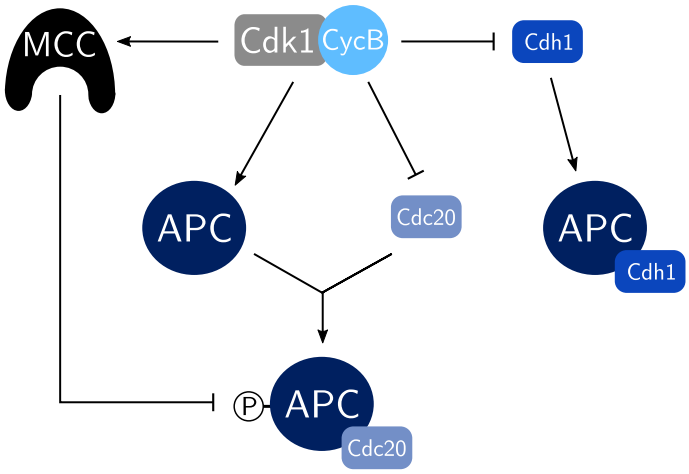

Figure 1.5: Summary of CDK-dependent pathways regulating APC/C activity in M-phase. Arrows indicate activatory interactions, bars indicate inhibition. Merging arrows indicate complex formation.

APC/C^{Cdh1} is active during late mitosis and promotes degradation of Cdc20

Cdh1 substrate specificity is similar but not identical to that of Cdc20. While it has previously been proposed that D-box and KEN-box degrons are associated with Cdc20- and Cdh1-dependent degradation respectively, it is now clear that both degrons can contribute to recognition by either co-activator [31, 56]. Perhaps of most significance, Cdh1 promotes ubiquitination and degradation of Cdc20, thereby promoting a distinct handover between the two co-activators once it becomes active in late mitosis [56]. Degradation of the major APC/C substrates Securin and CycB is catalysed by both APC/C^{Cdc20} and APC/C^{Cdh1} [57, 58].

APC/C is subject to multiple forms of CDK-dependent regulation

Both the APC/C core and its co-activators are CDK targets, but with opposite effects: phosphorylation of the APC/C core is required for APC/C^{Cdc20} activity (though not APC/C^{Cdh1} activity) [59, 60], while Cdh1 and Cdc20 are phosphorylated by CDKs at multiple sites, blocking their ability to activate APC/C [60, 61, 62]. CDK activity also influences APC/C^{Cdc20} via its role in activation of the mitotic checkpoint (See Section 1.4). These pathways are summarised in Figure 1.5.

The **APC/C core is phosphorylated at multiple sites** across its different subunits over the course of mitosis [63]. Phosphorylation by CDK and Polo-like kinase 1 (Plk1) are required for full activation of APC/C^{Cdc20}, but only CDK phosphorylation is essential for activity [63, 64]. Comparison of the X-ray structures of phosphorylated and unphospho-

rylated APC/C reveals that an **Auto-inhibitory Loop** of the **Apc1** subunit, containing multiple CDK target sites, blocks the co-activator binding site of APC/C when in its unphosphorylated form, thereby preventing Cdc20 binding. An additional phosphorylated domain on the **Apc3** subunit is responsible for enhancing CDK-dependent phosphorylation of the Apc1 loop [64, 65, 66]. The unphosphorylated auto-inhibitory loop does not inhibit Cdh1 binding to the APC/C core, possibly due to stronger interactions of Cdh1 with the core out-competing the loop for binding at the co-activator site [64].

In contrast, **CDK-dependent phosphorylation of Cdc20 and Cdh1** is inhibitory for APC/C activity. Cdc20 phosphorylation by Cdk1:CycB reduces its ability to act as an APC/C co-activator *in vitro* [67]. Loss of phosphorylation from a Cdc20 N-terminal fragment correlates with its association with the APC/C in *Xenopus* egg extracts, and an alanine mutant of the same construct will strongly out-compete the wild-type sequence for APC/C binding [62]. Cdc20 phosphorylation *in vivo* peaks in G2 and declines during G2/M [68]. These early phosphorylation events are the result of Cdk2:CycA activity, and this is important to prevent premature APC/C^{Cdc20} activity prior to mitotic entry [69]. Cdc20 phosphorylation has also been reported to be required for its effective inhibition by the SAC, however the mechanism by which this occurs remains unclear [70, 71].

Phosphorylation of Cdh1 is similarly inhibitory for its ability to activate APC/C [60, 61]. Cdh1 exists primarily in phosphorylated form from G1/S through to late mitosis, where it becomes active during mitotic exit and into G1 [60].

The requirement for both CDK-dependent phosphorylation on APC/C and loss of CDK-dependent phosphorylation on Cdc20 presents an apparent difficulty for explaining how APC/C^{Cdc20} activation can occur at M/A, and strongly suggests that significant differences in phosphorylation and dephosphorylation kinetics between the sites on the two species must exist. The **Residue-specificity** of the two species suggests that this is the case: the key phosphorylation sites on APC/C are **Serine**, while those on Cdc20 are **Threonine** [30]. This is significant since **PP2A-family phosphatases** (see Section 1.2.2) show a marked preference for phospho-threonine sites over phospho-serine [28, 29, 30]. These differences in the CDK-dependence of Cdc20 and APC/C activity have been proposed to contribute to cell cycle oscillations in *Xenopus* extract [72].

Since APC/C^{Cdh1} does not require APC/C phosphorylation for activity, this difficulty does not exist when explaining the ability of dephosphorylated Cdh1 to activate APC/C. The late activation of Cdh1 relative to Cdc20 means that its activity peaks at a time when the level of CDK-dependent phosphorylation in the cell is lower.

APC/C is regulated by stoichiometric inhibitors

Stoichiometric inhibitors provide another mechanism for APC/C regulation. These include the G1/S regulator **Emi1**, and the **Mitotic Checkpoint Complex (MCC)**, the major effector of the Spindle Assembly Checkpoint (see Section 1.4.3).

Emi1 is a stoichiometric inhibitor of the APC/C^{Cdh1} complex which becomes active at the G1/S transition. By preventing CycB degradation, it allows for a rise in CDK activity to promote S-phase entry [73]. Recently, Emi1 has been shown to undergo APC/C^{Cdh1}-dependent degradation, so that it acts as both a substrate and an inhibitor of APC/C^{Cdh1} [74]. The related inhibitor **Emi2** inhibits APC/C activity following the first meiotic division (see Section 1.5.2).

1.3 Systems Biology of the Cell Cycle

A simple description of the function of individual cell cycle regulators is insufficient to properly describe the behaviour of the cell cycle regulatory system. Regulators do not exist in isolation but participate in positive and negative interactions with other regulators to create a series of feedback loops. Understanding the behaviour of the resulting system requires a robust mathematical analysis. While the specific molecular details vary in each case, important similiarities exist both between organisms and between different phases within the cell cycle.

1.3.1 Biochemical Network Motifs

Much of the complex behaviour associated with biochemical reaction networks can be distilled down to a simpler series of recurring **Network Motifs** [75]. By network motif we mean a fixed pattern of interactions which is repeated in multiple systems at higher frequency than would be expected from a purely random network configuration of the same size. Separate incidences of a motif share the same network structure, but use a

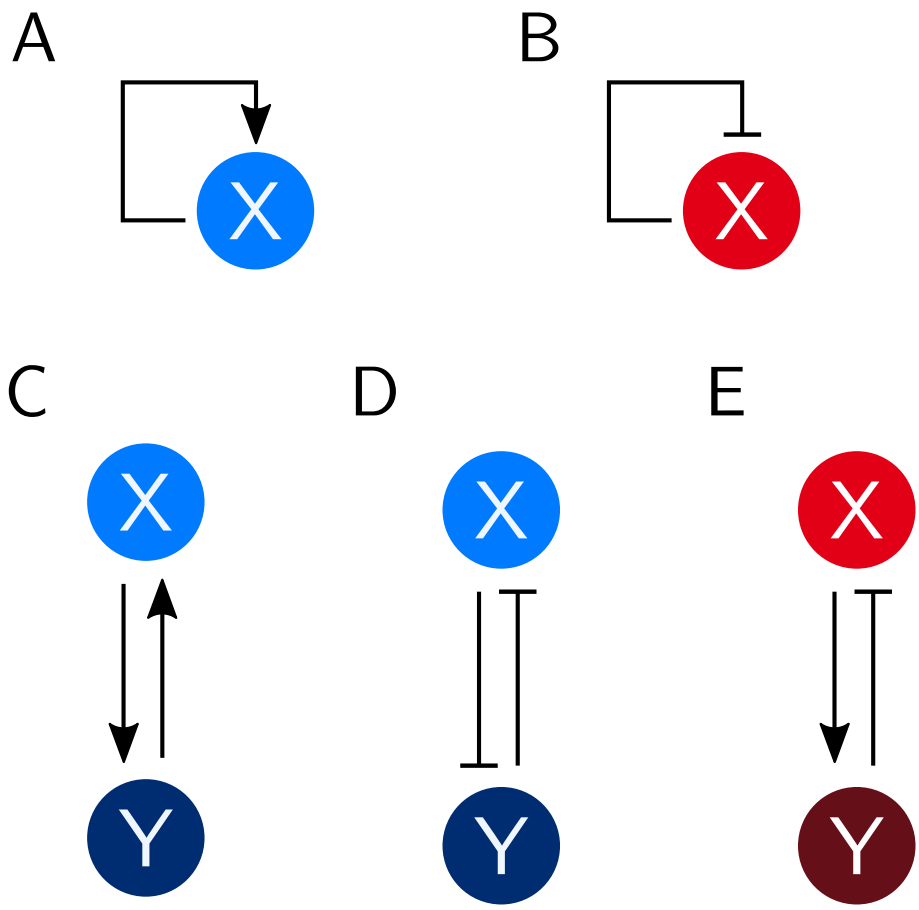

Figure 1.6: Examples of positive (blue) and negative (red) feedback loops. (A, B) One-component system with positive feedback (auto-activation) (A) and negative feedback (auto-inhibition) (B). (C, D) Two-component positive feedback loops: mutual activation (C) and mutual inhibition (double-negative feedback) (D). (E) Two-component negative feedback loop.

different set of components in each case. Understanding these generic motifs can therefore provide insight into a number of related biological examples. The most elementary motifs we will consider are **Positive and Negative Feedback Loops**, combinations of which give rise to much of the complex behaviour associated with the cell cycle.

1.3.2 Positive and Negative Feedback

Positive Feedback is a network motif in which activity of a component of the system has an activating effect on itself. Conversely, **Negative Feedback** is a network motif in which activity of a component has an inhibitory effect on itself.

The simplest case of either positive or negative feedback is a one-component system which directly activates or inhibits itself (Figure 1.6A, B). In more complex systems, positive or negative feedback can arise from a series of interactions between different components. For example, positive feedback can arise in a two-component system either

through mutual activation (**Simple positive feedback**, Figure 1.6C) or through mutual inhibition (**Double-negative feedback**, Figure 1.6D), while two-component negative feedback would require that one component act as an activator, and one as an inhibitor (Figure 1.6E). In general, any system of interactions between multiple components which forms a closed loop will produce positive feedback if the total number of negative interactions is even, and negative feedback if the total number of negative interactions is odd.

The uses of positive and negative feedback loops in biological systems are numerous and varied [76]. Positive feedback loops can contribute to signal amplification, while negative feedback is important for processes such as homeostasis and signal adaptation. Two of the most significant system behaviours associated with cell cycle network motifs are the **Cell Cycle Oscillator** and the **Bistable Switch**, which are discussed in detail below.

1.3.3 The Cell Cycle Oscillator

An oscillatory system displays periodic changes in the activity of its components. Simple cell cycles can operate entirely as autonomous biochemical oscillators, without the requirement for additional input from internal or external signals. In particular this applies to early embryonic systems where large cells with low nuclear:cytoplasmic ratio undergo rapid cycles of cell division uncoupled from requirements for growth or regulation from the comparatively small nuclear volume [78]. The classic example of such a system is the *Xenopus laevis* embryo, which displays oscillatory behaviour even in an enucleated extract [79].

One mechanism to generate an oscillator is to couple a positive feedback loop to a negative feedback loop (Figure 1.7A). The positive feedback loop allows the system to adopt one of two possible states, depending on whether the loop is in an 'on' or 'off' state. The negative feedback loop then constantly promotes the transition to the opposite state [76].

This mechanism is responsible for the cell cycle oscillations observed in *Xenopus* extract. In this system, CDK:Cyclin (also known as **Maturation/M-Phase–Promoting**

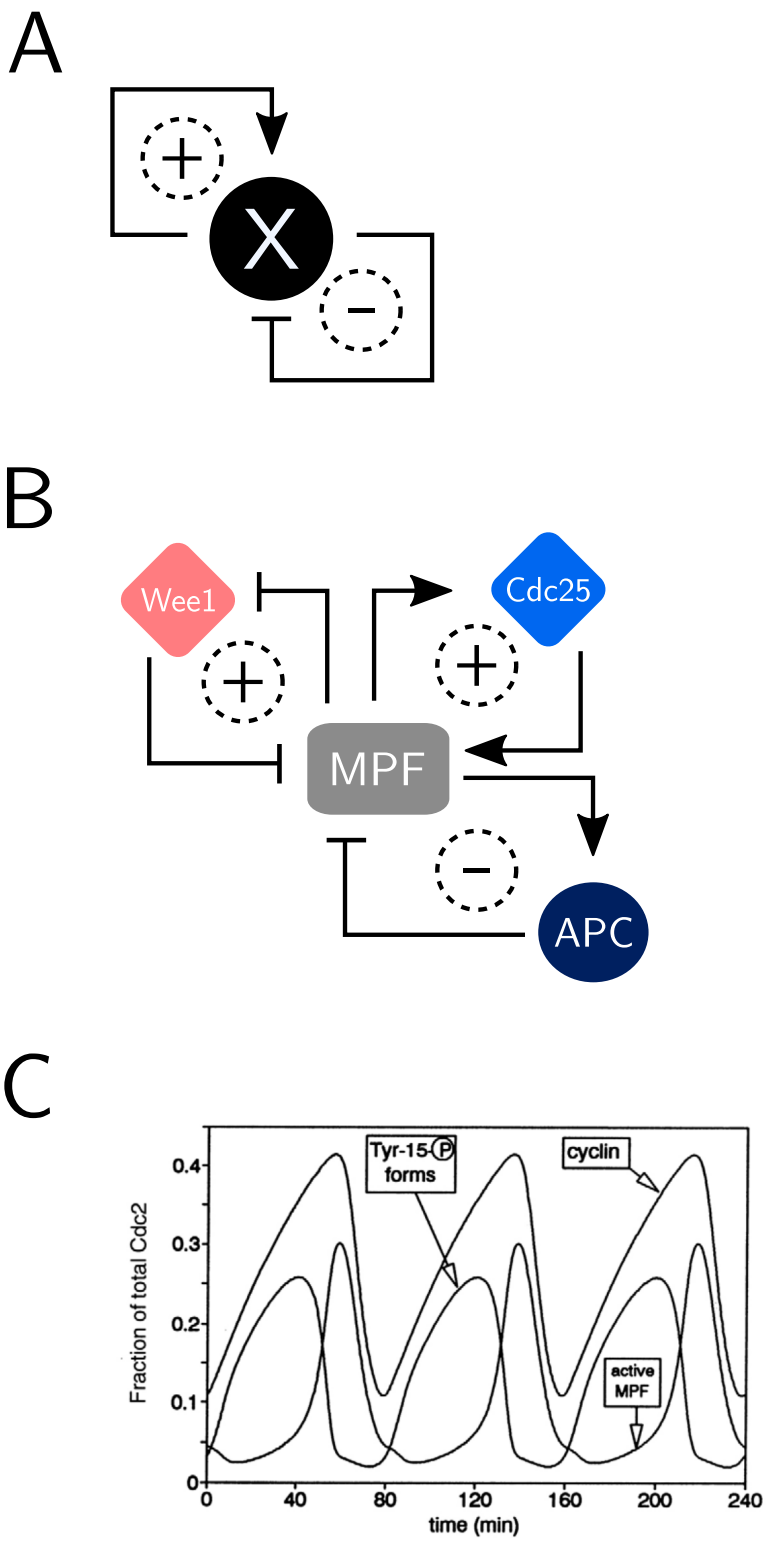

Figure 1.7: (A) Influence diagram for a generic positive-negative feedback oscillator. (B) Influence diagram for the cell cycle oscillator, an example of a positive-negative feedback oscillator. (C) Timecourse simulation of the network in (B), showing periodic oscillations in MPF. Figure (C) is reproduced with permission from the Journal of Cell Biology, `https://www.doi.org/10.1242/jcs.224501` [77].

Factor or **MPF**) and APC/C activities are linked to produce a biochemical oscillator (see influence diagram Figure 1.7B). As discussed earlier (Section 1.2.1), CDK activity is at the centre of positive feedback loops involving addition and removal of inhibitory phosphorylation from Cdk1 by Wee1 and Cdc25 respectively. At the same time, a negative feedback loop exists between CDK and APC/C, since CDK-dependent phosphorylation is required for APC/C activity, while APC/C inhibits CDK activity via CycB degradation (see Section 1.2.3). Combining these effects in a mathematical model produces an oscillating system which is consistent with the experimentally observed behaviour of the extract (Figure 1.7C) [77].

While *Xenopus* extract is an atypical system in which oscillations of the cell cycle components themselves are uncoupled from regulation by external events, its oscillatory behaviour is nonetheless relevant to a more general consideration of cell cycle events in other systems. The same components are also present in these cases, so the principles of an underlying oscillatory system remain the same. However, two important differences exist between the model *Xenopus* oscillator and a 'normal' cell cycle. Firstly, there are additional components operating in sequence (for example multiple CDK:Cyclin complexes), so the overall oscillatory mechanism is more complex. Secondly, rather than operating as a free-running oscillator, in a normal cell cycle the system is regulated by a series of cell cycle checkpoints (Section 1.1.3). These act as breaks in the oscillatory regime, during which further progression is delayed until a specific condition is satisfied.

1.3.4 Bistable Switches

Related to the idea of both cell cycle oscillators and checkpoints is the concept of a bistable switch. **Bistability** refers to the ability of a system to exist in either of two possible **Stable Steady States** for a fixed set of parameter values. This is illustrated on a **Bifurcation Diagram** (Figure 1.8), which plots the equilibrium points of the system as a function of one of the system parameters. The equilibrium points discussed in this thesis are principally stable and unsteady steady states (formally, stable and unstable nodes), however other equilibrium points such as saddle nodes or limit cycle foci are also possible. The process for generating a bifurcation diagram is discussed in more detail in

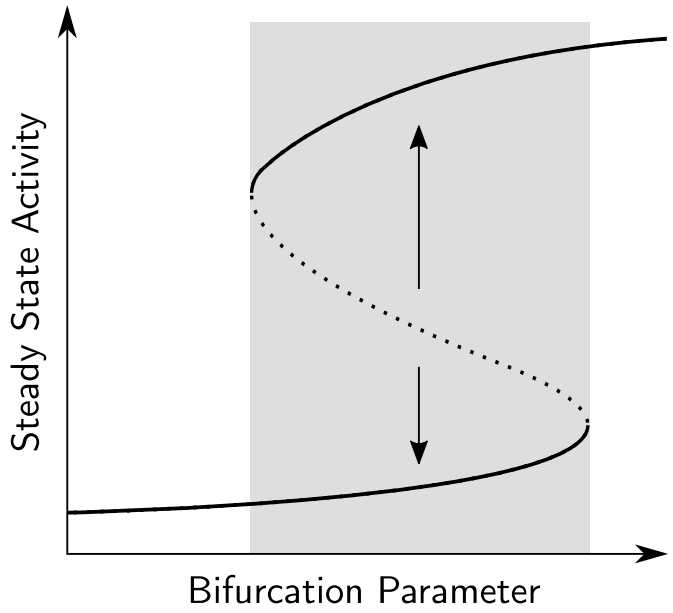

Figure 1.8: An example bifurcation diagram. Solid lines: stable steady states, Dotted line: unstable steady state. The shaded region shows the values of the bifurcation parameter for which two stable steady states exist, and in which the system is therefore bistable. Arrows represent example trajectories through the state-space.

Section 1.6.3.

The parameter chosen could represent a signal that changes to promote transition from one cell cycle stage to the next, for example the level of growth factor stimulation. For a given value of this signal parameter on the x axis, the bifurcation diagram displays the stable and unstable steady states of the system (solid and dashed curves respectively). A bistable system is one in which for certain values of the input parameter there exist two stable steady states, separated by an unstable steady state. This bistable region is indicated by the shaded area on Figure 1.8.

The unstable steady state does not represent an attainable physiological state, but instead marks the threshold separating regions of state-space from which the system will tend towards either of the two stable steady states (example trajectories shown by arrows in Figure 1.8).

Bistable systems such as this can display switch-like transitions between one state and the next in response to increase or decrease in an input signal. In the context of the cell cycle, these states can correspond to different cell cycle stages, where the input signal controlling the transition will either be an upstream cell cycle event itself, or the activity of an associated cell cycle regulator. Where each cell cycle stage is a different

state of a bistable system, this allows for switch-like transitions between states which are robust to perturbations to the input signal.

Requirements for Bistability

Bistability is an emergent property of systems which fulfil specific criteria. In such systems, there will exist certain parameter regimes in which a bistable state emerges. One essential requirement is for a positive feedback (or double-negative feedback) loop [80]. The presence of a positive feedback loop presents two possible options for the state of the system. For example, for a double-negative feedback loop (Figure 1.6D), where when one component is active, the other will tend to be inactive, and vice versa. Conversely, for a simple positive feedback loop (Figure 1.6C), the two options are for both components to be on, or both to be off. However, positive feedback alone is insufficient to produce a bistable system, since it does not guarantee the stability of the states described above. There is an additional requirement for a **Non-linear** or **Ultrasensitive** signal-response curve as part of the system. This can stabilise the two possible outcomes by separating them in state space without allowing either for one to dominate over the other, or for the system to stabilise at an intermediate point. These requirements for bistability, and their implications for the structure of cell cycle network motifs, are discussed in more detail in Chapter 2.

1.4 Mitosis and the Mitotic Checkpoint

Having introduced in general terms the basic functions of the cell cycle and its mechanisms of control, we will now consider in more detail the regulation of mitosis, since this will form one of the major topics of this thesis. In particular, we focus on the regulation of APC/C activation at the M/A transition, and the role of checkpoint mechanisms in preventing APC/C activation prior to this point.

1.4.1 Mitotic Checkpoint Overview

Correct chromosome alignment is the result of the physical movement of condensed mitotic chromosomes by the action of **Spindle Microtubules (MTs)** emanating from the spindle poles. Attachment of microtubules to the DNA occurs via the **Kinetochore**

(KT) associated with the centromere of each sister chromatid.

The **Mitotic Checkpoint (MC)**, or **Spindle Assembly Checkpoint (SAC)**, is the cell cycle checkpoint responsible for ensuring that chromosomes are correctly bioriented and aligned on the mitotic spindle prior to APC/C activation at the M/A transition. To do so, it must identify **Unattached Kinetochores (uKT)**, identify and eliminate incorrect attachments while stabilising correct attachments, and prevent APC/C activation until the checkpoint has been satisfied. These functions constitute distinct signalling modules, connected via common input and output pathways [81].

To prevent APC/C activation, MC signalling results in formation of a stoichiometric APC/C inhibitor, the **Mitotic Checkpoint Complex (MCC)**. Unattached kinetochores act as a site for catalytic assembly of MCC complexes, directly linking KT:MT attachment status to APC/C inhibition. A separate **Error Correction (EC)** pathway is responsible for the removal of incorrect KT:MT attachments. Each of these elements is discussed in more detail below.

The exact relationship between the EC and the attachment monitoring and MCC assembly pathways of the MC is the subject of ongoing debate (see below). This can make terminology confusing, since depending on the exact definition EC may or may not be referred to as a separate pathway from the MC/SAC. For the purposes of this thesis, we use **Spindle Assembly Checkpoint** to refer only to the attachment sensing and MCC generating pathways, but **Mitotic Checkpoint** to describe the entire checkpoint apparatus including EC. However, note that this is not a universally accepted use of these terms in the literature. Below, we first discuss the core SAC pathways, and then expand this to include EC.

1.4.2 Molecular Events of Chromosome Segregation

Before discussing further the mechanisms by which the SAC detects and responds to chromosome attachment status, we first revisit the mechanisms of chromosome segregation, and explain the molecular actors underpinning these chromosomal-level events, since these provide the physical link between attachment status and cell cycle progression.

Sister chromatid cohesion is maintained by cohesins and abolished by separase activation at M/A

Essential to the process of accurate chromosome segregation is the ability to maintain a physical link between sister chromatids prior to anaphase. At a molecular level, these events can be explained by the action of ring-shaped **Cohesin** proteins, which encapsulate both sisters to prevent their dissociation [82]. Cohesins are loaded onto DNA prior to S-phase (during G1 in budding yeast, but the preceding telophase in vertebrates) [83]. However, this initial loading produces only a transient association with chromosomes, and it is only during S-phase that cohesion is robustly established between newly replicated DNA strands via a mechanism involving acetylation of the cohesin Smc3 subunit [83, 84]. In metazoa most cohesin is lost from chromosome arms early in mitosis via the 'Prophase Pathway', however a core of centromeric cohesin persists to maintain cohesion into metaphase [85].

Once established, cohesion is maintained during prophase and prometaphase as chromosomes condense and align on the spindle. In order to subsequently separate the sister chromatids at anaphase, cohesins must be cleaved by the enzyme **Separase** [42]. Prior to this point, Separase is held in an inactive complex by its stoichiometric inhibitor **Securin** [86, 87]. Securin is an APC/C substrate (Section 1.2.3), so securin degradation and separase activation are tightly coupled to the activation of APC/C^{Cdc20} at the M/A transition [88, 89].

Kinetochore complexes link chromosomes to spindle microtubules

The kinetochore is a large multi-protein complex which assembles at the centromeric regions of eukaryotic chromosomes. Its structure has been recently subject of a comprehensive review [90], and is beyond the scope of this thesis, so here we highlight only those points which are necessary for subsequent discussion of its role in the mitotic checkpoint.

The kinetochore structure can be subdivided into 'inner' and 'outer' modules. The **Inner Kinetochore** mediates kinetochore:centromere binding, and is centred around the interaction between the centrosome-specific CENP-A nucleosome, and the Constitutive Centromere-Associated Network (CCAN), a complex of Centromeric Protein (CENP)

subunits which defines the inner kinetochore [91, 92, 90].

The **Outer Kinetochore** mediates KT:MT interactions, and predominantly comprises the **KMN** (Knl1, Mis12, Ndc80) complex [93, 92, 90]. Of these, **Ndc80** is the major site of microtubule interaction [93], while **Mis12** contains binding sites for inner kinetochore components, Ndc80, and Knl1 [90]. **Knl1** is an important signalling platform, containing binding sites for mitotic phosphatases and SAC components [90].

The outer kinetochore proteins are phosphorylated at multiple sites during mitosis, which is important for checkpoint function. Phosphorylation of Ndc80 by the kinase Aurora B (AurB) inhibits microtubule binding [94, 93].

Correct kinetochore:microtubule attachment generates tension across the kinetochore

The mitotic spindle comprises thousands of microtubules arising from two **Spindle Poles** on opposite sides of the cell [95]. In many cells, spindle poles are associated with **Centrosomes**, sub-cellular structures which direct microtubule organisation. However in others, for example mammalian oocytes, spindle poles are acentrosomal [96].

Microtubules are dynamically unstable structures which arise from the polymerisation and depolymerisation of $\alpha\beta$-tubulin monomers. Each tubulin monomer, and by extension the microtubule as a whole, has a plus end and a minus end, with polymerisation proceeding by addition of new monomers to the plus end of an existing microtubule [97].

Capture of kinetochores by the plus ends of spindle microtubules generates KT:MT attachments [90]. Following cohesin cleavage at anaphase, sister chromatids are pulled to opposite spindle poles via these attachments. This therefore requires a specific attachment geometry, since the two sister kinetochores must each be captured exclusively by MTs arising from opposite spindle poles (**Amphitelic Attachment**) in order to achieve correct alignment of chromosomes on the spindle. Correct attachments can be characterised by the existence of **Tension** as a result of the opposing pulling forces acting on the sister kinetochores. Attachment to a single spindle pole, or attachment of a single kinetochore to both spindle poles, does not result in generation of the correct tension. Incorrect attachments are recognised and eliminated by the Error Correction pathway (Section 1.4.4).

Drug	Mechanism	Spindle Formation	Attachment
Nocodazole (Noc) [98]	Blocks tubulin polymerisation	No Spindle	No Attachment
Monastrol [99]	Inhibits kinesin Eg5	Monopolar spindle	Tensionless attachment
Taxol [98]	Stabilises Microtubules	Multipolar Spindle	Incorrect Attachment

Table 1.2: Table showing commonly used spindle poisons, their effects on spindle formation and KT:MT attachment status.

Experimental assays of mitotic checkpoint function often make use of drugs which disrupt spindle formation (**Spindle Poisons**) in order to generate attachment defects and activate the checkpoint [98]. Different drugs have a range of effects on spindle formation, which influences how they activate the SAC and EC pathways. Table 1.2 gives a summary of some of the major spindle poisons used experimentally.

1.4.3 The Spindle Assembly Checkpoint

As discussed above, the key features of the SAC (as distinct from EC) are to detect unattached kinetochores and to prevent APC/C activation in response. This is achieved by formation of the APC/C inhibitor MCC, which is assembled at unattached kinetochores.

MCC is the SAC effector

Formation of MCC is essential for the SAC to inhibit APC/C^{Cdc20} activity prior to anaphase. However, the exact mechanisms by which this inhibition is achieved are less clear due to ambiguity surrounding the role of Cdc20, which in addition to its role as APC/C co-activator is also an essential component of the MCC.

MCC comprises 4 subunits: Mad2, Cdc20, BubR1 and Bub3 [100]. Of these, Bub3 forms a sub-complex with BubR1 and is non-essential for MCC function. Mad2 possesses two distinct conformations: an inactive 'open' (**o-Mad2**) form, and an active 'closed' (**c-Mad2**) form which is able to bind ligands including Cdc20 and the upstream SAC regulator **Mad1** [101, 102]. Formation of the MCC therefore requires a conformation change from o-Mad2 to c-Mad2. This change is catalysed by a second Mad2 molecule

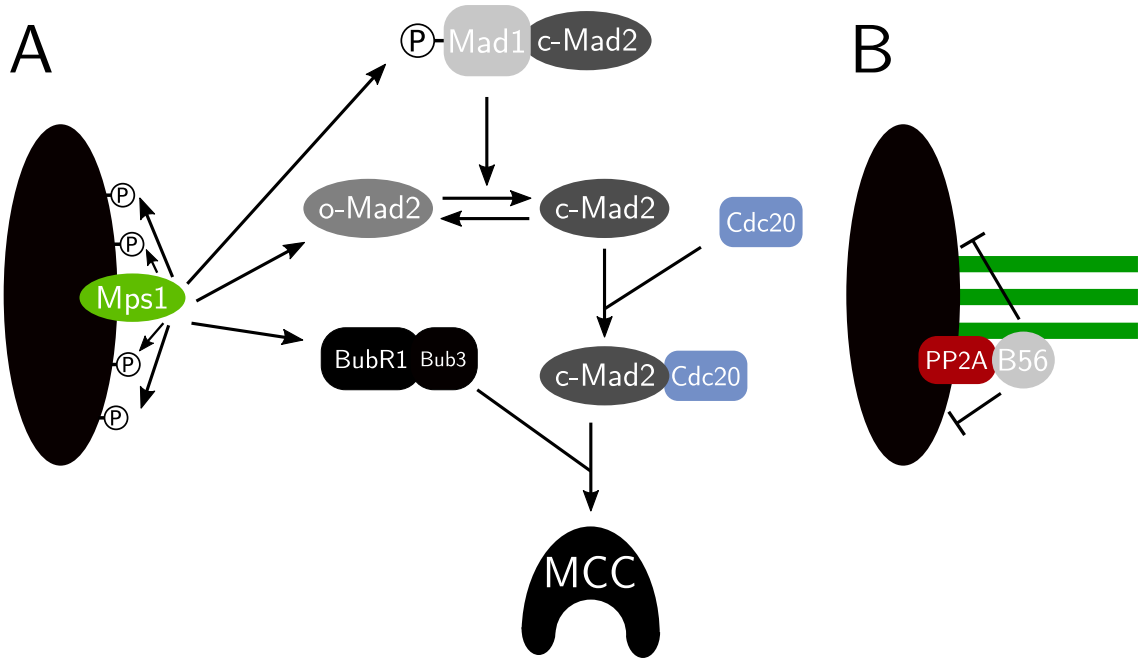

Figure 1.9: Diagram showing pathways of MCC assembly at the kinetochore. (A) Unattached kinetochores allow MPS1 binding and phosphorylation of target proteins. This recruits SAC components to the kinetochore and activates Mad1, allowing MCC assembly to occur. (B) Microtubule binding displaces MPS1. Dephosphorylation by PP2A:B56 silences SAC signalling.

in complex with **Mad1**. This Mad1:c-Mad2 complex binds free o-Mad2 and catalyses its interconversion via formation of an o-Mad2:c-Mad2 dimer [103, 104, 105]. Formation of c-Mad2 accelerates the assembly of Mad2:Cdc20 complexes, the rate-limiting step for MCC assembly [106]. Subsequent binding of BubR1:Bub3 to the c-Mad2:Cdc20 stabilises the complex and results in formation of the full MCC inhibitor. This interaction also prevents further downstream c-Mad2:o-Mad2 dimerisation which could result in ectopic SAC activation away from the kinetochore [107]. MCC assembly reactions are summarised in Figure 1.9A.

Attachment monitoring depends on MPS1-directed MCC assembly at unattached kinetochores

The monitoring of KT:MT attachment status is closely coupled to the formation of MCC (Figure 1.9). Unattached kinetochores are the site for catalytic assembly of MCC, and SAC components are recruited to kinetochores at the onset of prometaphase. As attachments are made, their localisation then decreases [33]. Attachment sensing centres on competition between spindle microtubules and the SAC kinase **MPS1** (*Monopolar Spindle-1*) for binding to the outer kinetochore component Ndc80 [108, 109].

MPS1 is, as the name suggests, essential for spindle pole body duplication in yeast [110, 111], and is likewise involved in duplication of the functionally equivalent centrosome in higher eukaryotes [112, 111]. However, it is its essential role in pathways of MCC assembly which explains the significance of its kinetochore localisation for attachment sensing [113, 114].

MPS1-dependent phosphorylation is required for kinetochore localisation and activation of multiple SAC targets. Firstly, MPS1 phosphorylation of **MELT motifs** in the kinetochore component Knl1 recruits the **Bub1:Bub3** complex to the kinetochore [115, 116, 117]. Bub1:Bub3 promotes localisation of other SAC proteins, including Mad1, BubR1, Mad2 and Cdc20, allowing MCC assembly to occur [118]. In addition to its phosphorylation of Knl1, MPS1 also directly phosphorylates Bub1 and Mad1 [119]. Bub1 phosphorylation is required for Bub1:Mad1 binding, and this interaction is essential for SAC function [119]. Pre-incubation of the Mad1:c-Mad2 complex with MPS1 greatly enhances its ability to catalyse formation of the Cdc20:c-Mad2 complex required for MCC formation [120].

Displacement of MPS1 following KT:MT attachment prevents assembly of SAC components and downstream signalling. In the absence of continued MPS1 activity, BubR1-dependent recruitment of PP2A:B56 ensures rapid turnover of MELT-repeat phosphorylation to silence further SAC signalling [121]. In this way, the attachment status of individual chromosomes is directly linked to their ability to generate an inhibitory MCC signal.

An outstanding question is to what extent this attachment status is an all-or-nothing response for a given kinetochore. While in yeast each kinetochore contains a binding site for a single microtubule, in higher eukaryotes each kinetochore can support multiple microtubule attachments, meaning that it does not have a single 'attached' or 'unattached' state but rather a range of states with varying levels of attachment [122]. How this relates to the activation status of the SAC is unclear.

Multiple mechanisms may contribute to APC/C inhibition by MCC

The structure and function of MCC immediately present two distinct mechanisms by which it can inhibit APC/C^{Cdc20}. Firstly, incorporation of Cdc20 into MCC acts to

sequester Cdc20 and reduce the amount available to act as an APC/C co-activator. Secondly, direct binding of MCC to APC/C allows it to act as a stoichiometric inhibitor. The relative contribution of these two mechanisms to APC/C inhibition by MCC is unclear.

Adding further to this picture is the recent discovery that MCC contains a binding site for an additional molecule of Cdc20 [123]. This presents the possibility either for additional sequestration (via formation of a free MCC:Cdc20 complex), or for targeted inhibition of APC/C^{Cdc20} complexes via the additional Cdc20:MCC interaction in preference to unproductive APC/C:MCC binding. Structures of the APC/C^{Cdc20}:MCC complex reveal distinct binding sites on both APC/C and MCC for the co-activator Cdc20 ($\mathbf{Cdc20_A}$) and the inhibitory Cdc20 within MCC ($\mathbf{Cdc20_M}$) [124, 125].

An additional puzzle is that a significant fraction of the APC/C population appears to exist in an unbound form (apo-APC/C) during checkpoint arrest, and therefore is not interacting with either its Cdc20 co-activator or MCC inhibitor [126, 127]. This is surprising since the existence of an APC/C^{Cdc20}:MCC complex implies that Cdc20 should be in sufficient excess over APC/C that it can provide both the co-activator and a stoichiometric amount of inhibitor to keep all Cdc20 inhibited. That APC/C remains unbound in this case suggests either that some other factor is responsible for inactivating a fraction of the APC/C pool, or that the Cdc20 pool is limiting for APC/C^{Cdc20} complex formation. In the latter case, preferential formation and binding of MCC would be needed to ensure that sufficient inhibitor exists to bind to any APC/C^{Cdc20} complexes that do form.

1.4.4 Error Correction

Kinetochore attachment state is not the only marker that the checkpoint system must monitor in order to ensure correct chromosome segregation at anaphase. **Incorrect attachments** (e.g. attachment of kinetochores to the same spindle pole) must also be avoided. An Error Correction (EC) pathway exists to recognise and destabilise such incorrect attachments, while permitting correct (amphitelic) attachments to persist.

Aurora B regulates stability of KT:MT attachments

The process of EC involves **Tension Sensing** across the kinetochore, and the destabilisation of attachments which do not produce the tension expected from an amphitelic attachment [128]. Central to this process is **Aurora B (AurB)**, which is responsible for regulating the stability of KT:MT attachments (The Aurora kinase Ipl1 performs this function in budding yeast [129]). Loss of AurB results in stabilisation of incorrect attachments, overriding SAC arrest in cases where it is induced by incorrect attachments (for example those resulting from abnormal spindle formation in taxol or monastrol), but not where it is induced by lack of attachment (for example in nocodazole) [130, 131]. Overexpression of AurB on the other hand leads to continuous disruption of attachments [132].

Tension-dependent changes in kinetochore structure control access of AurB to its target proteins

AurB phosphorylates multiple targets within the kinetochore *in vivo*, and is implicated in multiple pathways relating to chromosome alignment and segregation [133]. The proposed mechanism for tension sensing involves the spatial separation between AurB and its substrates at the outer kinetochore. AurB-dependent phosphorylation of KMN network components is responsible for the destabilisation of KT:MT interactions, and phosphorylation at these sites is increased in the absence of tension [134]. Microtubule-induced tension produces an increase in both the inter-kinetochore distance (distance between the inner kinetochore proteins of the two sister chromatids), and the intra-kinetochore stretch (the distance between the furthest ends of the inner and outer kinetochores) [135, 133]. AurB itself is located at the inner kinetochore through its association with the Chromosome Passenger Complex (CPC) [133], and this tension-dependent change in distance is proposed to regulate its interaction with its substrates at the outer kinetochore [136].

One problem presented by the tension-sensing error correction model is that to generate tension, both kinetochores must become attached, yet attachment at a single kinetochore (monotelic attachment) will not generate tension and so should activate the error correction machinery [137]. Models have been presented to resolve this paradox,

using a time delay in activation of error correction to provide time for a second attachment to take place in the time window before the monotelic attachment is destabilised [138, 139].

The mechanistic link between EC and SAC activation is unclear

The end result of activating error correction at a kinetochore is destabilisation of the attachment, resulting in an unattached kinetochore. The extent to which attachment status and intra-kinetochore tension are each responsible for the downstream activation of the SAC has been subject to significant debate in the field [137, 140]. There are two broad models for how this process works. In one, the SAC is activated only by unattached kinetochores, in which case the role of EC in activating the SAC is to generate these unattached kinetochores. Alternatively, the SAC may be activated directly by tensionless kinetochores, regardless of their attachment status.

A further sub-question for this second model is whether lack of tension is always a pre-requisite for SAC signalling. Insight into this latter question has been provided by the discovery of the competition-driven mechanism for attachment sensing (see Section 1.4.3). This model contains no intuitive mechanistic basis for a tension requirement for SAC signalling. This hypothesis has been confirmed experimentally by generating stable KT:MT attachments in the absence of tension, in which case the SAC still gets satisfied [141, 142, 122]. This suggests that lack of tension alone is insufficient to activate the SAC in the absence of unattached kinetochores, and that the presence of unbound Kmn1 to act as a binding site for MPS1 is an essential requirement for SAC signalling.

However, this does not exclude the possibility that in the absence of stable KT:MT attachments, lack of tension can contribute to enhancing SAC signalling beyond its role in generating unattached kinetochores through EC. Furthermore, the experiments above present an extreme case where all MT binding sites on the KT are occupied by stable long-lived interactions. In a normal cell, dynamic KT:MT interactions [122] may mean that even on an apparently 'attached' kinetochore there exists sufficient turnover of free sites to support SAC signalling in response to an appropriate stimulus.

Complicating matters is the role of the **AurB** kinase in SAC signalling. As discussed above, AurB is the key effector of the tension-sensing mechanism. Yet it is also has a

direct role in the SAC independently of EC, as shown by the ability of AurB inhibition to suppress SAC signalling in nocodozole, where the absence of any KT:MT interactions eliminates any effect of EC [143, 144]. However, the mechanistic basis for this effect remains unclear [145].

1.4.5 CDK-dependence of SAC signalling

We have already discussed the general role of CDK activity in cell cycle control, and in APC/C activity regulation (Section 1.2.1). However, CDK activity also plays a crucial role in regulation of the SAC. Without CDK activity, the SAC does not become active even in the complete absence of KT:MT attachment [146].

For the purposes of this discussion we must distinguish between two different modes of SAC activity. The SAC can be *active*, in the sense of monitoring for unattached kinetochores, irrespective of whether or not any unattached kinetochores exist. However it will only be *active*, in the sense of generating MCC to inhibit APC/C, when it is both active in the first sense and is in the presence of unattached kinetochores. We refer to the SAC in the first state as **'Licensed'**, and to the SAC in the second state as **'Active'**. SAC licensing is a necessary but not sufficient condition for SAC activity, which requires further stimulus in the form of unattached kinetochores. In this context, CDK activity is essential for SAC licensing.

This CDK requirement for SAC licensing creates a positive feedback loop between Cdk1:CycB and APC/C^{Cdc20}, since Cdk1:CycB indirectly inhibits APC/C^{Cdc20} by promoting formation of its MCC inhibitor, while APC/C^{Cdc20} promotes degradation of CycB (Figure 1.10). This positive feedback loop contributes to the irreversibility of checkpoint signalling, since once the SAC has been satisfied, the activation of APC/C will lead to loss of CDK activity and revoking of the SAC license, preventing reactivation in anaphase. If this feedback loop is removed by expressing non-degradable CycB in mouse embryos, cohesin cleavage results in checkpoint reactivation, preventing further progression through mitotic exit [147].

The mechanism or mechanisms for CDK-dependence of SAC licensing is discussed in greater detail in Chapter 3.

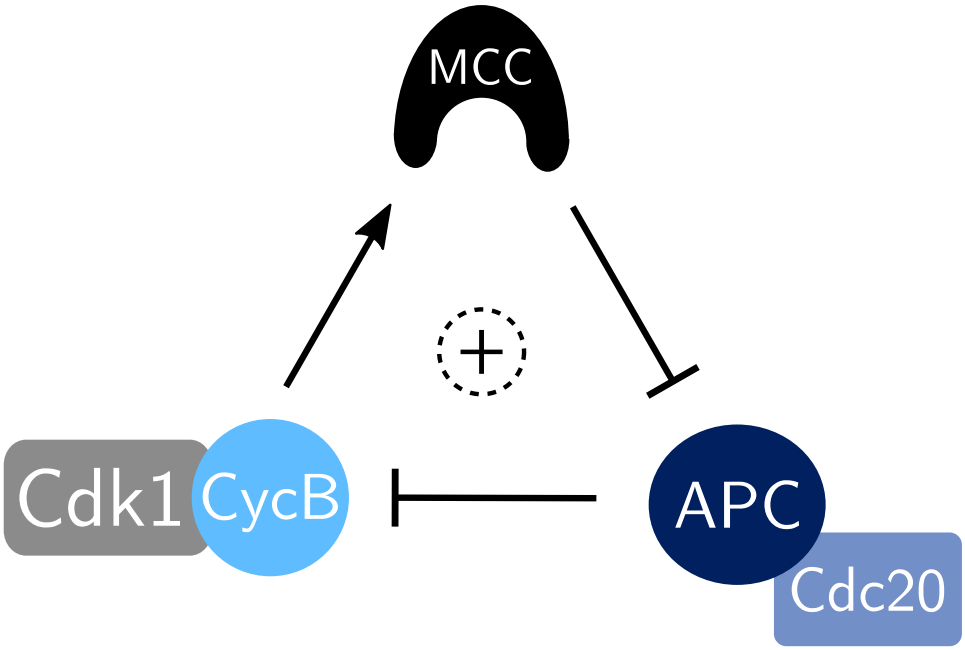

Figure 1.10: Generic SAC influence diagrams. Solid arrows: activatory interactions. Solid bars: inhibitory interactions.

1.4.6 Checkpoint Reactivation

Linked to the idea of a CDK:SAC:APC/C positive feedback loop is the concept of **Checkpoint Reactivation**. This refers to the ability of the cell to resume mitotic checkpoint signalling during late metaphase or early anaphase in response to a renewed kinetochore signal. This is not a normal state of the system, and in the absence of other experimental perturbation, formation of unattached kinetochores sufficiently late in metaphase will not delay checkpoint progression [148]. This implies that mechanisms exist to turn off the checkpoint during the M/A transition, creating an irreversible transition between the two states.

Related to this is the so-called **'Anaphase Problem'** [149, 150]. This refers to the apparent paradox that the state of chromosome attachment during anaphase is effectively identical to that in prometaphase, since following cohesin cleavage each daughter chromosome retains only a single kinetochore, and is not under tension (Figure 1.11). If the Error Correction pathway detects and destabilises tensionless kinetochores, then this loss of tension should cause destabilisation of KT:MT attachments and reactivation of the SAC, preventing progression through anaphase. In order to resolve this, some mechanism must exist to inactivate EC at anaphase.

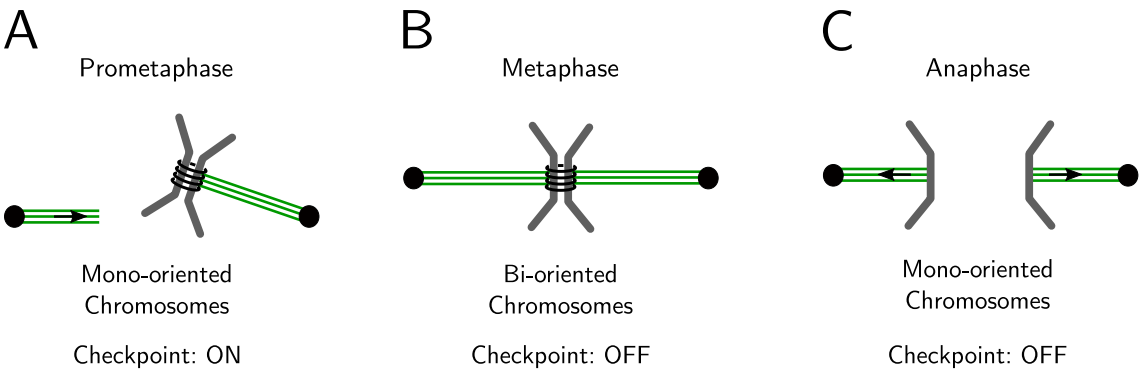

Figure 1.11: The anaphase problem. During prometaphase, the existence of mono-orientated kinetochores stimulates the mitotic checkpoint (A). Biorientation at metaphase places the kinetochore under tension and satisfies the checkpoint (B). Cohesin cleavage at anaphase causes chromosomes to separate, again becoming mono-oriented. However this does not cause reactivation of the checkpoint (C).

A variety of mechanisms may be responsible for preventing reactivation of the checkpoint during anaphase. AurB localisation is controlled by its association with the CPC, which relocalises to the central spindle at M/A via the action of the kinesin MKlp2 [151]. Depletion of MKlp2 results in retention of AurB at the kinetochore during anaphase, and recruitment of SAC components including MPS1 and BubR1 [152]. Crucially however, this does not result in a noticeable change in the rate of CycB degradation, or a delay in mitotic exit [152], suggesting that other factors must be responsible for the inability of the checkpoint to reactivate and inhibit APC/C in this case.

The CDK-dependence of SAC signalling described in the previous section provides another mechanism for checkpoint irreversibility [147]. Since CDK activity is lost at anaphase due to APC/C^{Cdc20}-dependent cyclin degradation, this should prevent further activation of the checkpoint. However, the exact point or points at which CDK activity acts are less clear. Previous modelling work suggests that a system where CDK promotes both EC (AurB) and SAC (MCC) pathways independently is most consistent with experimental results [153].

Note that the assumption that checkpoint reactivation during anaphase will have a disruptive effect on mitotic progression assumes that SAC activation can occur sufficiently quickly for degradation of APC/C^{Cdc20} substrates to be prevented. However, checkpoint reactivation in the presence of non-degradable CycB in fission yeast is relatively slow, so that despite the re-assembly of MCC, APC/C inhibition comes too late to prevent significant securin degradation [154].

1.4.7 Terminating SAC Signalling

Activation of APC/C following formation of the final KT:MT attachment requires that the inhibitory effects of the SAC can be reversed. This process has two components: firstly inactivation of SAC signalling at the kinetochore to prevent further MCC assembly, and secondly turnover of the existing pool of MCC complexes to release APC/C from inhibition.

Inactivation of kinetochore signalling depends on reversal of mitotic phosphorylation events by specific phosphatases. Several apparently independent components have been identified as contributing to disassembly of MCC complexes or sub-complexes, suggesting that multiple pathways may be responsible.

$Cdc20_M$ undergoes APC15-dependent turnover from within the APC/C^{Cdc20}:MCC complex

Cdc20 accumulates during S-phase and is highest during early mitosis, declining following the M/A transition. Loss of Cdc20 during late mitosis is at least in part due to APC/C^{Cdh1}-dependent degradation [155, 156]. A number of studies have identified Mad2 and APC/C-dependent Cdc20 turnover occurring during checkpoint arrest (and therefore prior to significant APC/C^{Cdh1} activation) [157, 158, 159, 160]. The APC/C subunit **APC15** is essential for this auto-ubiquitination reaction, but is not required for canonical APC/C^{Cdc20} or APC/C^{Cdh1} substrate degradation [127].

Previously, some disagreement existed about the role of this Cdc20 turnover for checkpoint function. One proposal was that Cdc20 degradation helps to maintain the checkpoint by limiting the pool of Cdc20 available to act as an APC/C co-activator [159, 157]. This was partly based on the observation that a non-ubiquitinatable Cdc20 mutant is able to override the SAC [157]. However, subsequent studies showed that this mutant is in fact also defective in MCC formation, which would explain this effect independently of Cdc20 degradation [160].

Alternatively, Cdc20 turnover can be explained as arising from turnover of Cdc20 within the MCC complex itself. This would act in opposition to checkpoint maintenance, but would contribute to more rapid release from checkpoint arrest following the cessation

of MCC assembly. Within this context, we can interpret the finding that MCC binds directly to the active APC/C^{Cdc20} complex [123] as supportive of a model where MCC acts as both a substrate and an inhibitor of APC/C^{Cdc20}.

Structures of the APC/C^{Cdc20}:MCC complex have backed up these biochemical results, confirming that APC/C can simultaneously bind both a co-activator Cdc20 ($Cdc20_A$) and an inhibitory Cdc20 within MCC ($Cdc20_M$) [124, 125]. Furthermore they show that there exist two distinct conformers of the APC/C^{Cdc20} complex. In the more abundant 'Closed' form, the binding site for the E2 enzyme required for the ubiquitination reaction is occluded by MCC, and the APC15 subunit is disordered. In contrast, in the less abundant 'Open' form, the APC15 is well defined and the E2 binding site is unobstructed. Deletion of APC15 results in the complex exclusively adopting the 'Closed' form. These studies confirm an important role for APC15 in APC/C-dependent degradation of the Cdc20 from within the APC/C^{Cdc20}:MCC complex, thereby providing a mechanism for APC/C to free itself from MCC-dependent inhibition [124, 125].

Active c-Mad2 is remodelled into inactive o-Mad2 via a TRIP13- and $p31^{comet}$-dependent pathway

A major pathway of significance for checkpoint silencing and a timely M/A transition is the extraction of c-Mad2 from MCC, followed by ATP-dependent remodelling of active c-Mad2 into inactive o-Mad2 [161, 162]. This process involves the AAA+ ATPase **TRIP13**, and the Mad2-binding protein **$p31^{comet}$**. $p31^{comet}$ promotes dissociation of Mad2 from MCC complexes during checkpoint arrest [163]. TRIP13 binds to a $p31^{comet}$:c-Mad2 complex, using ATP hydrolysis to drive unfolding of a region of the c-Mad2 protein, causing dissociation from $p31^{comet}$ and refolding as o-Mad2 [164, 165].

$p31^{comet}$ has also been implicated in the APC/C-dependent ubiquitination of Cdc20 [160], though it is unclear to what extent these pathways are linked. It has also been suggested that the two pathways act on APC/C-bound and free MCC respectively [33]. Recently it has been shown that $p31^{comet}$/TRIP13 can promote extraction of o-Mad2 from an APC/C^{Cdc20}:MCC complex in the absence of APC15 (required for Cdc20-ubiquitination), but that this occurs at a slower rate than extraction of o-Mad2 from free MCC [165], suggesting that the two pathways are independent, but may act

more efficiently on MCC in different contexts. Furthermore, $p31^{comet}$ associates with both MCC and APC/C^{Cdc20}, but TRIP13 does not, suggesting that $p31^{comet}$ may be necessary to extract c-Mad2 from either free or APC/C-bound MCC, before delivering it to TRIP13 for refolding [165].

MCC disassembly intermediates may retain the ability to inhibit APC/C

An important question when considering pathways of MCC disassembly is at which step in the process the MCC inhibitor ceases to function. In the simplest case, any modification or loss of MCC components would render it inactive as an APC/C inhibitor. In this scenario, any pathway acting directly on MCC itself would immediately remove its inhibitory function, and any steps further downstream would simply act to recycle SAC components. Alternatively, MCC disassembly intermediates may themselves have inhibitory properties, in which case the rate at which these are turned over by downstream pathways will influence the efficiency of checkpoint silencing.

A significant MCC disassembly intermediate is the complex formed when Mad2 is lost from MCC following extraction by $p31^{comet}$ [163]. The resulting BubR1:Bub3:Cdc20 complex is referred to as the **BBC** [163, 33]. This complex is functional as an APC/C inhibitor, and it has been proposed that Mad2 effectively plays a catalytic role in assembly of the BBC inhibitor, with no significant role for MCC itself [166]. However, the wealth of evidence for the existence of a strong and stable MCC complex and consideration of the kinetic properties of the binding reactions involved in complex formation argue against this model [33].

A related question is the extent to which ubiquitination of SAC components functions via directly inactivating them versus targeting them for proteasomal degradation. Enhanced ubiquitination of Cdc20 as a result of overexpressing an E2 ubiquitin-conjugating enzyme leads to dissociation of Mad2 and BubR1 from APC/C even in the presence of a proteasome inhibitor, suggesting that ubiquitination itself is inhibitory for SAC activity [158]. Although in most cases these two options will lead to qualitatively the same outcome, it is significant for the interpretation of experiments involving application of the proteasome inhibitor MG132, for example.

Specific phosphatases are responsible for reversing phosphorylation events required for checkpoint signalling

Just as phosphorylation events are crucial for driving the events of early mitosis, so removal of phosphorylation from these same sites is crucial to enable the cell to successfully exit mitosis and re-enter the subsequent cell cycle. In particular, we discuss here the role of the major mitotic exit phosphatases PP1 and PP2A.

PP2A:B56 PP2A:B56 is an important phosphatase opposing kinase activities involved in both the SAC and EC pathways [145]. It is the counteracting phosphatase for MPS1-dependent phosphorylation of Knl1 in the SAC pathway [121], and for AurB-dependent phosphorylations responsible for destabilisation of KT:MT interactions in the EC pathway [167].

PP2A:B56 activity is regulated via control of its kinetochore localisation. This is achieved by its binding to the KARD domain of BubR1 [168]. Phosphorylation of the KARD domain by Cdk1 and Plk1 is also required for this interaction [169]. Removal of PP2A:B56 from the kinetochore is dependent upon dephosphorylation by PP1 [170].

PP1 As discussed above, PP1 promotes removal of PP2A:B56 from the kinetochore, counteracting its stabilisation of KT:MT attachments [170]. Recruitment of PP1 to the kinetochore is itself dependent on removal of AurB-dependent phosphorylation from SILK and RVSF motifs on Knl1 [171]. Dephosphorylation of these sites is dependent on PP2A:B56, so that PP2A:B56 promotes its own removal from the kinetochore [170]. PP1 is also responsible for regulation of both PP2A:B55 and PP2A:B56 activity in a so-called 'phosphatase relay' [172].

PP2A:B55 PP2A:B55 is subject to regulation by the stoichiometric inhibitors α-Endosulfine (ENSA) and Arpp19 [174, 175] (Figure 1.12). Both are subject to similar regulation so we will refer generically to ENSA from this point onwards. Phosphorylation of ENSA by the kinase Greatwall (Gwl, also known as MASTL) converts it into its active phosphorylated form (p-ENSA), which binds to the PP2A:B55 active site [175]. p-ENSA is itself a substrate PP2A:B55, and undergoes slow dephosphorylation from the

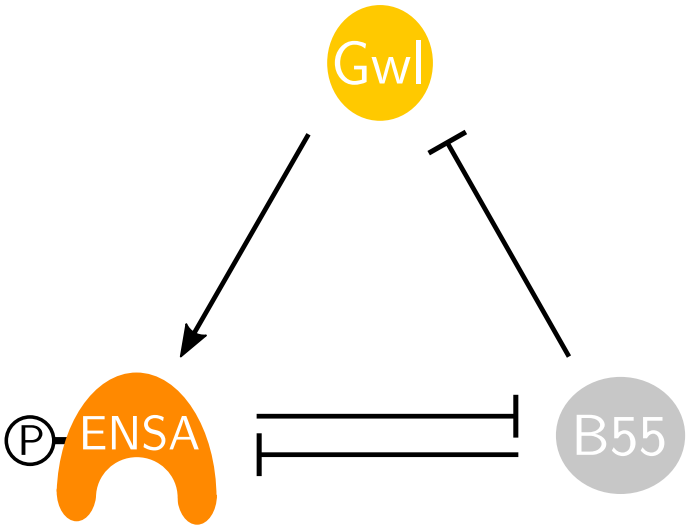

Figure 1.12: Influence diagram showing interactions between components of the B55/ENSA/Gwl (BEG) pathway [173]. See text for details.

inhibitory complex. This so-called 'unfair competition' mechanism nevertheless allows p-ENSA to function as a stoichiometric inhibitor of PP2A:B55, since its tight binding and slow turnover means that it prevents access of other substrates to the PP2A active site [176].

Gwl is itself regulated by activatory phosphorylation at multiple sites by CDK activity [177]. Removal of these phosphorylations is dependent in part on PP2A:B55 activity, resulting in a double-negative feedback loop between PP2A:B55 and Gwl, contributing to the bistability of mitotic entry and exit [178, 179]. PP1 also contributes to the initiation of Gwl dephosphorylation [180, 181, 182]. The time-delay provided by the B55/ENSA/Gwl (BEG) pathway is important for ensuring that PP2A:B55-dependent events of mitotic exit occur after chromosome segregation at anaphase [173].

1.5 Meiosis

In contrast to the mitotic cell cycle, where DNA replication strictly alternates with chromosome segregation and cell division, meiotic cells undergo two sequential divisions without an intervening round of DNA replication (Figure 1.13). In the first division (**Meiosis I**), homologous chromosomes pair up and undergo homologous recombination at chiasmata, linking together to form **Bivalents**. The subsequent anaphase results in formation of two haploid daughter cells. At the second division (**Meiosis II**), sister

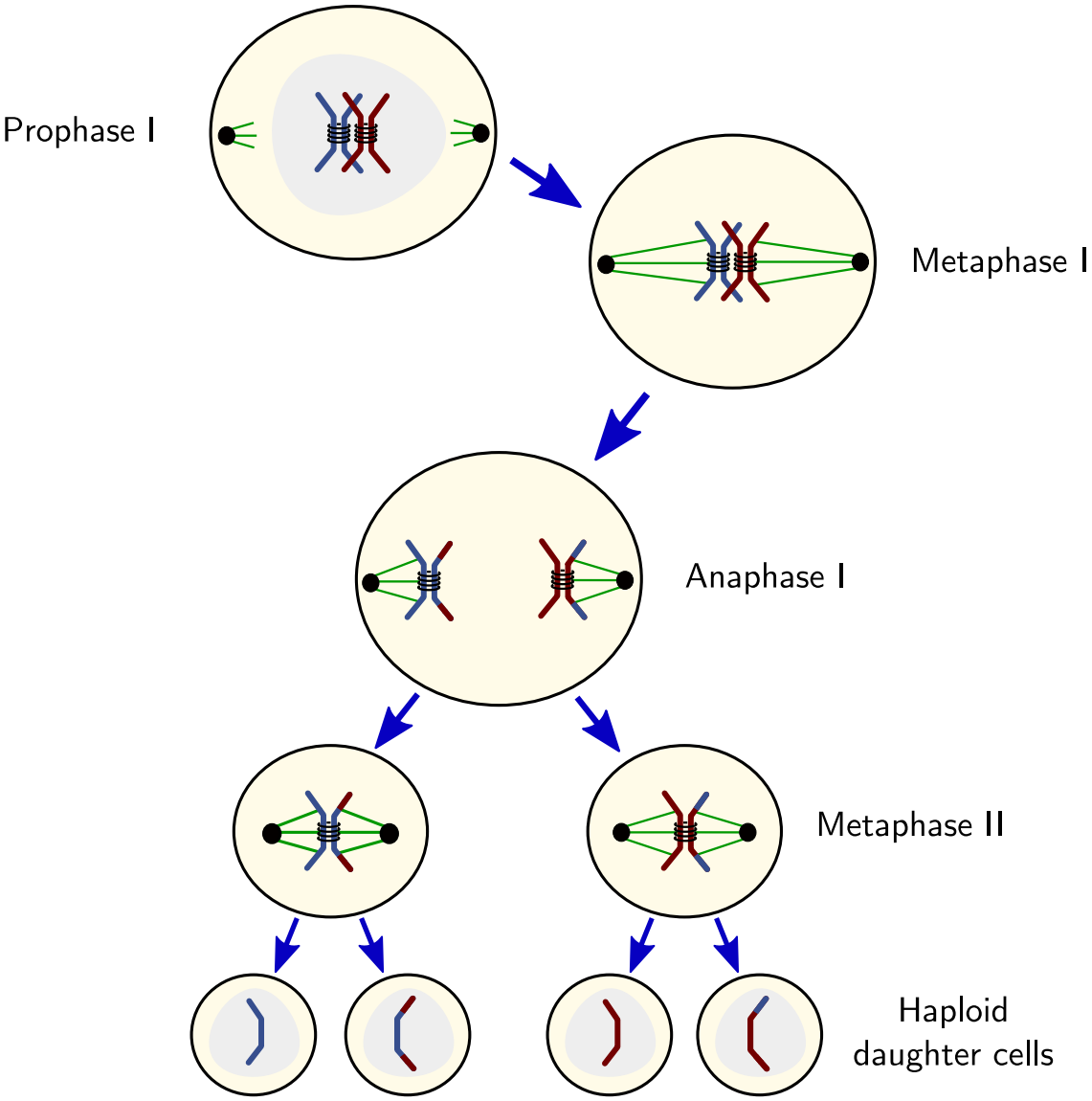

Figure 1.13: Overview of meiosis. Adapted from [1].

chromatids are segregated to generate a total of four haploid daughters [1].

Despite these differences, there exist important similarities between meiosis and the mitotic cell cycle. In particular, both use many of the same regulatory components, including APC/C and CDK:Cyclin complexes. For the most part it is the differences in regulation of these core components between mitosis and meiosis which allows the cell to achieve the required outcomes in each case.

Below, we highlight some of these important physiological and regulatory differences, which will be of relevance to modelling these meiotic processes in Chapters 4 and 5. In particular we focus on the regulation of meiosis in mammalian oocytes, since mouse oocytes are the experimental model used in each of these chapters.

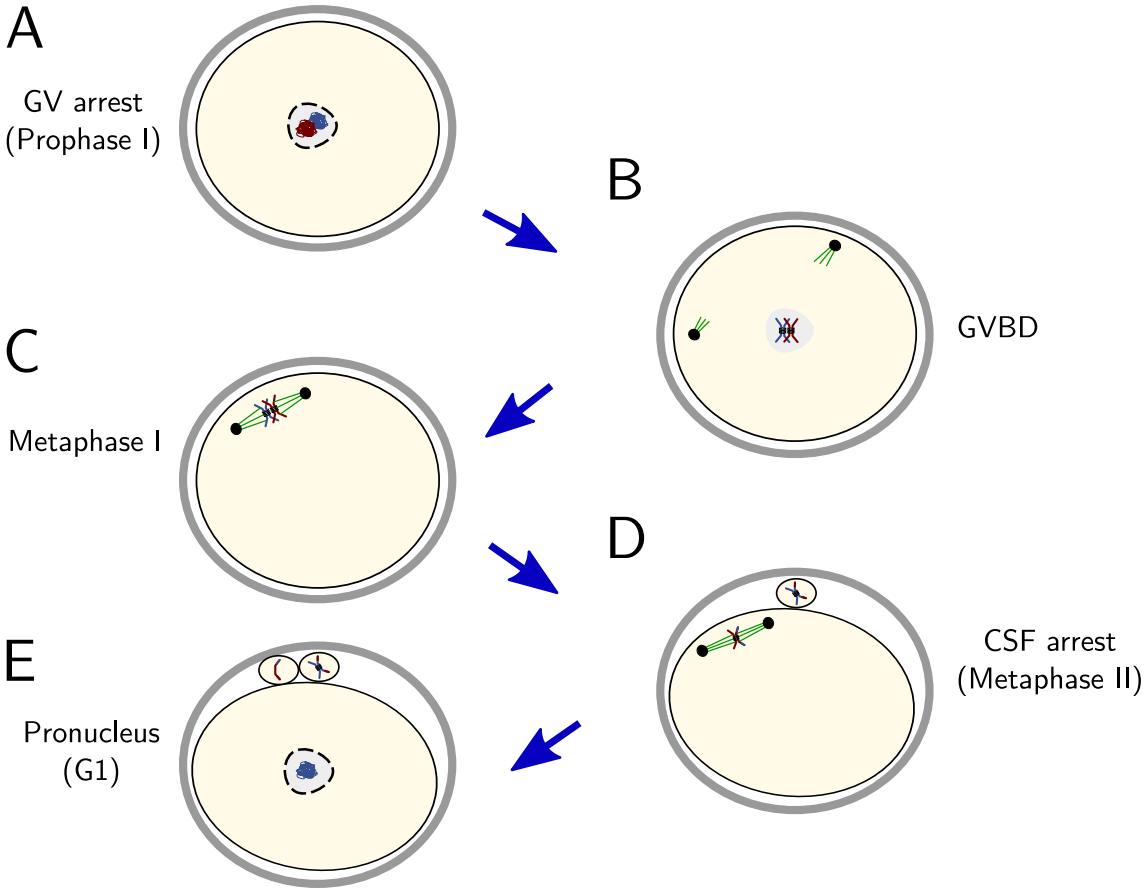

Figure 1.14: Overview of mammalian oogenesis. Figure adapted from [183] and [184].

1.5.1 GV arrest and meiotic resumption in mammalian oogenesis

In female animals, the first meiotic division comprises several different stages, the timing of which correspond to specific life events. During embryonic development, primordial follicle cells enter the cell cycle and undergo DNA replication, before reaching an arrest in prophase. This **Germinal Vesicle (GV)** arrest occurs at the diplotene stage of prophase I, after chromosomes have undergone alignment and chiasmata formation, but before chiasmata resolution and formation of the meiotic spindle (Figure 1.14A) [183, 184]. **Germinal Vesicle Breakdown (GVBD)**, also referred to as **Meiotic Resumption**, marks the release of the oocyte from GV arrest, and occurs in response to different stimuli depending on species. In mammals, meiotic resumption occurs at ovulation in response to an increase in Luteinizing Hormone (LH) [185].

Meiotic resumption requires CDK activity

Meiotic resumption is comparable to the mitotic G2/M transition, since in both cases regulation centres around the activation of Cdk1 [184]. Rising CDK activity promotes chromosome condensation and the formation of the meiotic spindle (Figure 1.14B) [186, 187]. However, the timing of spindle formation and stabilisation of KT:MT attachments is significantly delayed relative to the equivalent events in mitosis, and this delay corresponds to a slow rise in CDK activity during meiotic resumption [187, 188].

CDK activity is inhibited during GV arrest in response to cAMP/PKA signalling

GV arrest requires inhibition of CDK activity to prevent premature meiotic entry. This occurs via inhibitory phosphorylation of Cdk1 by the oocyte-specific Wee1-like kinase **Wee1B** [189]. Conversely, meiotic resumption requires removal of this inhibitory phosphorylation by the phosphatase **Cdc25B** [190]. This situation is analogous to the regulation of mitotic Cdk1 via inhibitory phosphorylation (See Section 1.2.1).

Regulation of these two reciprocally-acting processes is coordinated by the cAMP-dependent **Protein Kinase A (PKA)**, which catalyses activatory phosphorylation of Wee1B and inhibitory phosphorylation of Cdc25B [191, 192]. In the case of Wee1B, this activatory effect is direct [189], while PKA-dependent phosphorylation of Cdc25B promotes its translocation from the nucleus, preventing it from acting on Cdk1 [193, 192].

The transition from GV arrest to meiotic resumption is promoted by loss of cAMP signalling, thereby reducing PKA activity. This can occur either in response to hormonal signals acting on the follicles to promote ovulation, or through physically removing the primordial follicle cell from the surrounding follicle *in vitro* [184].

Inhibitory phosphorylation of Cdk1 is controlled by positive feedback loops

Although the initial stimulus for meiotic resumption is inactivation of PKA, further downstream effects act to reinforce this. Phosphorylation of Wee1B by Cdk1 also promotes its nuclear export [193], creating a double-negative feedback loop. In *Xenopus* oocytes, which do not contain Cdc25B, its homologue Cdc25C is activated by Cdk-dependent phosphorylation [194, 195]. This reciprocal regulation of Wee1 and Cdc25 is a conserved design motif across different species and cell cycle stages [19] (see also Section

1.2.1), although conclusive evidence of activatory phosphorylation of Cdc25B by Cdk1 in mammalian oocytes is currently lacking.

APC/C^{Cdh1} promotes CycB degradation during GV arrest

Inhibitory phosphorylation of Cdk1 is not the only factor controlling meiotic resumption in mouse oocytes. The availability of CycB will also determine the overall level of CDK activity. Degradation of CycB during GV arrest has been shown to depend on APC/C^{Cdh1} [196]. This is unusual relative to a mitotic cell cycle, where APC/C^{Cdh1} becomes active at mitotic exit and is inactivated at the G1/S transition. Loss of Cdh1 increases the rate of meiotic resumption in a CycB-dependent manner [197]. The significance of the interplay between Cdk1 phosphorylation and Cdh1-dependent regulation of CycB levels on overall CDK activity is discussed in detail in Chapter 4.

1.5.2 CSF Arrest and Meiosis II

Following GVBD, primary oocytes align bivalents on the spindle in metaphase I (Figure 1.14C), and undergo the first meiotic division to produce a large secondary oocyte, and a small polar body (Figure 1.14D). As mentioned above, the first meiotic division occurs at ovulation in mammals. However, the second meiotic division to produce the final mature ovum, along with a second polar body (Figure 1.14E) only occurs at the time of fertilisation, in response to Ca^{2+} signalling associated with the fertilisation event [183].

Prior to fertilisation, the secondary oocyte remains in metaphase II, in a state termed **'Cytostatic Factor' (CSF) Arrest** (Figure 1.14D) [183]. CSF arrest is a dynamic steady state characterised by high Cdk1:CycB and low but non-negligible APC/C^{Cdc20} activity, resulting in significant CycB turnover [198]. Under these conditions, APC/C activity is kept low by the action of its stoichiometric inhibitor **Emi2** [199, 200]. The steady state is maintained by a negative feedback loop in which Cdk1:CycB phosphorylates Emi2, reducing its binding to APC/C [201]. Counteracting dephosphorylation of Emi2 is via PP2A:B56 activity [201, 202]. PP2A:B56 can also bind to separase or separase:securin complexes, but not to separase:CycB complexes [203].

Release from CSF arrest occurs when an influx of Ca^{2+} associated with fertilisation promotes a calmodulin-dependent kinase cascade, resulting in phosphorylation and SCF-

dependent degradation of Emi2 [204]. This allows APC/C to become active and promote separase activation and cyclin destruction, leading to anaphase II and completion of the second meiotic division (Figure 1.14E).

1.5.3 Regulation of chromosome segregation

Just as in mitosis, correct alignment and segregation of chromosomes into daughter cells is an essential function of the two meiotic divisions. However, the first meiotic division presents a unique challenge of correctly aligning and segregating paired homologous chromosomes, while retaining cohesion between sister chromatids within each chromosome. Some of the ways in which chromosome segregation and checkpoint surveillance are adapted to this novel situation are explored in Chapters 4 and 5.

Sgol2 protects centromeric cohesin from cleavage during meiosis I

Retaining cohesion between sister chromatids into meiosis II requires that centromeric cohesin remains protected during meiosis I. This occurs via the activity of **Shugoshin-like Protein 2 (Sgol2)**, which binds to the centromere and recruits PP2A. Resulting dephosphorylation of the adjacent cohesin prevents it from being targeted for degradation by separase [205, 206]. Loss of centromeric cohesin from oocytes in aging mice is associated with loss of Sgol2 from chromosome arms [207].

The SAC response in meiosis I

SAC activity in meiosis I is thought to be less robust than in mitosis [208, 209]. The frequency of aneuploidy during meiosis is high [210], and lack of robust checkpoint controls are thought to be in part responsible for this [208]. Some animals, for example *Xenopus*, are unable to mount any checkpoint response [211], however a checkpoint response is observed in mouse oocytes [212], and is essential for correct chromosome segregation in meiosis I [213]. Nevertheless, the checkpoint remains highly error-prone, and SAC activation does not appear to respond robustly to incorrect attachment status [214, 215, 216]. Furthermore, attachment of bivalents to the spindle does not result in inter-kinetochore stretch, since KT:MT attachments from each homologue should all originate from the same spindle pole (mono-orientation), limiting the potential for

tension-dependent error correction pathways to act [217]. The question therefore remains as to how an essential role for the SAC in chromosome segregation can be reconciled with its apparent insensitivity to defects.

1.6 Mathematical Modelling

Mathematical modelling provides a framework with which to analyse the emergent behaviour of biochemical reaction networks. In this thesis, several modelling techniques are used to simulate and analyse the behaviour of systems of interest. We address a number of distinct but related biological systems in collaboration with different experimental groups, and use modelling to aid understanding and to make predictions to inform future experimental work. In general, we have favoured an approach of developing smaller, more specific models corresponding to the pertinent points of a particular experimental system, rather than developing a single over-arching model which could be applied to all systems. This has the advantage of producing a model more closely tailored to the specific experimental system of interest, and prevents potential over-fitting and redundancy associated with a large model containing all known interacting species. However, it also has limitations in potentially reducing the applicability of the findings from one particular model to a wider picture of cell cycle regulation.

Below, we give a general overview of the various modelling techniques used, but do not go into details of specific models beyond a simple example system. The details of the different models presented in the thesis will be discussed in the relevant chapters, and copies of each model and parameter values are included in Appendix A. Further evaluation of the modelling approaches chosen is presented in the discussion (Section 6.3).

1.6.1 Ordinary Differential Equations (ODEs)

The main technique used in this thesis is **Ordinary Differential Equation (ODE)** modelling. As the name suggests, an ODE model comprises a series of differential equations describing the rate of change of system components with respect to time. When combined with a set of **Parameters** and **Initial Conditions**, an ODE solver can

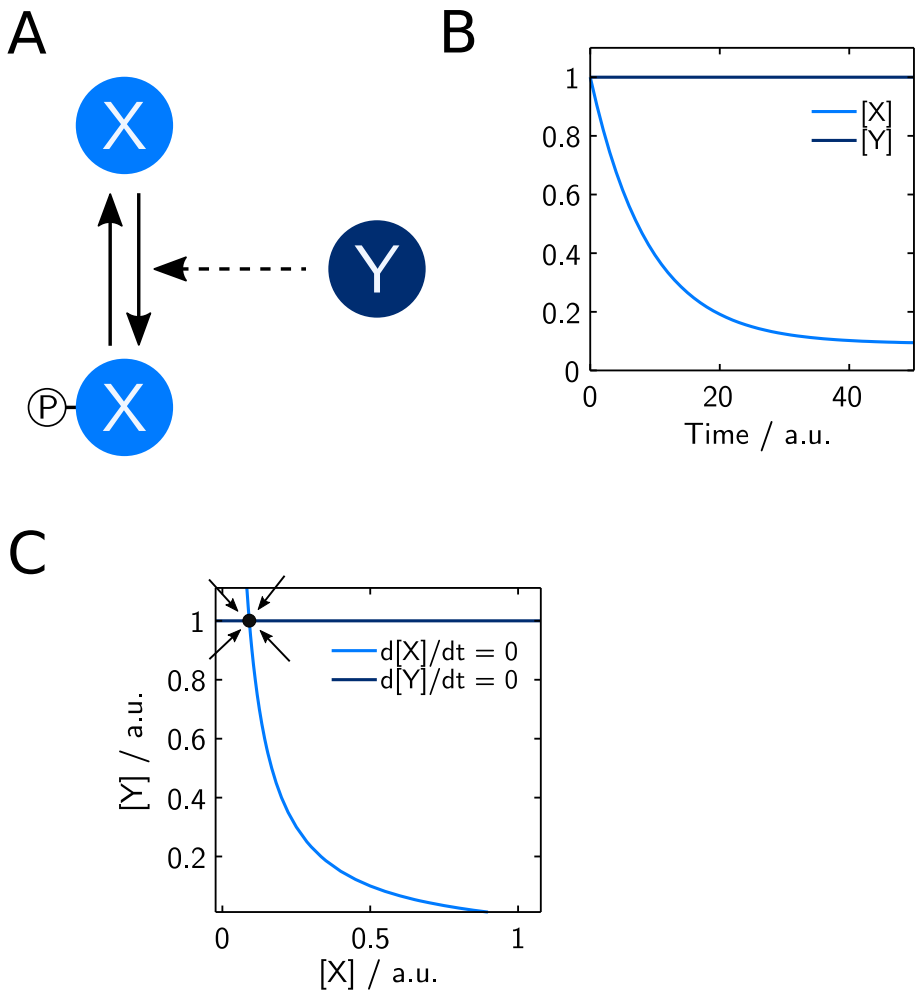

Figure 1.15: Wiring diagram (A), Timecourse simulation (B) and Phaseplane diagram (C) for example kinase-substrate reaction network.

then be used to generate a simulated timecourse showing how the state of the system evolves with time.

Defining a Series of ODEs

The starting point for an ODE model of a biochemical reaction network is a **Wiring Diagram** showing the relationships between all the species of interest in the network. A simple example of such a network wiring diagram is shown in Figure 1.15A, depicting a simple kinase-substrate reaction between a kinase Y, and its substrate X. From this diagram, we can then define variables $[\mathrm{X}]$, $[\mathrm{Y}]$ and $[\mathrm{pX}]$ corresponding to the activities of the species in the reaction network.

We can then define ODEs describing the rate of change of each component by considering the rate of each of the individual reactions it is involved in. For X, these are:

- Phosphorylation to form pX (catalysed by Y).
- Regeneration of X by dephosphorylation of pX (intrinsic).

For now, we will assume that phosphorylation and dephosphorylation of X occur via **Mass Action Kinetics**, i.e. that the rate is proportional to the concentration of the species involved in the reaction. This gives the following ODE:

$$\frac{d[\mathrm{X}]}{dt} = k_{dephos} \cdot [\mathrm{pX}] - k_{phos} \cdot [\mathrm{Y}] \cdot [\mathrm{X}] \tag{1.1}$$

Here $k_{phos} \cdot [\mathrm{Y}] \cdot [\mathrm{X}]$ is the rate of the phosphorylation reaction, and $k_{dephos} \cdot [\mathrm{pX}]$ is the rate of the dephosphorylation reaction.

For Y, in this simple example its concentration does not change during any reaction, so this is given simply by:

$$\frac{d[\mathrm{Y}]}{dt} = 0 \tag{1.2}$$

Since we already have an equation for $[\mathrm{X}]$, we do not require a separate ODE for $[\mathrm{pX}]$, since we also know from the wiring diagram that the total concentration of $[\mathrm{X}]$ and $[\mathrm{pX}]$ is constant (for convenience we denote this total value X_T). We can therefore use this relationship to define an **Algebraic Conservation Equation** for $[\mathrm{pX}]$.

$$[\mathrm{pX}] = X_T - [\mathrm{X}] \tag{1.3}$$

Parameter Selection

Given a series of ODEs and associated algebraic conservation equations, we must select appropriate parameters and initial conditions to use for the simulation. Depending on the particular experimental system we are studying, more or less information will be available to inform parameter and initial condition selection. Where specific values are known from literature data these can be used, but this is the minority of cases. More likely, literature data can be used to provide an indication of the relative magnitude of different parameter values, for example based on relative rates of measured reactions. Upper and lower limits can also be placed on parameter values based on typical ranges

of values for enzymatic reactions. Where available, suitable experimental data can also be used to fit the model. ODE models typically have a large number of parameters, and hence many degrees of freedom for model fitting, so that this approach alone is unlikely to produce an accurate representation of the true parameter values *in vivo*. However, by using data from multiple sources and different experimental conditions, additional constraints can be placed on the model, helping to refine the likely region of parameter space in which the system operates.

Simulation and Data Analysis

Defining a series of ODEs and assigning parameter values and initial conditions allows a simulation to be run showing how the state of the system changes over time. An example timecourse simulation of the model system laid out above is shown in Figure 1.15B. For numerical simulation of ODEs, we use the free ODE solver **XPPAUT**, (available from `http://www.math.pitt.edu/~bard/xpp/xpp.html`) [218]. XPPAUT '.ode' files for each of the models in this thesis are included in Appendix A. For more complex simulation variants (for example simulations where parameter values change mid-simulation), MATLAB [219] code was used to edit .ode model variants and run the XPPAUT solver from the command line. Simulation results were also imported into MATLAB for data analysis and plotting.

Population-level simulations

An ODE simulation is purely deterministic, so will always produce the same results for a given set of parameters and initial conditions. This approach is therefore not suitable to accurately reproduce experimental data which record the diversity of responses of a cell population to a given set of conditions.

We would expect that natural variation would exist within any cell population, which is absent from the deterministic ODE model. Reproducing these population-level effects therefore requires a simulation which can incorporate a suitable form of variation alongside the core deterministic mechanism. A purely stochastic simulation would be one way to achieve this, but would be computationally demanding for the number of variables and complexes considered in some models. In addition this would capture only

the intrinsic noise in the system (i.e. that caused by stochastic processes resulting from the low number of molecules present in each cell). It would not describe adequately extrinsic noise, caused by genuine heterogeneity within the cell population.

Therefore we instead favour an approach which approximates this variation by performing multiple deterministic simulations with parameter values or initial conditions selected from a suitable random distribution. These distributions can be centred on a mean of the 'true' value from the original deterministic simulation.

1.6.2 Phaseplane Diagrams

Timecourse simulations are useful for checking that proposed models are consistent with experimental data, as well as to make testable predictions about the behaviour of the system under novel conditions. However, they do not allow us to make a general statement about the overall behaviour of the system across a range of conditions. **Phaseplane Analysis** provides a tool with which to analyse the steady states or oscillations of a system, and the trajectories taken by the system through the phase space. This enables a more generalised understanding of the behaviour of a system under a wide range of conditions, which can then be related to specific physiological states.

By a phaseplane, we refer to a representation of possible states of the system on a two-dimensional set of axes. Onto these axes are plotted two curves (**Nullclines**), which show the points at which the rate of change of each of the axis variables is equal to 0 (i.e. the curves $\frac{d[\mathrm{X}]}{dt} = 0$ and $\frac{d[\mathrm{Y}]}{dt} = 0$). The phaseplane for the example system described above is shown in Figure 1.15C.

Where the nullclines intersect, the rate of change of both variables is 0, and so the system can be described as being in a steady state. These steady states can be **Stable** or **Unstable**, depending on whether an infinitesimal perturbation will result in the system returning to or diverging from the steady state. The stability of a given steady state can be computed formally by analysis of an eigenvector matrix, but for our purposes it is sufficient to observe by inspection the trajectories in the vicinity of each steady state. The rate of change of each variable will be positive on one side of the nullcline and negative on the other. These rates of change are indicated on the nullclines

by arrows and the resulting stable or unstable steady states indicated by filled or open circles respectively. In Figure 1.15C, the lines intersect in only one place, so the system has a single stable steady state.

Note that to generate a phaseplane diagram, the system must comprise precisely two ODEs, corresponding to the phaseplane axis variables. If the original system contains more than two variables, then the system must be reduced by converting ODEs for additional variables into algebraic equations expressed in terms of the chosen axis variables. This is achieved by making a steady state assumption about these variables: at steady state the rate of change is 0, so the ODE can be rearranged to express the variable in terms of the phaseplane axis variables.

1.6.3 Bifurcation Analysis

The other tool used for analysis of system behaviour in this thesis is the **Bifurcation Diagram**. Like a phaseplane diagram, the bifurcation diagram is used to summarise system behaviour across a range of conditions. As previously discussed in Section 1.3.4, it plots the steady state values of a system variable as a function of a system parameter (the bifurcation parameter). As the bifurcation parameter is increased, not only will the value of the steady state change, but also the number of steady states in existence. At a **Saddle-node Bifurcation Point**, an initial monostable state can split into a pair of stable states separated by an unstable state, and vice versa. These bifurcations give rise to characteristic S- and Z-shaped bifurcation curves.

In addition, **Two-parameter bifurcation diagrams** are used to show how the size of the bistable region produced by varying the first bifurcation parameter changes with a second bifurcation parameter. This can be useful to probe the effects of specific model parameters on the bistability of the system as a whole.

The **AUTO** function of **XPPAUT** was used for generating all bifurcation diagrams. The resulting data were then imported into Matlab for plotting.

Chapter 2

The FADS motif: a network motif providing bistability at multiple cell cycle transitions

2.1 Introduction

The bistability of cell cycle transitions is a central paradigm in the field. Bistability ensures that progression from one cell cycle stage to the next is an irreversible event. Mathematical modelling has been used with success to demonstrate how simple molecular interaction networks can give rise to bistable behaviour, however these can require complex assumptions about the reaction kinetics in order to generate the necessary mathematical relations between components to create a bistable system. In this chapter, we present a simple network motif, the **Feedback-Amplified Domineering Substrate (FADS)**, which we suggest represents a minimal set of components and kinetic complexity necessary to generate bistability. We show that this network motif is present in at least three distinct cell cycle transitions, analyse the features of this motif which are necessary for a bistable transition to arise, and speculate about the role of a simple motif such as this in the evolution of a bistable cell cycle transition. The work in this chapter formed the basis for a first-author paper published in Molecular Biology of the Cell in September 2017 [220].

2.1.1 Requirements for generating bistability

Before introducing the FADS network motif, it is necessary to return to the requirements for bistability discussed in Section 1.3.4 and provide a more robust description. As mentioned previously, while positive feedback is essential for bistability, it is not sufficient, with the additional requirement for an ultrasensitive signal-response curve. We can

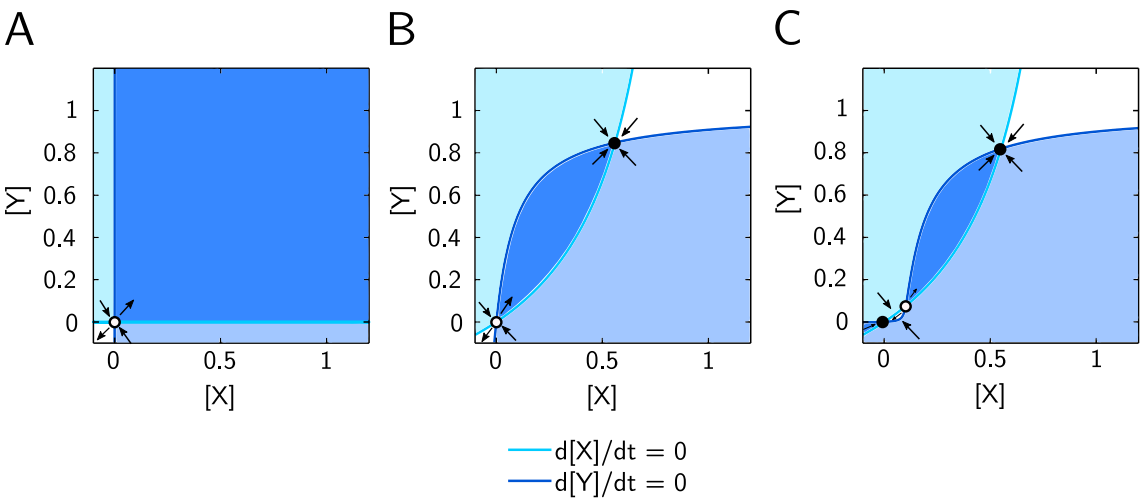

Figure 2.1: Phaseplane diagrams for a simple two-component positive feedback system, showing the impact of three different kinetic schemes on the steady state outcomes. Nullclines are plotted showing the points at which $\frac{d[\mathrm{X}]}{dt} = 0$ (light blue) and $\frac{d[\mathrm{Y}]}{dt} = 0$ (dark blue). Shading indicates the regions of the phaseplane where the corresponding variable is increasing (light blue: [X] increasing; dark blue: [Y] increasing; intersection (darkest blue): both increasing). Arrows show the overall direction of movement in each region. (A) Simple positive feedback with no upper limit on component activity. (B) Positive feedback with upper limit on [X] and [Y] activity, and constitutive background inactivation. (C) Positive feedback as in (B) with non-linear kinetics.

demonstrate this by considering a simple positive feedback system (e.g. Figure 1.6C), with two mutually activating components X and Y. Phaseplane analysis can be used to show how the behaviour of this system is dependent not only on overall network structure, but also the kinetics of the individual reactions in the network.

To plot a phaseplane, the equations of the nullclines are required. In the simplest case, we consider a simple linear system. Since the rate of change of both $[\mathrm{X}]$ and $[\mathrm{Y}]$ is linearly dependent on the other variable, we can describe the system as follows:

$$\frac{d[\mathrm{X}]}{dt} = k_1 \cdot [\mathrm{Y}] \tag{2.1}$$

$$\frac{d[\mathrm{Y}]}{dt} = k_2 \cdot [\mathrm{X}] \tag{2.2}$$

The nullclines $\frac{d[\mathrm{X}]}{dt} = 0$ and $\frac{d[\mathrm{Y}]}{dt} = 0$ are therefore the lines:

$$[\mathrm{Y}] = 0 \tag{2.3}$$

$$[\mathrm{X}] = 0 \tag{2.4}$$

These lines intersect in a single steady state at the origin (Figure 2.1A). This state is

unstable, since moving away from this point the system enters a region of phase space where both $[\mathrm{X}]$ and $[\mathrm{Y}]$ are increasing away from the origin (indicated by blue shading).

A more biologically meaningful way of modelling a system with simple positive feedback is to consider the activation and inactivation of each component via reversible post-translational modifications. These could represent commonly used biological modifications such as phosphorylation or ubiquitination. In some cases, modification can activate the substrate, while in others it can be inhibitory. By using post-translational modification as the mechanism for activity change, the maximum activity of each component is limited by the combined concentration of both modified and unmodified forms. Once the component is entirely in the modified or unmodified form, no further increase in its activity is possible, so the system will no longer tend towards infinity.

To model this in a 'toy' system, we assume that $X_T = 1$ and $Y_T = 1$ are the total amounts of the two mutually activating enzymes. X and Y each promote conversion of the other from its inactive to its active form. Conversion of active X or Y back to the inactive form is modelled as a first order process. We can describe this system with the following ODEs:

$$\frac{d[\mathrm{X}]}{dt} = ka_X \cdot (X_T - [\mathrm{X}]) \cdot [Y] - ki_X \cdot [\mathrm{X}] \tag{2.5}$$

$$\frac{d[\mathrm{Y}]}{dt} = ka_Y \cdot (Y_T - [\mathrm{Y}]) \cdot [X] - ki_Y \cdot [\mathrm{Y}] \tag{2.6}$$

Setting $\frac{d[\mathrm{X}]}{dt} = 0$ and $\frac{d[\mathrm{Y}]}{dt} = 0$ gives the following nullclines:

$$X = \frac{ka_X \cdot X_T \cdot [\mathrm{Y}]}{ka_X \cdot [\mathrm{Y}] + ki_X} \tag{2.7}$$

$$Y = \frac{ka_Y \cdot Y_T \cdot [\mathrm{X}]}{ka_Y \cdot [\mathrm{X}] + ki_Y} \tag{2.8}$$

These nullclines are plotted in Figure 2.1B. Now, rather than a straight line tending to infinity, the nullclines are hyperbolas tending to maxima at $[\mathrm{X}] = X_T$ and $[\mathrm{Y}] = Y_T$. These maxima represent the limiting case where all of X or Y has been converted to the active form. The resulting curves now intersect in two places, indicating that the

system has two possible steady states. As before, one of these states is at the point $([\mathrm{X}] = 0, [\mathrm{Y}] = 0)$, and is again unstable, since any infinitesimal increase in either X or Y will lead to activation of the other, and move the system into a region where both variables are increasing. The second intersection point is a stable steady state, occurring at a point where both X and Y are active, but further activation is limited by the decreasing pool of inactive X and Y available for further modification. The exact point at which this occurs will depend upon the parameters selected. The phaseplane shows that for any positive starting condition, the system will move towards this single stable steady state, so positive feedback alone is insufficient to generate a bistable system.

Bistability requires that the nullclines of the system intersect at three different intersection points (Figure 2.1C). This creates two stable steady states, separated by an unstable steady state. Achieving three intersection points requires that at least one of the nullclines is sigmoidal. The practical interpretation of such a sigmoidal curve is that the rate of change of $[\mathrm{X}]$ is most sensitive to changes in $[\mathrm{Y}]$ over a limited range, outside of which changes in $[\mathrm{Y}]$ have little effect. We refer to this property as ultrasensitivity. A combination of a positive feedback loop and an ultrasensitive signal-response curve is sufficient to generate a bistable system.

2.1.2 Sources of Ultrasensitivity

In the 'toy' model used to generate Figure 2.1C, non-linearity was introduced using a function where the rate constant for Y inactivation is inversely proportional to the concentration of Y:

$$ki_Y^{app} = \frac{ki_Y}{J_Y + [\mathrm{Y}]} \tag{2.9}$$

However, this is just an empirical function which produces a suitably non-linear curve. In reality, any non-linearity must arise as a direct consequence of the underlying biochemical reactions. Generating an ultrasensitive (sigmoidal) signal-response curve is therefore an important function of many biological systems. Multiple mechanisms have been identified by which simple biochemical interactions can give rise to a sigmoidal curve, and these have been recently reviewed [221]. We will explore a few of these mechanisms in

more detail below, however this does not represent an exhaustive list, as many reaction schemes of sufficient complexity have the capacity to produce a non-linear response.

Cooperativity

One mechanism for generating ultrasensitivity is to have multiple ligand binding sites on a target enzyme, where the ligand occupancy at one binding site influences the binding affinity at other sites. The classical example is the sigmoidal oxygen saturation curve for haemoglobin, which allows for near-complete saturation of haemoglobin in the lungs, followed by near-complete release to the tissues. In this case, cooperative binding of O_2 by the four sites of the haemoglobin tetramer results in an ultrasensitive binding curve.

Two competing models were proposed to account for the observed cooperativity in the haemoglobin:O_2 binding curve. The MWC model [222] proposes a symmetrical model in which haemoglobin can adopt either a high-affinity or low-affinity conformation, and where the transition between the low- and high-affinity states is enhanced by ligand binding. The KNF model [223] proposes an asymmetric, sequential model for ligand binding, where binding to each site influences the rate of ligand binding to the next site.

Multiple Modification

In a conceptually similar mechanism, multiple sequential modification sites on the same target can provide a source of ultrasensitivity. In the simplest case, independent (distributive) phosphorylation events occurring at multiple identical sites in the same target creates a non-linear dependence of the fraction of the target in the fully modified state on the concentration of the modifying enzyme. This occurs because full modification in a distributive reaction scheme requires multiple independent binding events, so is proportional to $[\mathrm{X}]^n$, where $[\mathrm{X}]$ is the enzyme concentration and n the number of modification sites. However, this mechanism only provides limited non-linearity for low values of n. In particular, while it is largely effective at preventing activation below a threshold value of $[\mathrm{X}]$, the curve does not undergo rapid switch-like activation above this point, instead increasing as a hyperbolic function of $[\mathrm{X}]$ [224].

In contrast, if the rate of reaction at one site is increased by prior modification at another site, this provides an amplification mechanism where as soon as a signal rises

sufficiently to promote modification at one site, this will then increase its ability to modify other sites, generating a more effective switch-like response curve [221]. This could happen for example where an initial phosphorylation site creates a docking site for a kinase to bind and catalyse modification at subsequent sites.

This mechanism has been modelled as part of the Substrate-Inhibitor-Multiply-Modified (SIMM) mechanism for describing the interaction between Sic1 and Cdk1 at the G1/S transition in budding yeast [225].

Positive feedback

Although positive feedback is required in addition to ultrasensitivity to generate a bistable system, positive feedback itself can produce ultrasensitivity [221]. For example, if a kinase which undergoes activatory auto-phosphorylation *in trans* is opposed by a decreasing level of counteracting phosphatase, then at a critical phosphatase threshold the system will rapidly transition from a mostly inactive to mostly active state, creating an ultrasensitive response curve. Coupling multiple positive feedback loops can therefore be sufficient to produce bistability.

Saturating Substrate kinetics

Goldbeter-Koshland kinetics [226] can generate ultrasensitivity in the case of a reversible post-translational modification where both the forward and reverse reactions are catalysed by enzymes operating in a saturating regime of substrate concentration. Since the enzymes are operating at saturation, the steady state level of the modified substrate depends almost entirely on the ratio of the V_{max} values of the two enzymes. The result is to amplify the differences in the relative rates of reaction, so that the substrate will tend to exist almost entirely in the modified or unmodified form, depending on which reaction is faster. Small changes to the V_{max} ratio in the critical range where the V_{max} for forward and reverse reactions are approximately equal can therefore lead to a large change in the proportion of substrate existing in the modified form.

Inhibitor Ultrasensitivity

Tight binding of a stoichiometric inhibitor to an enzyme catalysing reversible modification of a substrate can give rise to ultrasensitivity [227]. This is the basis of the ultrasensitivity

in the FADS motif proposed in this chapter, and will be described in more detail in Section 2.2.1.

Limitations of Ultrasensitivity mechanisms

While all of these mechanisms are valid and biologically meaningful ways to generate ultrasensitivity, they place important constraints on the kinetic properties of the underlying reactions. For example, multi-site cooperativity requires a multimeric enzyme, and a typically non-trivial mechanism to link the binding properties of distant binding sites in a productive manner. Multi-site phosphorylation requires the existence of multiple phosphorylation sites on the target protein, but to generate a true switch-like response a mechanism by which phosphorylation at one site can affect a downstream target is also needed. In each of these cases, a highly cooperative response is dependent on both the number of related binding or modification sites, and on the strength of the cooperative effect felt between sites.

While ultrasensitive responses can and do arise from cooperative mechanisms such as these, it is not necessarily appropriate to assume that just because a protein has multiple subunits or modification sites, that it will automatically produce a strongly switch-like signal-response curve.

Similarly, Goldbeter-Koshland kinetics requires that both the forward and reverse reactions are saturated by substrate over a wide concentration range. This assumption could be easily made for enzymatic catalysis of a small metabolite, present in concentrations orders of magnitude higher than the catalysing enzymes, but is less clearly the case when both the enzyme and the substrate are components of a protein interaction network. Similarly, previous work has shown that incorrectly applying assumptions of Michaelis-Menten enzyme kinetics to both reactions of a two-component positive feedback loop can cause loss of bistability [228].

These limitations reduce the confidence with which these mechanisms can be postulated *a priori* to describe the operation of cell cycle transitions. From a modelling perspective, identification of positive feedbacks in a regulatory network can produce the expectation that bistability should follow. Ultrasensitivity is necessary to produce this, but validating whether a particular mechanism for producing ultrasensitivity can apply

in a specific case may not always be possible with the available experimental data. Under these constraints, methods for producing ultrasensitivity with limited and reasonable assumptions about the required kinetic properties of the system are to be preferred. Furthermore, the more widely applicable the assumptions, the more likely it is that such a system could evolve from pre-existing cellular components in response to a specific demand.

2.2 Feedback-Amplified Domineering Substrate (FADS) motif

Having established the conditions necessary for generating a bistable switch, we now identify a biological network motif which fulfils these conditions. We suggest that stoichiometric inhibitor ultrasensitivity represents a simple and effective mechanism for producing ultrasensitivity with a limited set of components and kinetic assumptions, and that a straightforward extension of this basic mechanism can generate a bistable switch. We describe this network as a Feedback-Amplified Domineering Substrate or FADS motif, for reasons which are outlined in the description below.

We first describe a generic case of this motif and analyse how the properties of the network structure allow it to perform its biological function. We then describe in molecular detail how this motif operates at three distinct cell cycle transitions.

2.2.1 Binding of a stoichiometric inhibitor to a cell cycle activator creates an ultrasensitive cell cycle transition

We start with a simple network (Figure 2.2A) in which a cell cycle activator (A) catalyses post-translational modification (M) of multiple substrates (S), and thereby initiates a cell cycle transition (CCT). For simplicity, we describe this component generically as an activator with respect to the CCT, regardless of whether its effects on individual substrates is positive or negative. Counteracting de-modification is performed by a regenerating enzyme (R). Prior to the transition, the activator is kept inactive by tight binding of a stoichiometric inhibitor (I). This network creates an ultrasensitive response of substrate modification with respect to inhibitor level (Figure 2.3C). This ultrasensitivity

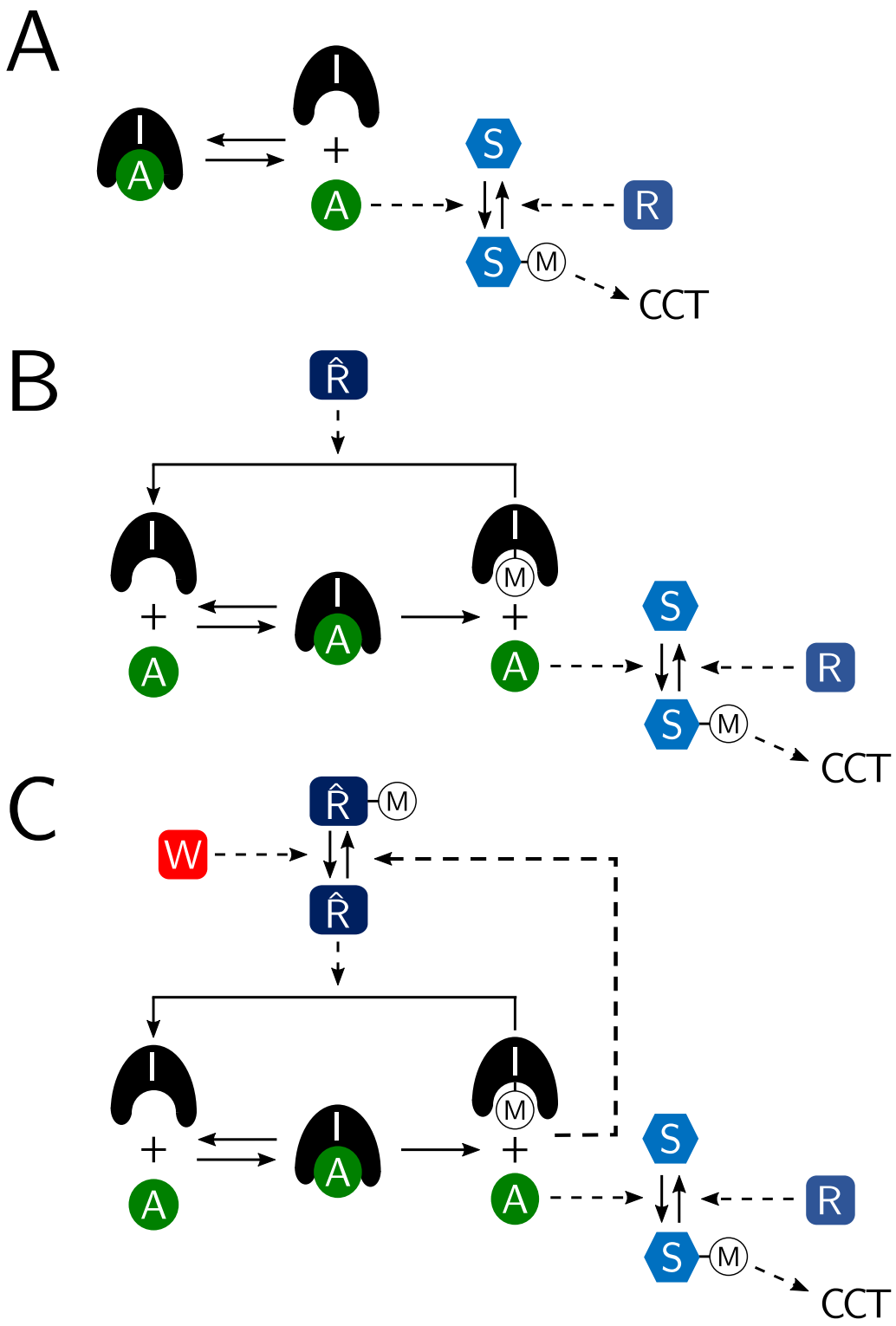

Figure 2.2: Wiring diagrams showing the development of the FADS network motif. Solid arrows indicate biochemical reactions, dashed arrows indicate rate enhancement of the targeted reaction. (A) Simple stoichiometric inhibition between an inhibitor (I) and activator (A) blocks modification of other substrates (S), thus preventing a cell cycle transition (CCT). (B) Modification of the inhibitor by the activator means it acts as a Domineering Substrate. A regenerating enzyme ($\hat{R}$) regenerates unmodified inhibitor. (C) Feedback from the activator onto the regenerating enzyme completes the Feedback-amplified Domineering Substrate motif.

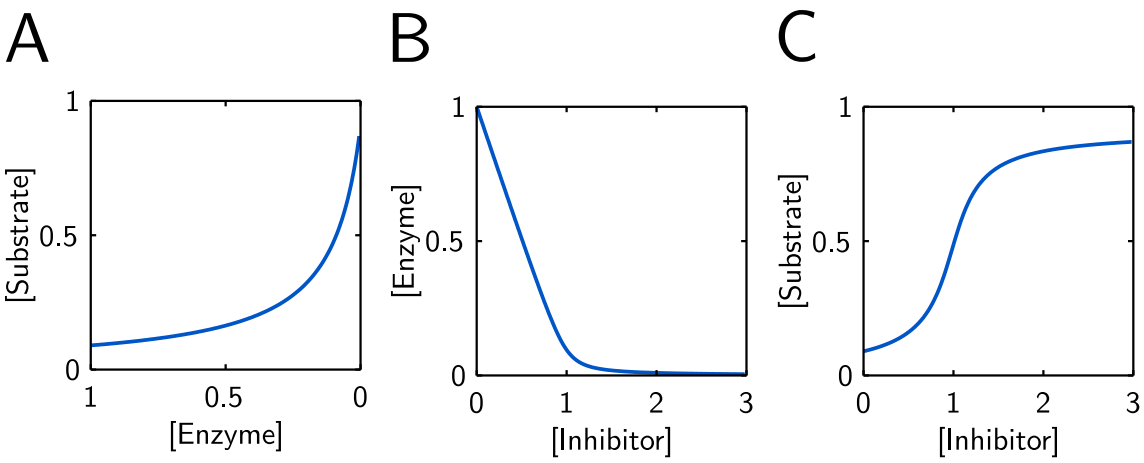

Figure 2.3: Example signal-response curves showing how a hyperbolic enzyme-substrate curve (A - note reversed x axis) can combine with a non-linear enzyme-inhibitor curve (B) to generate an ultrasensitive (sigmoidal) relationship between inhibitor concentration and substrate activity (C).

comes as a direct result of combining a hyperbolic enzyme-substrate response curve (Figure 2.3A) with a tight-binding inhibitor-enzyme curve (Figure 2.3B).

At inhibitor concentrations less than the total enzyme concentration, increasing the amount of inhibitor produces an almost equal decrease in enzyme activity, due to the efficiency of complex formation with the tight binding inhibitor. This can be seen in the initial linear region of Figure 2.3B. Transposing this linear decrease in enzyme activity onto the enzyme-substrate curve (Figure 2.3A) produces the rise in substrate with increasing inhibitor concentration in Figure 2.3C. There is an initial tail where decreasing enzyme activity does not produce a large change in substrate level, because the system starts in a regime where the substrate modification reaction is close to completion and is more limited by the availability of unmodified substrate than by enzyme concentration.

As inhibitor concentration is increased, and enzyme activity decreases further, it moves into a region of the hyperbolic enzyme-substrate curve where changes in enzyme activity have large effects on substrate modification. This produces the middle region of the sigmoid curve where sensitivity to change in inhibitor level is highest (middle section of Figure 2.3C). Once the inhibitor reaches a point at which it is in stoichiometric balance with the enzyme, the enzyme will exist almost exclusively in the inhibitor-bound form, and further addition of inhibitor can have little effect on its activity (flattened tail of Figure 2.3B). As a result, further inhibitor addition will have little effect on the level of substrate modification. This produces the upper tail of the sigmoidal curve (final section

of Figure 2.3C).

2.2.2 A 'Domineering Substrate' mechanism provides a pathway for rapid release from inhibition

With this system we therefore have a mechanism to generate an ultrasensitive CCT, but not a bistable one. Furthermore, to allow for rapid transition from one cell cycle stage to the next, a mechanism must exist to inactivate or destroy the inhibitor to reduce its level below that of the activator.

Since the properties of a competitive inhibitor require it to bind tightly and typically in close proximity to the active site of an enzyme, one plausible inactivation pathway is modification of the inhibitor by the inhibited enzyme itself (Figure 2.2B). The inhibitor would therefore act as a 'bad' substrate of the activator, binding with high affinity but relatively low turnover, so as to prevent access by other substrates. Provided that the active inhibitor is continuously regenerated at a sufficient rate by a suitable regenerating enzyme ($\hat{R}$), the activator will be maintained in the inactive form despite constant inhibitor turnover. However, if the pathway providing for inhibitor regeneration is turned off, the intrinsic ability of the enzyme to catalyse inactivation of the inhibitor provides a mechanism to rapidly free itself from inhibition.

This mechanism has been previously described by Goldberg et al. [176], who coined the phrase 'unfair competition' to describe the relationship between enzyme and inhibitor-substrate. However, we are unclear what is 'unfair' about the process, since relative to a pure example of competitive inhibition where the inhibitor is not modified by the enzyme, the so-called 'unfair competition' does not give any additional benefit to the competitor relative to the true substrate. If anything it provides an additional helping hand to the true substrate by providing a way to inactivate the inhibitor. Instead, we prefer to refer to the inhibitor as a 'domineering substrate', reflecting that the inhibitor is a *bona fide* substrate of the enzyme, but that by tight binding and slow turnover rate it dominates the occupancy of the enzyme's active site to the exclusion of all other substrates.

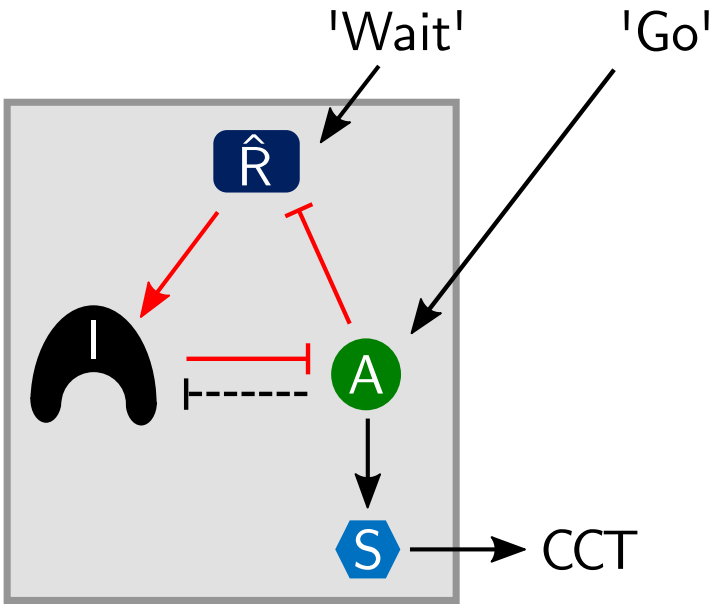

Figure 2.4

Influence diagram describing the FADS motif (inside box), and its relationship to external events and signals (outside box). A: Cell Cycle Activator; I: Stoichiometric inhibitor; R̂: regenerating enzyme; S: Substrate; CCT: Cell Cycle Transition. Arrows and bars represent activatory and inhibitory interactions respectively. The positive feedback loop between activator, regenerating enzyme and inhibitor is highlighted in red. Dashed bar between A and I indicates that this interaction does not comprise a true double-negative feedback loop between activator and inhibitor (see Discussion Section 2.4.2 for details).

2.2.3 'Feedback-amplification' creates bistability

The final component of the network motif necessary to generate a bistable switch is the presence of a positive feedback loop. If the regenerating enzyme responsible for converting inactive inhibitor back into its active form is itself a substrate of the cell cycle activator, this can generate such a loop (Figure 2.2C).

2.2.4 Formal Description of FADS Motif

Putting together these different interactions creates the FADS motif. A simplified influence digram showing the internal network structure and its interactions with external signals is shown in Figure 2.4.

Assuming that the total concentrations of all the components are constants (I_T, A_T and $\hat{R}_T$), and that both I and R̂ are inter-converted by reversible post-translational modifications between active (I and R̂) and inactive (I_M and $\hat{R}_M$) forms, these ideas can

be described by the following differential equations:

$$\frac{d[\mathrm{A:I}]}{dt} = k_{ass} \cdot [\mathrm{I}] \cdot [\mathrm{A}] - (k_{dis} + k_{cat}) \cdot [\mathrm{A:I}] \tag{2.10}$$

$$\frac{d[\mathrm{I_M}]}{dt} = k_{cat} \cdot [\mathrm{A:I}] - k_{demI} \cdot [\hat{\mathrm{R}}] \cdot [\mathrm{I_M}] \tag{2.11}$$

$$\frac{d[\hat{\mathrm{R}}]}{dt} = k_{demR} \cdot [\hat{R}_M] - k_{modR} \cdot [\mathrm{A}] \cdot [\hat{\mathrm{R}}] \tag{2.12}$$

Where:

$$\begin{aligned} [\mathrm{I}] &= I_T - [\mathrm{I_M}] - [\mathrm{A:I}] \\ [\mathrm{A}] &= A_T - [\mathrm{A:I}] \\ [\hat{\mathrm{R}}_\mathrm{M}] &= \hat{R}_T - [\hat{\mathrm{R}}] \end{aligned} \tag{2.13}$$

We assume that A:$\hat{\mathrm{R}}$ and A:S complexes are turned over more rapidly than the A:I complex and do not have a significant residence time. We therefore model these processes using mass action kinetics.

Formation of the A:I complex is assumed to be fast and reversible, allowing us to make a pseudo–steady-state approximation for its concentration, reducing the system to a series of two ODEs:

$$[\mathrm{A:I}] = \frac{A_T + I_T - [\mathrm{I_M}] + K_M - \sqrt{(A_T + I_T - [\mathrm{I_M}] + K_M)^2 - 4 \cdot A_T \cdot (I_T - [\mathrm{I_M}])}}{2} \tag{2.14}$$

Here $K_M = \frac{k_{dis}+k_{cat}}{k_{ass}}$ is the Michaelis constant for activator-catalysed inhibitor inactivation.

2.2.5 The FADS motif produces a bistable system

We can analyse the behaviour of the FADS model using a bifurcation diagram (Figure 2.5), which clearly demonstrates the bistable behaviour of the system. On the diagram, the upper steady state (high [$\hat{\mathrm{R}}$], low [A]) is the pre-transition state, where the activator is kept inactive by unmodified inhibitor. The lower steady state (low [$\hat{\mathrm{R}}$], high [A]) is

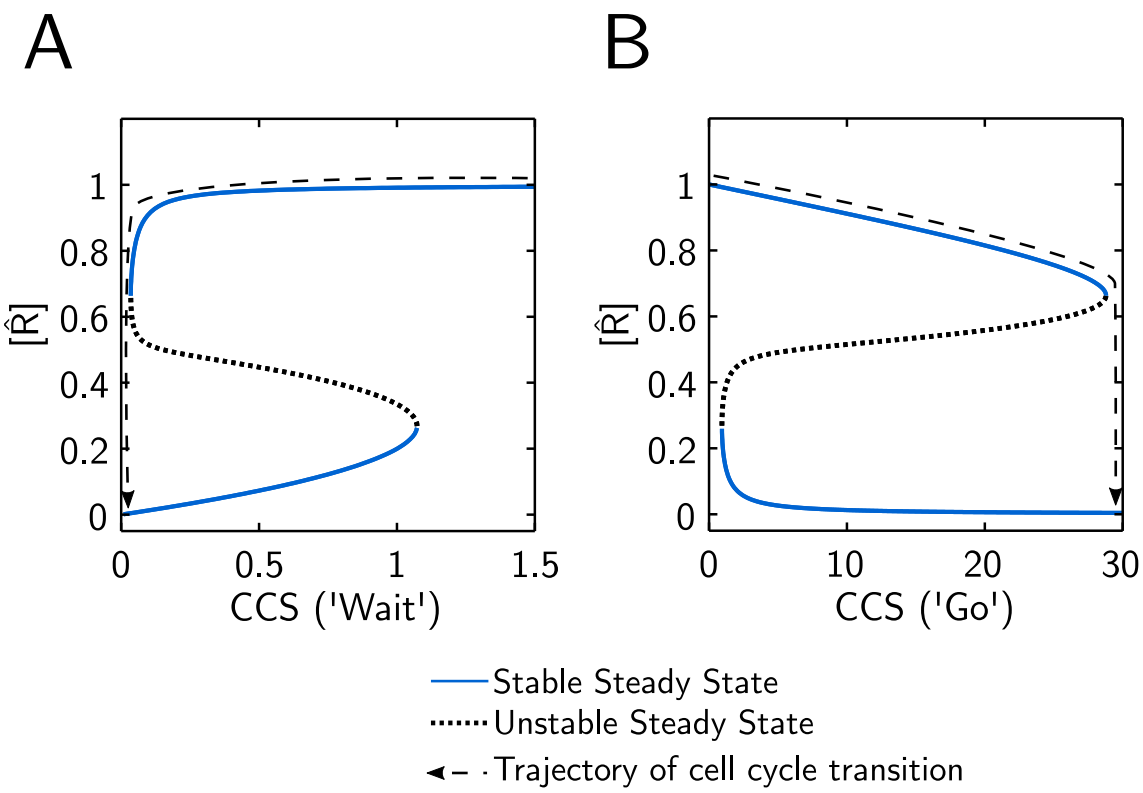

Figure 2.5: Bifurcation diagrams plotting the steady states of the generic FADS motif as a function of either a 'Wait' (A) or 'Go' (B) upstream cell cycle signal (CCS).

the post-transition state, where the activator overcomes its inhibitor, and inactivates the regenerating enzyme. Biologically, the bifurcation parameter corresponds to the upstream Cell Cycle Signal (CCS), which dictates the timing of the transition from one stable steady state to the next. This CCS can take the form of a 'Wait' signal which must be removed to trigger the transition (Figure 2.5A), or a 'Go' signal which increases to promote passage into the next cell cycle stage (Figure 2.5B). In these examples, we include the CCS in the model by modification of equation 2.12:

Wait:

$$\frac{d[\hat{\mathrm{R}}]}{dt} = k_{demR} \cdot CCS \cdot [\hat{\mathrm{R}}_{\mathrm{M}}] - k_{modR} \cdot [\mathrm{A}] \cdot [\hat{\mathrm{R}}] \tag{2.15}$$

Go:

$$\frac{d[\hat{\mathrm{R}}]}{dt} = k_{demR} \cdot [\hat{\mathrm{R}}_{\mathrm{M}}] - k_{modR} \cdot CCS \cdot [\mathrm{A}] \cdot [\hat{\mathrm{R}}] \tag{2.16}$$

However in principle (and as will be seen in practice later), the upstream CCS could exert its effect at any of the individual reactions within the system, so this only serves as a single example of each type of signal.

Regardless of their point of input, Wait and Go signals produce characteristic S-shaped

or Z-shaped curves respectively (Figure 2.5). Note that assuming a steady change in CCS without fluctation, 'Time', which is not explicitly plotted, in general runs from right to left on Figure 2.5A as the 'Wait' signal is reduced, but from left to right on Figure 2.5B as the 'Go' signal increases. The resulting trajectories as the system moves from the upper to the lower steady state in response to changes in CCS are indicated by arrows.

Having demonstrated that the system is bistable, we can also analyse the factors contributing to that bistability using phaseplane diagrams (Figure 2.6). These are effectively cross-sections of the system shown in Figure 2.5, taken for a fixed value of the CCS parameter. For simplicity, we only analyse the 'Wait' signal bifurcation diagram, an elongated version of which is included in Figure 2.6D for comparison. We consider three separate cases: $CCS = 1.5$ (monostable, upper steady state), $CCS = 0.75$ (bistable) and $CCS = 0$ (monostable, lower steady state). On each phaseplane, two nullclines are plotted, representing the points at which $\frac{d[\mathrm{I_M}]}{dt} = 0$ (black) and $\frac{d[\hat{\mathrm{R}}]}{dt} = 0$ (blue).

The $[\mathrm{I_M}]$ nullcline (black) is not affected by the value of CCS, since it does not appear in the corresponding ODE (Equation 2.11). The $[\hat{\mathrm{R}}]$ nullcline (blue) on the other hand is affected by the value of CCS, since it appears in Equation 2.15. In the pre-transition state (Figure 2.6C), the high value of CCS pushes up the $[\hat{\mathrm{R}}]$ nullcline, so that it intersects the $[\mathrm{I_M}]$ nullcline at only a single point, corresponding to a high $[\hat{\mathrm{R}}]$, low $[\mathrm{A}]$ state. As the wait signal reduces, the $[\hat{\mathrm{R}}]$ nullcline is pushed downwards, so that it begins to intersect the $[\mathrm{I_M}]$ nullcline at two additional points (Figure 2.6B). These points are a lower stable steady state, corresponding to the post-transition state, and an intervening unstable state, separating the pre- and post-transition states. As CCS is reduced further, the $[\hat{\mathrm{R}}]$ nullcline collapses and falls below the $[\mathrm{I_M}]$ nullcline, so that only a single intersection point remains (Figure 2.6A).This lower state corresponds to the post-transition state. The CCS threshold at which the upper intersection between the nullclines is lost and the system loses bistability defines the point at which the cell undergoes the cell cycle transition.

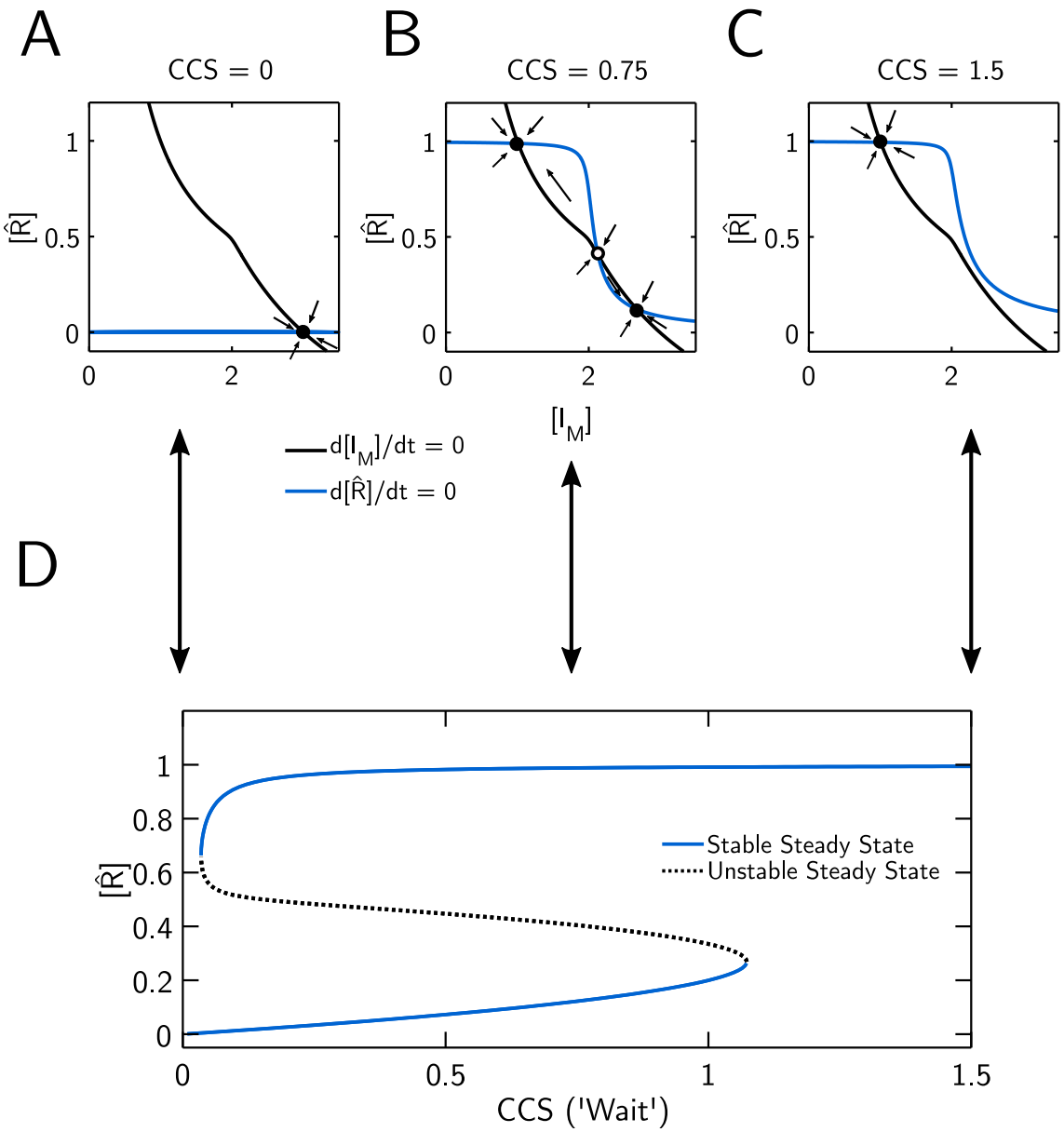

Figure 2.6: Phaseplane diagrams for the generic FADS motif (A-C) corresponding to specific points on the bifurcation diagram (D). Note that (D) is simply an enlarged version of Figure 2.5A, shown here for direct comparison.

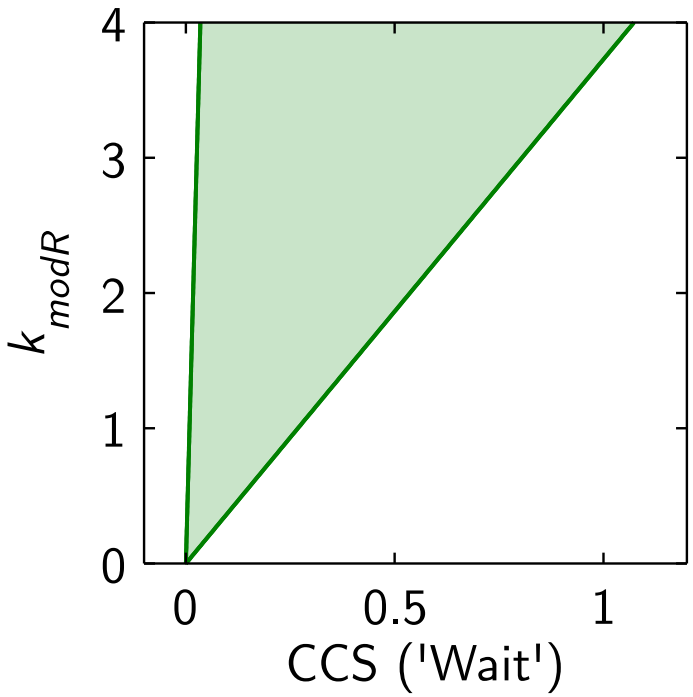

Figure 2.7: Two-parameter bifurcation diagram for the generic FADS motif. The graph shows the change in 'on' and 'off' thresholds of a one-parameter bifurcation diagram with bifurcation parameter CCS, as the second bifurcation parameter k_{modR} is changed. The threshold values are indicated by solid green lines. The shaded region indicates the size of the bistable region between these two thresholds.

2.2.6 Bistability depends on the FADS feedback-amplification loop

Having demonstrated that the FADS motif is able to generate a bistable cell cycle transition, we can test our original assertion that the feedback-amplification loop is necessary to convert a simple domineering substrate system into a bistable switch. Figure 2.7 shows that increasing the rate at which the regenerating enzyme is modified by the activator (k_{modR}), the difference between the upper and lower CCS threshold increases. The bistable region (green shading) exists between these two thresholds. When k_{modR} is reduced to 0, the two thresholds converge, and the system is no longer bistable, demonstrating that completing the feedback-amplification loop is necessary to generate a bistable system.

2.2.7 Inhibitor binding strength

As discussed so far, the FADS motif requires a tight-binding interaction between the stoichiometric inhibitor (domineering substrate) and the cell cycle activator, in order to

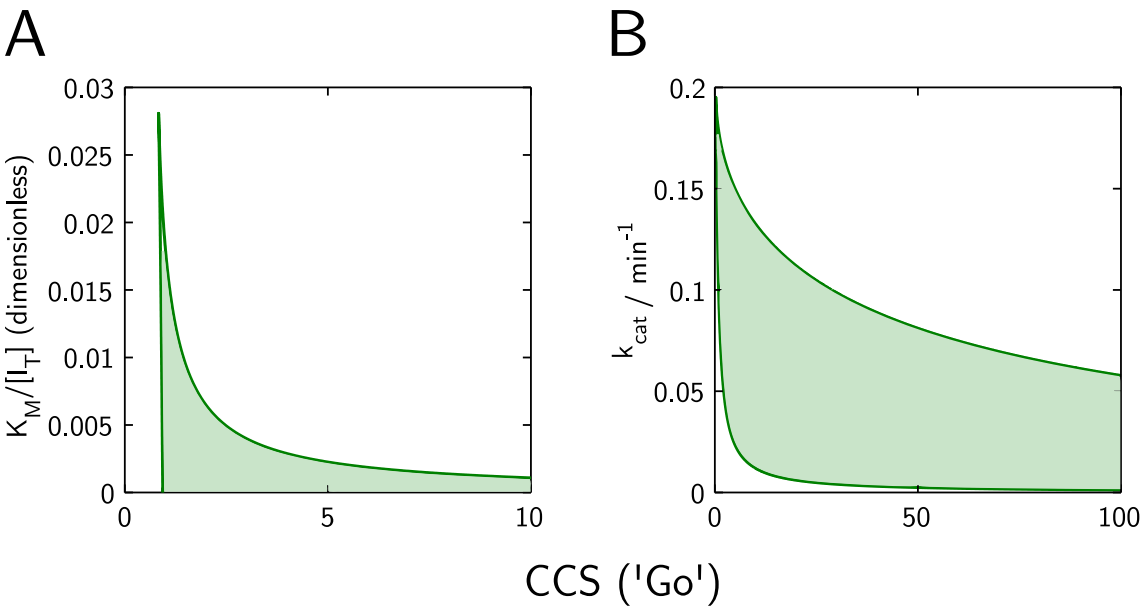

Figure 2.8: Two-parameter bifurcation diagrams showing the effects of kinetic parameters affecting activator:inhibitor interactions on the bistability of the FADS motif. Note different x axis scaling between figures.

generate the necessary non-linearity required for bistability. In order to analyse the significance of this binding affinity, and to assess whether the mechanism we have proposed could realistically be expected to generate bistability *in vivo*, we analysed the effects of altering kinetic parameters associated with A:I complex formation and disassembly.

The relative sizes of the k_{ass}, k_{dis} and k_{cat} parameters will all affect the stability of the A:I complex. However, k_{ass} and k_{dis} do not appear independently from each other in the model. They occur only in the algebraic equation for A:I complex formation (Equation 2.14), in which they are always expressed in terms of K_M ($K_M = \frac{k_{cat}+k_{dis}}{k_{ass}}$). As a result, for a fixed value of k_{cat}, any change in k_{ass} can be offset by a change in k_{dis} which maintains a fixed value of K_M. We therefore choose not to consider the effects of varying k_{ass} and k_{dis} individually, instead looking at the global effects of changing K_M. Since K_M is expressed in units of concentration, which are arbitrary in our generic FADS model, we plot the ratio $K_M/[I_T]$, giving the value of K_M as a fraction of the total possible substrate concentration.

Unlike k_{dis} and k_{ass}, k_{cat} occurs both inside and outside of the expression for K_M, since in Equation 2.11, $k_{cat} \cdot [\mathrm{A:I}]$ gives the rate of I_M generation from the A:I complex. k_{cat} therefore has effects on the system separate to its contribution to K_M. However, if k_{cat} is used as a bifurcation parameter, changes to its value will also result in changes

to K_M, making it difficult to separate its effects on K_M from its role in I_M formation. To circumvent this problem, we make a variant of the model where K_M is set to a constant value, rather than being calculated from k_{ass}, k_{diss} and k_{cat}. In doing so, we are implicitly adjusting the k_{ass} parameter to offset the effect of changes to k_{cat} on K_M, rearranging the K_M definition to give $k_{ass} = \frac{k_{dis}+k_{cat}}{K_M}$.

Two-parameter bifurcation diagrams were plotted, showing the CCS thresholds between which the system exhibits bistable behaviour as a function of K_M (Figure 2.8A) and k_{cat} (Figure 2.8B). The right-hand branch is the CCS required to promote movement from the pre-transition to post-transition state ('on' threshold), while the left-hand branch is the CCS below which the system will revert to the pre-transition state ('off' threshold). The shaded region in between these two thresholds indicates that the system is bistable within this range of parameter values.

Effects of K_M

Figure 2.8A shows that the extent of bistability is strongly dependent on the strength of inhibitor-activator binding. At low values of K_M, the system is bistable across a large range of CCS, and as K_M tends towards 0, the CCS 'on' threshold tends to infinity. In contrast, as K_M is increased, the system is funnelled into a narrow region of bistability, and eventually the system is no longer bistable at all.

In addition to the general trends, the specific values of $K_M/[I_T]$ used here are also important to consider. Since our aim in this Chapter has been to highlight the important features of the FADS motif, and to identify known cell cycle transitions where we believe it to be working, in general we have not attempted to rigorously fit parameters to experimental data. However, in the case of the relative rates of binding of domineering and regular substrates to the cell cycle activator, the relative rates are highly significant to the FADS mechanism.

In this case, the total inhibitor concentration is far in excess of the K_M, implying that the activator should be almost entirely saturated by the unmodified inhibitor. It is this tight binding which provides non-linearity, since as soon as the total amount of unmodified inhibitor becomes sub-stoichiometric with respect to the activator, free activator rapidly becomes available, where a similar fall in inhibitor concentration which remained

above the stoichiometric balance would have very little effect on enzyme activity.

Effects of k_{cat}

Figure 2.8B shows that k_{cat} sensitivity follows a similar pattern to that of K_M, with the bistable region falling within a distinct range of values of k_{cat}. However, of perhaps more significance is the effects of low values of k_{cat} on the system. In these cases, the 'on' threshold of CCS required to move the system into the post-transition state moves to increasingly high values, meaning that the system will be locked into a pre-transition state in the absence of an extreme perturbation.

This highlights the role that inhibitor turnover via the domineering substrate mechanism plays in this system. Inhibitor turnover itself is not a specific requirement to generate bistability using stoichiometric inhibitor ultrasensitivity. This can be seen at the bottom of Figure 2.8A, where the bistable region persists even as K_M falls to 0. Since for K_M to be 0, both k_{dis} and k_{cat} must be 0, this amounts to the same thing. (The same trend is true of Figure 2.8B, but the relevant region occurs at too high a level of CCS to be easily shown.) Nevertheless, we clearly see that domineering substrates are a recurring feature of cell cycle transitions. Figure 2.8B clearly shows the advantage of a domineering substrate over a simple stoichiometric inhibitor. By allowing the activator to inactivate its own inhibitor, the system always retains the ability to fully overcome inhibition as inhibitor regeneration is turned off. This gives the cell the freedom to develop a strong and robust inhibition pathway, which nevertheless retains the ability to be readily inactivated. In this way, the cell can reconcile the opposing pressures for a cell cycle which is fast and efficient, while also being strictly controlled at specific checkpoints.

2.3 FADS motif in cell cycle regulation

We argue that the FADS motif operates at multiple cell cycle transitions *in vivo* and is responsible for their switch-like nature. We illustrate this claim by discussing the molecular mechanisms of three consecutive cell cycle transitions in detail. Components comprising FADS motifs at G1/S, M/A and mitotic exit are summarised in Table 2.1, and the resulting influence diagrams are shown in Figure 2.9.

Transition	Activator	Inhibitor	Modification	Regenerating Enzyme	Signal
G1/S	Cdk1:Clb5	Sic1	Phosphorylation	Swi5	Cdk1:Cln2 ('Go')
M/A	APC/C^{Cdc20}	MCC	Ubiquitination	CycB	uKT ('Wait')
Mitotic Exit	PP2A:B55	p-ENSA	Dephosphorylation	Gwl	Cdk1:CycB ('Wait')

Table 2.1: Table showing the different components of the FADS motif at different cell cycle stages.

In each case, while the underlying network structure is unchanged (Figure 2.9), the different nature of the interaction mechanisms (phosphorylation and dephosphorylation, synthesis and destruction etc.) require differences in the precise molecular description of the system in the wiring diagram and ODEs. In this section, we describe each of the transitions in turn, first summarising the biological background, and then explaining the specific modifications made to the model to capture the unique features of each transition.

2.3.1 G1/S in Budding Yeast

The G1/S transition in budding yeast operates as a bistable switch generated by a FADS motif comprising the activator Cdk1:Clb5, inhibitor Sic1 and regenerating 'enzyme' (in this case a transcription factor) Swi5. The relationship between these components is summarised in the influence diagram in Figure 2.9A, and detailed in the wiring diagram in Figure 2.10.

While higher eukaryotes use multiple CDKs to control their cell cycle progression, budding yeast rely on a single CDK, Cdk1 [14]. The S-phase Cdk1:Cyclin complex is Cdk1:Clb5/6 in budding yeast [229], but for simplicity we will use 'Clb5' to refer to both Clb5 and Clb6 in the model. The Cdk1:Clb5 complex is responsible for initiation of DNA replication and corresponds to the activator in the generic FADS motif.

Prior to G1/S, Cdk1:Clb5 is inhibited by the CKI Sic1, corresponding to the stoichiometric inhibitor in the generic FADS motif [22, 230]. As required for the FADS motif, Sic1 is also a substrate for Cdk1-dependent phosphorylation [231, 232]. Indeed,

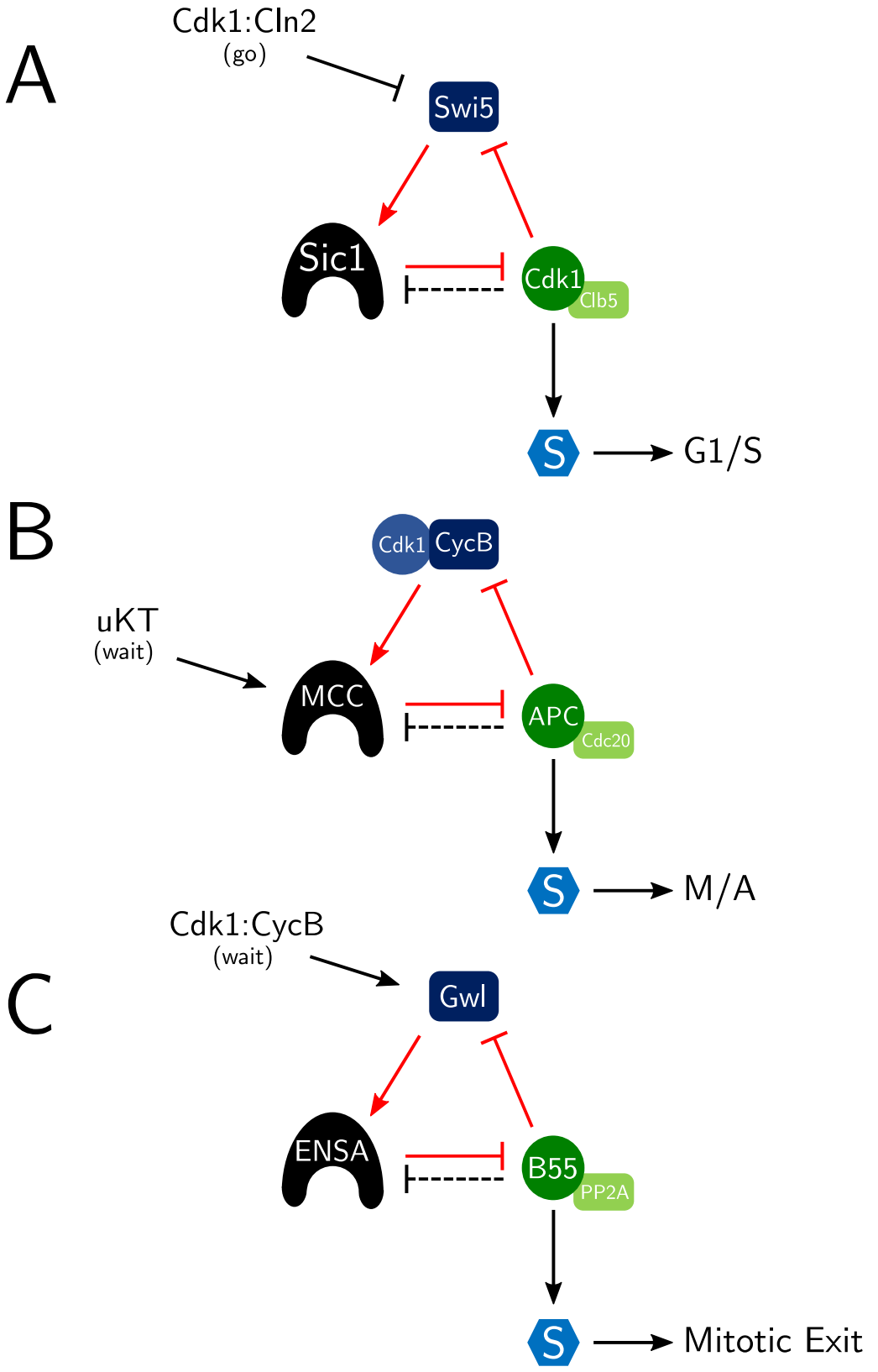

Figure 2.9: Influence diagrams showing how the FADS motif described generically in Figure 2.4 operates at three different cell cycle transitions. (A) G1/S in budding yeast. (B) Spindle Assembly Checkpoint. (C) Mitotic Exit.

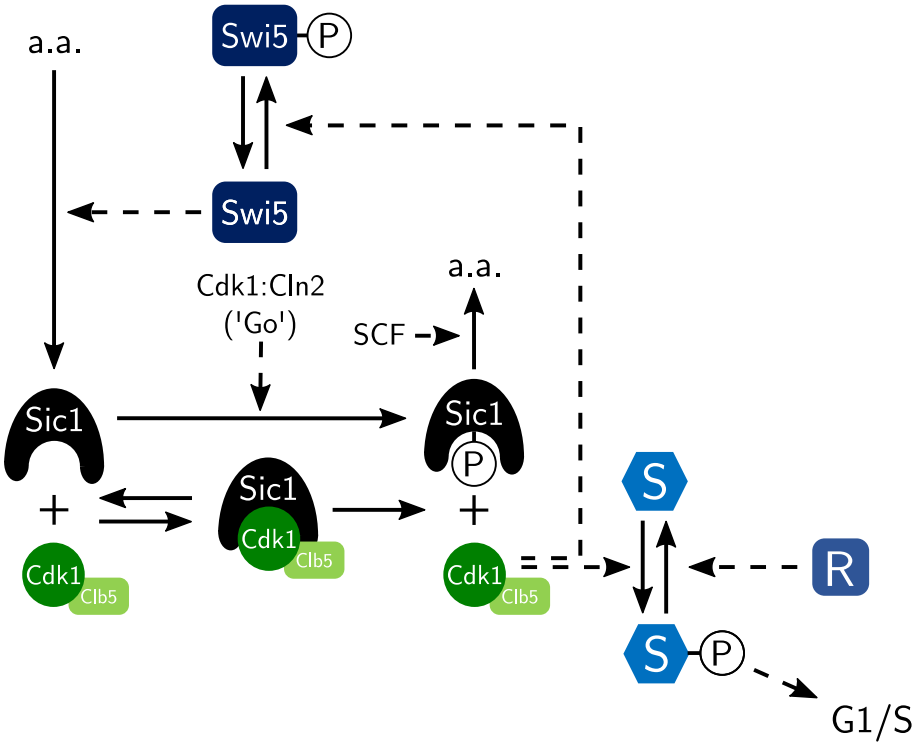

Figure 2.10: Wiring diagram for the FADS model of the G1/S transition in budding yeast. Solid arrows indicate biochemical reactions, dashed arrows indicate rate enhancement of the targeted reaction. Arrows to or from 'a.a.' (amino acids) indicate protein degradation and synthesis respectively.

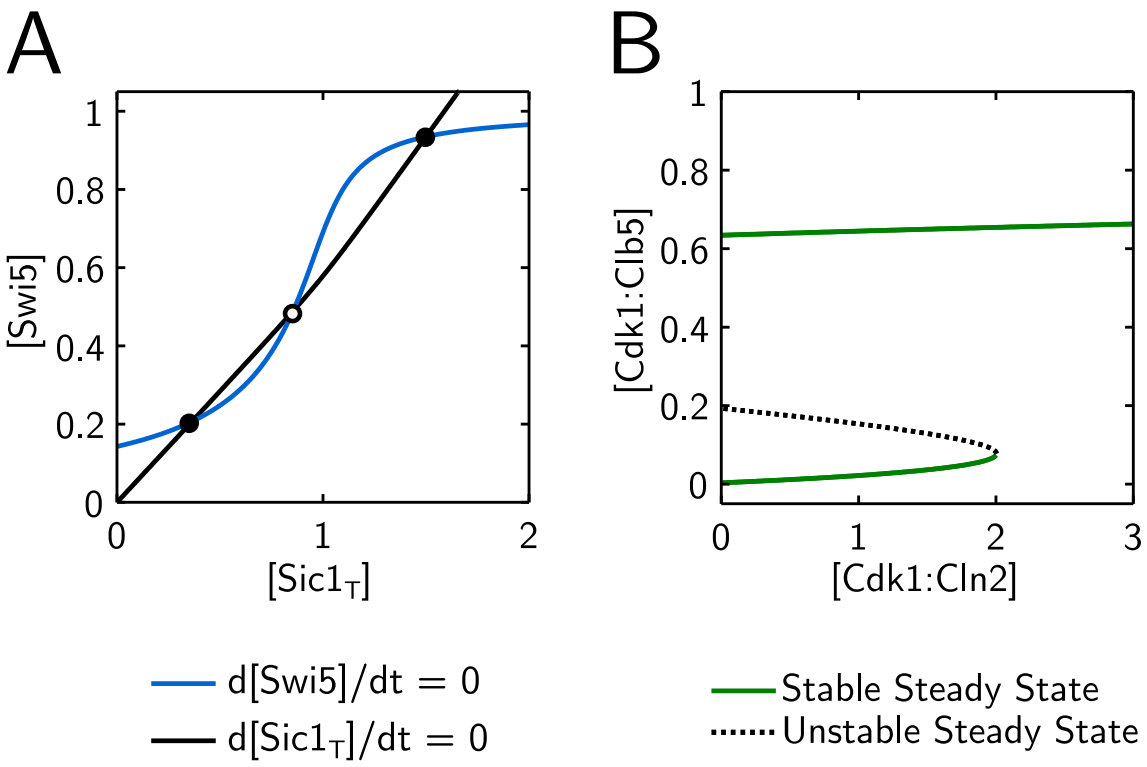

Figure 2.11: (A) Phaseplane diagram for G1/S FADS model. (B) Bifurcation diagram for G1/S FADS model, showing steady state [Cdk1:Clb5] as a function of [Cdk1:Cln2], the upstream starter kinase.

the name Sic1 was originally coined as '**S**ubstrate/**I**nhibitor of **C**dk**1**' [233], since both aspects of the protein's interaction with Cdk1 were separately identified during its early characterisation. Phosphorylation of Sic1 does not inhibit it directly, but promotes its SCF-dependent ubiquitination and degradation [234, 235].

One of the substrates of the activated Cdk1:Clb5 complex is Swi5, the transcription factor for Sic1, which provides the positive feedback loop required to complete the FADS motif. Cdk1-phosphorylated Swi5 is excluded from the nucleus [236], which terminates the production of Sic1.

In addition to phosphorylation by Cdk1:Clb5, Sic1 is also subject to phosphorylation by the G1-specific CDK:Cyclin complex Cdk1:Cln2, which also contributes to its SCF-dependent degradation. In this way, rising Cdk1:Cln2 activity acts as the upstream 'Go' signal driving the transition between the G1- and S- phases of the cell cycle.

The production of Cdk1:Cln2 itself is subject to control by the budding yeast 'Start' checkpoint, controlling entry into the cell cycle. Once a decision is made to commit to a new cell cycle at Start, Cdk1:Cln2 levels increase in late G1, providing an upstream trigger to initiate the G1/S transition. Once in S-phase, high levels of Cdk1:Clb5 can self-maintain high levels of Swi5 phosphorylation and low levels of Sic1, so that the initial Cdk1:Cln2 input signal is no longer required. This feedback loop provides the bistability associated with the FADS motif.

While we have referred here to the situation in budding yeast, the same principles can be applied to the fission yeast cell cycle. Here the relevant components are Cdk1:Cig2 (Activator) and Rum1 (Inhibitor) [22].

In order to represent the budding yeast G1/S transition using our generic FADS model, it is necessary to make some modifications to reflect that rather than a strictly reversible process, inhibitor activation and inactivation occur through synthesis and phosphorylation-dependent degradation of Sic1 respectively. Specifically, the parameter I_T from the generic FADS model becomes a dynamic variable ($[\mathrm{I_T}]$) in the G1/S model, allowing for change in the total inhibitor concentration in response to synthesis and degradation.

This gives the following system of ODEs:

$$\frac{d[\mathrm{A:I}]}{dt} = k_{ass} \cdot [\mathrm{I}] \cdot [\mathrm{A}] - (k_{dis} + k_{cat}) \cdot [\mathrm{A:I}] \tag{2.17}$$

$$\frac{d[\mathrm{I_T}]}{dt} = k_{syn} \cdot \hat{R} - k_{cat} \cdot [\mathrm{A:I}] - k_{phosI} \cdot G \cdot [\mathrm{I}] - k_{deg} \cdot [\mathrm{I_T}] \tag{2.18}$$

$$\frac{d[\hat{\mathrm{R}}]}{dt} = k_{demR} \cdot CCS \cdot [\hat{\mathrm{R}}_{\mathrm{M}}] - k_{modR} \cdot [\mathrm{A}] \cdot [\hat{\mathrm{R}}] \tag{2.19}$$

Where:

$$\begin{aligned} [\mathrm{I}] &= [\mathrm{I_T}] - [\mathrm{A:I}] \\ [\mathrm{A}] &= A_T - [\mathrm{A:I}] \\ [\hat{\mathrm{R}}_{\mathrm{M}}] &= \hat{R}_T - [\hat{\mathrm{R}}] \end{aligned} \tag{2.20}$$

As in the generic FADS model, we make a pseudo–steady-state approximation for $[\mathrm{A:I}]$, reducing the system to two ODEs:

$$[\mathrm{A:I}] = \frac{A_T + [\mathrm{I_T}] + K_M - \sqrt{(A_T + [\mathrm{I_T}] + K_M)^2 - 4 \cdot A_T \cdot [\mathrm{I_T}]}}{2} \tag{2.21}$$

This network generates a bistable switch in Cdk1:Clb5 activity as a function of the upstream CCS Cdk1:Cln2 (Figure 2.11). This corresponds to the *in vivo* function of the G1/S transition. For the chosen parameter set, the 'off' Cdk1:Cln2 threshold is to the left of the y-axis, making the transition irreversible.

2.3.2 The Spindle Assembly Checkpoint

The SAC operates as a bistable switch, generated by a FADS motif comprising the activator APC/C^{Cdc20}, its inhibitor MCC, and a form of regenerating 'enzyme', in that MCC assembly is catalysed at unattached kinetochores in a process requiring CDK-dependent phosphorylation. The relationship between these components is summarised in the influence diagram in Figure 2.9B and detailed in the wiring diagram in Figure 2.12.

Accumulation and activation of mitotic Cdk1:CycB during G2 is the trigger for mitosis. Following spindle formation in prophase and chromosome biorientation during

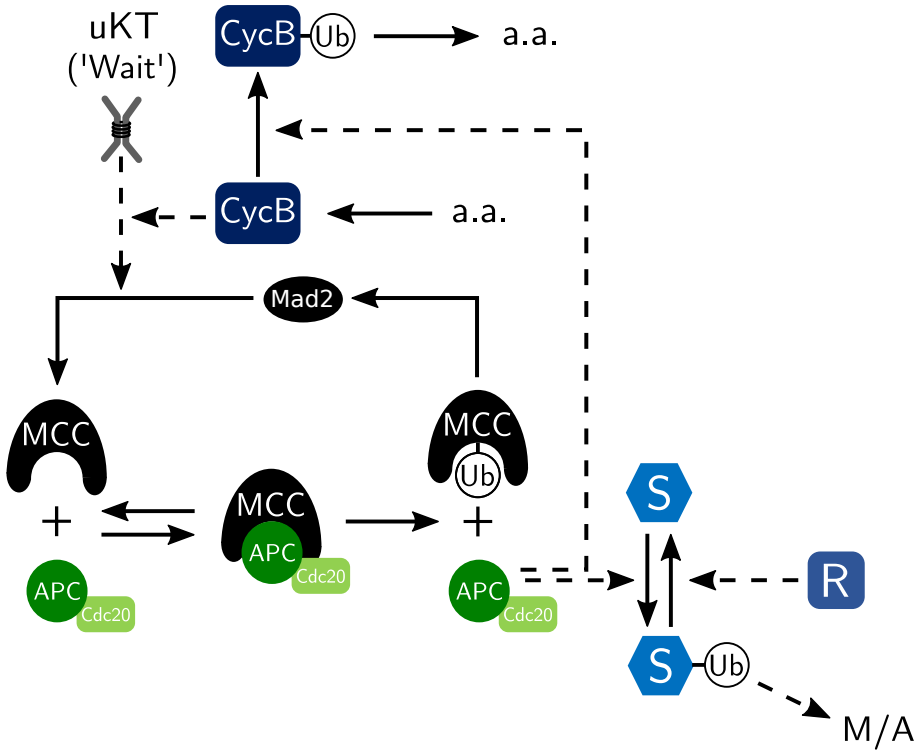

Figure 2.12: Wiring diagram for the FADS model of the SAC. Solid arrows indicate biochemical reactions, dashed arrows indicate rate enhancement of the targeted reaction. Arrows to or from 'a.a.' (amino acids) indicate protein degradation and synthesis respectively.

prometaphase, further mitotic progression requires activation of APC/C^{Cdc20}, which initiates anaphase and mitotic exit by promoting ubiquitin-mediated degradation of Securin and CycB. APC/C^{Cdc20} therefore corresponds to the activator in the generic FADS motif.

As described in the introduction (Section 1.4), it is essential for successful chromosome segregation that anaphase onset is delayed until all chromosomes undergo correct microtubule attachment and biorientation. APC/C must be kept inactive until these processes are complete, which is achieved by MCC assembly at unattached kinetochores. The Cdc20 within MCC ($Cdc20_M$) is itself targeted for ubiquitination within the APC/C^{Cdc20}:MCC complex, promoting MCC disassembly and relieving APC/C^{Cdc20} from inhibition. It therefore follows that MCC can be described as a domineering substrate of APC/C.

To complete the FADS motif, we require a regenerating enzyme to close the feedback-amplification loop between activator and inhibitor. Since the enzymatic activity of APC/C promotes MCC disassembly, the regeneration reaction requires *de novo* assembly of MCC rather than demodification, but otherwise the same principles apply. Since MCC

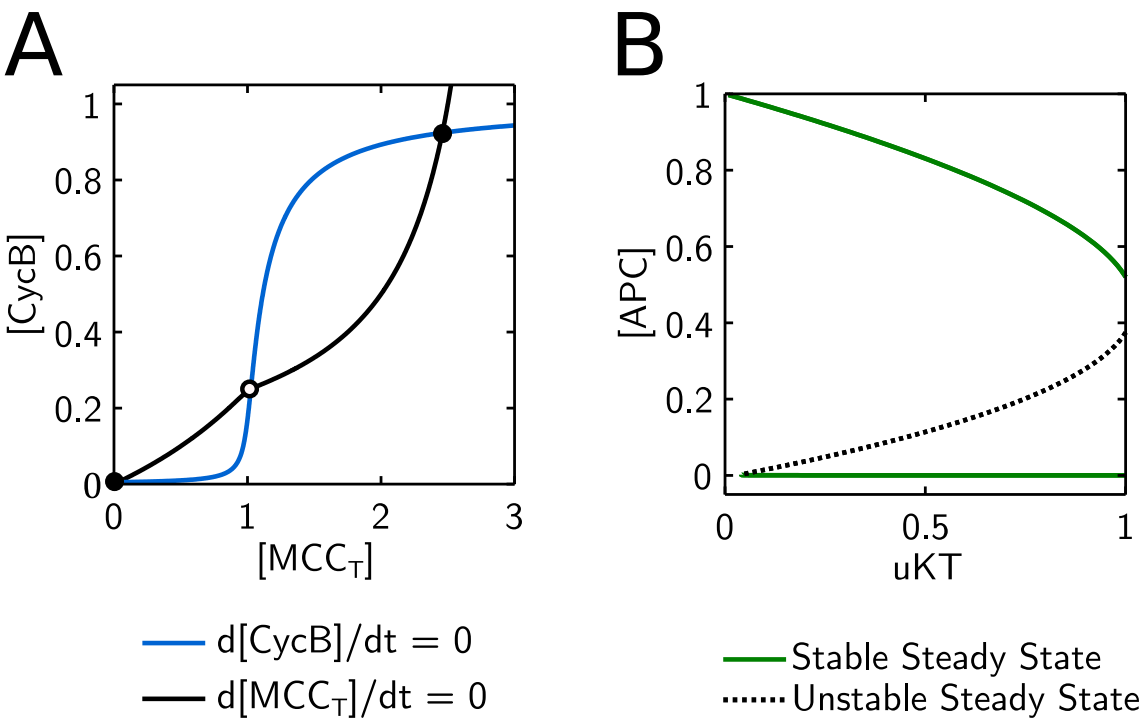

Figure 2.13: (A) Phaseplane diagram for SAC FADS model. (B) Bifurcation diagram for SAC FADS model, showing steady state [APC] as a function of uKT, the upstream 'Wait' signal.

assembly at unattached kinetochores requires CDK activity, and CycB is itself targeted by APC/C^{Cdc20}, this creates the necessary feedback-amplification loop. With this loop, the FADS motif is complete, and the system can adopt either a high Cdk1:CycB state (metaphase), or a high APC/C^{Cdc20} state (anaphase) (Figure 2.13A).

The final part of the model is the requirement for a upstream signal to promote the transition from metaphase into anaphase. In the case of the SAC, the presence of unattached kinetochores provides the necessary wait signal to maintain the metaphase state until all chromosomes are correctly aligned on the spindle. Unattached kinetochores (uKT) act as the site of MCC assembly, so that as attachment proceeds during prometaphase the rate of MCC regeneration decreases, until it is no longer sufficient to counteract the turnover of MCC from the APC/C^{Cdc20} complex. This creates a bistable switch in APC/C^{Cdc20} activity as a function of uKT, the upstream 'Wait' signal for the M/A transition (Figure 2.13B).

In order to represent the SAC using our generic FADS model, it is necessary to modify the generic FADS equations to reflect that inhibitor activation and inactivation occur through assembly and ubiquitin-mediated disassembly of the MCC complex, and that

$\hat{\text{R}}$ (CycB) activation and inactivation occurs through synthesis and degradation rather than by reversible modification. Furthermore, the upstream 'Wait' signal (uKT) feeds in at the level of MCC assembly. The requirement to keep track of a second complex (MCC) in addition to the A:I (APC:MCC) complex also means that it is convenient to rewrite the ODEs in terms of the specific complex names in this case rather than use generic ones. The I_T parameter in the generic model therefore corresponds to the $[\text{MCC}_\text{T}]$ variable in the SAC model, while $[\text{CycB}]$ and $[\text{APC} : \text{MCC}]$ correspond to $[\hat{\text{R}}]$ and $[\text{A} : \text{I}]$ respectively.

This gives the following ODEs:

$$\frac{d[\text{CycB}]}{dt} = k_{syn} - (k'_{deg} + k_{deg} \cdot [\text{APC}]) \cdot [\text{CycB}] \tag{2.22}$$

$$\frac{d[\text{MCC}_\text{T}]}{dt} = -k_{cat} \cdot [\text{APC} : \text{MCC}] + k_{assemb} \cdot uKT \cdot [\text{CycB}] \cdot [\text{Mad2}] \tag{2.23}$$

$$\frac{d[\text{APC} : \text{MCC}]}{dt} = k_{ass} \cdot [\text{MCC}] \cdot [\text{APC}] - (k_{dis} + k_{cat}) \cdot [\text{APC} : \text{MCC}] \tag{2.24}$$

Where:

$$\begin{aligned} [\text{MCC}] &= [\text{MCC}_\text{T}] - [\text{APC} : \text{MCC}] \\ [\text{APC}] &= APC_T - [\text{APC} : \text{MCC}] \\ [\text{Mad2}] &= Mad2_T - [\text{MCC}_\text{T}] \end{aligned} \tag{2.25}$$

As in the generic FADS model, we make a pseudo–steady-state approximation for $[\text{APC} : \text{MCC}]$, reducing the system to 2 ODEs:

$$\begin{aligned} [\text{APC} : \text{MCC}] = \quad & 0.5 \cdot ([\text{APC}_\text{T}] + [\text{MCC}_\text{T}] + K_M \\ & - \sqrt{([\text{APC}_\text{T}] + [\text{MCC}_\text{T}] + K_M)^2 - 4 \cdot [\text{APC}_\text{T}] \cdot [\text{MCC}_\text{T}]}) \end{aligned} \tag{2.26}$$

2.3.3 Mitotic Exit

Exit from mitosis also operates as a bistable switch, generated by a FADS motif comprising the activator PP2A:B55, its inhibitor phosphorylated Endosulfine (p-ENSA), and the regenerating enzyme Gwl. The relationship between these components (the 'BEG' pathway) is summarised in the influence diagram in Figure 2.9C, and detailed in the

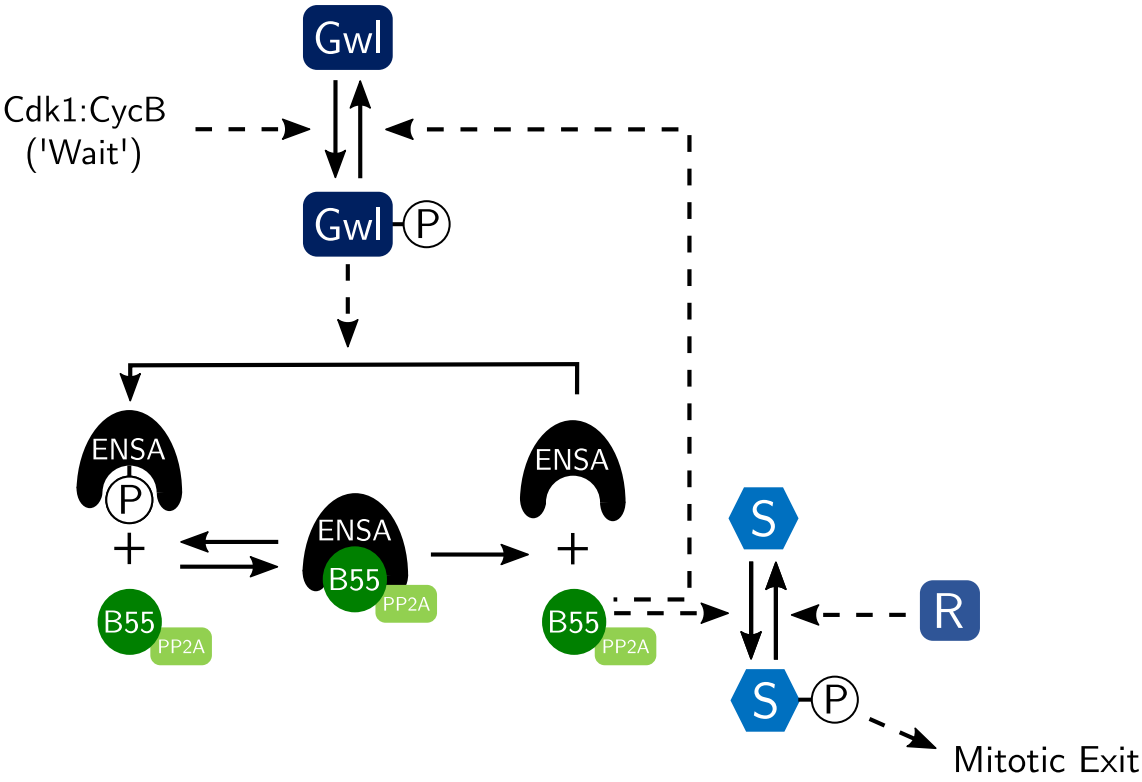

Figure 2.14: Wiring diagram for the FADS model of mitotic exit. Solid arrows indicate biochemical reactions, dashed arrows indicate rate enhancement of the targeted reaction.

wiring diagram in Figure 2.14.

During mitosis, CDK-dependent phosphorylation of hundreds of targets contributes to maintaining the mitotic state and driving the events of mitosis. Exit from mitosis requires that many of these phosphorylations are reversed by counter-acting phosphatases. Reciprocal regulation of kinase and phosphatase activity is necessary to coordinate entry into and exit from mitosis, ensure a clean transition between these distinct cell cycle stages, and prevent futile cycling. PP2A:B55 is one of the major mitotic exit phosphatases, and we therefore consider it as the activator in the FADS motif controlling mitotic exit.

As discussed in Section 1.4.7, regulation of PP2A:B55 occurs via its stoichiometric inhibitor ENSA. In its phosphorylated form (p-ENSA), it binds strongly to PP2A:B55 and blocks its activity towards other substrates. The p-ENSA phospho-site is itself a target for PP2A:B55-dependent dephosphorylation from within the complex, making p-ENSA a domineering substrate (or 'unfair competitor') of PP2A:B55.

Regeneration of inhibitory p-ENSA requires phosphorylation of the free ENSA pool.

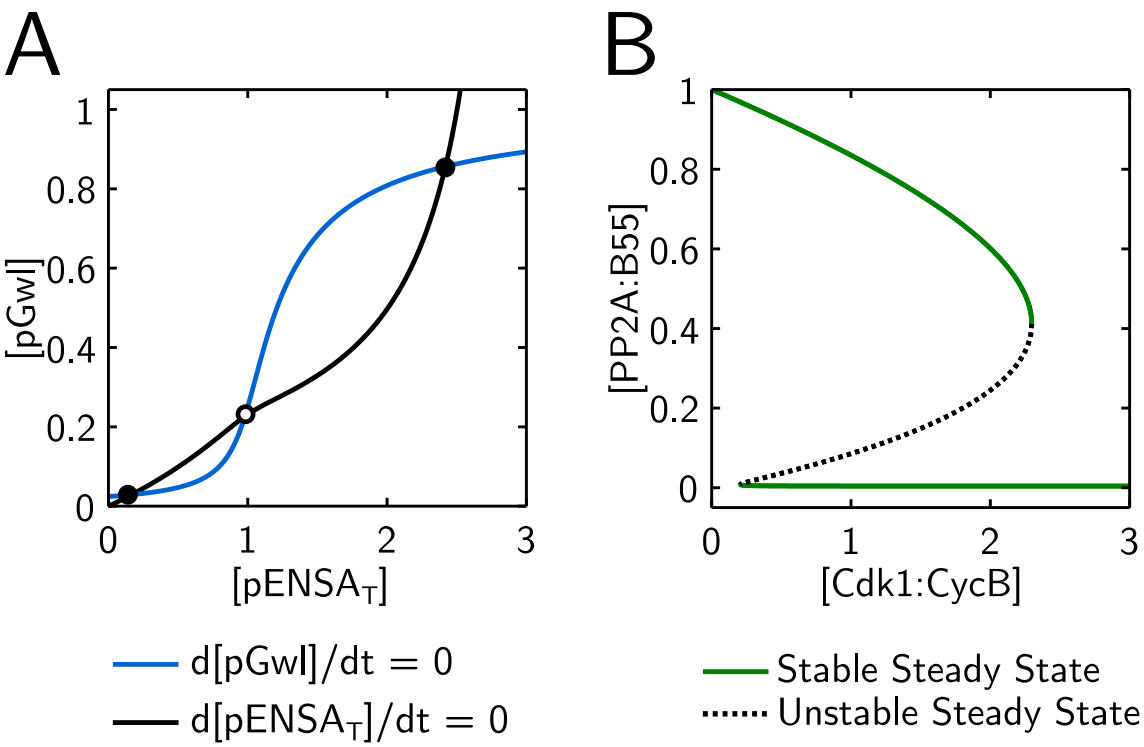

Figure 2.15: (A) Phaseplane diagram for Mitotic Exit FADS model. (B) Bifurcation diagram for Mitotic Exit FADS model, showing steady state [PP2A:B55] as a function of [Cdk1:CycB], the upstream 'Wait' signal.

This reaction is catalysed by Gwl, which plays the role of the regenerating enzyme from the generic FADS motif. Removal of activatory phosphorylation from Gwl by PP2A:B55 activity creates a double-negative feedback loop, which completes the FADS motif. This results in a bistable system which can adopt either a low PP2A, high Gwl state (mitosis) or a high PP2A, low Gwl state (mitotic exit) (Figure 2.15A).

The transition between these states requires an upstream cell cycle signal. This is provided by the CDK-dependence of Gwl phosphorylation. During mitosis, high CDK activity keeps Gwl in its active phosphorylated state. When CycB levels decline following APC/C^{Cdc20} activation at M/A, this reduces Gwl activity, allowing PP2A:B55 to overcome inhibition by p-ENSA and promote mitotic exit. This creates a bistable transition between the mitosis and mitotic exit states as a function of the decreasing Cdk1:CycB 'Wait' signal (Figure 2.15B).

As described above, the BEG pathway controlling mitotic exit corresponds exactly to the generic FADS motif set out previously. Note however that the 'modification' catalysed by the activator in this case is dephosphorylation, so that $[\mathrm{pENSA}]$ and $[\mathrm{pGwl}]$

correspond to [I] and [$\hat{\mathrm{R}}$], while [ENSA] and [Gwl] correspond to [$\mathrm{I_M}$] and [$\hat{\mathrm{R}}_\mathrm{M}$] in the generic model. This gives the following series of ODEs:

$$\frac{d[\mathrm{B55:pENSA}]}{dt} = k_{ass} \cdot [\mathrm{pENSA}] \cdot [\mathrm{B55}] - (k_{dis} + k_{cat}) \cdot [\mathrm{B55:pENSA}] \tag{2.27}$$

$$\frac{d[\mathrm{ENSA}]}{dt} = k_{cat} \cdot [\mathrm{B55:pENSA}] - k_{pENSA} \cdot [\mathrm{Gwl}] \cdot [\mathrm{ENSA}] \tag{2.28}$$

$$\frac{d[\mathrm{pGwl}]}{dt} = k_{pGwl} \cdot Cdk1 \cdot [\mathrm{Gwl}] - k_{dpGwl} \cdot [\mathrm{B55}] \cdot [\mathrm{pGwl}] \tag{2.29}$$

Where:

$$\begin{aligned} [\mathrm{pENSA}] &= ENSA_T - [\mathrm{ENSA}] - [\mathrm{B55:pENSA}] \\ [\mathrm{B55}] &= B55_T - [\mathrm{B55:pENSA}] \\ [\mathrm{Gwl}] &= Gwl_T - [\mathrm{pGwl}] \end{aligned} \tag{2.30}$$

This is reduced to a two-ODE system by making a pseudo–steady-state approximation for [B55 : pENSA]:

$$\begin{aligned} [\mathrm{B55:pENSA}] = 0.5 \cdot (&B55_T + [\mathrm{pENSA_T}] + K_M \\ &- \sqrt{(B55_T + [\mathrm{pENSA_T}] + K_M)^2 - 4 \cdot B55_T \cdot [\mathrm{pENSA_T}]}) \end{aligned} \tag{2.31}$$

Where:

$$[\mathrm{pENSA_T}] = ENSA_T - [\mathrm{ENSA}] \tag{2.32}$$

2.4 Discussion

We have identified a conserved regulatory motif (FADS) present at three different cell cycle transitions. This motif uses a tight-binding stoichiometric inhibitor to generate an ultrasensitive relationship between inhibitor concentration and the modification of substrates of the target enzyme. The stoichiometric inhibitor is itself a target of the enzyme, and so we describe it as a 'Domineering Substrate'. Given the presence of this ultrasensitive response, it is possible to generate a bistable switch by the addition of a feedback amplification loop. In the motif we have identified this occurs via the inhibitory action of the cell cycle activator on the regenerating enzyme, creating a double-negative

feedback loop.

2.4.1 Alternative models for cell cycle transitions

Although we describe the role of the FADS motif at multiple cell cycle transitions, we by no means claim that all cell cycle transitions proceed exclusively via a FADS mechanism. We only claim that it is a simple yet robust mechanism for generating such a transition. Other mechanisms besides domineering substrates can be used to generate ultrasensitivity, and other network motifs featuring domineering substrates can incorporate the necessary positive feedback for bistability without involving direct action of the cell cycle activator on a regenerating enzyme.

Bistability without a domineering substrate

Other cell cycle transitions use alternative mechanisms to generate the non-linear or ultrasensitive response necessary for bistability. For example, the Start transition in budding yeast uses multi-site CDK-dependent phosphorylation of Whi5, an inhibitor of the SBF transcription factor, to generate ultrasensitivity [237, 238]. Bistability is generated by coupling this ultrasensitivity with positive feedback loops involving inhibitory phosphorylation of Cdk1 by Wee1 and dephosphorylation by Cdc25.

Another example occurs at the G1/S transition in budding yeast. While we have described this motif as occurring via a FADS motif involving Cdk1:Clb5, Sic1 and Swi5, additional regulation via mutual antagonism between Cdk1:Clbs and APC/C^{Cdh1} may also contribute, since this creates a positive feedback loop, and can also potentially generate non-linearity via a SIMM motif [225].

This second example also shows that rather than the FADS motif (or any other motif) necessarily existing in isolation, that multiple signalling motifs can be combined in a modular way. These additional regulatory motifs can provide increased robustness, tune the response to achieve a specific timing of cell cycle events, or integrate a core cell cycle transition motif with other cellular signalling pathways.

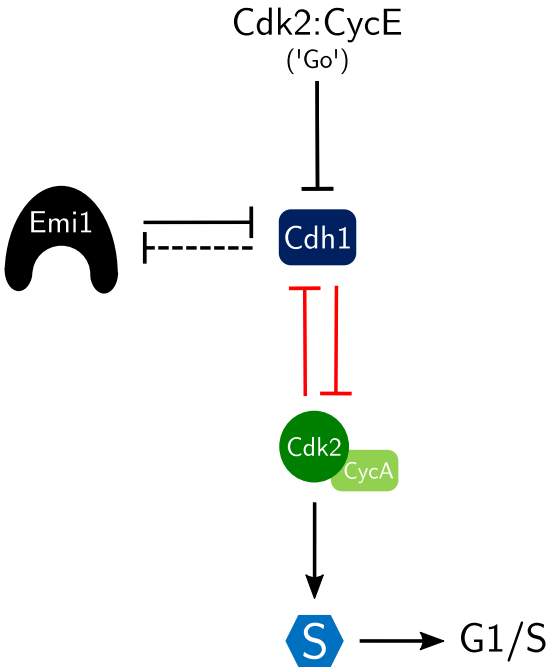

Figure 2.16: Influence diagram for Emi1/Cdh1/Cdk2:CycA model of the G1/S transition. The positive feedback loop between Cdh1 and Cdk2:CycA is highlighted in red. Dashed bar between Emi1 and Cdh1 indicates that this interaction does not comprise a true double-negative feedback loop.

Domineering substrates without a FADS motif: Cdh1 and Emi1

Although we have highlighted examples of cell cycle transitions where a domineering substrate is coupled to a positive feedback loop via inhibition of its regenerating enzyme, in principle any network structure involving both a domineering substrate and a positive feedback loop is potentially bistable.

As an example of such an alternative case, we consider the regulation of APC/C^{Cdh1} activity by Emi1 at the G1/S transition in mammals. The resulting network structure is shown in Figure 2.16. APC/C^{Cdh1} is active during G1, where it maintains low CDK activity by promoting ubiquitin-mediated cyclin degradation. Following the G1/S transition, Cdk2 activity phosphorylates Cdh1 and prevents it from activating APC/C, thus creating a double-negative feedback loop between APC/C^{Cdh1} and Cdk2:Cyclin complexes. In addition to this phospho-regulation, Cdh1 is also inhibited by Emi1 binding. Levels of Emi1 are low in G1, but rise during the G1/S transition.

Recently it has been shown that Emi1 is not only an inhibitor of APC/C^{Cdh1}, but also a substrate [74]. While the authors of that paper propose a model based on poly-ubiquitination of Emi1 and distinct catalytic and inhibitory binding sites for Emi1 on

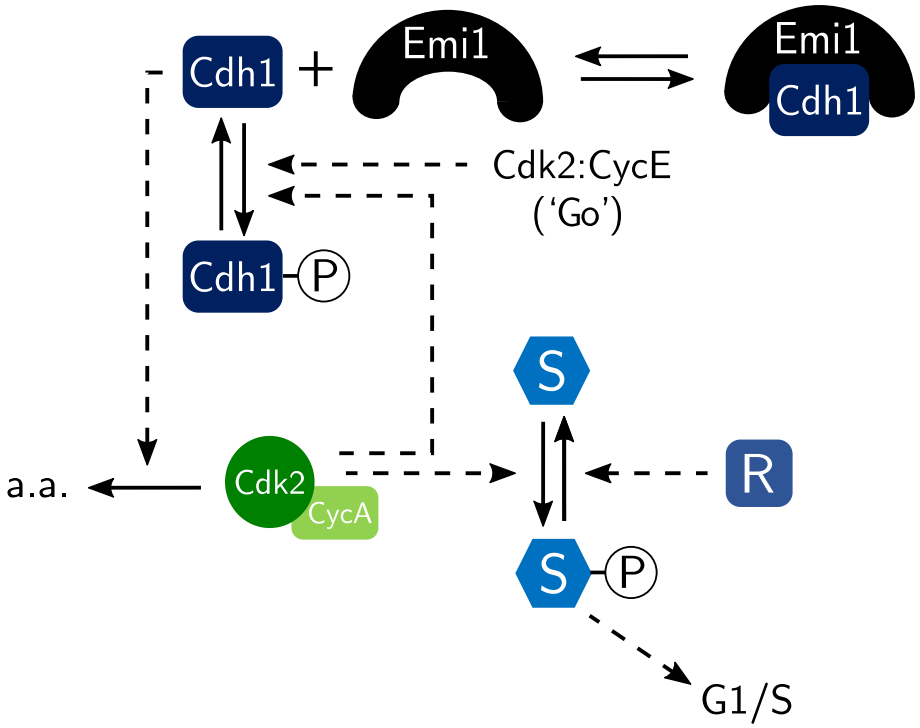

Figure 2.17: Wiring diagram for Emi1/Cdh1/Cdk2:CycA model of the G1/S transition. Solid arrows indicate biochemical reactions, dashed arrows indicate rate enhancement of the targeted reaction. Arrows to 'a.a.' (amino acids) indicate Cyclin A degradation. Note that Cdk2:CycA binding is not explicitly modelled and CycA is used as a proxy for Cdk2:CycA activity in the model.

Cdh1, we propose that a simpler model can also produce a bistable G1/S transition by treating Emi1 as a simple domineering substrate with a single binding site on Cdh1.

The wiring diagram for our model is shown in Figure 2.17. The principles of the model are much the same as those of the generic FADS motif, with the exception that the 'activator' of the G1/S transition, Cdk2:CycA, is not the component subject to inhibition by a domineering substrate. Instead, the domineering substrate (Emi1) acts on an inhibitor of the activator (Cdh1). Feedback amplification occurs not through the action of Cdk2 on a regenerating enzyme for Emi1, but instead on Cdh1, its own inhibitor. Nevertheless, the role of Emi1 as a domineering substrate is essential to provide the non-linearity necessary to generate a bistable cell cycle transition.

A phaseplane and bifurcation diagram for this model are shown in Figure 2.18, showing that the system is able to produce an irreversible, bistable transition between G1-phase (low $[\text{Emi1}_T]$) and S-phase (high $[\text{Emi1}_T]$). Notably the phaseplane is qualitatively different to those from the transitions modelled using the standard FADS motif. [CycA] is bistable as a function of $[\text{Emi1}_T]$. This occurs because the positive feedback loop is

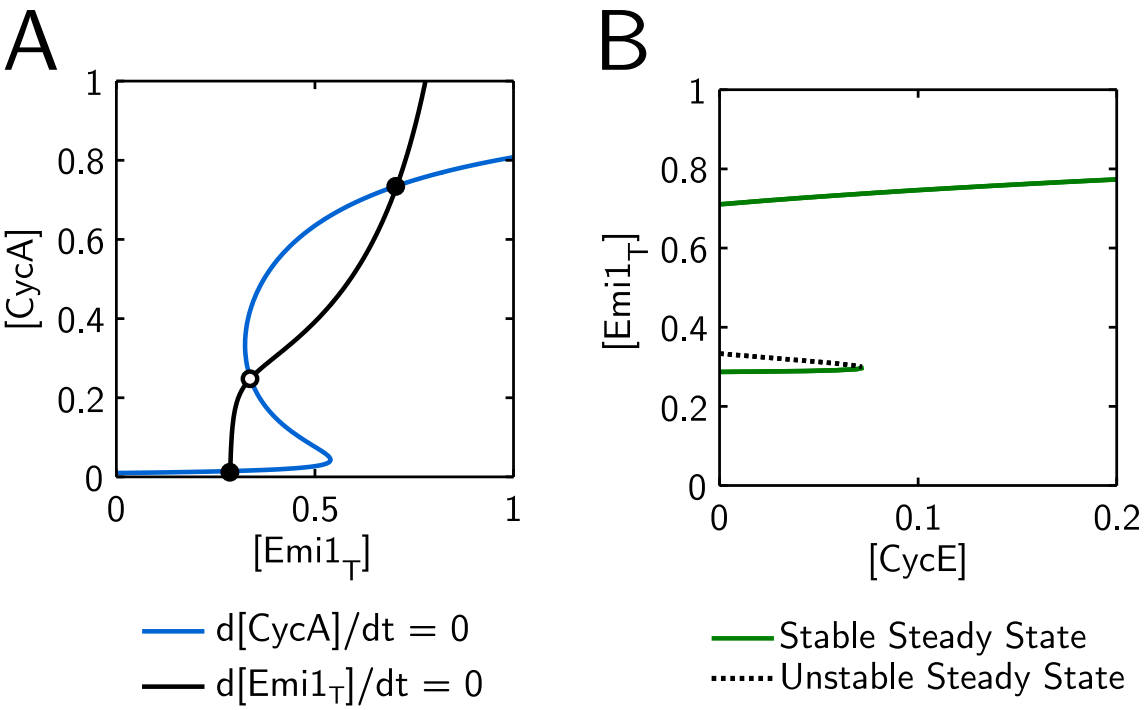

Figure 2.18: (A) Phaseplane diagram for G1/S domineering substrate model. (B) Bifurcation diagram for G1/S domineering substrate model, showing steady state [Emi1$_T$] as a function of [CycE], the upstream 'Go' signal.

external to the two variables used to plot the bifurcation diagram. Nevertheless, the bifurcation diagram shows that these differences to the underlying network structure are still able to construct a robust bistable transition responding to changes in an upstream cell cycle signal.

2.4.2 Domineering Substrates alone do not produce a positive feedback loop

One question that might arise from an initial examination of the FADS motif in Figure 2.4, is why the feedback amplification loop is necessary. A bistable transition requires both an ultrasensitive response and a positive (or double-negative) feedback loop, and from inspection of the influence diagram, the domineering substrate appears to provide both. The inhibitor (I) inhibits the activator (A) through stoichiometric binding, while the activator inhibits the inhibitor through post-translational modification, creating an apparent double-negative feedback loop.

However, although the activator and inhibitor are mutually inhibitory, this is not sufficient to produce a double-negative feedback loop. The reason for this is that inactivation

of the inhibitor by the activator proceeds entirely from the A:I complex. Therefore the maximum rate of inhibitor inactivation occurs when the concentration of A:I is at its highest, i.e. the point at which the activator is subject to most inhibition. As the level of free A increases, this corresponds to a decrease, not an increase, in the rate of inhibitor inactivation, since there is no longer so much A:I complex for inhibitor inactivation. For a true double-negative feedback loop, this would require that as the level of free A increased, the rate of I inactivation also increases, and that as the level of I increased, the rate of inactivation decreases. In fact the reverse is true, and so the system does not provide the positive feedback that would be necessary for bistability.

We can test these theoretical considerations using the CRNT toolbox (freely available from https://crnt.osu.edu/CRNTWin) [239]. We create a network comprising the following reactions, representing the core domineering substrate mechanism:

$$A + I \longleftrightarrow AI \tag{2.33}$$

$$AI \longrightarrow A + I_M \tag{2.34}$$

$$I_M \longrightarrow I \tag{2.35}$$

Using the toolbox to analyse this network confirms that it cannot generate a bistable system with multiple positive steady states for any values of the kinetic parameters. In contrast, if we add in the following reactions to complete the feedback amplification loop, the toolbox analysis confirms that this reaction network does admit the existence of multiple steady states (i.e. bistability) for certain parameter values.

$$A + \hat{R} \longleftrightarrow A + \hat{R}_M \tag{2.36}$$

$$\hat{R}_M \longrightarrow \hat{R} \tag{2.37}$$

Thus both the domineering substrate and the feedback amplification loop are required for the bistability of the FADS motif.

2.4.3 Evolution of the FADS motif

A key attraction of the domineering substrate mechanism for modelling bistable cell cycle transitions is the simplicity of the resulting model. The major assumption required is the tight binding of the domineering substrate to its target enzyme. This contrasts to alternative mechanisms for generating ultrasensitivity, for example multiple-modification of substrates, or a high level of co-operativity between binding sites on a multimeric enzyme. In these cases, a more complicated model is typically required to describe multiple sequential binding reactions, each with different kinetic parameters. While such methods can produce good results, and can often be backed by experimental observations from the system in question, the kinetic properties they require of these reactions are specific and complex, so are less suitable to use as an *a priori* assumption about an unknown system.

By analogy, since domineering substrates can be used to create a simple mathematical model of a cell cycle transition, this same simplicity may suit their adoption by natural selection to evolve a bistable cell cycle transition. We propose that this could happen in the following manner.

We would expect that a bistable cell cycle transition should evolve from a simpler system which is not bistable. While bistability provides robustness and irreversibility to the system, it is not essential for a cell to undergo a transition. Such a simple system could comprise a single cell cycle activator, the activity of which is responsive to an upstream cell cycle signal. Modification of substrates by the activator in response to this signal would promote transition to the next stage of the cell cycle.

The potential problem with this system is that there is no way to delay the cell cycle transition in response to cellular events. The cell therefore risks entering into the next cell cycle stage before the events of the previous stage have been completed. The next evolutionary step could therefore be to reduce this risk, either by creating a time-delay mechanism to provide more time during which cell cycle events can be completed, or by creating a cell cycle checkpoint, explicitly linking progression into the next cell cycle stage with completion of upstream events. In both cases, a stoichiometric inhibitor can be used to slow cell cycle progression, coupling the successful completion of stage-specific

events with transition to the next cell cycle stage.

One possible method of action of a competitive stoichiometric inhibitor is to bind directly to the active site of its target enzyme, preventing the binding of alternative substrates. Evolution of such an inhibitor could naturally proceed from an existing substrate of the enzyme, since this will already possess the ability to bind to the enzyme active site. Point mutations which favour tight binding at the expense of efficient catalysis and product release could then adjust the kinetic properties of the substrate so that it behaves more like a pure competitive inhibitor. The presence of this inhibitor can provide a time-delay during which cell cycle events associated with the pre-transition cell cycle state can occur, while the retained ability of the enzyme to inactivate the inhibitor ensures that transition to the next cell cycle stage is not blocked indefinitely.

The final step to add additional robustness to the system is to generate a feedback amplification loop, whereby the system evolves so that the cell cycle activator gains the capacity to modify and inactivate the regenerating enzyme responsible for synthesis or de-modification of the stoichiometric inhibitor. Once this occurs, the transition has the potential to be bistable for a certain range of kinetic parameters.

Thus we have outlined how at each step, sequential addition of single components or interactions can lend additional robustness to a primitive cell cycle transition, finally culminating in a FADS motif. We suggest that the three cell cycle transitions we have described in this chapter may represent separate occasions where natural selection has adopted this motif. In each case, the activator/domineering substrate pairing uses an entirely different post-translational modification, strongly suggesting that this is convergent evolution towards a simple and efficient design, rather than the divergent evolution of a proto-FADS motif to give rise to the different transitions.

2.4.4 Other FADS Motifs

Considering the widespread applicability of domineering substrates in general, and the FADS motif in particular, in cell cycle regulation, it is worth considering whether the same principles may be applicable elsewhere in biology. The idea that an enzyme substrate with high affinity but poor turnover can act as an inhibitor towards other substrates

is not unique to the cell cycle. A non–cell-cycle example of a domineering substrate is the inhibition of myosin light-chain phosphatase (MLCP) by the phosphorylated inhibitor pCPI-17 during muscle contraction, and the subsequent dephosphorylation of the inhibitor by MLCP during muscle relaxation [240]. Other examples almost certainly exist in other biological regulatory systems, but these are difficult to identify from a standard literature search given the frequency of the terms 'substrate' and 'inhibitor' in biochemical and pharmacological contexts.

It remains to be seen whether a non–cell-cycle example of a FADS motif exists, but the utility of bistable switches for generating robust transitions between distinct regulatory states means that they could well play a useful role in contexts such as development or gene regulation.

2.5 Conclusion

The cell cycle comprises a series of distinct stages, during which the events of DNA replication, chromosome segregation and cell division must occur in a highly ordered sequence. Robust and irreversible transitions between these stages are required to ensure that each stage occurs once and only once in sequence. Bistable transitions provide both robustness and irreversibility, since the level of signal needed to activate the transition is higher than the level at which it will revert to the pre-transition state. This provides a critical window where the system will remain in the post-transition state despite changes in the input signal. This makes the system robust to stochastic fluctuations in signal strength around the transition point, as well as to programmed shutting off of upstream signals in response to later cell cycle events.

However, creating a bistable system is a potentially difficult problem for evolution to solve. Bistability requires a non-linear (ultrasensitive) signal-response curve, coupled to a positive feedback loop. Our proposed FADS motif provides one possible mechanism by which such a system could evolve. A cell cycle activator can be regulated by a stoichiometric inhibitor, itself evolving from a substrate molecule which is selected for higher affinity (lower K_M) but lower k_{cat} relative to other substrates. This provides a simple and evolutionarily accessible mechanism for developing an ultrasensitive switch,

which can function as a simple cell cycle transition. The additional robustness provided by bistability can then be accessed by completing the feedback amplification loop between the cell cycle activator and the regenerating enzyme responsible for inhibitor production or activation.

This trio of cell cycle activator, domineering substrate, and regenerating enzyme, coupled together in the form of a FADS motif, can be seen at multiple eukaryotic cell cycle transitions. It provides a simple mechanism for generating a robust bistable toggle switch, which nevertheless retains the ability to rapidly transition from one stage to the next when required.

Chapter 3

CDK-dependence of APC/C^{Cdc20} activity in mitosis

3.1 Introduction

The work in this chapter is the result of a collaboration with experimentalists in the labs of Ulrike Gruneberg (Dunn School of Pathology, University of Oxford) and Francis Barr (Department of Biochemistry, University of Oxford), and Section 3.2 forms the basis of a co-authored manuscript (Hayward et al.) [241] published in the Journal of Cell Biology in January 2019.

In this chapter we present several models for CDK-dependence of APC/C^{Cdc20} activity. As discussed in the introduction, CDK activity has a variety of effects on APC/C^{Cdc20} (Figure 1.5):

- CDK requirement for mitotic checkpoint licensing
- Activatory phosphorylation of APC/C core
- Inhibitory phosphorylation of Cdc20

Since CDK activity is itself inversely dependent on APC/C^{Cdc20} activity due to APC/C-dependent cyclin degradation, these interactions have the potential to generate positive and negative feedback loops between CDK and APC/C. We discuss the implications of these feedback loops with reference to two sets of experimental data. Firstly, the CDK-dependence of the mitotic checkpoint is discussed using data identifying an essential CDK and PP2A:B55 target site on the MPS1 kinase. Secondly, CDK-dependent phosphorylation of Cdc20 is discussed in the context of data suggesting a checkpoint-independent acceleration of APC/C substrate degradation following CDK inhibition. Finally, the

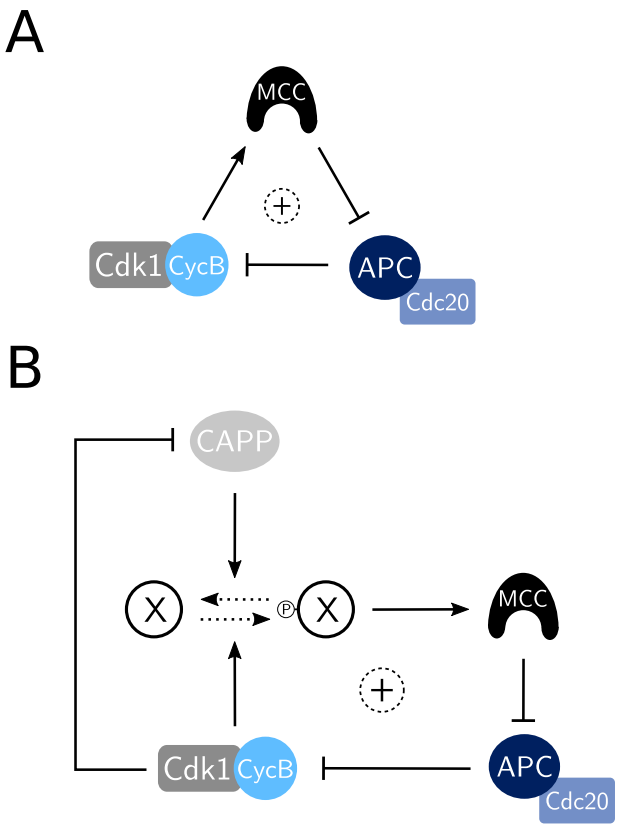

Figure 3.1: Generic SAC influence diagrams. Solid arrows: activatory interactions. Solid bars: inhibitory interactions. Dotted arrows: direct interconversion between species. Positive feedback loops are indicated by a circled '+' at the centre of the loop. CAPP: Counter-acting protein phosphatase. (A) Core SAC double-negative feedback loop. (B) Simplified influence diagram for the He et al. model [242].

implications of the simultaneous activatory and inhibitory roles that CDK activity has on APC/C^{Cdc20} via phosphorylation of the APC/C core and its Cdc20 co-activator are modelled and discussed.

3.2 CDK-dependent phosphorylation of MPS1

The MPS1 kinase is essential for SAC signalling at the kinetochore, and forms a core part of the detection mechanism for KT:MT attachment (see Section 1.4.3). Work by collaborators in the Gruneberg and Barr labs has identified that CDK phosphorylation of MPS1 is essential for its kinetochore localisation. Here we present a model describing the implications of this interaction for the robustness and irreversibility of mitotic checkpoint inactivation at M/A. Experimental and some modelling figures, and the model description in Section 3.2.2, are adapted from the joint manuscript produced from this collaboration [243].

3.2.1 Cdk1-dependence of the SAC

The CDK-dependence of the SAC is well established (see Section 1.4.5), however the mechanism by which this is achieved remains an open question. The existence of this interaction creates a positive feedback loop between APC/C, CDK and the MCC (Figure 3.1A). A previously published SAC model by **He et al.** [242] proposed that irreversibility could be the consequence of an unspecified CDK target present at unattached kinetochores (X), which was dephosphorylated by a CDK-inhibited counteracting phosphatase (CAPP, Figure 3.1B). This network motif creates a double-negative feedback loop between Cdk1:CycB, the MCC, and APC/C. Tight binding between MCC and APC/C generates the non-linearity required to produce a bistable cell cycle transition (in effect the model operates as an extended version of the FADS motif described in Section 2.3.2). One limitation of this model was that the identity of the CDK target within the SAC was unknown, limiting the ability to test the model and to provide specific predictions about checkpoint function.

Here we describe experiments performed by collaborators in the Gruneberg and Barr labs which have identified the checkpoint kinase MPS1 as a suitable candidate for the CDK-dependent SAC target. The counteracting phosphatase is identified as PP2A:B55. We use these results to develop a model of the SAC, with which we can further analyse the dynamic behaviour of the checkpoint.

3.2.2 Model Description

The mathematical model is an updated version of the He et al. model [242], supplemented with the B55-ENSA-Gwl pathway [179]. The unified model consists of an MPS1 and an APC/C regulatory module (Figure 3.2). The phosphorylation state and kinetochore localization of MPS1 is regulated by Cdk1:CycB and its counteracting phosphatase PP2A:B55, whose activity is controlled by the CDK-dependent Gwl-ENSA pathway. APC/C is regulated by MCC, which binds and inhibits APC/C-dependent degradation of CycB and is itself inactivated by APC/C activity.

The two modules are coupled in a mutually inhibitory relationship. The APC/C module inhibits the input of the MPS1 module (CDK1) through APC/C-dependent

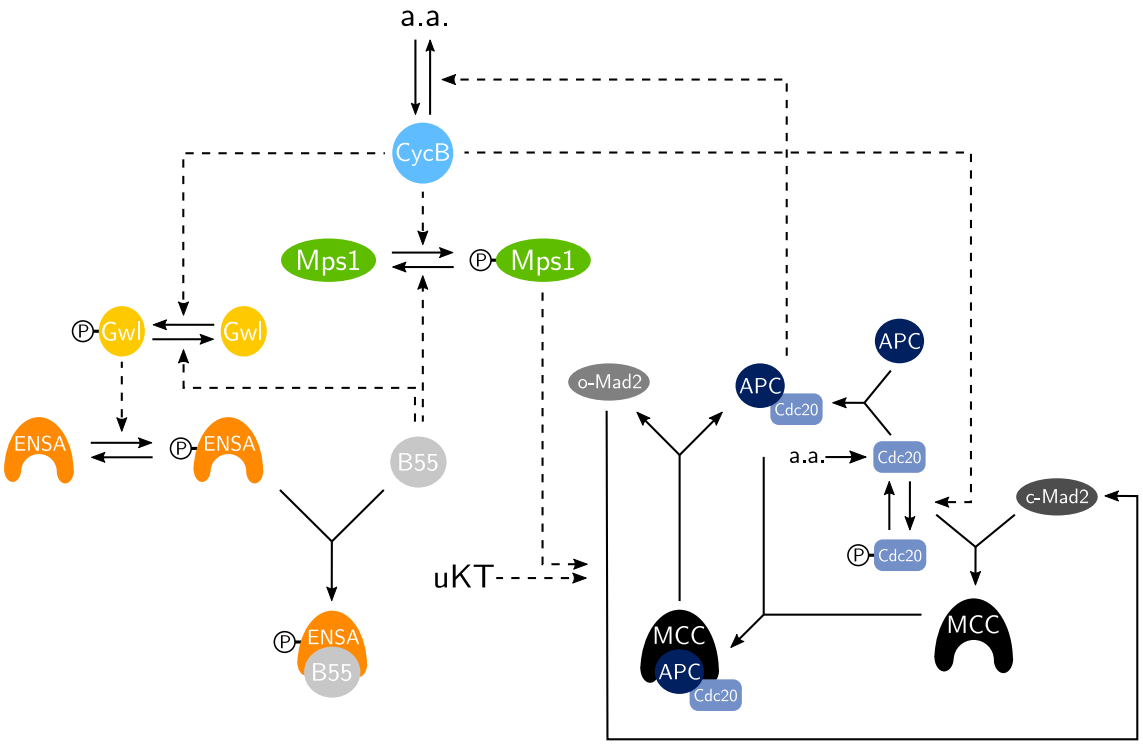

Figure 3.2: Wiring diagram for SAC model. Solid arrows indicate biochemical reactions, dashed arrows indicate rate enhancement of the targeted reaction. Arrows to or from 'a.a.' indicate protein degradation and synthesis respectively.

CycB degradation. In return, the output of the MPS1 module (pMPS1) inhibits APC/C through activation of MCC assembly. The strength of this inhibition is determined by the fraction of unattached kinetochores (uKT). This antagonism between the two modules creates two mutually exclusive states: checkpoint arrest (high pMPS1 and CycB, inactive PP2A:B55 and APC/C^{Cdc20}) and mitotic exit (inverse conditions).

We assume that the level of Cdk1:CycB and APC/C^{Cdc20} complexes is limited by their regulatory subunits CycB and Cdc20 respectively, so these names are used in the model equations to denote the entire complex. The synthesis of CycB is CDK-dependent, while Cdc20 synthesis is constant. Both CycB and Cdc20 are degraded in an APC/C- and proteasome- (Psome) dependent manner. Gwl and ENSA are phosphorylated by Cdk1 and Gwl respectively, and dephosphorylated by both PP2A-B55-dependent and -independent reactions. Formation of active c-Mad2 (Mad2a) from inactive o-Mad2 is catalysed by pMPS1-bound unattached kinetochores ($pMps1_{KT}$). Mad2a associates with free Cdc20 (Cdc20f) into MCC. Free Cdc20 undergoes CDK-dependent inhibitory phosphorylation, and only the dephosphorylated form can bind and activate APC/C (this interaction is discussed in more detail in Section 3.3). Free MCC (containing Cdc20)

binds to APC/C^{Cdc20}, so their complex (MCCAPC) contains two molecules of Cdc20. APC/C^{Cdc20} promotes the disassembly of MCC by proteasome-dependent degradation of $Cdc20_M$. This MCC disassembly is accompanied by inactivation of Mad2.

Kinetics and Parameter Selection

An ODE model of the system described above was created using exclusively mass-action kinetics:

ODEs

$$\begin{aligned}\frac{d[\mathrm{CycB}]}{dt} &= ks_{cyc} + ks2_{cyc} \cdot [\mathrm{Cdk1}] \\ &\quad - (kd2_{cyc} + kd_{cyc} \cdot Psome \cdot [\mathrm{Cdc20}]) \cdot [\mathrm{CycB}]\end{aligned} \tag{3.1}$$

$$\begin{aligned}\frac{d[\mathrm{pMps1}]}{dt} &= k_{an} \cdot [\mathrm{Cdk1}] \cdot ([\mathrm{Mps1_T}] - [\mathrm{pMps1}]) \\ &\quad - k_{in} \cdot ([\mathrm{B55}] + PP) \cdot [\mathrm{pMps1}]\end{aligned} \tag{3.2}$$

$$\begin{aligned}\frac{d[\mathrm{pENSA_T}]}{dt} &= kp_{ENSA} \cdot [\mathrm{pGwl}] \cdot ([\mathrm{ENSA_T}] - [\mathrm{pENSA_T}]) \\ &\quad - kdp_{ENSA} \cdot [\mathrm{ENSAB55}] \\ &\quad - k_{inact} \cdot ([\mathrm{pENSA_T}] - [\mathrm{ENSAB55}])\end{aligned} \tag{3.3}$$

$$\begin{aligned}\frac{d[\mathrm{Mad2a_T}]}{dt} &= ka_{mad} \cdot [\mathrm{pMps1}] \cdot \mathrm{uKT} \cdot [\mathrm{Mad2i}] \\ &\quad - ki_{mad2} \cdot [\mathrm{Mad2a_T}] - k_{cat} \cdot Psome \cdot [\mathrm{Comp}]\end{aligned} \tag{3.4}$$

$$\begin{aligned}\frac{d[\mathrm{MCC_T}]}{dt} &= kas1 \cdot [\mathrm{Mad2a}] \cdot [\mathrm{Cdc20f}] \\ &\quad - (kdi1 + ki_{mad2} + kd_{20}) \cdot [\mathrm{MCC_T}] \\ &\quad - k_{cat} \cdot Psome \cdot [\mathrm{Comp}]\end{aligned} \tag{3.5}$$

$$\begin{aligned}\frac{d[\mathrm{Comp}]}{dt} &= kas2 \cdot [\mathrm{MCC}] \cdot [\mathrm{Cdc20}] \\ &\quad - (kdi2 + kdi1 + ki_{mad2} + 2 \cdot kd_{20} + k_{cat} \cdot Psome) \cdot [\mathrm{Comp}]\end{aligned} \tag{3.6}$$

$$\begin{aligned}\frac{d[\mathrm{pGwl}]}{dt} &= ka_{gw} \cdot [\mathrm{Cdk1}] \cdot (Gwl_T - [\mathrm{pGwl}]) \\ &\quad - (ki_{gw2} + ki_{gw} \cdot [\mathrm{B55}]) \cdot [\mathrm{pGwl}]\end{aligned} \tag{3.7}$$

$$\frac{d[\mathrm{Cdc20_T}]}{dt} = ks_{20} - kd_{20} \cdot [\mathrm{Cdc20_T}] - k_{cat} \cdot Psome \cdot [\mathrm{Comp}] \tag{3.8}$$

$$\frac{d\mathrm{uKT}}{dt} = -attach \cdot \mathrm{uKT} \tag{3.9}$$

Algebraic equations

$$[\mathrm{Mad2i}] = Mad2_T - [\mathrm{Mad2a_T}] \tag{3.10}$$

$$[\mathrm{Mad2a}] = [\mathrm{Mad2a_T}] - [\mathrm{MCC_T}] \tag{3.11}$$

$$[\mathrm{MCC}] = [\mathrm{MCC_T}] - [\mathrm{Comp}] \tag{3.12}$$

$$[\mathrm{Cdk1}] = \frac{[\mathrm{CycB}] + \epsilon}{1 + ki_{CDK}} \tag{3.13}$$

$$[\mathrm{Cdc20f}] = [\mathrm{Cdc20_T}] - [\mathrm{MCC_T}] - [\mathrm{Comp}] \tag{3.14}$$

$$[\mathrm{Cdc20}] = \frac{[\mathrm{Cdc20f}]}{1 + \alpha \cdot [\mathrm{Cdk1}]} \tag{3.15}$$

$$\mathrm{BB} = [\mathrm{pENSA_T}] + B55_T + \frac{k_{dis} + kdp_{ENSA}}{kass} \tag{3.16}$$

$$[\mathrm{ENSAB55}] = \frac{2 \cdot [\mathrm{pENSA_T}] \cdot B55_T}{\mathrm{BB} + \sqrt{\mathrm{BB}^2 - 4 \cdot [\mathrm{pENSA_T}] \cdot B55_T}} \tag{3.17}$$

$$[\mathrm{B55}] = B55_T - [\mathrm{ENSAB55}] \tag{3.18}$$

Parameter estimation was performed by fitting to mitotic exit experiments with three different conditions (Figure 3.3). All of the rate constants have a dimension of min^{-1}, because the dynamic variables representing concentrations are expressed on a relative scale in the model, so the concentration units are arbitrary.

3.2.3 Population Level Simulations

As discussed in the introduction (Section 1.6.1), deterministic ODE simulations are not able to reproduce the diversity of responses observed in a cell population. For example, Figure 3.5A shows the cumulative frequency of mitotic exit with time for different cell populations, whereas a deterministic simulation would describe a uniform time of mitotic

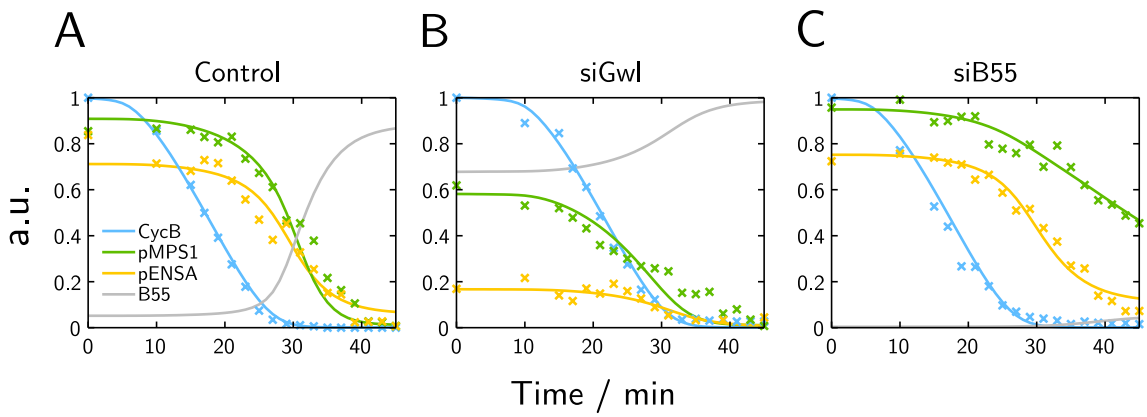

Figure 3.3: Experimental data (x) and model simulations (solid lines) of MPS1 dephosphorylation kinetics measured by mass spectrometry, under Control (A), Gwl siRNA ($Gwl_T = 0.1$) (B) or B55 siRNA ($B55_T = 0.2$) (C) conditions. MS experiments performed by Mike Cundell and James Holder, MS data analysis by Lukas Hutter and Francis Barr; figure adapted from [243] (DOI: 10.1083/jcb.201808014) under a Creative Commons 4.0 License (`https://creativecommons.org/licenses/by/4.0/`).

exit, which could at best be interpreted as the average response of the cell population. For this reason, population-level simulations are used to approximate random variation in the cell population. In this case, we use a lognormal distribution to select values for relevant initial conditions and parameter values, since this avoids the selection of non-zero values which would be nonsensical and could prevent correct simulation of the model.

3.2.4 CDK and PP2A:B55 regulate SAC activity

The first series of experiments used for developing the model above involved identifying MPS1 S281 as a CDK target required for SAC activity. The counteracting phosphatase was also identified as PP2A:B55.

Inhibition of CDK activity prevents checkpoint reactivation during MG132 arrest

The CDK-dependence of SAC activity has previously been demonstrated by observing the behaviour of cells arrested by the proteasome inhibitor MG132 in the presence of nocodazole [146]. MG132 does not interfere with spindle formation or chromosome alignment, but prevents proteasome-dependent degradation of CycB and securin following APC/C activation. As a result, cells arrest in metaphase with a fully-formed mitotic spindle (Figure 3.4A). Since KT:MT attachments are correctly formed, the SAC

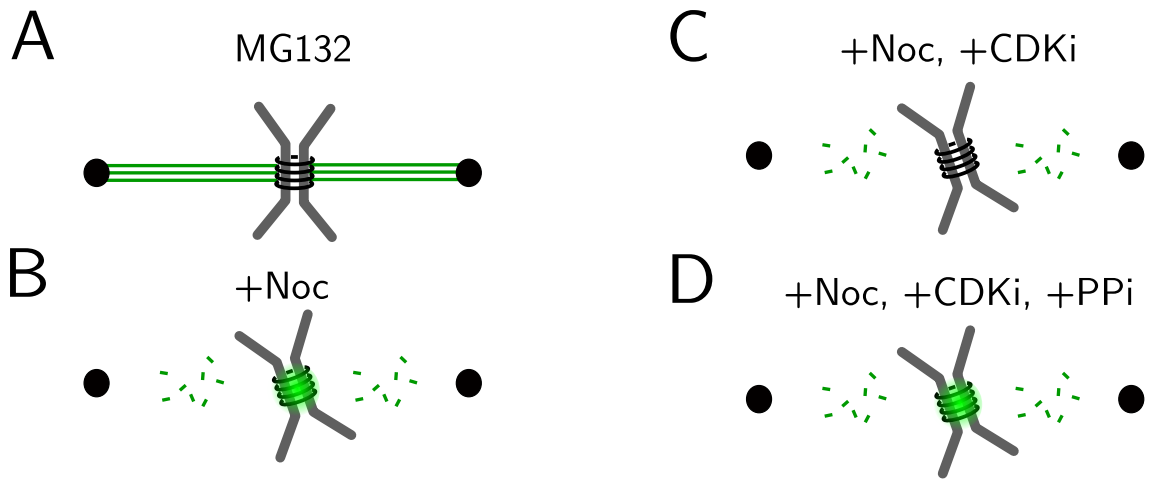

Figure 3.4: Schematic of SAC licensing experiment. MG132 arrests cells in metaphase with bioriented chromosomes (A). Application of nocodazole causes MT depolymerisation and activation of the SAC (Mad2-GFP to kinetochore) (B), but this effect is reversed by CDK inhibition (+CDKi), (C). In the presence of phosphatase inhibitor (+PPi), Mad2-GFP returns to the kinetochore (D)

is satisfied, which can be observed by the absence of fluorescence-labelled checkpoint proteins from the kinetochore. However, under these conditions, addition of nocodazole to disrupt KT:MT interactions results in checkpoint reactivation and relocalisation of SAC components to the kinetochore (Figure 3.4B).

This MG132-arrest system can be used as an assay for SAC function. Application of the CDK inhibitor flavopiridol (+CDKi) alongside nocodazole (+Noc) is sufficient to prevent SAC reactivation, suggesting that CDK activity is required to maintain SAC activity (Figure 3.4C). This is in agreement with the He et al. model, providing evidence for the existence of a double-negative feedback loop between CDK activity and APC/C via CDK-dependence of SAC signalling.

PP2A:B55 is the counteracting phosphatase for CDK-dependent SAC activity

Collaborators in the Gruneberg and Barr labs have extended the MG132 SAC assay experiments from reference [146] to additionally consider the role of counteracting phosphatases. In these new experiments, SAC activation is measured by localisation of GFP-Mad2 to kinetochores. Addition of a broad-spectrum inhibitor of PP1 and PP2A (+PPi) alongside flavopiridol prevented disruption of SAC signalling (Figure 3.4D). Further experiments showed that knockdown of the PP2A co-activator B55, but not PP1, was able to maintain SAC signalling in the presence of flavopiridol.

MPS1 S281 dephosphorylation kinetics suggest it is a CDK and PP2A:B55 target in the SAC

Having shown that B55 counteracts the CDK-dependence of the SAC, a proteomic Mass Spectrometry (MS) analysis of mitotic phosphatase targets identified **MPS1 S281** as a suitable candidate for B55-dependent dephosphorylation. The MS data provided timecourses of MPS1 S281 phosphorylation in WT cells, and in RNA knockdowns of B55 and Gwl, slowing and accelerating dephosphorylation kinetics respectively (Figure 3.3).

Since B55 is indirectly subject to inhibition from CDK activity (via CDK activation of Gwl), this makes MPS1 a suitable candidate for a CDK target in the SAC pathway which is dephosphorylated by a CDK-inhibited phosphatase, equivalent to the chromosomal target 'X' originally postulated in the He et al. model. These experiments therefore prompted the development of a new SAC model by adapting the He et al. model to take into account the specific regulation of MPS1 by CDK- and B55-dependent phosphorylation and dephosphorylation (See Section 3.2).

The mass spectrometry timecourses were used to guide parameter selection for the new model, and the resulting fit of the model to the experimental data is shown by the solid lines in Figure 3.3. The chosen parameters are used for all other simulations described in this section.

S281A mutants show shortened mitotic duration

Non-phosphorylable MPS1 S281A and phospho-mimetic S281D mutants were created to characterise further the effects of phosphorylation at this site. Experimentally, S281A mutants show shortened mitotic duration compared to both control and S281D cells (Figure 3.5A), consistent with a role for phosphorylation at this site in promoting SAC activity and hence delaying exit from mitosis during chromosome alignment. Using the model, we were able to reproduce these effects by using parameter changes to simulate either non-phosphorylable MPS1 S281A ($k_{an} = 0$), or constitutively active MPS1 S281D ($k_{in} = 0$) in a population-level simulation (Figure 3.5B).

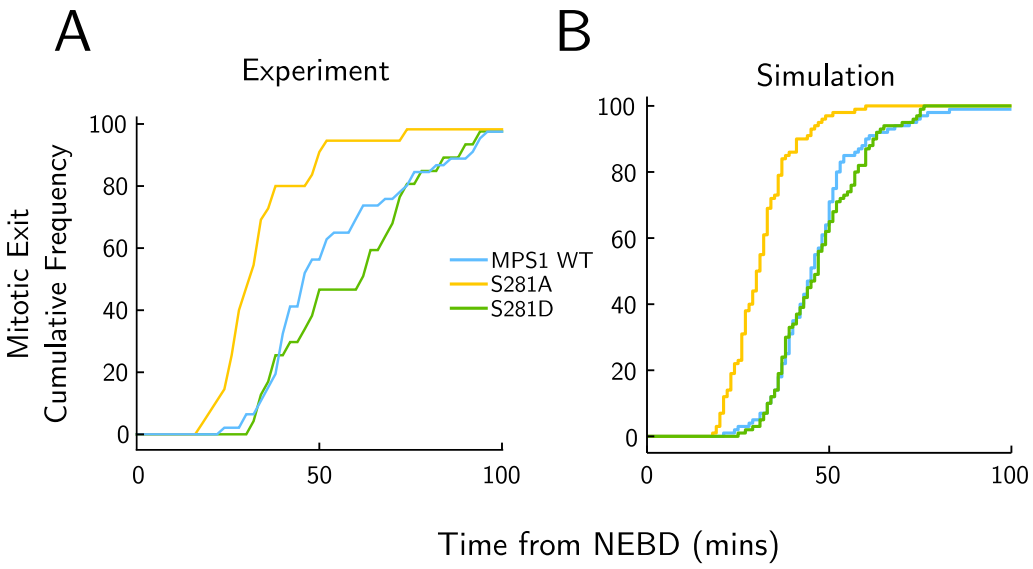

Figure 3.5: Simulation (A) and experimental data (B) showing cumulative frequency of mitotic exit during normal mitosis for cells with either WT, S281A MPS1 ($k_{an} = 0$) or S281D MPS1 ($k_{in} = 0$). Experimental data adapted from [243] (DOI: 10.1083/jcb.201808014) under a Creative Commons 4.0 License (`https://creativecommons.org/licenses/by/4.0/`). A population-level simulation was performed by randomly varying both the ki_{uKT} parameter and the [CycB] initial condition to simulate variation within the mitotic cell population. These values were sampled from lognormal distributions with means of 0.25 and 1.09 respectively. The log standard deviation was 0.5 in both cases. Initial conditions for all other variables correspond to an early mitotic state with full checkpoint signalling (from running a simulation with $\mathrm{uKT} = 1, \quad Psome = 0, \quad ki_{uKT} = 0$). At $t = 0$, $Psome$ is set to 1, and ki_{uKT} to the randomly sampled value.

3.2.5 SAC reactivation depends on PP2A:B55

A key prediction of the original He et al. model is that the CDK-dependent double-negative feedback loop (Fig 3.1A) creates a bistable switch and therefore enables an irreversible M/A transition. While it is clear that at some point in anaphase sufficient cyclin degradation will revoke SAC licensing, the point at which this occurs is not. This is significant since if the license is revoked too early then the SAC may fail to respond to errors arising late in prometaphase, while if it is revoked too late then mitosis may be delayed by errors arising during chromosome segregation, at which point it may be too late to rectify the problem by inhibiting APC/C activity. We therefore use the model to explore the contexts in which SAC reactivation can and cannot occur.

PP2A:B55 is necessary to reverse CDK-dependent activation of the SAC

As an initial starting point, we used the model to simulate the MG132 arrest and checkpoint reactivation experiment described above (Figure 3.6) for Control, CDK inhibition (CDKi), B55 knockdown (siB55), and joint inhibition (CDKi, siB55) cases. Starting

from an initial MG132-induced metaphase arrest ($Psome = 0$, $\mathrm{uKT} = 0$), we simulate addition of nocodazole ($ka_{uKT} = 0.1$) at $t = 0$. CDK inhibition ($flavo = 100$) and B55 knockdown ($B55_T = 0.2$) are simulated by changing the relevant parameters in the initial simulation set-up.

As expected, the model showed that in MG132-arrested control and siB55 cells, addition of nocodazole results in checkpoint reactivation as measured by return of MPS1 to the kinetochores ([pMps1$_{\mathrm{KT}}$], Figure 3.6A, C). In contrast, CDK inhibition prevents full activation of the checkpoint in control cells (Figure 3.6B). The reason for this effect is the availability of phosphorylated Mps1: in the absence of CDK inhibition, Mps1 remains in a phosphorylated state, and is able to return to the kinetochores immediately that unattached kinetochores re-appear to give a full checkpoint response (Figure 3.6A). In contrast, when CDK activity is inhibited, the drop in [pMPS1$_{\mathrm{T}}$] limits the amount of pMps1 available to return to the kinetochore (Figure 3.6B). This loss of MPS1 phosphorylation requires B55 activity, which rises in response to CDK inhibition (Figure 3.6B). In siB55 cells dephosphorylation is much slower, so the checkpoint still undergoes significant activation in the presence of CDK inhibition (Figure 3.6D). Although this initial activation declines as residual B55 activity slowly promotes Mps1 dephosphorylation, MPS1 remains at the kinetochore during the observation window for the experiment (the fixation reaction is started after 5 minutes of nocodazole arrest). We would therefore not expect to detect this later loss of [pMps1$_{\mathrm{KT}}$] in this assay unless the system were allowed to run for more time before fixing and imaging.

This simulation and accompanying experiment therefore demonstrate the important role that PP2A:B55 plays in counteracting CDK-dependent licensing of the checkpoint. This is significant since during normal mitotic progression CDK activity will decline following activation of APC/C at metaphase. Based on these results, we would expect that as CDK activity drops during metaphase and into anaphase, the ability of the checkpoint to reactivate in response to perturbations will be lost in the presence of PP2A:B55 activity. In the absence of PP2A:B55, MPS1 should remain phosphorylated and able to mount a checkpoint response later into anaphase.

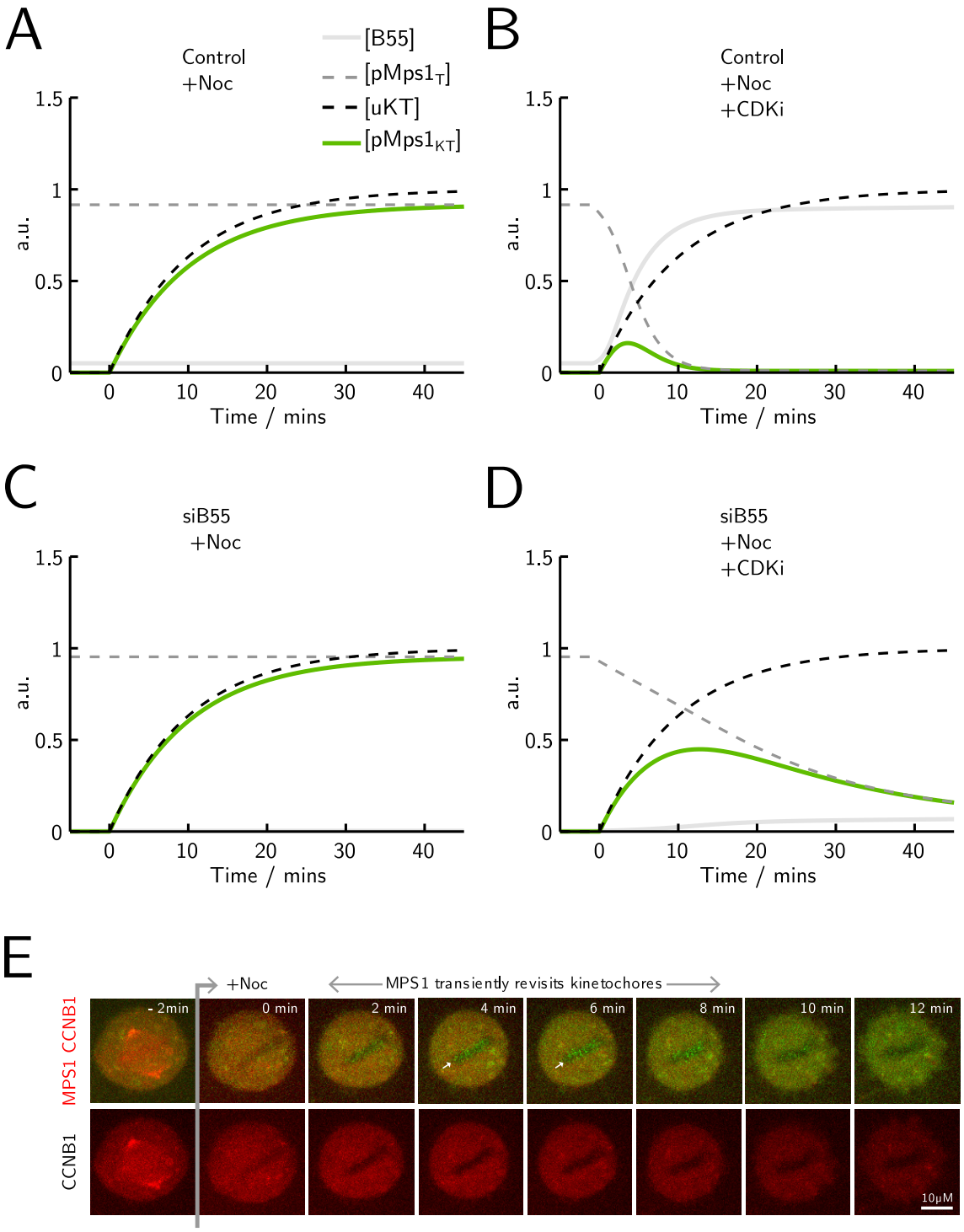

Figure 3.6: Timecourse simulation of checkpoint reactivation in the presence (A, C) or absence (CDKi: B, D) of the CDK inhibitor flavopiridol. Simulations are performed for Control (A, B) and B55 knockdown (siB55: C, D) cells. (E) HeLa MPS1-GFP/CCNB1-mCherry cells in mitosis were imaged until all chromosomes had aligned and MPS1 removed from kinetochores. 3μM nocodazole was added (+Noc) to trigger checkpoint activation (t=0min). Images from 2min prior to nocodazole addition until 12min after addition are shown. Panel E experiments performed by Dan Hayward; panel E adapted from [243] (DOI: 10.1083/jcb.201808014) under a Creative Commons 4.0 License (`https://creativecommons.org/licenses/by/4.0/`).

Transient SAC reactivation occurs during CDK inhibition but is insufficient to mount a checkpoint response

In addition to reproducing the endpoint results of the MG132 checkpoint reactivation experiments, the simulations also produced the unexpected prediction that while CDK inhibition does not permit full activation of the checkpoint, a transient activation does occur (Figure 3.6B).

Since the initial starting point has high CDK activity and low PP2A:B55 activity, MPS1 starts in a highly phosphorylated state. Inhibiting CDK causes MPS1 phosphorylation to decline, but sufficiently slowly that a significant pool of MPS1 remains available to localise to kinetochores in the event of nocodazole addition. This localisation causes an initial increase in [$pMPS1_{KT}$], but this is then counteracted by the ongoing dephosphorylation of MPS1 by PP2A:B55. The result is a transient spike in [$pMPS1_{KT}$] which is insufficient to promote full scale checkpoint activation.

To test this model prediction, cells were challenged with nocodazole shortly after anaphase and the checkpoint response measured by localisation of fluorescence-labelled MPS1 to the kinetochore (Figure 3.6E). In this period, CycB concentration is reduced by the activity of APC/C and so we would expect the conditions to mimic those of CDK inhibition in the MG132 case. Transient reactivation of the checkpoint was observed, suggesting that in the absence of CDK activity, residual phosphorylated MPS1 will attempt to mount a checkpoint response, but that continued loss of this signal via B55-dependent dephosphorylation will prevent full activation.

PP2A:B55 is necessary for checkpoint irreversibility

Having established that PP2A:B55 is necessary to counteract CDK-dependent activation of the checkpoint, the next step was to determine more precisely the extent to which the B55/ENSA/Gwl pathway contributes to checkpoint bistability and irreversibility. This is important since in principle the system has the capacity for bistability in its absence based only on the CDK/MCC/APC double-negative feedback loop shown in Figure 3.1A (see for example the FADS model of the SAC in Chapter 2).

Bifurcation analysis was therefore used to examine the effects of PP2A:B55 on the system. Using the fraction of unattached kinetochores (uKT) as a bifurcation param-

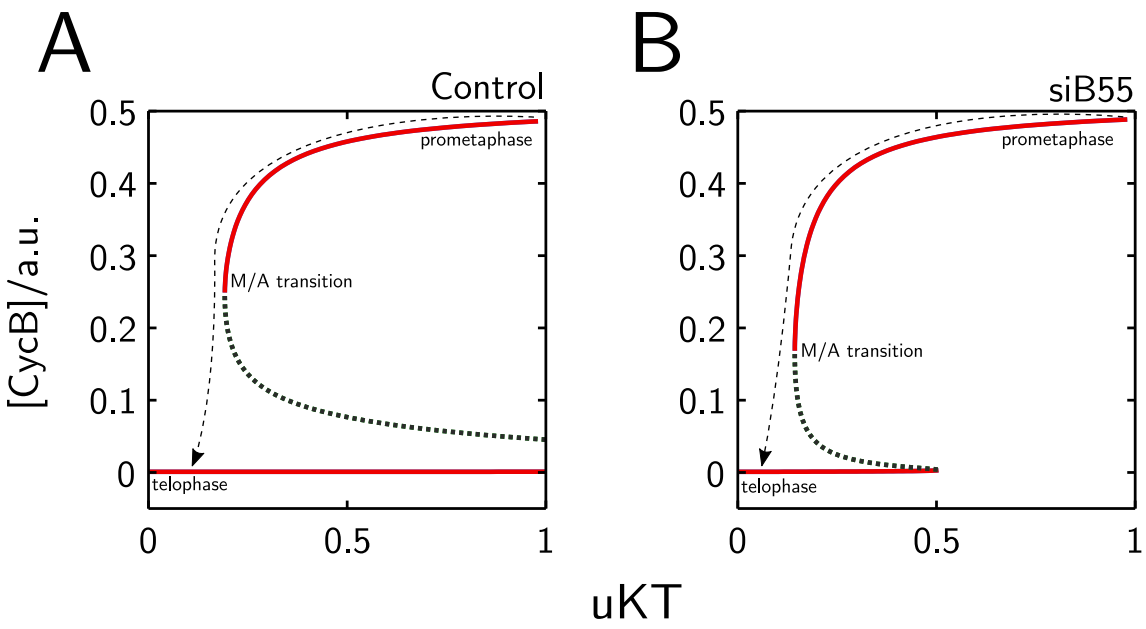

Figure 3.7: Bifurcation digrams showing the steady state level of CycB as a function of fraction of unattached kinetochores (uKT) for (A) Control and (B) B55 knockdown ($B55_T = 0.2$) cells.

eter[1], modelling the behaviour of a control cell shows that the system comprises an irreversible bistable switch (Figure 3.7A). Starting from an initial condition where all kinetochores are unattached and [CycB] is high (top right), a decrease in uKT as chromosomes undergo attachment and biorientation promotes a switch-like transition to a low [CycB] anaphase state (bottom left). Once this state is reached, the transition is irreversible, since the upper uKT threshold required for the reverse transition is out of the possible range of uKT values (bottom right).

In contrast, when B55 depletion is simulated (siB55: $B55_T = 0.2$), the size of the bistable region is considerably reduced (Figure 3.7B). While the system retains the capacity to undergo a normal transition from the high [CycB] prometaphase state to the low [CycB] anaphase state in response to reducing uKT, this transition is no longer irreversible. From the anaphase state, increasing [CycB] beyond a certain threshold will mean that the low [CycB] steady state is no longer stable, and the system will undergo transition back to a prometaphase-like state. In practical terms, this would correspond to the system being able to reactivate the SAC and recover CycB levels in response to the presence of unattached kinetochores during anaphase.

To show the effect of PP2A:B55 on the bistability of the system in more detail, a

[1]This replaces its use as an ODE variable in the model description in Section 3.2.

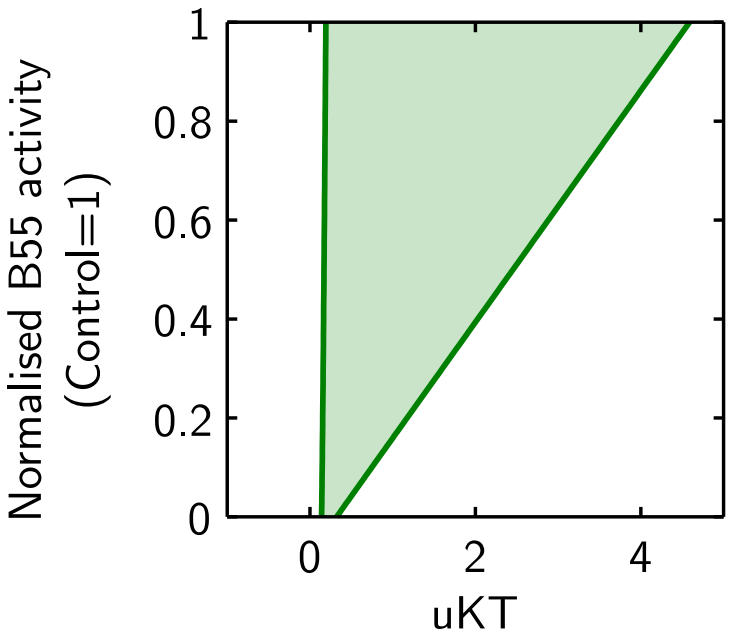

Figure 3.8: Two-parameter bifurcation diagram showing how the size of the bistable region (shaded) varies with the extent of B55-dependent MPS1 dephosphorylation. Note that uKT is defined here as the fraction of unattached kinetochores, so physiological values are between 0 and 1. The axis is extended beyond 1 to show the trend in bistability, but these higher upper thresholds would not be accessible in a physiological setting.

two-parameter bifurcation diagram was plotted, showing how the upper and lower uKT thresholds for transition between high [CycB] and low [CycB] states are affected by changing the B55-dependence of MPS1 phosphorylation (Figure 3.8). In the model, MPS1 dephosphorylation comprises both a B55-dependent and B55-independent component. As the B55-dependent component is reduced, so is the extent of the bistable region. This is consistent with the differences between the two 1-parameter bifurcation diagrams in Figure 3.7, which effectively represent individual cross-sections of the two-parameter bifurcation diagram in Figure 3.8 at different levels of B55 activity. Notably, even when the B55-dependent contribution is reduced to 0, the upper and lower thresholds do not completely converge, so the system still shows a small bistable region even in the absence of B55. This is the result of the CDK-dependence of MPS1 phosphorylation, which completes the CDK/APC/SAC double-negative feedback loop. However, the presence of B55 makes the bistability considerably more robust, and is important for ensuring irreversibility by pushing the upper uKT threshold for the reverse transition out of a physiologically accessible range.

Checkpoint reactivation

The bifurcation analysis described above uses a steady state approach to analyse system reversibility. While this allows a more rigorous mathematical analysis of the problem, in reality the reversibility or otherwise of the checkpoint in response to a specific set of events is the property of a dynamic system which has not yet reached steady state. For this reason, we supplemented the bifurcation analysis with timecourse simulations of checkpoint reactivation trajectories (Figure 3.9). In control cells, the ability of the checkpoint to successfully reactivate depends on the time at which nocodazole addition is simulated (Figure 3.9A), with the extent of reactivation reducing with time from the initial release. In contrast, B55 knockdown simulations (Figure 3.9B) are always able to reactivate the checkpoint, while in Gwl knockdown simulations (Figure 3.9C), only a limited and transient reactivation is possible even at the earliest timepoints. This supports the hypothesis that control of PP2A:B55 activity is important to regulate the point at which the checkpoint license is irreversible revoked.

To test these predictions experimentally, it was not possible to develop a suitable reactivation assay which precisely mimicked the simulation conditions. This is because obtaining a suitably uniform starting population from which to test reactivation at different time-points is not possible due to cell-to-cell variation. Instead, this variability in the cell population was used by collaborators in the Gruneberg and Barr labs to test the simulations by identifying mitotic cells in which checkpoint signalling was switched off (as measured by loss of MPS1 from the kinetochore) and treating them with nocodazole to promote checkpoint reactivation. Fluorescence microscopy was used to measure levels of CycB and kinetochore-localised MPS1 following nocodazole addition.

Since the initial levels of CycB vary within the cell population, this effectively provides an equivalent situation to the checkpoint reactivation simulations in Figure 3.9, since each starting point will exist somewhere on the CycB curve defined in that figure. For the purposes of visualisation, we therefore aligned [$MPS1_{KT}$] simulations to the point at which nocodazole addition was simulated (Figure 3.10A). This is then compared to the experimentally measured curve for [$MPS1_{KT}$] (Figure 3.10B). The corresponding CycB curves are shown in Figure 3.10C.

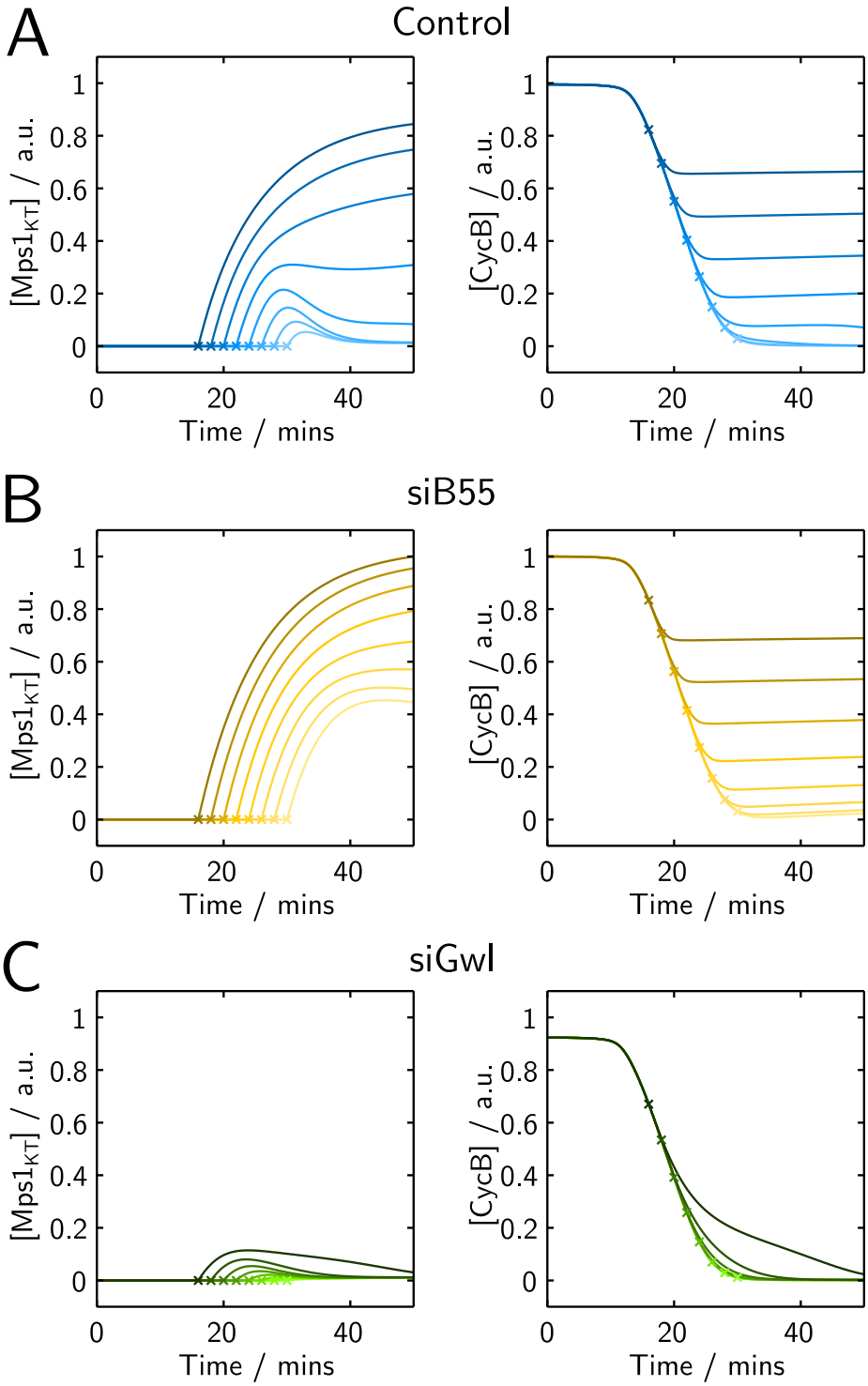

Figure 3.9: Simulations of checkpoint reactivation occurring at different stages during mitotic progression. Simulations begin from an initial checkpoint arrest condition, which is released by setting $uKT = 0$. Checkpoint reactivation is simulated by setting $uKT = 1$ at 2-minute time intervals between 16 and 30 minutes; these reactivation points are indicated by crosses, with colours matched to the corresponding timecourse (darkest = 16 mins, lightest = 30 mins). $[MPS1_{KT}]$ values are normalised to the maximum value across all three cell types.

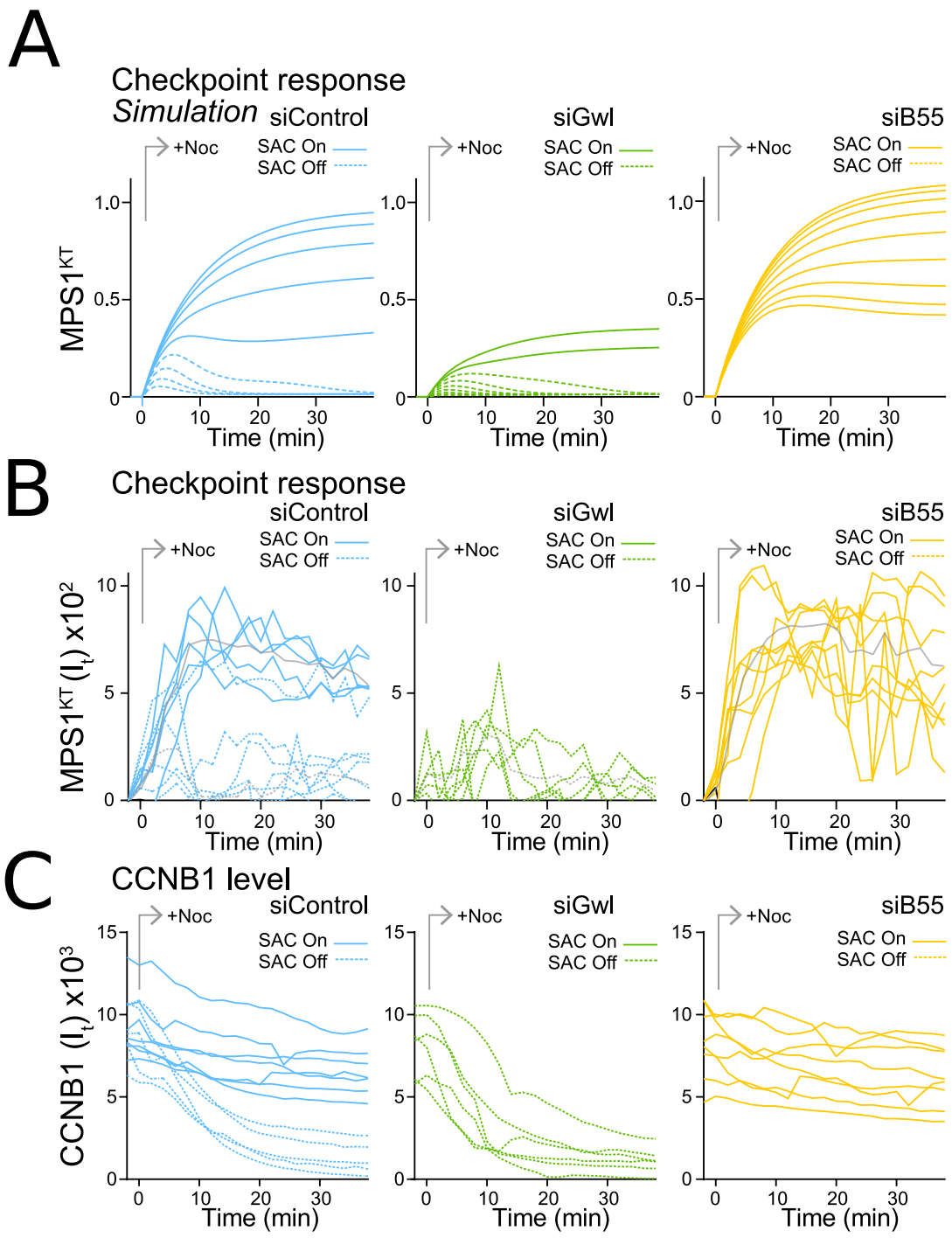

Figure 3.10: Timecourse of kinetochore-associated MPS1 levels ([$pMPS1_{KT}$]) during nocodazole-induced checkpoint re-activation (B), and from timecourse simulations (A). Different lines in the model simulation are generated by realigning simulations of checkpoint reactivation at variable timepoints (e.g. Figure 3.9) to the point of reactivation. Variation in measured CycB levels is shown in (C). Experiments for panels B and C performed by Dan Hayward; experimental figures adapted from [243] (DOI: 10.1083/jcb.201808014) under a Creative Commons 4.0 License (`https://creativecommons.org/licenses/by/4.0/`).

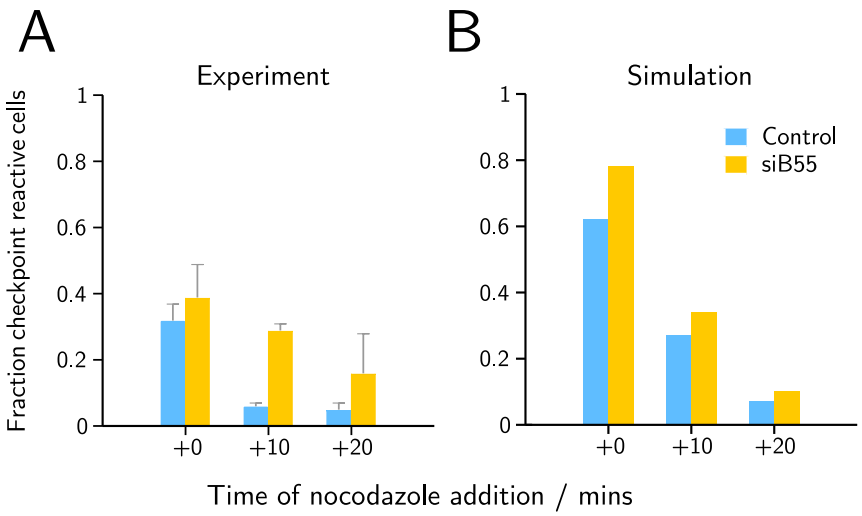

Figure 3.11: Experiment (A) and population-level simulation (B) of SAC reactivation following nocodazole addition. (A) Prior to nocodazole addition, cells were arrested in monastrol, followed by washout for 25 minutes. Nocodazole was then added at timepoints 0, 10 and 20 mins after this point, and checkpoint reactivation monitored by the return of Mad1 to the kinetochore. (B) Population-level simulations were performed by randomly varying the ki_{uKT} parameter and the [CycB] initial condition. ki_{uKT} was sampled from a lognormal distribution with mean 0.25 and log standard deviation 0.5. CycB was sampled from a lognormal distribution with mean 0.5 and log standard deviation 0.5. Initial conditions for all other variables correspond to a metaphase block with checkpoint signalling ($Psome = 0$, $uKT = 1$, $ki_{uKT} = 0$). At the designated time, checkpoint reactivation was simulated by setting $ki_{uKT} = 0$, $ka_{uKT} = 0.1$. 100 simulations were performed for each nocodazole addition time. Checkpoint reactivation was defined as $[\mathrm{pMps1_{KT}}] > 0.5$ at 5 minutes after nocodazole addition. Panel A experiments performed by Dan Hayward; experimental figure adapted from [243] (DOI: 10.1083/jcb.201808014) under a Creative Commons 4.0 License (`https://creativecommons.org/licenses/by/4.0/`).

This combination of simulation and experiment clearly shows that the existence of a B55-dependent checkpoint reactivation threshold predicted by the model is observed experimentally. In control cells, addition of nocodazole results in one of two possible responses: a sustained reactivation of the checkpoint; or a small transient increase in [$\mathrm{MPS1_{KT}}$] which is not sufficient to stabilise [CycB]. In contrast, the Gwl and B55 knockdowns do not show this behaviour. In the Gwl knockdown, the system is unable to reactivate the checkpoint sufficiently to stabilise [CycB], showing only a limited and/or transient increase in [$\mathrm{MPS1_{KT}}$] in response to nocodazole addition. In the B55 knockdown, the checkpoint reactivates sufficiently to stabilise [CycB] in all cases. Thus PP2A:B55 plays an important role in determining the ability of the checkpoint to reactivate during anaphase in response to renewed stimulus. The distinct split in the behaviour of control cells between those which fully activate the checkpoint and those which do not suggests that activation of PP2A:B55 during the course of anaphase switches the system from a checkpoint-responsive to non-responsive state.

To test this hypothesis further, we simulated the results of a SAC reactivation experiment in which cells were synchronised in prometaphase with monastrol, before washout for 25 minutes to allow correct spindle formation and progression into metaphase. Application of nocodazole 0, 10 or 20 minutes after this point was then used to disrupt KT:MT attachments and reactivate the SAC (Figure 3.11). In both experiment and simulation, the ability of the cells to reactivate the checkpoint declined with time, indicating that the checkpoint remains reactivatable only for a certain time following metaphase. Furthermore, B55-depleted cells retained the ability to reactivate the checkpoint for longer, again confirming the significance of B55-dependent dephosphorylation in revoking the checkpoint license at anaphase.

Determining the CycB threshold for SAC inactivation

Having established that during normal anaphase cells transition from a state in which the checkpoint is re-activatable to one in which it is not, this leaves the question of where exactly the transition point between these two states lies.

If we consider the bifurcation diagram in Figure 3.7A, we can describe the reactivation experiment in terms of positions within this diagram. The initial starting point is with [CycB] high, but uKT=0. This corresponds to a point in the upper left of the bifurcation diagram. From this point, the only possible steady state is the low [CycB] steady state in the bottom left, so the system will move in this direction and degrade CycB. When nocodazole is added, the effect is to jump the system horizontally to a point with the same CycB concentration, but uKT=1. This region of the bifurcation diagram is bistable, so the outcome will depend on the starting position. If the horizontal jump crosses the unstable state separating the upper and lower steady states, then the system will be attracted towards the upper [CycB] steady state, so will slowly accumulate CycB. However, if [CycB] is sufficiently low that the horizontal jump does not cross the unstable steady state, the system will still be attracted to the lower [CycB] steady state, meaning that reactivation will not occur. The point at which the unstable steady state crosses the line uKT=1 is therefore the crucial [CycB] threshold below which checkpoint reactivation is no longer possible.

To determine quantitatively the position of this threshold in real cells, collabora-

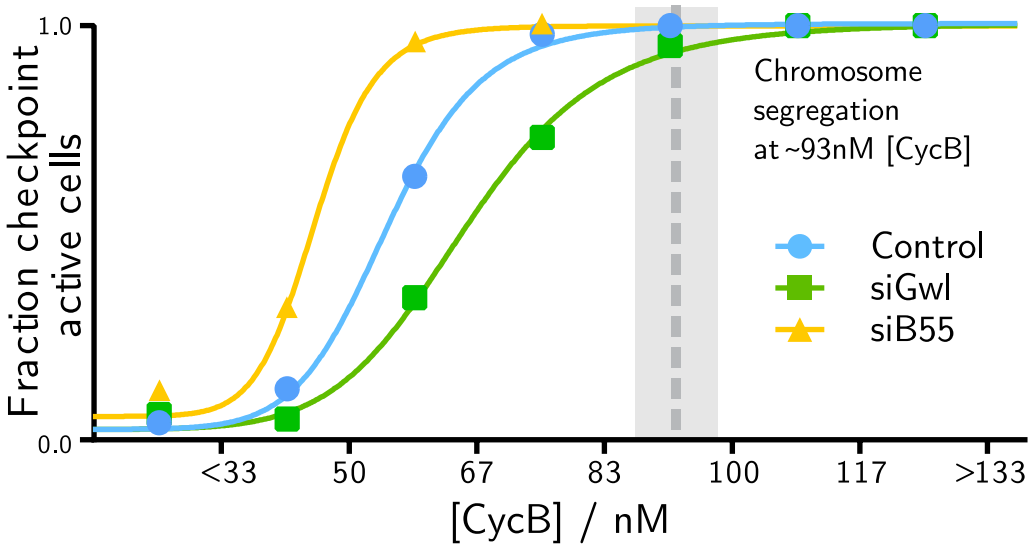

Figure 3.12: Populations of control (siControl), Gwl- (siGwl) and B55- (siB55) depleted HeLa CCNB1-GFP cells were released from a thymidine block for 10h and then challenged with 3M nocodazole for 5min and stained for MAD1. Checkpoint status, either on or off, and total CCNB1 (CycB) levels were determined. The fraction of checkpoint active cells was plotted for bins of 100 fluorescence units of CCNB1 on the graph for n=880, 895 or 657 cells for siControl, siB55 and siMASTL, respectively. Experiments performed by Dan Hayward; experimental figure and description adapted from [243] (DOI: 10.1083/jcb.201808014) under a Creative Commons 4.0 License (`https://creativecommons.org/licenses/by/4.0/`).

tors in the Gruneberg and Barr labs performed population-level analysis of cells subject to checkpoint reactivation. Control, B55 knockdown and Gwl knockdown cells were synchronised in mitosis and then challenged with nocodazole for 5 minutes before imaging the checkpoint response (MAD1 at the kinetochore) and total CycB concentration through fluorescence microscopy. Binning the CycB fluorescence data allowed the fraction of checkpoint active cells for a given CycB concentration to be determined (Figure 3.12).

These results show that there is considerable variation within the cell population, but that as expected, the probability that a given cell will activate the checkpoint increases with CycB concentration. Furthermore, loss or gain of B55 activity respectively increase and decrease the [CycB] threshold for checkpoint activation. Additionally, the reactivation threshold is in all cases significantly lower than the [CycB] threshold associated with the onset of chromosome segregation. This is consistent with the known timing of B55 activation via the BEG pathway in late anaphase [173], which occurs after chromosome segregation.

However, these results present another puzzle, namely the physiological significance

of this threshold in preventing spurious checkpoint reactivation, since it still permits the possibility of (presumably) futile checkpoint reactivation occurring after chromosome segregation. One possibility is that the B55-dependent threshold is just one of several CDK-dependent mechanisms contributing to checkpoint activation and inactivation. In the rest of this chapter we address some of these additional CDK-dependent pathways, before returning to the broader question of the role of these multiple pathways in checkpoint licensing and activity in the discussion.

3.3 Cdc20 phosphorylation

The text originally presented in this section cannot be made freely available via ORA due to confidentiality agreements.

3.3.1

The text originally presented in this section cannot be made freely available via ORA due to confidentiality agreements.

Figure 3.13: This figure cannot be made freely available via ORA due to confidentiality agreements.

3.3.2

The text originally presented in this section cannot be made freely available via ORA due to confidentiality agreements.

3.3.3

The text originally presented in this section cannot be made freely available via ORA due to confidentiality agreements.

3.3.4 Modelling Cdc20 phosphorylation

For these reasons, we incorporated an inhibitory effect of Cdk1 activity on Cdc20 into the model. Phosphorylation of free Cdc20 converts it into a form which is not active for promoting degradation of APC/C substrates:

$$[\mathrm{Cdc20}] = \frac{[\mathrm{Cdc20f}]}{1 + \alpha \cdot [\mathrm{Cdk1}]} \tag{3.19}$$

Using the model presented previously, we simulate the effects of the CDK and MPS1 inhibition experiments on [CycB] and [Cdc20p] (Figure 3.13, 3rd column). The model is in agreement with the experiment in predicting an acceleration of CycB degradation when

CDK is inhibited. This corresponds with a greater proportion of unphosphorylated Cdc20 capable of supporting APC/C activity (Figure 3.13C). Note that securin degradation was not simulated separately since in the model there is no distinction between degradation of different APC/C substrates, so we would expect this to follow the same pattern as seen with CycB.

3.3.5 The counteracting phosphatase for CDK phosphorylation of Cdc20 is unknown

The existence of this interaction naturally invites the question of why the system is wired in this way. We have already discussed how the CDK-dependence of checkpoint signalling could provide a mechanism for switching off checkpoint reactivation during anaphase. However, this inhibitory effect of CDK on Cdc20 is checkpoint independent. One possibility is that the positive feedback inherent in this reaction allows for amplification of an initial APC/C^{Cdc20} activation to promote fast and irreversible progression through anaphase and mitotic exit. Once CycB degradation begins, the resulting loss of CDK activity will further increase its degradation via increasing the amount of Cdc20 available to activate APC/C. Implicitly, this reasoning assumes the presence of a suitable phosphatase counteracting the inhibitory phosphorylation on Cdc20. Given that Cdc20 phosphorylation does decline during this period (Figure 3.13C), it is reasonable to assume that such a reaction takes place. However, it is not presently known which mitotic exit phosphatase is responsible for this reaction, and this would provide further clarification of the role of this particular feedback loop relative to others such as the MPS1/B55 pathway discussed above.

3.4 APC/C and Cdc20 phosphorylation

One apparent puzzle arising from the identification of CDK-dependent inhibition of Cdc20 is that APC/C itself shows the exact opposite dependence on CDK-dependent phosphorylation. As discussed in the introduction, phosphorylation of APC/C is required to promote removal of an auto-inhibitory loop from its active site. APC/C^{Cdc20} activity therefore requires that APC/C is in a CDK-phosphorylated state, but that Cdc20 is

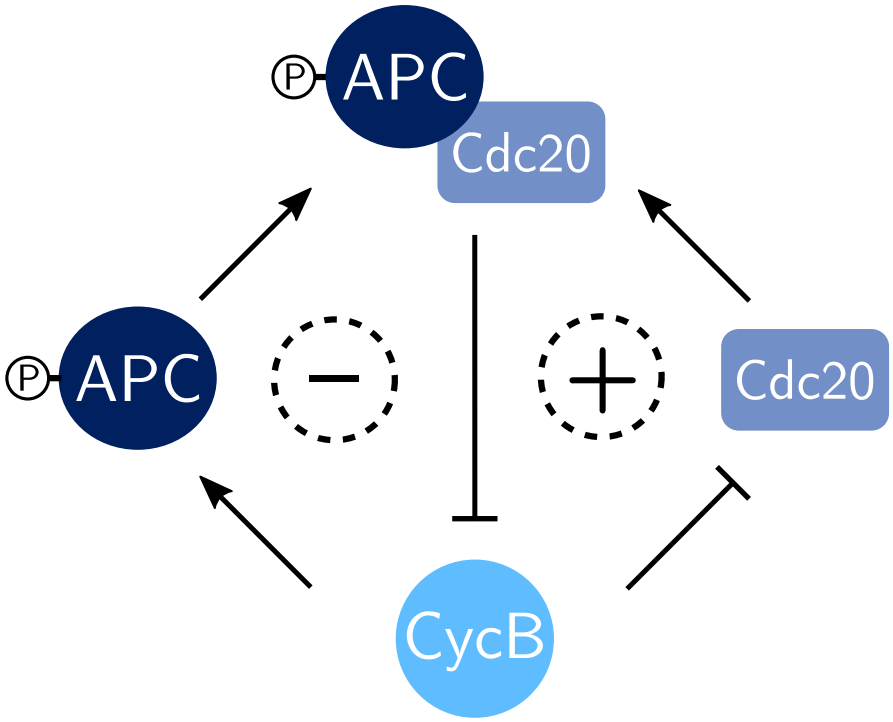

Figure 3.14: Influence diagram showing phosphorylation-dependent regulation of the APC/C^{Cdc20} complex. Positive and negative feedback loops are indicated by '+' and '-' in the centre of the loop.

in a dephosphorylated state. Formation of active APC/C^{Cdc20} would therefore require significant differences in the kinetics of APC/C and Cdc20 phosphorylation and dephosphorylation. In particular, APC/C dephosphorylation at anaphase must be slow relative to Cdc20 dephosphorylation and APC/C substrate degradation. This would allow for a window of APC/C^{Cdc20} activity during anaphase and mitotic exit during which substrate degradation can occur.

The interactions described above place APC/C^{Cdc20} activity at the centre of both a double-negative feedback loop (APC/C^{Cdc20} degrades CycB, Cdk1:CycB phosphorylates Cdc20), and a negative feedback loop (APC/C^{Cdc20} degrades CycB, Cdk1:CycB phosphorylates APC/C) (Figure 3.14). We developed a simple 'toy' model of this system in order to analyse the implications of this network motif for cell cycle function. The interactions in this model are shown in the wiring diagram in Figure 3.15.

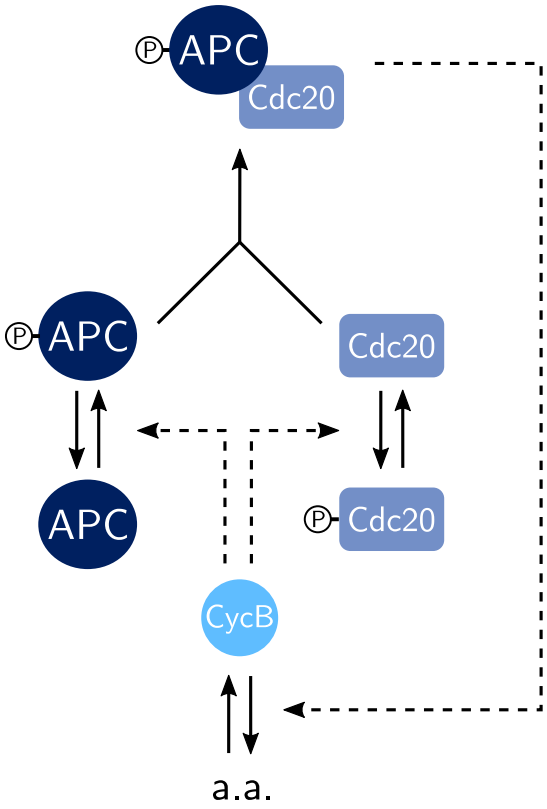

Figure 3.15: Wiring diagram for APC/C and Cdc20 phosphorylation model. Note that only formation of the active APCpC20 complex is shown here. In the model complex formation is not modelled explicitly: phos-/dephosphorylation proceed directly from all four possible APC/C:Cdc20 complexes.

ODEs

The model comprises the following series of ODEs:

$$\begin{aligned}\frac{d[\mathrm{CycB}]}{dt} &= ks_{CycB} - (kd1_{CycB} + kd2_{CycB} \cdot [\mathrm{APCpC20}] \ldots \\ &+ kd3_{CycB} \cdot [\mathrm{APCC20}] + kd4_{CycB} \cdot [\mathrm{APCpC20p}] \ldots \\ &+ kd5_{CycB} \cdot [\mathrm{APCC20p}]) \cdot [\mathrm{CycB}]\end{aligned} \tag{3.20}$$

$$\frac{d[\mathrm{APCp_T}]}{dt} = Vp_{APC} \cdot [\mathrm{Cdk1}] \cdot [\mathrm{APCdp_T}] - Vdp_{APC} \cdot [\mathrm{APCp_T}] \tag{3.21}$$

$$\begin{aligned}\frac{d[\mathrm{APCC20}]}{dt} &= Vdp_{APC} \cdot [\mathrm{APCpC20}] + Vdp_{C20} \cdot [\mathrm{APCC20p}] \\ &- (Vp_{C20} + Vp_{APC}) \cdot [\mathrm{Cdk1}] \cdot [\mathrm{APCC20}]\end{aligned} \tag{3.22}$$

$$\begin{aligned}\frac{d[\mathrm{APCpC20}]}{dt} &= Vdp_{C20} \cdot [\mathrm{APCpC20p}] - Vdp_{APC} \cdot [\mathrm{APCpC20}] \\ &- (Vp_{C20} + Vp_{APC}) \cdot [\mathrm{Cdk1}] \cdot [\mathrm{APCpC20}]\end{aligned} \tag{3.23}$$

Algebraic Equations

And the following algebraic conservation equations:

$$[\mathrm{APCpC20p}] = [\mathrm{APCp_T}] - [\mathrm{APCpC20}] \tag{3.24}$$

$$[\mathrm{APCdp_T}] = Cdc20_T - [\mathrm{APCp_T}] \tag{3.25}$$

$$[\mathrm{APCC20p}] = [\mathrm{APCdp_T}] - [\mathrm{APCC20}] \tag{3.26}$$

$$[\mathrm{Cdc20p_T}] = [\mathrm{APCC20p}] + [\mathrm{APCpC20p}] \tag{3.27}$$

$$[\mathrm{Cdc20dp_T}] = Cdc20_T - [\mathrm{Cdc20p_T}] \tag{3.28}$$

$$[\mathrm{Cdk1}] = \frac{[\mathrm{CycB}]}{1 + ki_{CDK}} \tag{3.29}$$

Phosphorylation and Dephosphorylation Kinetics

In the ODEs above, the terms Vp_{APC}, Vdp_{APC}, Vp_{C20} and Vdp_{C20} are expressions for the apparent rate constant for the relevant phosphorylation or dephosphorylation reaction. The exact expression depends on whether mass action or Goldbeter-Koshland kinetics are used.

Mass action:

$$Vdp_{C20} = kdp_{C20} \tag{3.30}$$

$$Vp_{C20} = kp_{C20} \tag{3.31}$$

$$Vdp_{APC} = kdp_{APC} \tag{3.32}$$

$$Vp_{APC} = kp_{APC} \tag{3.33}$$

Goldbeter-Koshland:

$$Vdp_{C20} = \frac{kdp_{C20}}{J_{C20} + [\mathrm{Cdc20p_T}]} \tag{3.34}$$

$$Vp_{C20} = \frac{kp_{C20}}{J_{C20} + [\mathrm{Cdc20dp_T}]} \tag{3.35}$$

$$Vdp_{APC} = \frac{kdp_{APC}}{J_{APC} + [\mathrm{APCp_T}]} \tag{3.36}$$

$$Vp_{APC} = \frac{kp_{APC}}{J_{APC} + [\mathrm{APCdp_T}]} \tag{3.37}$$

Phaseplane analysis

To analyse the behaviour of the model graphically, we reduce the system of ODEs to allow plotting of a two-dimensional phaseplane digram. To do so, we make the assumption that Cdc20 phosphorylation and dephosphorylation are fast relative to both APC/C phosphorylation and dephosphorylation, and to CycB synthesis and degradation. This allows us to make a pseudo–steady-state assumption for the proportion of phosphorylated Cdc20.

Equations 3.22 and 3.23 are therefore converted from ODEs to algebraic expressions by setting $\frac{d[\mathrm{APCC20}]}{dt} = 0$ and $\frac{d[\mathrm{APCpC20}]}{dt} = 0$. The solution varies depending on whether Goldbeter-Koshland or mass action kinetics are used in each case.

Mass action:

$$[\mathrm{APCC20}] = \frac{[\mathrm{APCdp_T}] \cdot kdp_{C20}}{kp_{C20} \cdot [\mathrm{Cdk1}] + kdp_{C20}} \tag{3.38}$$

$$[\mathrm{APCpC20}] = \frac{[\mathrm{APCp_T}] \cdot kdp_{C20}}{kp_{C20} \cdot [\mathrm{Cdk1}] + kdp_{C20}} \tag{3.39}$$

Goldbeter-Koshland:

$$[\mathrm{APCC20}] = [\mathrm{APCdp_T}] \cdot \mathrm{GK}(kdp_{C20}, kp_{C20} \cdot [\mathrm{Cdk1}], J_{C20}, J_{C20}) \tag{3.40}$$

$$[\mathrm{APCpC20}] = [\mathrm{APCp_T}] \cdot \mathrm{GK}(kdp_{C20}, kp_{C20} \cdot [\mathrm{Cdk1}], J_{C20}, J_{C20}) \tag{3.41}$$

For brevity, the function $\mathrm{GK}(v_1, v_2, K_1, K_2)$ is used for Goldbeter-Koshland reactions to describe the proportion of substrate in the dephosphorylated form. The input parameters refer to the V_{max} and K_M of the dephosphorylation and phosphorylation reactions respectively. A precise definition of this function is provided in Appendix B.

Model variants with different phosphorylation kinetics

As described above, the generic model allows for either mass-action or Goldbeter-Koshland kinetics to be used to describe APC/C and Cdc20 phosphorylation and dephosphorylation. The reason for this is that the kinetic scheme chosen significantly changes the properties and behaviour of the model. In this reduced model framework we are not aiming to accurately capture the entire cell cycle regulatory network, but instead to

examine the possible consequences of the particular network motif of interest. For this reason we examine different kinetic schemes in turn since this provides information on the range of possible outcomes arising from the given network motif.

Specifically, we consider the following model variants: all mass action; all Goldbeter-Koshland; and mass action APC, Goldbeter-Koshland Cdc20. We do not consider the alternative case of mass action Cdc20, Goldbeter-Koshland APC, since the Cdc20 concentration in the cell is much greater than that of APC/C. It is therefore unlikely that there would exist a scenario where APC/C was able to saturate kinase and phosphatase active sites while Cdc20 was not able to.

Phaseplane analysis was used for an initial comparison of the model variants above (Figure 3.16). The reduced version of each model variant is used to plot a phaseplane diagram showing APCpT and CycB nullclines. Doing so reveals that the system has the capacity to function in distinct ways depending on the non-linearity of the phosphorylation kinetics.

Phosphorylation kinetics determines the behaviour of the model as an oscillator or a bistable switch

In the simplest case of mass-action kinetics, there is no non-linearity and the two nullclines are simple hyperbolas (Figure 3.16A). As a result, there is a single intersection point corresponding to a stable steady state.

Addition of Goldbeter-Koshland Cdc20 phosphorylation kinetics converts the [CycB] nullcline to a Z-shaped curve, so that it intersects the [$APCp_T$] nullcline in three places, corresponding to two stable steady states separated by an unstable steady state.

Since both of these model variants describe a system which produces a steady state solution, any change in APC/C or Cdc20 phosphorylation state during cell cycle progression must result from external influences which change the value of internal system parameters. For example, the total available Cdc20 ($Cdc20_T$) may vary in response to the activity of the SAC in sequestering it as MCC. To test the response of these two model variants to change in $Cdc20_T$, bifurcation diagrams were plotted (Figure 3.17), showing the concentration of the active APC/Cp^{Cdc20} complex as a function of $Cdc20_T$. This demonstrates how the bistable system shown in Figure 3.16B differs from

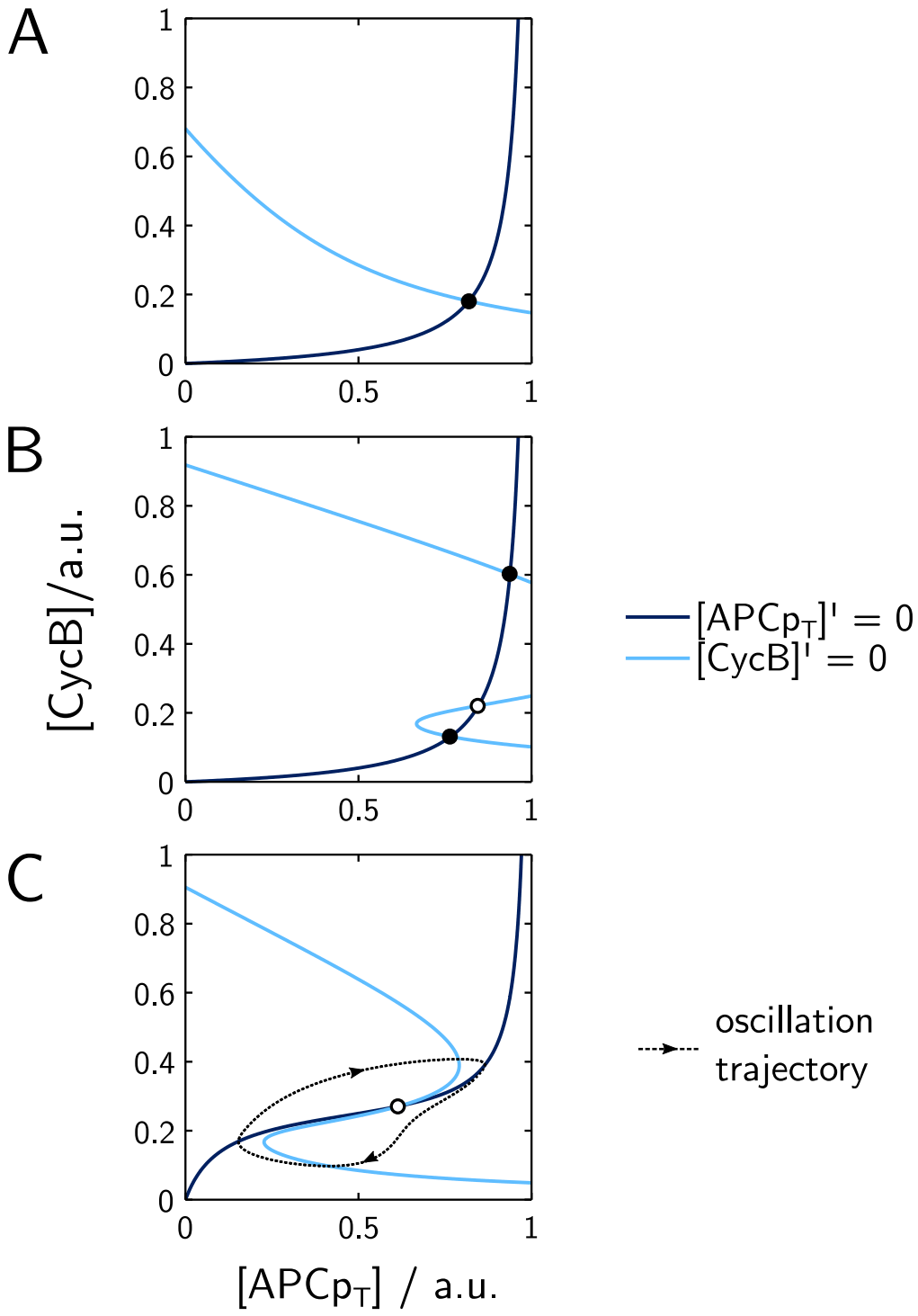

Figure 3.16: Phaseplanes showing the behaviour of APC/C and Cdc20 phosphorylation model variants with different kinetic schemes. (A) Mass action APC/C and Cdc20 phosphorylation produces a single stable steady state. (B) Goldbeter-Koshland Cdc20 phosphorylation kinetics produces a bistable system. (C) Goldbeter-Koshland kinetics for both APC/C and Cdc20 phosphorylation produces a limit cycle oscillator.

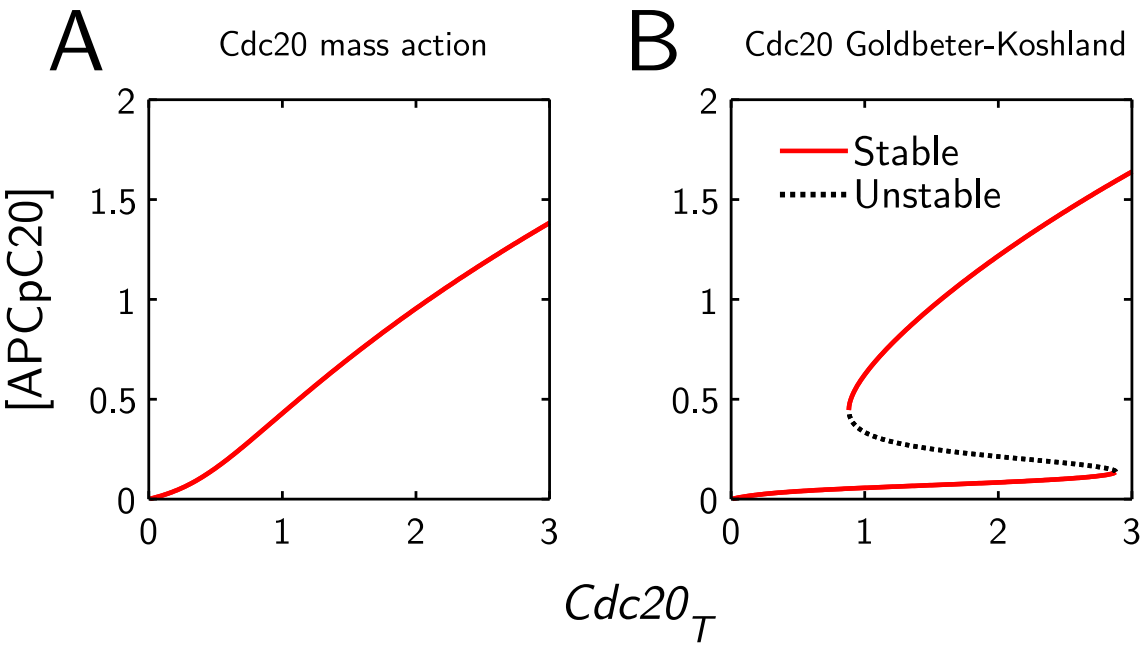

Figure 3.17: Bifurcation diagrams showing steady state APC/Cp^{Cdc20} activity as a function of $Cdc20_T$ for model variants with (A) mass action or (B) Goldbeter-Koshland Cdc20 phosphorylation kinetics. APC/C phosphorylation is mass action in both cases.

the monostable system in generating a distinct on and off threshold for APC/Cp^{Cdc20}.

In contrast to the first two variants, the model variant in which both APC/C and Cdc20 phosphorylation are described using Goldbeter-Koshland kinetics does not form a stable steady state, since the two Z-shaped nullclines intersect only once in an unstable steady state (Figure 3.16C). Instead, the system functions as a stable cell cycle oscillator, undergoing periodic activation and inactivation of APC/Cp^{Cdc20} and Cdk1:CycB. The trajectory of these oscillations is indicated by the dotted arrow loop in Figure 3.16C, while a timecourse simulation of the full model is shown in Figure 3.18.

APC/C and Cdc20 phosphorylation may interact with other cell cycle oscillatory mechanisms

This finding that Cdc20 and APC phosphorylation can act as the driving force for an intrinsic cell cycle oscillator is interesting to consider alongside other proposed oscillators such as the classic model of *Xenopus* oocyte extract [77]. In both cases, the negative feedback loop between Cdk1:CycB (MPF) and APC/C forms one half of the oscillator. The models differ in the nature of the positive feedback loop: the *Xenopus* model relies on inhibitory phosphorylation of Cdk1 by Wee1 and removal by Cdc25; our model uses

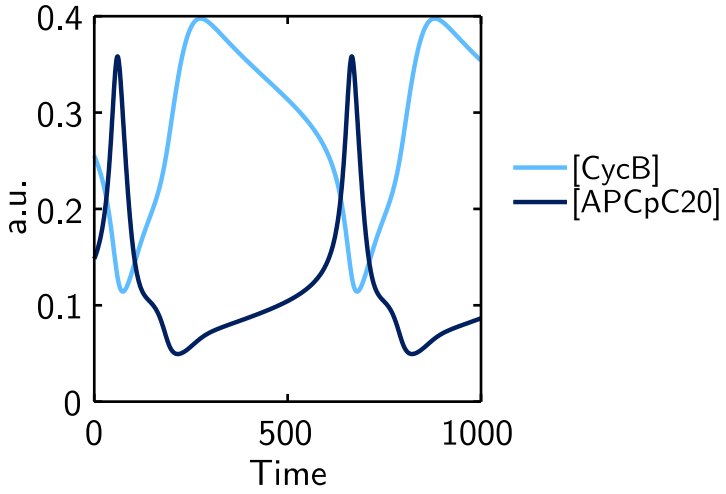

Figure 3.18: Timecourse simulations of oscillations in the model variant with Goldbeter-Koshland kinetics for both APC/C and Cdc20 phosphorylation.

inhibitory phosphorylation of Cdc20 by Cdk1:CycB. In both cases, CycB levels increase in the absence of APC/C activity, until it reaches a critical threshold where APC/C becomes active enough to destroy CycB. Inactivation of APC/C follows the loss of CycB, but with a time delay, so that CycB destruction is near-complete. Once APC/C is inactive, CycB can re-accumulate, and the cycle repeats.

APC/C and Cdc20 phosphorylation have previously been modelled as contributing to *Xenopus* oscillations in an extension of the MPF/APC model described above [72]. In this case, oscillations are permitted even with mass action phosphorylation kinetics for both APC and Cdc20 phosphorylation. However, in this model additional non-linearity is provided both by Goldbeter-Koshland kinetics of inhibitory CDK phosphorylation, and by modelling the stoichiometric inhibition of Cdc20p by Mad2 binding. Thus by placing simple network motifs such as the APC/Cdc20 phosphorylation module into a wider cell cycle context, their effects on the system can be amplified. This is important, since as discussed in Chapter 2, the assumptions of Goldbeter-Koshland kinetics may not be valid in all cases. This model demonstrates how alternative kinetic schemes, and in particular binding of stoichiometric inhibitors, can give rise to the necessary non-linearity.

The significance of APC/C and Cdc20 phosphorylation as the driver of a cell cycle oscillator *in vivo* is unknown. It is perhaps unlikely that this mechanism would constitute the major driving force of the cell cycle oscillator in mammalian cells, given the multiple layers of regulation at different cell cycle stages which are independent of the phosphory-

lation status of Cdc20 or APC/C. However, this model does highlight that such a simple system can admit periodic oscillations in CDK and APC/C activity, which has important implications for the evolution of the cell cycle and the mitotic checkpoint in particular.

3.5 Discussion

Bringing together the different effects of CDK-dependent phosphorylation on APC/C activity discussed above is crucial to understanding the regulation both of mitosis and of the associated mitotic checkpoint. The irreversibility of cell cycle events such as the M/A transition is an important paradigm in cell cycle research. Irreversibility depends on the existence of positive feedback loops which create systems capable of undergoing switch-like transitions between two alternative steady state regimes.

However, the existence of multiple positive feedback loops controlling the same underlying mechanism complicates this picture. We have already discussed how CDK negatively regulates APC/C activity via phosphorylation of both MPS1 and Cdc20. Both of these interactions have the potential to create a bistable switch, but how do these two switch mechanisms interact? Does one switch dominate over the other, or do both give rise to switch-like behaviour? If both are significant, do they act at the same point, contributing to a single threshold, or are they arranged in series so that it is possible to reach an intermediate state where one is switched on, and the other off?

Extending this picture further sees additional complications arise when we consider the role of other known system components subject to similar forms of CDK-dependent regulation, for example APC/C^{Cdh1}, or other CDK-inhibited phosphatases, e.g. PP1. In this discussion we consider how the arrangement of these different network motifs may contribute to the overall picture of checkpoint regulation in mitosis.

3.5.1 Irreversible checkpoint inactivation depends on PP2A:B55

As the cell undergoes mitosis it transitions between states with different levels of checkpoint activity and responsiveness. In prometaphase, the SAC is actively responsive to unattached kinetochores, preventing further mitotic progression until all chromosomes are correctly aligned on the spindle. In addition, EC pathways are actively disrupting

incorrect KT:MT interactions, regenerating unattached kinetochores in the process. At metaphase, correct biorientation of chromosomes is achieved, satisfying the SAC, and promoting the transition to anaphase. Checkpoint reactivation refers to any point where SAC signalling resumes after this initial satisfaction of the SAC at metaphase.

During normal mitotic progression, the checkpoint will not resume signalling after metaphase, as to do so would disrupt APC/C activity and prevent downstream events in mitotic exit. However, if the cell encounters problems during anaphase, for example the disruption of KT:MT interactions, checkpoint reactivation could provide additional time to rectify these problems prior to completion of chromosome segregation. Control of checkpoint reactivation must balance these two competing demands. The possible role of checkpoint reactivation after anaphase is unclear. Experiments which artificially induce unattached chromosomes shortly after metaphase have shown that there is a window of time following metaphase in which reactivation can occur [148]. However it is unclear how frequently defects such as this would be encountered physiologically (the frequency is 0/21 of the control cells in the same study, suggesting these are rare events, but a meaningful estimate of the true frequency is not possible from these data).

One problem with reactivating the checkpoint during anaphase is that cohesin cleavage has already occurred, so there is no way to return to a state where chromosomes are correctly aligned on the spindle. Inhibition of APC/C via SAC reactivation does however affect the rate of cyclin degradation: successful reactivation can be observed as a rapid stabilisation of CycB levels. By preventing cyclin degradation and maintaining CDK activity, downstream events of mitotic exit will be delayed, since many are dependent on removal of CDK-dependent phosphorylations by CDK-inhibited phosphatases. However, it is unclear to what extent delaying such processes could enable recovery from the conditions that might induce the SAC physiologically under these conditions (namely chromosome detachment).

Linked to the question of SAC reactivation in anaphase is the role of checkpoint silencing in turning off error correction pathways to resolve the so-called 'anaphase problem'. During prometaphase, incorrect KT:MT interactions are detected and removed by the EC pathway. In order to distinguish incorrect from correct attachment, tension

across the kinetochore is detected, since only correct attachment and biorientation will generate tension. The problem arises since cleavage of cohesin at the M/A transition should result in loss of tension. If EC is active during anaphase this would therefore be expected to lead to catastrophic loss of KT:MT attachments. Since this does not occur, a mechanism must exist to inactivate EC at or close to the M/A transition. Note however that this is a distinct question from the reactivation of the SAC itself: detachment experiments have shown that the cell retains the capacity to respond to unattached kinetochores should they arise spontaneously.

Key questions therefore remain:

- What is the window during which the checkpoint can be reactivated?
- How and why does this differ between EC and the SAC itself? (the 'Anaphase Problem')
- Which physiological events during chromosome segregation have the capacity to induce the SAC if licensing is not revoked?

Interestingly, we have already seen that a constitutively licensed S281D mutant shows only a small difference in mitotic exit timing experimentally, and no difference in the model (Figure 3.5). We must therefore conclude that the existence of a permanently licensed checkpoint does not appear to substantially delay mitotic exit, despite its continued ability to signal via MPS1. Two possible explanations for this finding are:

- Post-anaphase defects capable of inducing transient SAC reactivation are rare or non-existent.
- Phosphorylation of an additional component by CDK creates another layer of feedback which also contributes to preventing reactivation.

Evidence for the first of these possibilities would require further work to identify if or when post-anaphase defects in chromosome attachment and segregation do occur. This is likely to be a low-frequency event, so would require analysis of a large cell population to identify the true incidence level. The role of the second possibility of additional CDK-dependent feedback loops on checkpoint reactivation is more complex to determine and analyse, and is discussed in more detail below.

3.5.2 Sequential inactivation of surveillance mechanisms during mitotic exit is driven by a series of negative feedback loops

In this chapter we have described how CDK activity has a negative effect on APC/C activity during mitosis, both via MPS1-dependent SAC licensing, and via inhibitory Cdc20 phosphorylation. Although not modelled here in detail, we have also discussed the likely role of CDK-dependent activation of the EC pathway in resolving the so-called 'anaphase problem'. At this point it is also worth considering the well-characterised role of CDK-dependent inhibition of APC/C^{Cdh1}. Furthermore, the wide variety of CDK target proteins during mitosis does not exclude that further CDK-dependent phosphorylation sites may also play a related role.

In each case, we see a common regulatory motif. CDK activity during early mitosis is responsible for promoting the activity of a checkpoint surveillance pathway, preventing premature APC/C activation prior to correct chromosome alignment. At anaphase, cyclin degradation by APC/C reduces CDK activity. This has a double effect: reducing the CDK activity available to maintain checkpoint surveillance, and activation of a series of phosphatases as CDK activity drops below the level required to maintain their inhibition. In the initial stages, challenging the checkpoint with a renewed stimulus (e.g. by disrupting KT:MT attachment during anaphase) will be detected by the still-active surveillance mechanism, resulting in re-activation of the checkpoint effector mechanisms and stabilisation of cyclin levels via renewed APC/C inhibition. However, once CDK activity has fallen below a critical threshold, continued activity of the surveillance pathway is turned off, locking the system into a post-checkpoint state with no capacity to reactivate in response to renewed stimulus.

Crucially however, components of these various CDK-regulated pathways differ in their sensitivity to CDK activity, and in particular are subject to regulation by different mitotic exit phosphatases. They are therefore likely to be inactivated with different timing and in response to different CDK activity thresholds. Each of these points can potentially act as an irreversible bistable switch since at the very least it completes a double-negative feedback loop between APC/C and CDK activity. Mitotic exit phosphatase regulation can provide additional robustness to these switches.

The presence of this series of switches has the potential to provide a ratchet-like mechanism for the cell to coordinate the series of events required for mitotic exit. At each stage, further cyclin degradation can be halted in response to a specific stimulus and further progression into mitotic exit. At the same time, this can be achieved without the risk of total recovery of CDK activity and reactivation of upstream mitotic pathways, which could have deleterious consequences to a cell already committed to anaphase.

Though this is an attractive model for reconciling the existence of multiple overlapping feedback loops in mitosis, the relationship between these layers of switches is not yet clearly defined. It is unclear which of them represent genuine thresholds associated with distinct physiological states of the cell. Alternatively, closely linked bistable mechanisms may end up contributing to a single threshold, without discrete transitions between intermediate states. Further discussion of future approaches to characterise these different possibilities is provided in Section 6.1.3.

3.5.3 Similarities between Cdc20 and Cdh1 regulation

One particular aspect of overlap between different CDK-regulated targets in mitosis is the similarity between the regulation of both Cdc20 and Cdh1 by inhibitory CDK-dependent phosphorylation. The double-negative feedback loop between APC/C^{Cdh1} and CDK-Cyclin complexes has long been established as a key regulatory element of the cell cycle, specifically its role in regulating mitotic exit as APC/C^{Cdh1} is turned on in late mitosis, as well as its control of the G1/S transition, where its activity must be switched off to allow progression into S-phase. The regulation of Cdc20 by inhibitory phosphorylation has only been characterised more recently, and the significance of the similarities between these two regulators is not known.

It is possible that the two co-activators do not play a substantially different role in the underlying cell cycle mechanism at the point at which their activity overlaps (i.e. late anaphase). In this context the purpose of having two separate co-activators rather than a single CDK-regulated co-activator would be to allow for specific regulatory functions at the points where their expression does not overlap. The early APC/C co-activator (Cdc20) is subject to regulation by the SAC, while the late APC/C co-activator (Cdh1)

is not, but is subject to Cdh1-specific regulation by Emi1 at the G1/S transition. Where their activity overlaps in anaphase, regulation by the same mechanism (CDK-dependent phosphorylation) could allow for a smooth transition from primarily Cdc20-dependent APC/C activity in early mitosis to primarily Cdh1-dependent APC/C activity in late mitosis. It may also provide redundancy between the two co-activators, allowing greater levels of Cdc20 to compensate for Cdh1 or vice versa.

3.6 Conclusion

In this chapter we have shown how CDK activity affects the activity of APC/C^{Cdc20} via activatory and inhibitory phosphorylation of multiple targets. CDK-dependent phosphorylation of MPS1 is required for checkpoint licensing, and reversal of this phosphorylation by PP2A:B55 determines a point-of-no-return for checkpoint inactivation in anaphase. Inhibitory phosphorylation of Cdc20 by CDK provides an additional input downstream of the checkpoint which may contribute to acceleration of APC/C activation at anaphase. In conjunction with activatory CDK-dependent phosphorylation of the APC/C core it may also contribute to an intrinsic biochemical oscillator controlling APC/C^{Cdc20} activation via cycles of phosphorylation, APC/C activation and dephosphorylation. Although not explicitly modelled here, CDK-dependent regulation of other pathways such as APC/C^{Cdh1}, or AurB-dependent error correction, also contributes to M-phase APC/C activity regulation.

These interactions comprise a series of overlapping feedback loops regulating the activation of APC/C during mitotic M-phase. The exact relationship between these various switch-like mechanisms remains poorly understood, but likely contributes to the ordered regulation of the precise series of events needed to achieve successful progression through mitosis.

Chapter 4

Regulation of APC/C^{Cdh1} during GV arrest and meiotic resumption

4.1 Meiosis Overview

In this and the next chapter we address key questions regarding the regulation of the first meiotic M-phase, and in particular the role of APC/C activity in this process. The modelling presented here was done as part of an experimental collaboration with 2 groups studying the first meiotic division in mouse oogenesis.

In this chapter, we present work done in collaboration with Ahmed Rattani and Kim Nasmyth (Department of Biochemistry, University of Oxford), investigating the role of Cdh1 in regulating the timing of meiosis I. This work resulted in a co-authored Current Biology publication in May 2017 [244]. In Chapter 5 we present a related project in collaboration with Martin Anger (CEITEC, Brno), where we use a mathematical model to derive APC/C activity in meiosis I from *in vivo* timecourses showing the level of fluorescence-labelled substrates.

Analysis of the relationship between these two sets of work on meiosis can be found in the concluding discussion chapter (Section 6.2).

4.2 Introduction

Working in collaboration with Ahmed Rattani and colleagues, we used a combined experimental and modelling approach to identify and characterise the role of Cdh1 in GV arrest and subsequent meiotic resumption. We produced an ODE model of GV arrest and meiotic resumption, and validated this by simulating the outcomes from a range of oocyte-specific gene knock-outs. We show that the presence of Cdh1 in the network

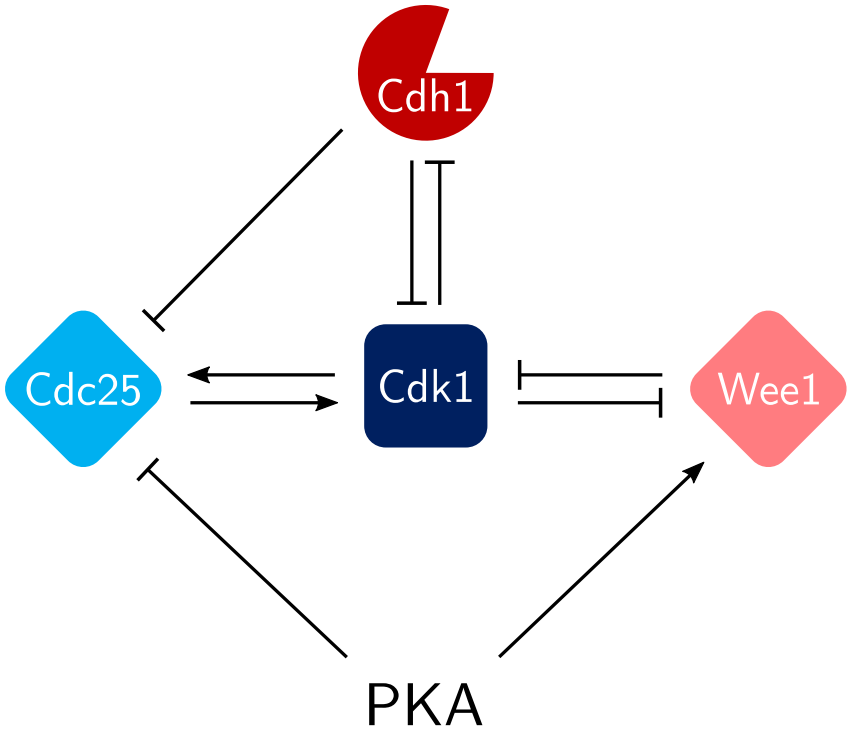

Figure 4.1: Influence diagram for model of GV arrest and meiotic resumption in mammalian oocytes. Arrows represent activatory interactions, bars represent inhibitory interactions.

structure results in a critical-slowing-down phenomenon that produces a slow rise in CDK activity during meiotic resumption, in agreement with experimental observations. This slow rise is essential to allow a sufficient time window of low CDK activity for the removal of Sgol2 from chromosome arms by Aurora B/C, so that chromosomes can undergo correct cohesin cleavage and dyad separation during anaphase I.

4.3 Description of Mathematical Model

An ODE model was developed describing the interactions between APC/C^{Cdh1}, Cdk1:CycB, Wee1B and Cdc25B (henceforth referred to in the context of the model as Cdh1, Cdk1, Wee1 and Cdc25) during GV arrest and meiotic resumption. The network structure which this creates is summarised in the influence diagram in Figure 4.1. For more detail about these interactions and the wider context of GV arrest during mammalian oogenesis, see Section 1.5.1.

Cdk1 activity is central to the model. This activity is dependent both on the availability of CycB, which is synthesised at a constant rate and degraded by Cdh1, and on

the level of inhibitory phosphorylation, which is added and removed by Wee1 and Cdc25 respectively.

Cdk1 activity creates three distinct positive feedback loops by inhibitory phosphorylation of its inhibitors (Wee1 and Cdh1), and activatory phosphorylation of its activator (Cdc25). Further positive feedback is generated through the Cdh1-dependent degradation of Cdc25 [244].

PKA maintains the GV arrest state by inhibiting Cdc25 and activating Wee1. Reducing the level of PKA promotes meiotic resumption. To simulate these effects, PKA is not modelled explicitly as a dynamic variable of the model, but as a parameter that can be adjusted to simulate different experimental conditions.

4.3.1 Full model

The influence diagram in Figure 4.1 was converted into a wiring diagram (Fig. 4.2). This was then used to formulate a series of six ODEs, and four algebraic conservation equations, describing the behaviour of the different components of the system.

In the model, $[\mathrm{Cdk1}]$ represents the activity of the Cdk1:CycB complex, rather than free Cdk1. We do not explicitly model Cdk1:CycB binding, and assume that CycB is the limiting component for complex formation, so $[\mathrm{CycB_T}] = [\mathrm{Cdk1}] + [\mathrm{Cdk1p}]$. The variable $[\mathrm{Cdk1p}]$ refers to a Cdk1:CycB complex where Cdk1 has undergone inhibitory phosphorylation.

Phosphorylation and dephosphorylation of Cdc25, Wee1 and Cdh1 are modelled using Goldbeter-Koshland kinetics. This provides the necessary non-linearity for the system to exhibit bistable behaviour.

ODEs

$$\begin{aligned}\frac{d[\mathrm{Cdk1}]}{dt} &= ks_{CycB} - Vd_{CycB} \cdot [\mathrm{Cdk1}] \\ &\quad + (Va''_{Cdk1} \cdot [\mathrm{Cdc25p}] + Va'_{Cdk1} \cdot [\mathrm{Cdc25}]) \cdot [\mathrm{Cdk1p}] \\ &\quad - (Vi''_{Cdk1} \cdot [\mathrm{Wee1}] + Vi'_{Cdk1} \cdot [\mathrm{Wee1p}]) \cdot [\mathrm{Cdk1}]\end{aligned} \tag{4.1}$$

$$\frac{d[\mathrm{Cdh1}]}{dt} = \frac{Va_{Cdh1} \cdot [\mathrm{Cdh1p}]}{J_{Cdh1} + [\mathrm{Cdh1p}]} - \frac{Vi_{Cdh1} \cdot [\mathrm{Cdk1}] \cdot [\mathrm{Cdh1}]}{J_{Cdh1} + [\mathrm{Cdh1}]} \tag{4.2}$$

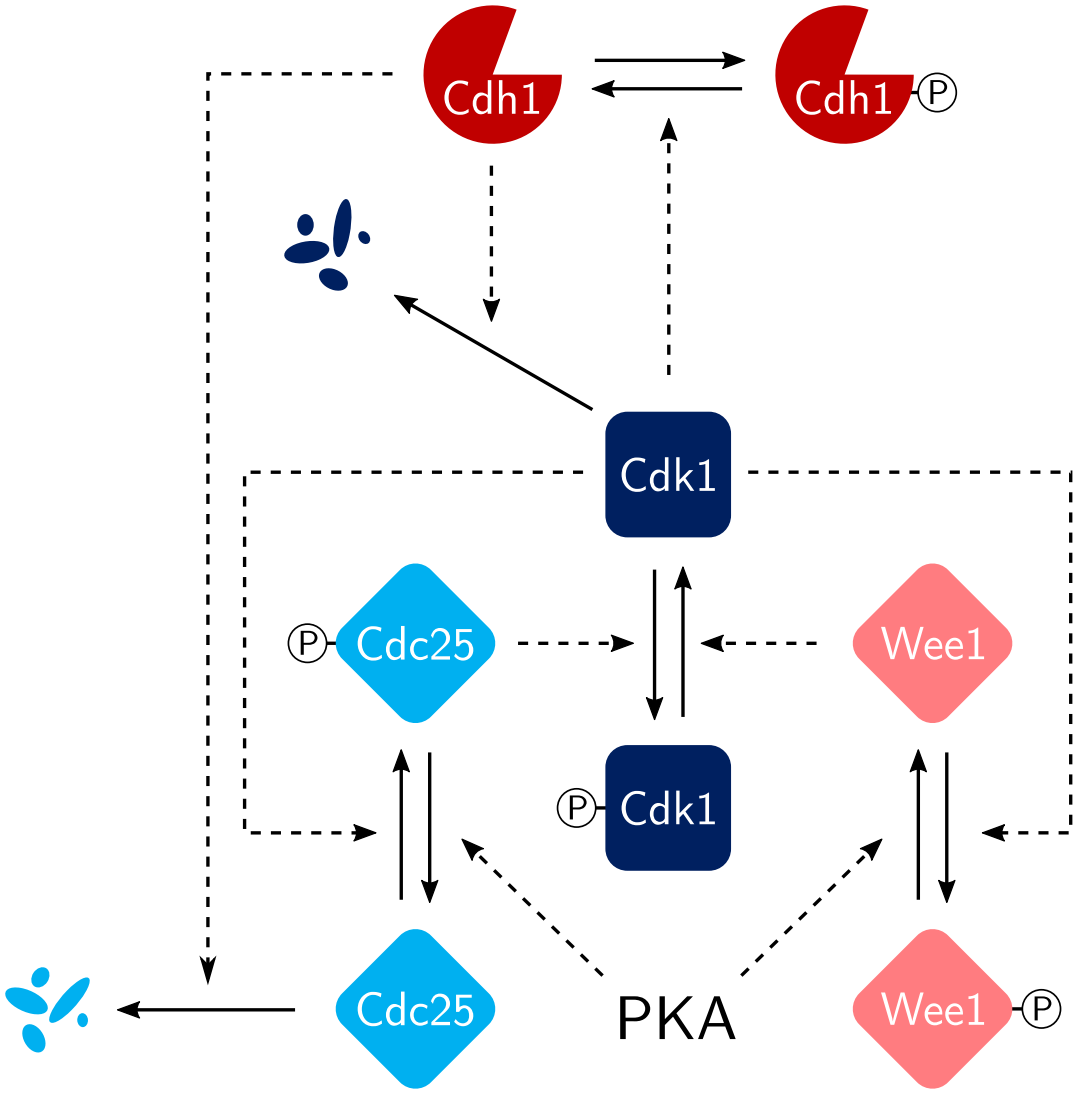

Figure 4.2: Wiring diagram for model of GV arrest and meiotic resumption in mammalian oocytes. Solid arrows indicate interconversions between model species. Dotted arrows represent enzymatic catalysis of the indicated reaction. Note that Cdk1 (CycB) and Cdc25 degradation reactions occur equally from both phosphorylated and unphosphorylated forms, but only the reaction from the unphosphorylated form is shown here for simplicity. Corresponding synthesis reactions are included in the model but not shown.

$$\frac{d[\mathrm{CycB_T}]}{dt} = ks_{CycB} - Vd_{CycB} \cdot [\mathrm{CycB_T}] \tag{4.3}$$

$$\frac{d[\mathrm{Cdc25p}]}{dt} = \frac{Va_{25} \cdot [\mathrm{Cdk1}] \cdot [\mathrm{Cdc25}]}{J_{25} + [\mathrm{Cdc25}]} - \frac{Vi_{25} \cdot [\mathrm{Cdc25p}]}{J_{25} + [\mathrm{Cdc25p}]} - Vd_{25} \cdot [\mathrm{Cdc25p}] \tag{4.4}$$

$$\frac{d[\mathrm{Wee1}]}{dt} = \frac{Va_{Wee} \cdot [\mathrm{Wee1p}]}{J_{Wee} + [\mathrm{Wee1p}]} - \frac{Vi_{Wee} \cdot [\mathrm{Wee1}] \cdot [\mathrm{Cdk1}]}{J_{Wee} + [\mathrm{Wee1}]} \tag{4.5}$$

$$\frac{d[\mathrm{Cdc25_T}]}{dt} = ks_{25} - Vd_{25} \cdot [\mathrm{Cdc25_T}] \tag{4.6}$$

Where:

$$\begin{aligned} Vd_{CycB} &= kd'_{CycB} + kd''_{CycB} \cdot [\mathrm{Cdh1}] \\ Vd_{25} &= kd'_{25} + kd''_{25} \cdot [\mathrm{Cdh1}] \end{aligned} \tag{4.7}$$

Algebraic conservation equations

$$[\mathrm{Cdc25}] = [\mathrm{Cdc25_T}] - [\mathrm{Cdc25p}] \tag{4.8}$$

$$[\mathrm{Wee1p}] = Wee1_T - [\mathrm{Wee1}] \tag{4.9}$$

$$[\mathrm{Cdk1p}] = [\mathrm{CycB_T}] - [\mathrm{Cdk1}] \tag{4.10}$$

$$[\mathrm{Cdh1p}] = Cdh1_T - [\mathrm{Cdh1}] \tag{4.11}$$

4.3.2 Reduced two-dimensional model

For analytical purposes, the model was reduced to a two-dimensional form by assuming that the activities of Wee1 and Cdc25, and the concentrations of CycB and Cdc25, are in pseudo–steady-state. This allows us to express these variables in terms of the remaining dynamic variables (Cdk1 and Cdh1). This reduced system can be plotted as two nullclines on a phaseplane with axes corresponding to $[\mathrm{Cdh1}]$ and $[\mathrm{Cdk1}]$, allowing us to estimate the steady states and system behaviour under different conditions.

The ODEs for $[\mathrm{Cdk1}]$ and $[\mathrm{Cdh1}]$ remain as in the full model (Eqs. 4.1 and 4.2). The remaining ODEs (Equations 4.3-4.6) are converted to algebraic expressions using a

pseudo–steady-state assumption:

$$[\mathrm{CycB_T}] = \frac{ks_{CycB}}{Vd_{CycB}} \tag{4.12}$$

$$[\mathrm{Cdc25p}] = [\mathrm{Cdc25_T}] \cdot \mathrm{GK}(Va_{25} \cdot [\mathrm{Cdk1}], Vi_{25}, \frac{J_{25}}{[\mathrm{Cdc25_T}]}, \frac{J_{25}}{[\mathrm{Cdc25_T}]}) \tag{4.13}$$

$$[\mathrm{Wee1}] = [\mathrm{Wee1_T}] \cdot \mathrm{GK}(Va_{Wee}, Vi_{Wee} \cdot [\mathrm{Cdk1}], \frac{J_{Wee}}{[\mathrm{Wee_T}]}, \frac{J_{Wee}}{[\mathrm{Wee_T}]}) \tag{4.14}$$

$$[\mathrm{Cdc25_T}] = \frac{ks_{25}}{Vd_{25}} \tag{4.15}$$

For brevity, the solutions for $[\mathrm{Cdc25p}]$ and $[\mathrm{Wee1}]$ are expressed using the function $\mathrm{GK}(v_1, v_2, K_1, K_2)$ to describe the proportion of the substrate in the modification state produced by the designated 'forward' reaction. The input parameters refer to the V_{max} and K_M of the forward and reverse reactions respectively. A precise definition of this function is provided in Appendix B.

4.4 Results

Based on the models, we suggest that the meiotic resumption transition functions as a bistable switch, and analyse the behaviour of this system when subjected to different experimental perturbations. Using data provided by Ahmed Rattani and collaborators in the Nasmyth lab, we then validate the behaviour of the model for a range of conditions and genotypes. Phaseplane analysis of the reduced 2-dimensional model is then used to draw conclusions about the significance of the role of Cdh1 during GV arrest and meiotic resumption.

4.4.1 Timecourse Simulations

Timecourse simulations were performed using the full ODE model (Section 4.3.1). To simulate GV arrest, system parameters are initially set so that Wee1 activity is high, and Cdc25 activity is low ($VaWee = 0.375, Vi25 = 0.375$), and the system run to steady state. This steady state is then used as the initial condition for the subsequent simulation of meiotic resumption.

From these starting conditions, the system was run for 100 minutes before Wee1 and Cdc25 activities were altered to simulate the effects of PKA withdrawal at meiotic

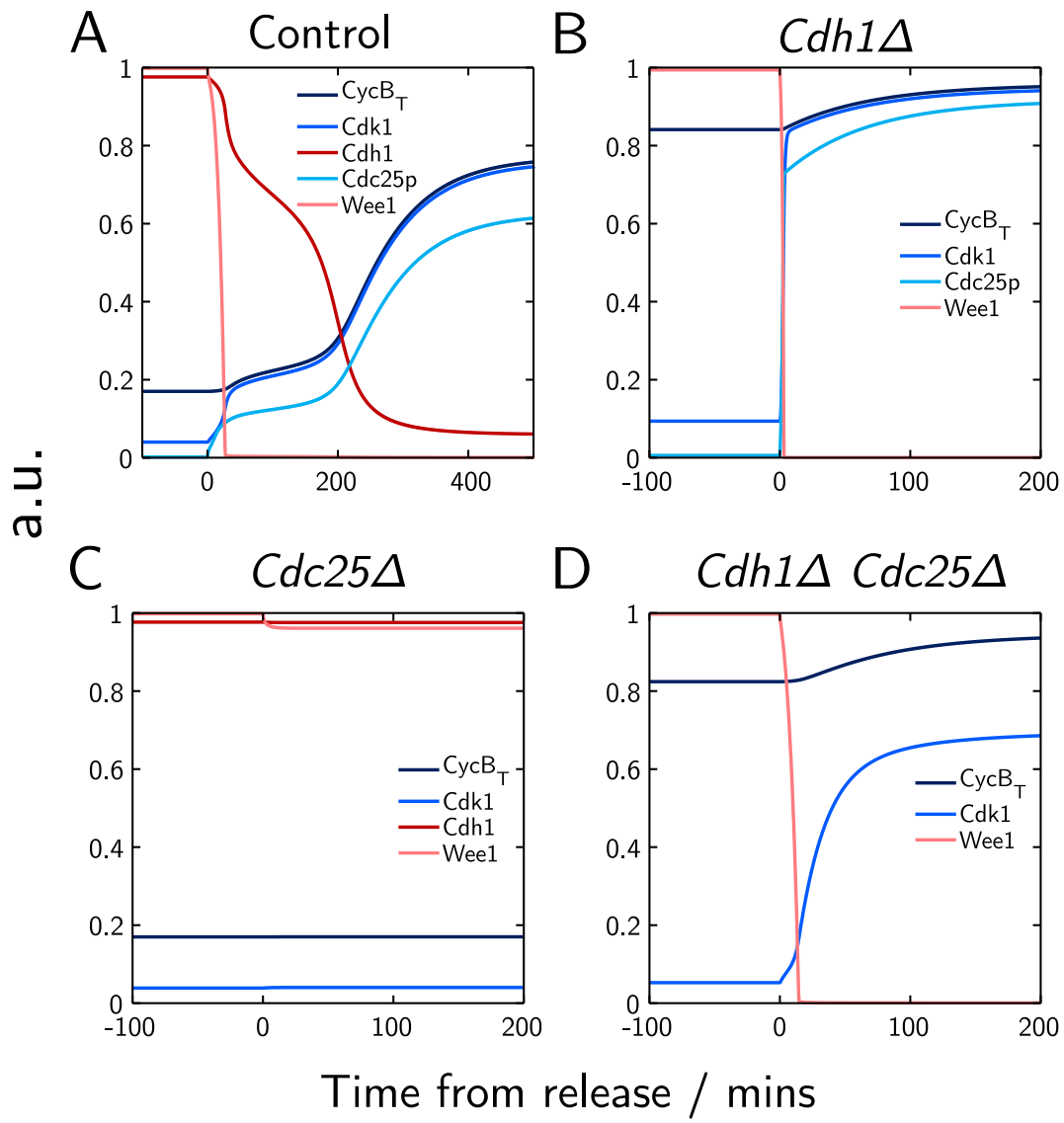

Figure 4.3: Timecourse simulations of meiotic resumption. Simulations run from GV arrest steady state ($Va_{Wee} = 0.375$, $Vi_{25} = 0.375$). At t=0, Va_{Wee} and Vi_{25} are both set to 0.075 to simulate loss of PKA signalling.

Genotype	$Cdh1_T$	ks_{25}
Control	1	0.015
Cdh1Δ	0.05	0.015
Cdc25Δ	1	0.0003
Cdh1Δ Cdc25Δ	0.05	0.0003

Table 4.1: Parameters for simulating Cdh1 and Cdc25 knock-out genotypes

resumption ($VaWee = 0.075$, $Vi25 = 0.075$). This point was defined as t = 0 for the purposes of plotting. In the experimental set-up, PKA activity is lost upon incubation in fresh medium lacking the phosphodiesterase inhibitor IBMX.

To simulate the response of different genotypes during meiotic resumption, four simulations were run, with parameters corresponding to either wild type or knock-out of Cdh1 and Cdc25 (Table 4.1). For each knock-out, the level of the relevant component is reduced to 5% of its wild type level. These non-zero values represent the persistence of residual activity in the cell even after disruption of the targeted gene sequence.

Timecourse simulation of control cells (Fig. 4.3A) shows that an initial rapid fall in Wee1 and rise in Cdc25 activity follows loss of PKA activity. This allows Cdk1 activity to increase almost to the level of total CycB as inhibitory phosphorylation is lost. Once Cdk1 is entirely in the dephosphorylated state, the availability of CycB becomes the only limiting factor for CDK activity. However, accumulation of CycB is initially slow, because APC/C^{Cdh1} remains active and continues to delay the transition into prometaphase until it becomes gradually inactivated by CDK activity. Therefore in contrast to mitosis, inactivation of Cdk1 inhibitory phosphorylation produces only a gradual increase in CycB levels, and hence Cdk1 activity, during meiotic resumption. In the absence of APC/C^{Cdh1} in the knock-out mutant, Cdk1 activation becomes fast and similar to mitosis, because inhibitory phosphorylation is the only factor holding back Cdk1 activation (Fig. 4.3B).

The dual role of inhibitory phosphorylation and Cdh1-dependent CycB degradation can be seen by comparing the relevant single knock-outs to the double knock-out *Cdh1Δ Cdc25Δ*. In the *Cdc25Δ* mutant (4.3C), Cdk1 remains almost entirely phosphorylated,

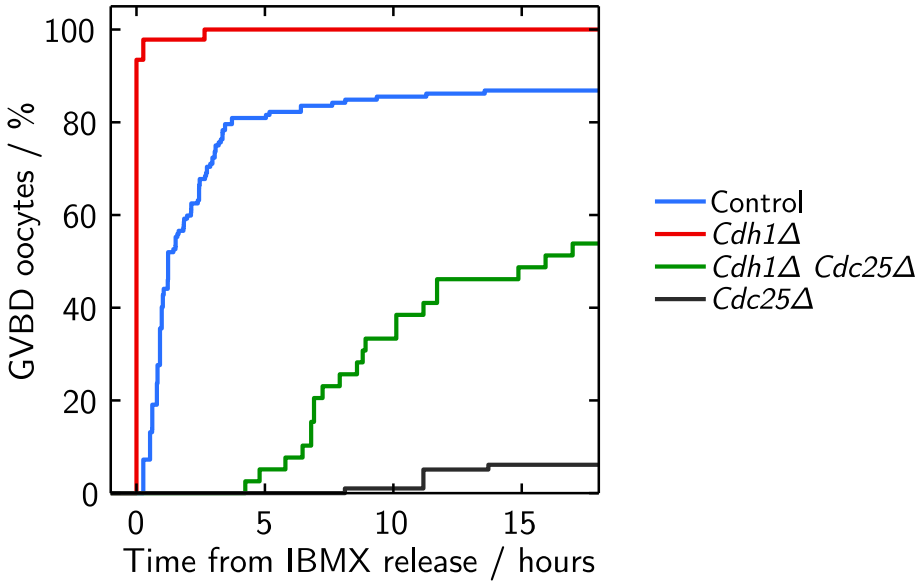

Figure 4.4: Percentage of oocytes undergoing GVBD following release from IBMX for *Cdh1Δ* (n=46), *Cdc25Δ* (n=98) and *Cdh1Δ Cdc25Δ* (n=39) and control cells (n=152). Control data are aggregated from individual control experiments using different floxed genotypes (*$Cdh1^{f/f}$*, *$Cdc25^{f/f}$*, *$Cdh1^{f/f}$ $Cdc25^{f/f}$*) lacking germline-specific Cre recombinase expression. Experiments performed by Ahmed Rattani. Figure adapted from [244] (DOI: 10.1016/j.cub.2017.04.023) under a Creative Commons 4.0 License (`https://creativecommons.org/licenses/by/4.0/`).

so there is no appreciable rise in CDK activity following loss of PKA signalling at t = 0. In contrast, in the *Cdh1Δ Cdc25Δ* double mutant (Fig. 4.3D), the lack of Cdh1 to maintain low levels of CycB means that even the residual Cdc25 activity is sufficient to generate a small Cdk1 activation following loss of PKA signalling. This initial activity can then tip the balance of the Wee1/Cdk1 double-negative feedback loop so that Wee1 is inactivated and Cdk1 becomes fully active, allowing meiotic resumption to proceed.

4.4.2 Experimental Validation

The mutant simulations discussed above correspond to oocyte-specific gene knockouts in mice generated by Ahmed Rattani and collaborators in the Nasmyth lab [244]. These were produced by crossing female *$Cdh1^{f/f}$*, *$Cdc25B^{f/f}$* or *$Cdh1^{f/f}$ $Cdc25B^{f/f}$* mice with male mice expressing Cre recombinase under the control of oocyte-specific expression markers (*Gdf9-iCre* or *Zp3-Cre*). Oocytes of both control and knock-out genotypes were harvested in the presence of the phosphodiesterase inhibitor IBMX to maintain cAMP signalling and therefore PKA activity. They were then released into an IBMX-free medium and imaged for 18 hours. The fraction of cells that underwent GVBD was

recorded over time.

Cdh1Δ and Cdc25Δ show good agreement between simulation and experiment

As can be seen from these results (Fig. 4.4), GVBD does not occur in a synchronised manner under these conditions. Instead, the proportion of cells undergoing GVBD continues to increase over time, presumably due to random variation in the initial starting conditions. Direct comparison of these experimental results with the deterministic time-course simulations is therefore not possible, since the deterministic model represents an idealised picture of the process occurring in a single cell, without any random variation.

Nevertheless, the general trends in time taken for meiotic resumption can be compared between experiment and model. The extreme cases of *Cdh1*Δ and *Cdc25*Δ produce a good fit to the model predictions. In the *Cdh1*Δ, almost all cells undergo rapid GVBD prior to the first observation point 30 mins after IBMX release. Similarly, in the model *Cdh1*Δ rapidly activates Cdk1 following loss of PKA activity. In contrast, in *Cdc25*Δ, cells do not undergo GVBD at all within the first 8 hours, and even by the end of the observation period at 18 hours, less than 10% of cells have undergone GVBD. This is consistent with the model simulation, where *Cdc25*Δ remains in the high [Cdh1], low [Cdk1] GV-arrested state following loss of PKA signalling.

The model predicts a biphasic rise in Cdk1 activity during normal meiotic resumption in control cells

A significant feature of the control simulation is the biphasic rise in CDK activity, with an initial rise associated with loss of inhibitory Cdk1 phosphorylation, followed by a slower rise associated with accumulation of CycB against opposition from Cdh1-dependent degradation. While the overall result is that activation of Cdk1 is slower than in *Cdh1*Δ, which is reflected in the experimental results, it is not possible to infer the biphasic rise from the data available in Figure 4.4 alone.

However, comparing to existing published data shows that such a biphasic rise in Cdk1 activity is observed during meiotic resumption *in vivo*. Experiments measuring H1 kinase activity (a standard assay for CDK activity) in mouse oocytes have recorded a slow rise in activity over the course of 6-8 hours [187, 188]. Although the biphasic characteristic of

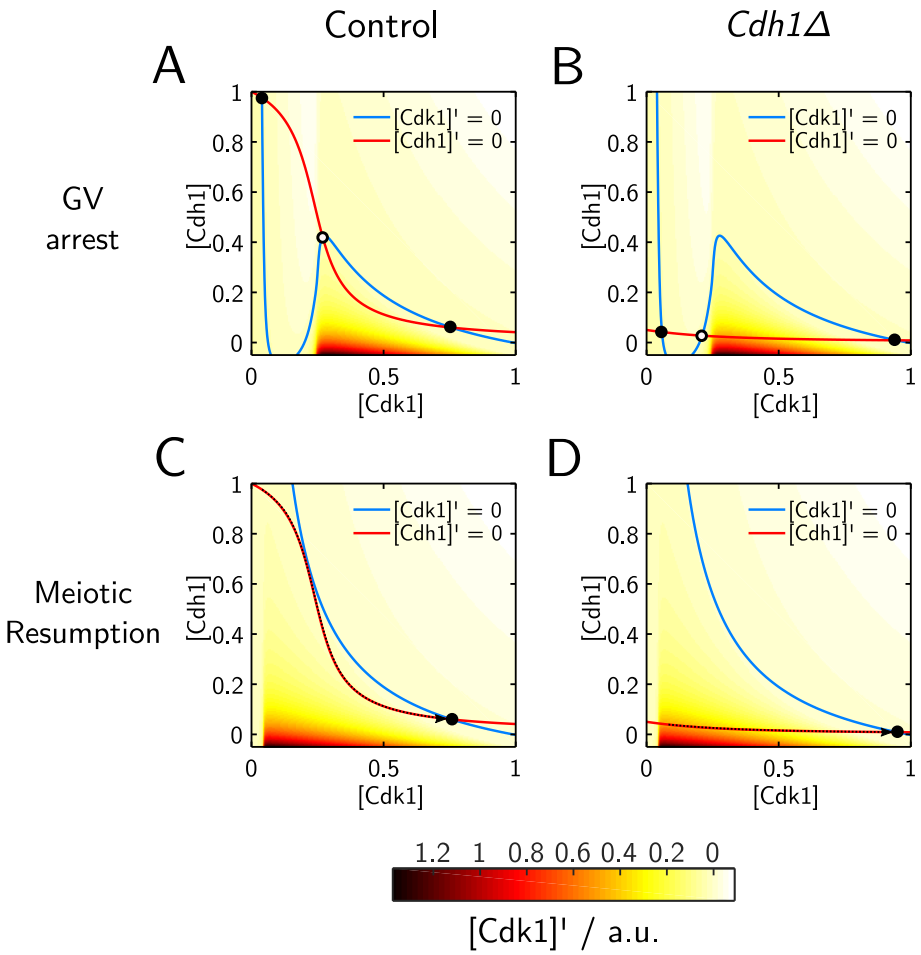

Figure 4.5: Phaseplane analysis of the reduced model. [Cdk1] and [Cdh1] nullclines are plotted for GV arrest and meiotic resumption for both Control and Cdh1 knock-out oocytes. Shading is used to indicate the rate of change of the Cdk1 variable at each point in the phaseplane.

this rise has not previously been commented on, it is observable in both sets of published data. The similarities between the simulated Cdk1 curve and these experiments provides good validation of the model, and suggests that meiotic resumption occurs in two distinct phases: an initial activation of existing Cdk1:Cyclin complexes by removal of inhibitory phosphorylation from Cdk1, followed by a slow accumulation of CycB to reach maximal CDK activity.

Discrepancy between model and experiment for the double knock-out may reflect differences in the level of Cdk1 activation

The double knock-out does not show such a good fit between the model and the experimental data as the control and single knock-out. The model predicts that meiotic resumption in the double knock-out should occur rapidly (~100 mins). This is slower than the time taken in the Cdh1 knock-out, but much faster than the control. However,

in the experiment the double knock-out oocytes start to undergo GVBD only after an initial lag of at least 4 hours, slower than both the Cdh1 knock-out and control. In addition, less than 60% of cells undergo GVBD at all during the 18 hour observation window, compared with over 80% of control cells.

One plausible explanation for this discrepancy relates to the difference in the absolute levels of Cdk1 activation between different conditions. Although Cdk1 activation in the control cells takes longer than in the double knock-out, the final [Cdk1] steady state reached is higher. The exact [Cdk1] threshold in the model that would correspond to GVBD is not known. If we assume that meiotic resumption in real cells proceeds similarly to the deterministic model but with some random variation in initial conditions and parameter values due to cell-cell variability, then this lower [Cdk1] set-point could translate into a smaller fraction of cells achieving sufficient Cdk1 activation to undergo GVBD.

4.4.3 Phaseplane analysis

To understand the behaviour of the system in more detail, we use the reduced model (Section 4.3.2) to plot phaseplanes showing the steady states of the system for Control and *Cdh1*Δ cells during GV arrest and meiotic resumption (Figure 4.5).

GV arrest and prometaphase correspond to distinct stable steady states on the phaseplane

In control cells (Figure 4.5A), the [Cdh1] nullcline (red curve) is a sigmoidal decreasing function of [Cdk1] because of inhibitory CDK-dependent phosphorylation of Cdh1. In *Cdh1*Δ (Figure 4.5B), this nullcline is flattened because the total Cdh1 concentration is significantly reduced. In both Control and *Cdh1*Δ, the [Cdk1] nullcline (blue curve) is bistable with respect to [Cdh1] during GV arrest as a result of the double-negative/positive feedback loops between Wee1/Cdc25 and Cdk1.

During GV arrest in both control and *Cdh1*Δ oocytes, the system has two possible stable steady states at the intersection points of the two nullclines (filled circles), separated by an unstable steady state (open circle). In control cells (Fig. 4.5A), these correspond to a high-[Cdh1], low-[Cdk1] GV arrest state (top left) and a low-[Cdh1],

high-[Cdk1] prometaphase state (bottom right). The intermediate unstable steady state acts as an energy barrier preventing transition from GV arrest into prometaphase. In *Cdh1*Δ cells (Fig. 4.5B), the GV arrest steady state (bottom left) differs from control since Cdh1 activity is low. This means that under these conditions the major limiting factor maintaining low CDK activity is the inhibitory phosphorylation of Cdk1 by Wee1.

Meiotic resumption occurs due to loss of the GV arrest steady state

In both control and *Cdh1*Δ, partial inactivation of inhibitory Cdk1 phosphorylation resulting from loss of PKA activity at meiotic resumption shifts the [Cdk1] nullcline to the right, eliminating the GV arrested state (Fig. 4.5C, D). The system therefore becomes irreversibly committed towards the other stable attractor in the bottom right corner with high [Cdk1] and low [Cdh1], corresponding to prometaphase.

The trajectories traced out towards the prometaphase state in control and *Cdh1*Δ cells are indicated by the dotted arrows in Figures 4.5C and 4.5D. Importantly, while the position of the prometaphase steady state is similar in both control and *Cdh1*Δ cells, the trajectories through the phaseplane are considerably different, due to the differences in starting position and to the flattened [Cdh1] nullcline in *Cdh1*Δ.

To understand how the different trajectories affect the rate of meiotic resumption, the phaseplanes have been shaded according to the magnitude of the [Cdk1]' vector at each point. Darker shading indicates that [Cdk1] is increasing quickly in that region of the phaseplane. A more detailed intuitive description of the shape of the vector field is included in Appendix C.

Control and Cdh1Δ oocytes follow different meiotic resumption trajectories

By comparing the meiotic resumption trajectories of control and *Cdh1*Δ oocytes in Figures 4.5C and 4.5D, we see that the *Cdh1*Δ results in a trajectory passing through a region of the phaseplane where [Cdk1]' is relatively high. By definition, higher [Cdk1]' means that Cdk1 activity is increasing more quickly, so the transition to the prometaphase state happens over a shorter time period. This has already been shown with the time-course simulations of the full model (Figure 4.3B), and is consistent with the experimental observations (Figure 4.4). In contrast, the meiotic resumption trajectory in the

control passes through regions of the phaseplane with comparatively low [Cdk1]', and so consequently take longer to activate Cdk1 and reach the prometaphase state, which is again consistent with both timecourse simulations (Figures 4.3A) and experiment (Figure 4.4)).

Slow activation of Cdk1 in control cells results from a Cdh1-dependent 'critical slowing down'

The reason for the slow transition in the control is a 'critical slowing down' phenomenon associated with the close proximity between the [Cdh1] and [Cdk1] nullclines. Where two nullclines approach each other, the system is close to being at a steady state, since the derivative of both variables is close to 0. Following loss of PKA activity, the [Cdk1] nullcline in Figure 4.5C is shifted upwards, but in doing so it is brought close to the [Cdh1] nullcline. In contrast, in $Cdh1\Delta$ the [Cdh1] nullcline is much lower (since the maximum possible [Cdh1] is limited by the much reduced $Cdh1_T$). This means that the same shift in the [Cdk1] nullcline results in a much larger separation between the two nullclines.

In both cases, since the [Cdh1] nullcline is unaffected by loss of PKA activity, the initial starting point of the meiotic resumption trajectory (previously the GV arrest steady state) is located on this nullcline. Since at all points on the line [Cdh1]' $= 0$, the initial tendency for the system is to move horizontally towards the [Cdk1] nullcline. Physiologically, this corresponds to a decrease in inhibitory phosphorylation and an increase in CycB. As [Cdk1] increases, this will lead to a decrease in the [Cdh1] steady state towards the new value of the [Cdh1] nullcline. The rate of Cdh1 phosphorylation is fast relative to the rate of CycB synthesis, so the overall effect is to trace out the path of the [Cdh1] nullcline towards the prometaphase steady state.

The greater separation between the nullclines in $Cdh1\Delta$ means that the meiotic resumption trajectory passes through a region of the phaseplane where [Cdk1] is increasing more quickly compared to the control. In control cells, the [Cdk1] trajectory passes through a region of the phaseplane where the two nullclines are close together, with the result that [Cdk1] rises more slowly.

The physical interpretation of the close proximity between the nullclines is that during

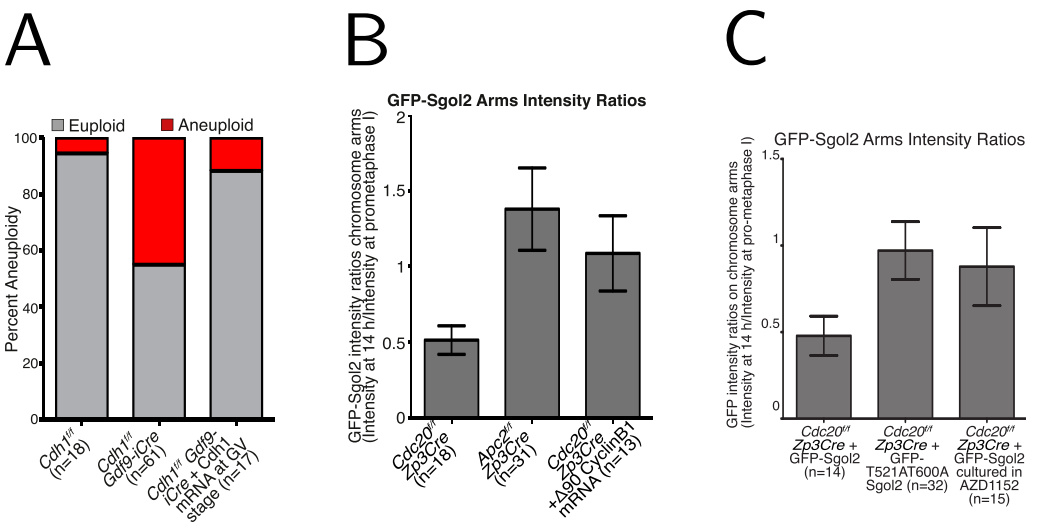

Figure 4.6: Selected experimental data figures reproduced from the co-authored Rattani et al. paper [244] (DOI: 10.1016/j.cub.2017.04.023) under a Creative Commons 4.0 License (`https://creativecommons.org/licenses/by/4.0/`). Experiments by Ahmed Rattani and colleagues. (A) Frequency of aneuploidy observed in chromosome spreads from Control cells, (*Cdh1*$^{f/f}$), *Cdh1*Δ cells (*Cdh1*$^{f/f}$ *Gdf9-iCre*), and *Cdh1*Δ cells with Cdh1 mRNA rescue. (B) Normalised GFP-Sgol2 fluorescence intensity on chromosome arms for *Cdc20*$^{f/f}$ *Zp3Cre* control is compared with *Apc2*$^{f/f}$ *Zp3Cre* and with injected non-degradable CycB mRNA (Δ90 CyclinB1). (C) GFP-Sgol2 fluorescence intensity on chromosome arms. T521A T600A Sgol2 is mutated at Aurora B/C target sites. AZD1152 is an Aurora B/C inhibitor.

meiotic resumption, control cells approach closely to a high-[Cdh1], low-[Cdk1] steady state, where inhibitory Cdk1 phosphorylation is removed, but Cdh1-dependent degradation of CycB limits Cdk1 activation. This state corresponds to the initial levelling off of the [Cdk1] curve in Figure 4.3A. This state would correspond to a true steady state if the nullclines actually intersected, and in that case we would expect the [Cdk1] curve to level off at that point and not undergo further activation. Since the nullclines do not intersect, this state is one that the system approaches, but does not attain. CycB synthesis is always slightly higher than Cdh1-dependent degradation, so the system continues to move towards the prometaphase state through slow accumulation of CycB. As the system moves further along the [Cdh1] nullcline, the additional Cdk1 activity leads to further inhibition of Cdh1, resulting in an acceleration in Cdk1 activation which can be seen as the second phase of the [Cdk1] curve in Figure 4.3A.

4.5 Discussion

Our model has demonstrated that the presence of Cdh1 during GV arrest and meiotic resumption is responsible for the observed slow, biphasic rise in CDK activity during

meiotic resumption. However, this leaves open the question of the physiological significance of this slow rise, and hence the major role of Cdh1 in meiosis I. Work by Ahmed Rattani and other collaborators, outlined here and described in more detail in our joint paper [244], provides important insight into the physiological implications of the model findings.

Cdh1 is necessary for efficient chromosome segregation

Cells lacking Cdh1 have a higher incidence of aneuploidy during the first meiotic division than control cells (Fig. 4.6A) [245]. This suggests that the ability to limit the rise in CDK activity during meiotic resumption may be necessary to allow chromosome pairs to segregate normally.

Cdh1-dependent cyclin degradation and AurB/C kinase activity are required for efficient removal of Sgol2 from chromosome arms

An explanation for this observation is the effect of APC/C^{Cdh1} activity on Sgol2 localisation, since Sgol2 is responsible for protection of centromeric cohesin from cleavage during meiosis I (see Section 1.5.3). In the absence of APC/C-dependent CycB degradation, Sgol2 persists on chromosome arms for many hours after GVBD. This effect is seen both when APC/C activity is lost through Apc2 depletion, or by injection of non-degradable CycB (Figure 4.6C). Further work showed that phosphorylation of Sgol2 by AurB/C kinases is necessary for its dissociation from chromosome arms during meiotic resumption. Expressing a mutant Sgol2 with alanine substitution at two AurB/C target sites, or inhibiting AurB/C activity with AZD1152 both resulted in greater retention of Sgol2 at chromosome arms than in control cells (Figure 4.6B).

APC/C^{Cdh1} provides a time window of low CDK activity during which AurB/C can act on Sgol2

Bringing together these experimental findings with the modelling results gives the following explanation for the Cdh1-dependence of efficient chromosome segregation during meiotic resumption (Figure 4.7). During GV arrest, Sgol2 is located along the entire chromosome arm and maintains cohesin in a dephosphorylated state through recruitment of PP2A. Without phosphorylation, cohesin can be stably maintained during the long GV

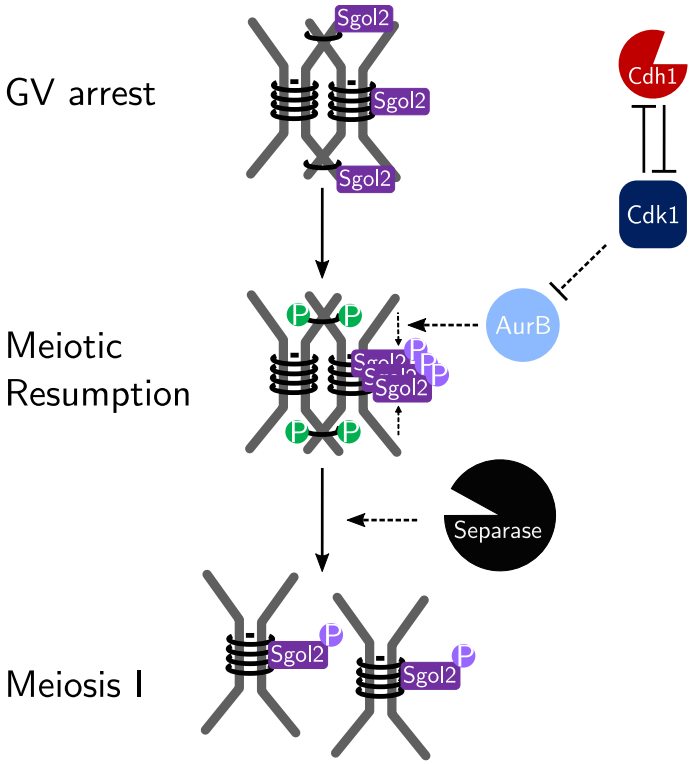

Figure 4.7: Proposed mechanism for Cdh1-dependence of efficient chromosome segregation during meiotic resumption. See text for details.

arrest. Cdk1 activity is kept low by inhibitory phosphorylation and by Cdh1-dependent degradation of CycB.

At meiotic resumption, Aurora B/C activity phosphorylates Sgol2, promoting its relocation to the centromeres. As a result, arm cohesin is no longer protected from phosphorylation, making it a suitable target for cleavage at anaphase I. The slow rise in Cdk1 activity as a result of counteracting Cdh1 activity prevents Cdk1 from rising too quickly before this process is complete. Once Cdk1 has risen sufficiently, it will inhibit AurB and promote entry into prometaphase, leading eventually to separase activation and cohesin cleavage at anaphase I. If relocalisation of Sgol2 has not been completed prior to separase activation, arm cohesin may not be cleaved, or centromeric cohesin may be insufficiently protected from cleavage, leading respectively to non-segregation of homologous chromosomes, or premature sister chromatid separation.

4.6 Conclusion

Mitosis and meiosis use much of the same cell cycle machinery, but with important differences in the sequence and timing of their activities. These crucial differences not

only ensure fulfilment of the essential meiotic functions of undergoing two sequential rounds of chromosome segregation and cell division without an intervening S-phase, but also allow for different stages of meiosis to be separated in time, for example in mammalian oogenesis.

One such component with distinct mitotic and meiotic functions is the APC/C coactivator Cdh1. In mitosis, Cdh1 becomes active during mitotic exit, and remains so during G1 until shut off by a combination of Emi1-dependent inhibition and CDK-dependent phosphorylation at the G1/S transition. In contrast, meiotic Cdh1 is active during GV arrest in mammalian oocytes, corresponding to a block in prophase of the cell cycle.

We have developed a mathematical model for GV arrest and subsequent meiotic resumption in mouse oocytes. In the model, the activity of the Cdk1:CycB complex is regulated by the availability of its CycB subunit, and by inhibitory phosphorylation of Cdk1 by PKA-dependent Wee1 activity. Although Cdh1 contributes to low CDK activity during GV arrest by promoting cyclin degradation, its presence is not strictly required since inhibitory phosphorylation of Cdk1 is sufficient to maintain the arrest.

Instead, we show that the presence of Cdh1 during meiotic resumption results in a significant delay in accumulation of CycB and hence CDK activity. Compared to mitosis, where the G2/M transition occurs over a timecourse of minutes, the rise in CDK activity during meiotic resumption takes around 6-8 hours. Our model is consistent with this timing, and with Cdh1 and Cdc25 knock-out experiments performed by Ahmed Rattani. Further experimental work detailed in our joint paper [244] has shown that the Cdh1-dependent delay in Cdk1 activation is essential to provide a time-window of low CDK activity in which centromeric cohesin can be protected by Sgol2.

Chapter 5

Calculating APC/C Activity in Meiosis I

5.1 Introduction

In this chapter we present work in collaboration with Martin Anger (CEITEC, Brno), investigating the role of the SAC in regulating APC/C activity in mouse oocytes during meiosis I. The extent to which the SAC is active during meiosis I is the subject of considerable uncertainty, and we were interested to investigate how checkpoint activity affected APC/C activity. To do so, we use a mathematical model of substrate degradation kinetics to derive APC/C activity timecourses from *in vivo* data showing the level of fluorescence-labelled substrates in the cells over time. This enables us to precisely link APC/C activation and inactivation during meiosis I with cellular events including anaphase and loss of Mad1 from kinetochores.

We find that the rise in APC/C activity following GVBD is closely linked to checkpoint inactivation, but that this APC/C activation is only slightly altered in the presence of persistent chromosomal abnormalities. This suggests that, while active in oocytes, the checkpoint is a less significant force for regulating APC/C activation than in mitotic cells. We also examine the effect of completely removing chromosomal input on APC/C activation by calculating APC/C activity profiles in enucleated cytoplasts, and find that lack of chromosomal regulation can permit repeated spikes of APC/C activity.

5.2 Calculating APC/C activity from substrate curves

In order to determine the effects of the checkpoint on APC/C activation, we needed a technique to determine the level of APC/C activity so that it could be compared to the timing of checkpoint activation and inactivation. While a direct read-out of APC/C

activity was not possible, we used a modelling approach to infer APC/C activity from the degradation profile of a fluorescence-labelled substrate. Previous work has used a similar method to determine the APC/C activity profile in oocytes [212], however we refine this method by directly determining the required kinetic parameters rather than simply fitting to the expected shape of the curves. Here we describe the principles behind our method and the accompanying experiments required to generate the necessary substrate degradation timecourses.

5.2.1

The text originally presented in this section cannot be made freely available via ORA due to confidentiality agreements.

5.2.2 APC/C Substrate Degradation Kinetics

Using these fluorescence timecourses, we make simplifying assumptions about the system behaviour which allow us to infer APC/C activity from the data. We assume that the rate of change in the substrate concentration ($[\mathrm{S}]$) is dependent upon a basal rate of synthesis from the injected mRNA, and upon both APC/C-dependent and APC/C-independent degradation (this latter pathway could also incorporate fluorescence bleaching). We summarise these terms with the following rate expressions:

- Synthesis rate: k_S
- APC/C-dependent degradation rate: $k_d \cdot [\mathrm{APC/C}] \cdot [\mathrm{S}]$
- Intrinsic degradation rate: $k'_d \cdot [\mathrm{S}]$

This gives the following ODE for the substrate concentration:

$$\frac{d[\mathrm{S}]}{dt} = k_s - (k_d \cdot [\mathrm{APC/C}] + k'_d) \cdot [\mathrm{S}] \tag{5.1}$$

This can then be rearranged to give an expression for APC/C activity:

$$k_d \cdot [\mathrm{APC/C}] = \frac{\frac{d[\mathrm{S}]}{dt} + k_s}{[\mathrm{S}]} - k'_d \tag{5.2}$$

5.2.3 Parameter estimation

Calculating APC/C activity using Equation 5.2 requires that the values of the parameters k_s and k'_d are known. To estimate these values, we consider a simplified system where APC/C is inactive. In this case, Equation 5.1 is reduced to:

$$\frac{d[\mathrm{S}]}{dt} = k_s - k'_d \cdot [\mathrm{S}] \tag{5.3}$$

In this situation, a linear regression can be used to fit this equation to a graph of $\frac{d[\mathrm{S}]}{dt}$ against $[\mathrm{S}]$, and hence estimate the parameters k_s and k'_d. To achieve this experimentally, nocodazole was used to arrest cells expressing CFP-labelled securin. We assume that APC/C is kept inhibited by the SAC during nocodazole arrest, meaning that the assumptions required for Equation 5.3 hold true, and allowing estimation of k_s and k'_d.

$\frac{d[\mathrm{S}]}{dt}$ is estimated using a finite difference approximation:

$$\frac{d[\mathrm{S}]}{dt} \approx \frac{[\mathrm{S}]_{t+\Delta t} - [\mathrm{S}]_t}{\Delta t} \tag{5.4}$$

Multiple sets of k_s and k'_d parameters were calculated corresponding to different substrates (securin or CycB), and in some cases to a different genetic background. These parameters were then used for APC/C activity calculations for the corresponding cell type/substrate combination. For each set of parameters, the window size (Δt) was chosen to reduce the impact of experimental noise on the outcome.

Details of the nocodazole samples used for parameter estimation, and the corresponding parameter values, are given in Table 5.1. For some experiments (notably those using cytoplasts and fusion oocytes) it was not possible to obtain nocodazole data for the

Substrate	Cell-type	n	k_s / 10^{-3} a.u. min^{-1}	k'_d / 10^{-3} min^{-1}
Securin	Control	13	3.5	1
Cyclin B	Control	21	5.4	2.2
	ZP3+	8	12	0.78
	ZP3-	7	20	1

Table 5.1: Table of k_s and k'_d parameters measured for different combinations of cell type and/or substrate.

corresponding cell type, in which case control parameters were used.

5.2.4 Data Processing

Due to variation in measurement conditions and instrument settings, the fluorescence intensity data does not provide an estimate of Securin or CycB concentration that can be compared directly between cells. To get around this problem, which would otherwise prevent us from using parameters estimated with one set of data to calculate APC/C activity in another set, data are normalised to the value at GVBD. Where GVBD annotation is not available, data are normalised to the first measured timepoint. We assume that the level of substrate at GVBD is constant, so that the parameters calculated from one set of data can be directly applicable to another. The implementation of this data analysis was performed in MATLAB [219].

5.2.5 APC/C peak identification

Figure 5.1 shows an example securin curve, alongside the corresponding calculated APC/C curve. This example illustrates how this approach can reveal details about the shape and timing of the underlying APC/C activity profile which are not intuitively obvious from the substrate degradation curve alone.

While clear peaks in APC/C activity are identifiable in the calculated profiles, a more rigorous framework for characterising this profile was necessary to allow for quantitative comparison between different cells and cell types. To do so, we developed a MATLAB

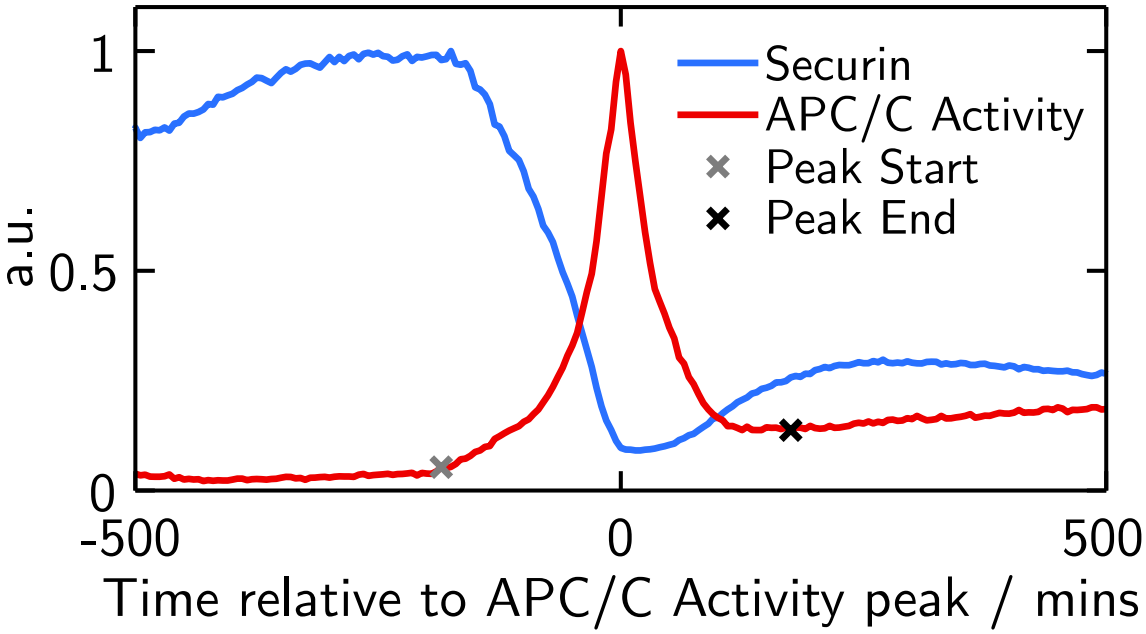

Figure 5.1: Example Securin degradation curve (blue) and corresponding APC/C activity (red). The APC/C activity curve is annotated with the start- and end-points of the APC/C activity peak as identified by the peak identification protocol.

protocol to identify the start and finish of each APC/C activity peak. This protocol had to robustly identify these features across data from different cell types and detection conditions, with peaks which varied significantly in shape, noise and amplitude. It also had to cope with timecourses containing varying numbers of peaks. Below we outline the steps included in this protocol.

Peak identification via APC/C activity maximum

To determine the position and number of peaks within a dataset, the inbuilt MATLAB function *findpeaks()* was used to identify local maxima within the APC/C activity profile. The function allows for specific identification of peaks with sufficient prominence over the surrounding data points, allowing for exclusion of transient local maxima arising from signal noise. This prominence was set at 0.0025.

The typical pattern of peak placement within the timecourse is for the initial peak to occur within a few hours of GVBD. In some cells, this does not occur, and a misshapen noisy peak appears at the very end of the recording time, characterised by a near-vertical spike in the activity profile. These peaks share neither the typical profile nor the timing of other meiotic APC/C peaks, and are not likely to represent a normal meiotic APC/C activation. We therefore opt to identify peaks only where the initial peak occurs

within 600 minutes of GVBD (this threshold is then extended by 250 minutes for each subsequent peak).

In the majority of cells, only a single APC/C peak is present. The exception is enucleated cytoplasts (see later for more detailed discussion). When comparing between non-cytoplast datasets, where peak number is not a significant point of interest, a simplified method of finding the peak position is simply to take the maximum of the APC/C activity profile in each cell.

APC/C activation threshold

A fixed threshold for APC/C activity cannot be used to determine the beginning and end of the APC/C activity peaks because in general the post-activation state has a higher baseline of APC/C activity than the pre-activation state. Furthermore, these basal levels of activity differ between cells. Instead, we use the shape of the curve rather than the precise values of APC/C activity associated with it. The initial point of activation is determined by combining a fixed APC/C activity threshold with a test to determine whether the point is part of a larger spike in APC/C activity. Doing so prevents the erroneous identification of transient crossings of the activation threshold as part of the general background noise as APC/C activation.

The first point of the curve higher than the fixed APC/C activity threshold (0.003) is a candidate for the start of the APC/C activity peak. However, to minimise the effects of noise, two tests were applied to this point to determine whether it represented the start of a true APC/C activity peak. These tests are:

$$APC_t < \frac{\sum_{\tau=1}^{5} APC_{t+\tau}}{5} \tag{5.5}$$

And:

$$APC_t < \{APC_{t+\tau} | 4 < \tau < 11\} \tag{5.6}$$

Where APC_t is the APC activity measured at timepoint t. The first test checks that the APC/C activity at the chosen threshold point is less than the mean value of the next five subsequent timepoints. This ensures that the APC/C activity is locally rising, while smoothing out the effects of localised noise in APC/C activity. The second test checks

further forward in time, and checks that all values of APC/C activity are larger than the threshold value across this range. The rate of increase of APC/C activity after the initial activation, and the low level of noise on the APC/C peak itself means that these two checks can simply and effectively identify whether a given point above the activation threshold is part of a true activity peak. In cases where it is not, the next point above the threshold is instead chosen and again tested, until a point is found which satisfies these criteria.

APC/C minima

Following each APC/C peak, the activity tends to fall to a local minimum, either overshooting before recovering to a post-activation steady state, or falling before a second peak of APC/C activation occurs. Capturing this point provides a convenient endpoint from which to measure the timing of APC/C activation associated with each peak.

An inbuilt MATLAB function, *islocalmin()* was used to identify the first local minimum following each APC/C peak. A prominence threshold was set to exclude some cases where transient local minima occurred close to the top of the APC/C peak due to signal noise. However, by doing so this occasionally prevented the identification of any local minimum at all on other curves. Therefore an iterative search process was used where the prominence threshold was sequentially reduced if a search with a higher prominence threshold failed to return a local minimum in the expected location in the data. In addition, since the amplitude of both the APC/C peak and the subsequent minimum varied substantially between different cells and conditions, the initial prominence threshold used in each case was set as a fraction of the maximum APC/C amplitude in each cell. Thus, a peak with lower amplitude would have a lower prominence requirement for identification of the subsequent local minimum.

5.3 Results

The initial aim of this investigation was to determine the extent to which APC/C activation during meiosis I is affected by the SAC. To do so APC/C activity profiles were annotated with the timing of cytological events (GVBD and anaphase), and the strength of SAC signalling was determined by monitoring the number of kinetochores decorated

with fluorescence-labelled Mad1. Comparing the relative timings of these events with APC/C activity allowed relationships between these events and the activation or inactivation of APC/C to be inferred.

5.3.1

The text originally presented in this section cannot be made freely available via ORA due to confidentiality agreements.

5.3.2

The text originally presented in this section cannot be made freely available via ORA due to confidentiality agreements.

Figure 5.2: This figure cannot be made freely available via ORA due to confidentiality agreements.

Figure 5.3: This figure cannot be made freely available via ORA due to confidentiality agreements.

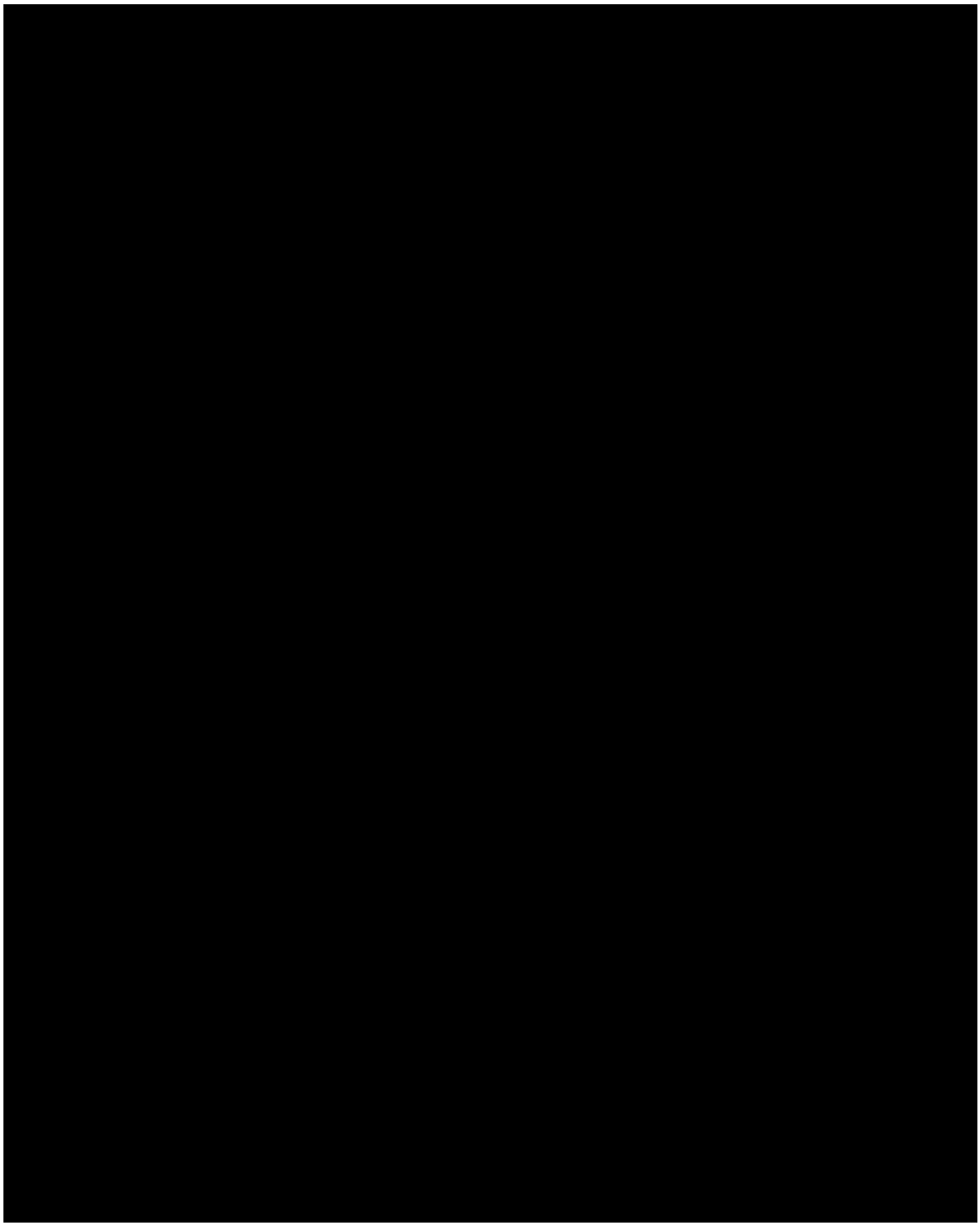

Continued on next page.

Figure 5.3: *Continued*

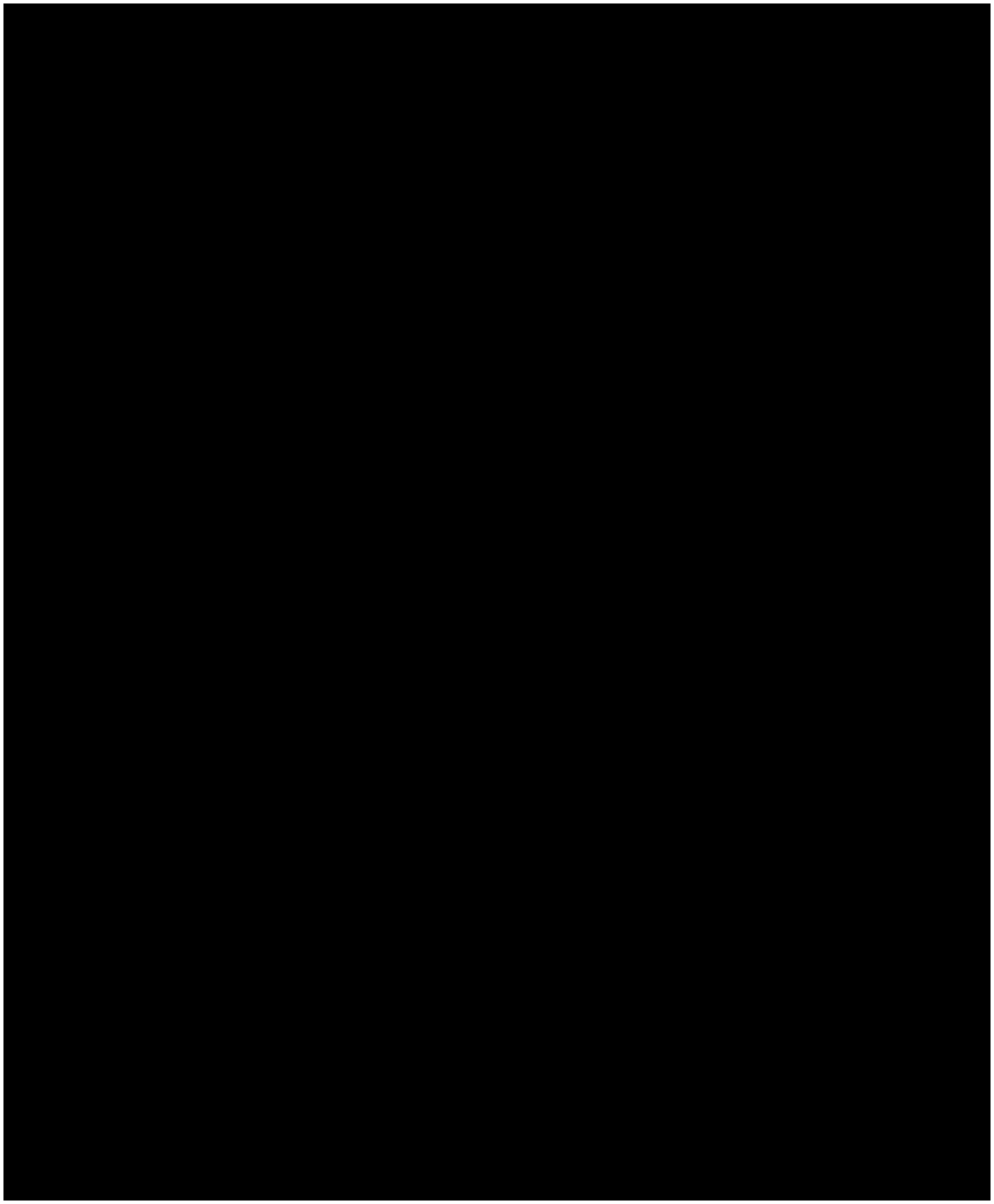

Figure 5.4: This figure cannot be made freely available via ORA due to confidentiality agreements.

5.3.3

The text originally presented in this section cannot be made freely available via ORA due to confidentiality agreements.

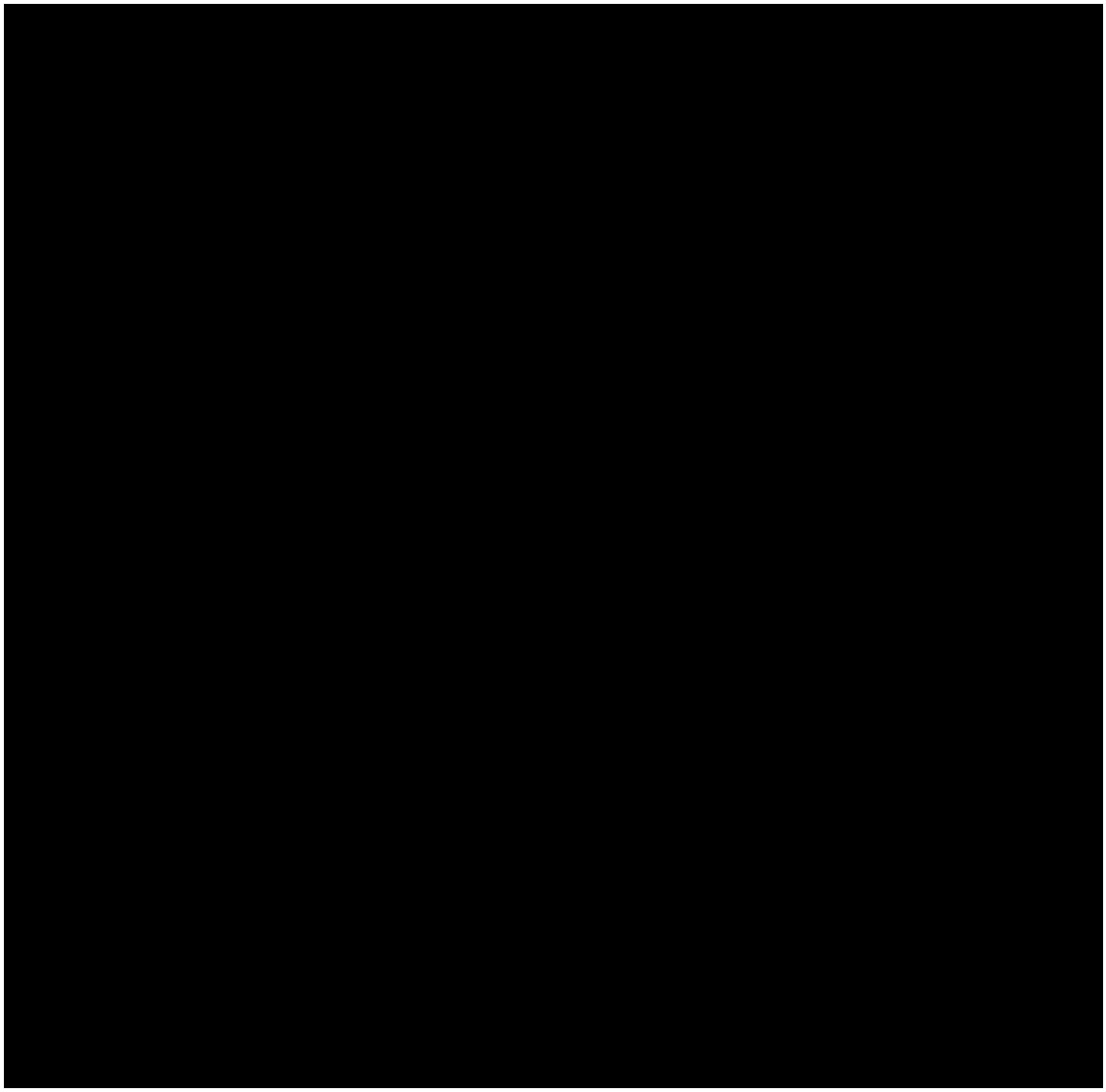

Figure 5.5: This figure cannot be made freely available via ORA due to confidentiality agreements.

Figure 5.6: This figure cannot be made freely available via ORA due to confidentiality agreements.

5.3.4

The text originally presented in this section cannot be made freely available via ORA due to confidentiality agreements.

Figure 5.7: This figure cannot be made freely available via ORA due to confidentiality agreements.

5.3.5

The text originally presented in this section cannot be made freely available via ORA due to confidentiality agreements.

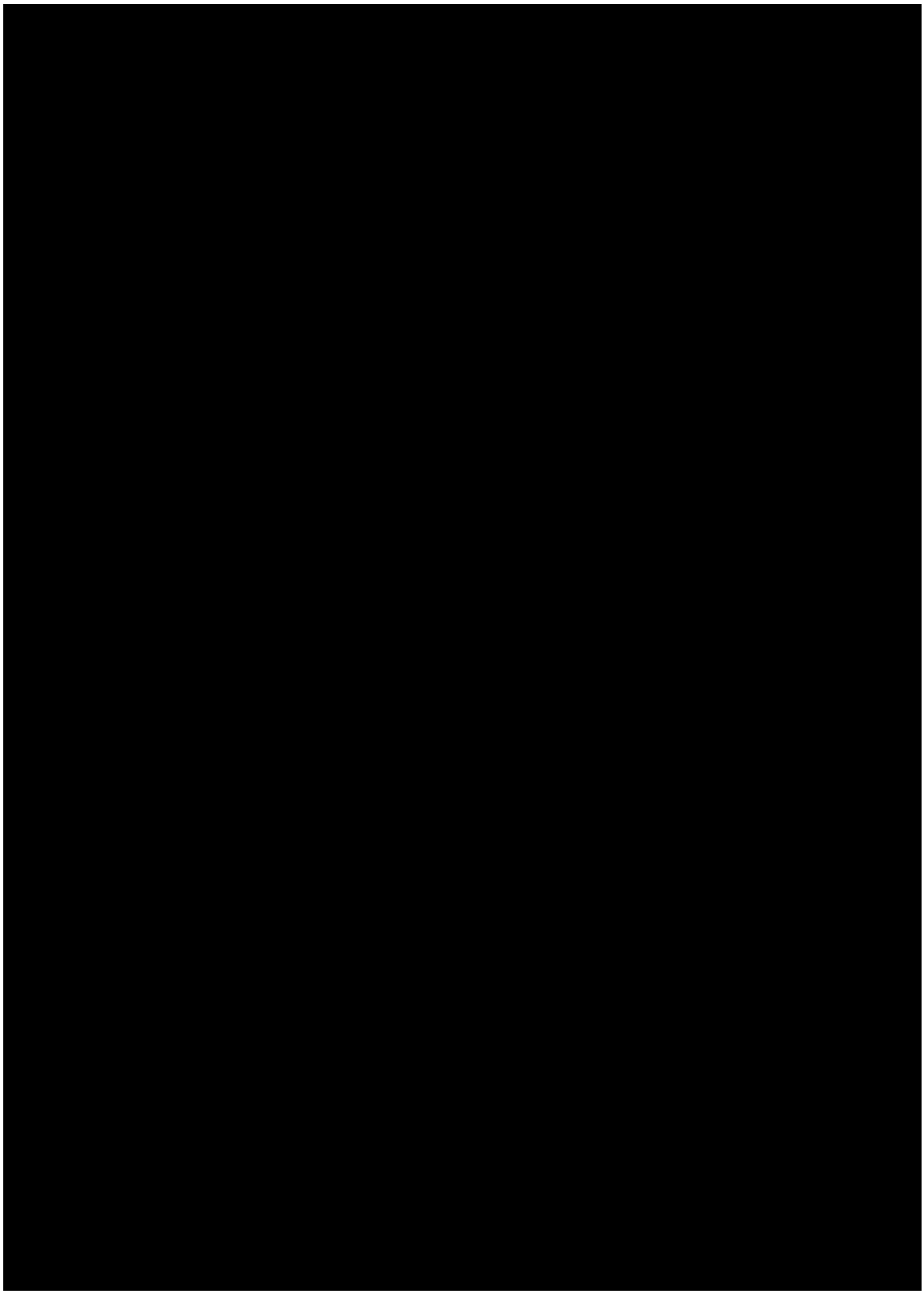

Figure 5.8: This figure cannot be made freely available via ORA due to confidentiality agreements.

Figure 5.9: This figure cannot be made freely available via ORA due to confidentiality agreements.

Figure 5.10: This figure cannot be made freely available via ORA due to confidentiality agreements.

5.4 Discussion

5.4.1 SAC activity in meiosis I

As discussed in Section 1.5.3, there is mixed evidence for the effectiveness of the SAC in meiosis I, and our results are consistent with the literature description of an active but error-prone checkpoint. As evidence for checkpoint activity, nocodazole induces a checkpoint-arrested state, and we have used this fact to estimate kinetic parameters for use in APC/C activity determination. Furthermore, the close correlation between $Mad1_{off}$ and the rise in APC/C activity in control oocytes following GVBD suggests that the checkpoint is important for determining the timing of APC/C activation during a normal meiosis I. However, the failure of the checkpoint to delay anaphase in fusion oocytes with constitutive chromosome segregation errors suggests a more limited ability of the checkpoint to influence the timing of APC/C activation in the case of perturbations

short of full nocodazole arrest. This agrees with previous studies showing failure of the SAC to respond directly to specific chromosomal defects in meiosis I in mouse oocytes. This behaviour contrasts with the functioning of the checkpoint during a similar situation in a mitotic cell cycle, where checkpoint activation can delay anaphase in response to a single unattached kinetochore.

A role for the SAC in attachment sensing without a corresponding contribution from error correction could potentially explain how the checkpoint is functional under normal conditions, but is not responsive to chromosomal alignment defects. We have shown here that the rise in APC/C activity is closely linked to loss of SAC signalling under normal conditions. However if only attachment were detected, then misaligned chromosomes with sufficient incorrect attachments could also silence the checkpoint, allowing these defects to persist into anaphase I. In nocodazole by contrast, no attachments are made, so the checkpoint can become fully active and the system undergoes SAC arrest. A limited checkpoint response such as this would still provide a suitable delay during prometaphase to allow spindle formation and attachment, but would be less robust to more complex alignment errors. Further targeted experiments would be necessary to test this hypothesis, for example by contrasting the effects of MPS1 and AurB inhibition on the APC/C activation profile.

5.4.2 Cytoplast Oscillations

A second observation revealed by the APC/C activity timecourses in this chapter is the ability of enucleated cytoplasts to undergo repeated cycles of APC/C activation. It is interesting to compare this behaviour with the well-studied *Xenopus* embryonic extract, which also permits oscillations in APC/C activity in the absence of a significant nuclear input. In *Xenopus*, this oscillation has been well characterised in a classic model of the eukaryotic cell cycle, as already detailed in Section 1.3.3. In mouse cytoplasts, in contrast to *Xenopus* extract, the oscillations appear to be self-limiting, with the majority of oscillating cells stopping after only a single additional spike.

While it is possible that the underlying oscillator in mouse oocytes is similar to that seen in the *Xenopus* extract, it is necessary to consider the implications of the state of

the system in each case. In the mouse system, the point at which we observe additional oscillations corresponds to the transition between meiosis I and meiosis II, during which we would normally expect to see the system enter into a CSF-arrested state. During CSF arrest, APC/C activity is inhibited and CDK levels are maintained in order to prevent the cell from dropping out of meiosis into a G1-like state. In cytoplasts, we instead see re-activation of APC/C, suggesting that some process is counteracting the ability of the cell to enter CSF arrest.

In contrast, *Xenopus* extracts initially correspond to an interphase state immediately following meiosis II [79], in which case the cell is primed to undergo repeated cycles of cell division following fertilisation. There are obvious similarities between the two systems, with both deriving from an oocyte precursor with nuclear material removed (though this is subsequently re-added in *Xenopus* extract, in which sperm nuclei are used as a marker for M-phase events). However, the difference in the point at which the model system is created defines a distinct set of components and initial conditions, so the oscillations observed in both cases do not necessarily result from the same network structures.

One additional observation of interest concerns the effects of using fluorescence-labelled CycB, rather than securin as the marker for APC/C activation. In this case, the appearance of APC/C peaks in cytoplasts is significantly reduced. The presence of this additional CycB under control of a constitutive promoter may perturb the system and push it into a regime where oscillations are no longer favoured. This observation would support a role for CDK activity in the oscillatory mechanism.

5.5 Conclusion

In this chapter we have used a model of APC/C substrate degradation kinetics to analyse the role of the SAC in regulating APC/C activity in meiosis I. We find that while loss of checkpoint signalling is closely linked to the onset of the initial rise in APC/C activity in control oocytes, that only minor differences in timing and SAC activation are observed in fusion oocytes with persistent chromosomal defects. This suggests that SAC signalling may not be such a powerful regulator of APC/C activity in Meiosis I as in the equivalent stages of mitosis, and suggest that a weakened error correction pathway may be one

explanation for these effects. We also found that in the complete absence of chromosomal signalling in enucleated cytoplasts, APC/C undergoes multiple cycles of activation and inactivation, indicating that nuclear signals may be responsible for regulating an underlying oscillator-like system for APC/C activation.

This work raises several questions about regulation of APC/C activity in mouse oocytes. In particular, the mechanisms underlying the timing of the rise, peak, and fall in APC/C activity remain unclear. Furthermore, the mechanism driving the oscillator-like behaviour in the cytoplasts is also unknown. The established protocol for APC/C activity determination presented here could be easily applied to investigate these questions by generating APC/C activity profiles from oocytes under different experimental perturbations.

Chapter 6

General Discussion

The four preceding chapters have each explored a particular area in which mathematical modelling and experimental data have been used to address questions important for the regulation of M-phase progression. While the individual models and their results have been discussed at the end of each chapter, here we again summarise the key findings and bring together the different aspects of the work to make general comments about the implications of this work for our understanding of M-phase regulation in both mitosis and meiosis. We also evaluate the modelling approaches used, and speculate about possible future work arising from outstanding questions raised in this thesis.

6.1 Network motifs controlling M-phase progression

Successful progression through M-phase requires the cell to face multiple decision-making points in order to ensure that each daughter receives a complete copy of the genetic information from the parent cell. These decision-making points correspond to the successful completion of specific processes. For example, entry into M-phase requires that DNA replication in S-phase, and the subsequent gap phase G2 have been successfully completed. Likewise, progression from metaphase into anaphase requires that chromosomes are correctly attached and aligned on the mitotic spindle. Cytokinesis and exit from M-phase should occur only once chromosome segregation has successfully taken place. These decision-making points correspond to switch-like mechanisms in the underlying control network. In creating these switch-like transitions, the cell frequently adopts common network motifs to solve similar design problems. Here we discuss the use of these recurring network motifs in the context of the models we have introduced in this thesis.

6.1.1 Double-negative feedback loops regulating APC/C activation

Close control of APC/C activity is essential for cells to undergo a normal M-phase. APC/C activity is responsible both for the timing of the central events of chromosome segregation at anaphase, and for the successful completion of later mitotic events and resetting the cell cycle for entry into the next G1-phase. These roles for APC/C correspond respectively to degradation of its two major M-phase substrates: securin and CycB.

We started with an analysis of a generic network motif (FADS) with the potential to create a bistable switch at multiple cell cycle transitions, including at M/A. This introduced the double-negative feedback loop between APC/C, Cdk1:CycB and the SAC (Figure 3.1) which is at the core of the checkpoint signalling system. We demonstrated that this simple 3-component network is able to generate a unidirectional bistable response to the fraction of unattached kinetochores (Figure 2.13). In Chapter 3 the same double-negative feedback loop forms the core of the SAC model presented, but this is significantly extended with a more detailed description of the checkpoint pathway and its CDK dependence, with the additional B55/ENSA/Gwl-dependent regulation of MPS1 dephosphorylation, and with inhibitory CDK-dependent phosphorylation of Cdc20 (Figure 3.2). These additional mechanisms create further double-negative feedback loops between APC/C^{Cdc20} and CDK activity. Ultimately, exit from mitosis requires prolonged activation of APC/C in the form of APC/C^{Cdh1}, again operating via a double-negative feedback loop between CDK and APC/C activity.

As discussed in Section 3.5.2, exit from mitosis requires that each of these double-negative feedback loops is overcome. The extent to which this is a sequential versus a concerted process is less clear. Some ordering of events is evident, for example since APC/C^{Cdc20} is essential for substrate degradation at anaphase, even if APC/C^{Cdh1} can take over this role later in the process. However, whether for example the irreversible inactivation of error correction (via AurB dephosphorylation) and MCC assembly (via MPS1 dephosphorylation) occur simultaneously with falling CDK activity, or whether two distinct thresholds exist is unclear.

6.1.2 B55/ENSA/Gwl

The multiple roles of the B55/ENSA/Gwl pathway in M-phase progression can also be examined in the context of these models. In Chapter 2 we present a FADS mitotic exit model comprising these three components, which creates a bistable mitotic exit switch (Figure 2.15). Indeed, the B55:pENSA interaction is the archetypal example of an Activator : Domineering Substrate (or 'unfair competition') motif [176]. The same switching mechanism, acting in the opposite direction, is also important for regulating entry into mitosis by control of Wee1 and Cdc25 dephosphorylation [247]. Meanwhile in Chapter 3 we have also described a role for B55-dependent dephosphorylation of MPS1 S281 in preventing checkpoint reactivation during anaphase.

These multiple roles raise important questions about the timing of B55 activation during mitosis. While it is clear that B55 is inactivated at M-phase onset, and becomes active again during mitotic exit, the exact timing of this reactivation is important for understanding the role played by B55 in irreversibility of M-phase progression. We have demonstrated that B55-dependent dephosphorylation of MPS1 controls checkpoint inactivation, implying that the timing of this process is highly sensitive to the exact point at which B55 becomes active following anaphase. It has previously been suggested that B55 is the subject of a time-delayed switching mechanism (the so-called 'EG-timer') due to the time taken for sufficient p-ENSA dephosphorylation to occur to enable B55 to target other substrates [173]. ENSA/Gwl-depletion in the same study is associated with a 'cut' phenotype (premature cytokinesis), suggesting that B55 activity is associated with the regulation of post-anaphase mitotic events. This places a tight time restriction on the window of B55 activation, since checkpoint inactivation is only meaningful in the context of chromosome segregation, which must by necessity precede cytokinesis. Preferential dephosphorylation of MPS1 over cytokinesis-related substrates might provide one possible way out of this problem, however it is not clear whether or not this is the case. If B55 activation does occur later in mitosis then the relevance of its role in SAC signalling via MPS1 may not correspond directly to the requirement for irreversible checkpoint inactivation at anaphase. As discussed in Section 3.5.2, additional feedback loops may also play a role in regulating checkpoint activity. In this context, later B55-

dependent inactivation may be an additive effect on top of other pathways (for example those acting on AurB), providing a final shut-off on checkpoint activity as the cell commits to mitotic exit.

6.1.3 Future work: Overlapping feedback loops

By breaking down complex network structure into combinations of simple network motifs, mathematical modelling can demonstrate which features of the network are required for its core behaviour, and which provide more precise control around this core functional structure.

As discussed above, our work identifies multiple mechanisms by which double-negative feedback loops act to regulate APC/C and mitotic checkpoint activation during the course of M-phase progression. While we have explored some of the implications of this finding in this thesis, the picture remains unclear. In particular, the relative significance of these different potential thresholds in regulating progression through mitosis is not clearly defined. Similarly, it is not known to what extent the double-negative feedback mechanisms controlling APC/C activation at M/A and during mitotic exit integrate into a single irreversible switch, versus a series of switches associated with different thresholds of APC/C or CDK activity. A more thorough understanding of the relationship between the different switching mechanisms is therefore required.

Future work could address these questions by more precise characterisation of intermediate states (i.e. attempting to isolate cases where one checkpoint mechanism is on, but another off), and assessing the effects on potential checkpoint reactivation. Knocking out individual pathways may enable the system to access intermediate states which it would normally only pass through transiently. This has been recently demonstrated for interlinked B55- and CDK-dependent bistable switches in mitotic entry [248], where partial CDK inhibition was able to trap cells in an intermediate prophase-like state. Further studies of this nature could be used to dissect the complex series of switches with the potential to control checkpoint inactivation, cytokinesis and mitotic exit.

Another important question of broad relevance to this field is understanding the true rates of spontaneous spindle defects at different stages of mitosis. Although spindle

defects are well characterised during prometaphase, evidence for late metaphase or early anaphase spindle defects or their effects on mitotic progression is lacking. In these cases the ability of the system to respond to artificially-induced defects, for example nocodazole addition, is often used as a proxy in experimental studies. However, the logic behind the existence of checkpoint reactivation as a discussion topic at all implies that there exists the potential for post-anaphase defects which would cause the SAC to reactivate if checkpoint licensing were not revoked prior to this point. Better characterisation of this process would therefore inform discussion of the significance of the various checkpoint inactivation pathways.

6.2 Meiosis re-purposes mitotic cell cycle regulators to achieve distinct outcomes

In this thesis we have explored two distinct aspects of APC/C regulation of meiosis in mouse oocytes. Firstly, we examined the essential role of APC/C^{Cdh1} both in maintaining low CDK activity during GV arrest in prophase I, and in ensuring a slow rise in CDK activity during meiotic resumption (Chapter 4). We then explored the role of the SAC in regulating APC/C activity during meiosis I, while also considering SAC-independent features of the APC/C activity curve, and the ability of enucleated cytoplasts to undergo repeated cycles of APC/C activation and inactivation (Chapter 5).

Taken together, these chapters demonstrate that a series of regulatory events acting on APC/C are crucial for enabling the precise ordering and timing of events during meiosis. Mammalian oogenesis adds further complexity by the additional requirement to separate the events of a single meiosis across much of the life-span of the organism. This requires mechanisms to achieve robust blocks on the process which can persist for many years, while retaining the ability to undergo timely resumption of meiotic progression in response to the correct stimulus.

In many cases, the regulators controlling progression through meiotic M-phase are the same as those active during the mitotic cell cycle. This raises the question of how this largely unchanged cast of regulators is re-purposed to enable the differential ordering of events necessary to generate a haploid daughter cell.

The role of Cdh1 during meiotic resumption is a clear example of such a re-purposing approach. In the mitotic cell cycle, Cdh1 does not become active until late M-phase, once CDK activity has dropped sufficiently due to APC/C^{Cdc20}-dependent cyclin degradation. In contrast, during meiosis Cdh1 is active during GV arrest (prophase), and its continued presence during meiotic resumption is essential for the gradual rise in CDK activity necessary for de-protection of cohesin at chromosome arms prior to the first meiotic division. Cdh1 acts on the same substrates and is subject to similar mechanisms of regulation as in mitosis, but the difference in timing of these events causes a distinct meiosis-specific outcome.

Following meiotic resumption, the cell then activates APC/C^{Cdc20} to promote anaphase during the first meiotic division. This process is captured by the APC/C activity time-courses in Chapter 5, which show a clear rise in APC/C activity following loss of check-point signalling at kinetochores. While this activation is the same as the role played by APC/C^{Cdc20} at the same stage of mitosis, the timing is distinctly different occurring over a timescale of several hours. The reasons for this slow rise in activity are unclear. One possibility is that the large size of the oocyte relative to a typical somatic cell may create a greater resistance to change, for example due to the existence of a larger pool of MCC than would be possible in a smaller cell. Furthermore, APC/C activation is required not to segregate individual chromatids, but pairs of homologous chromosomes, which might place different requirements on the system with regards to timing of cohesin cleavage. In any case, these observations again suggest that differences in regulation can contribute to achieving distinct meiotic functions.

Following APC/C activation at anaphase I, its activity then declines and the cell enters CSF arrest in metaphase II. We have shown here that in the absence of chromosomal signals, the oocyte retains the capacity to undergo multiple cycles of APC/C activation instead of entering into this arrest phase. The similarity between these oscillations and those seen in embryonic *Xenopus* extract suggests that here again a meiosis-specific factor is normally responsible for changing the underlying oscillatory system behaviour from that of a somatic cell. Note however that this analysis assumes that the physical similarity between the two sets of oscillations is indicative of similarity in their network

structure: further work is required to determine whether or not this is in fact the same in both cases.

In these ways, we have shown how APC/C regulation in meiosis makes use of much of the same regulatory networks which apply during a normal mitotic cell cycle. By making subtle changes to these underlying networks, the same components can be effectively re-purposed to achieve the specific requirements of the two meiotic divisions.

6.2.1 Future Work: Intrinsic regulation of APC/C activity in mouse oocytes

Although the work in this thesis had provided important insights into some of the ways in which APC/C is regulated in meiosis, outstanding questions remain. In particular, the analysis of APC/C activity timecourses in Chapter 5 revealed several interesting features about these curves, but was unable to lead to firm conclusions about the underlying mechanisms. Extending our established methods for APC/C activity calculation and applying them to a broader set of experimental conditions could provide greater understanding of the underlying processes regulating APC/C activity in this system, with important implications for control of oogenesis.

In particular, we were unable to resolve which factors regulate the inactivation of APC/C after its peak, or to explain why this peak is so closely associated with anaphase onset. The ability of the system to undergo repeated cycles of APC/C activation and inactivation in enucleated cytoplasts is also unexplained, but hints at an intrinsic oscillator (or damped oscillator) within the reaction network which is normally kept in check by chromosome-mediated signalling. Future work could aim to more precisely characterise this behaviour, and to identify which components are responsible.

One possibility is that the oscillator is the same as the well-characterised *Xenopus* extract oscillator, in which case measurements of inhibitory phosphorylation on CDK should also show oscillatory patterns of behaviour. Alternatively, reactivation of Cdh1 following cyclin degradation could promote a return to a GV-like state from which the cell could re-undergo a meiotic-resumption-like process. The role of Emi2, which under normal conditions should be responsible for inhibiting APC/C activity after meiosis I, is

also unclear.

Measurements to observe which, if any, of these components undergo periodic cycles of activation in cytoplasts could help to distinguish between these possibilities, while knockdown mutants could also potentially aim to disrupt the ability of the cell to repeatedly activate APC/C. Any such work would naturally be well suited for a combined modelling and experimental approach, since modelling should be able to reconstruct any proposed oscillator in agreement with these experimental results. With a better understanding of the underlying network structure governing APC/C activation, we would be better placed to interpret the additional effects of the SAC in modulating this intrinsic behaviour.

6.3 Evaluation of modelling approaches used

In this thesis, we have primarily used ODE models to explore the biochemical interaction networks underpinning M-phase progression. These models have the advantage of simplicity of design and implementation, since any biochemical wiring diagram can be converted to a series of ODEs, and the resulting equations can be rapidly solved by a desktop ODE solver such as XPPAUT. This makes them well suited to testing assumptions about different possible network structures or parameter regimes, since generating and testing model variants is relatively quick. Furthermore, bifurcation analysis in AUTO simplifies this process further, allowing for steady state solutions for a near-continuous range of parameter values to be plotted. For networks with limited numbers of variables, using pseudo–steady-state assumptions to reduce the system to a two-dimensional one is also a powerful tool, since this allows the plotting of phaseplane diagrams which provide additional insight into system behaviour. Nevertheless, there are limitations and drawbacks to this approach, which we discuss below.

6.3.1 Network Structures

One of the most powerful applications of ODE models of biochemical reaction networks is to demonstrate how complex behaviours can arise from simple reaction networks. For example, the classic Novak-Tyson model [77], which uses a minimal set of components

to describe oscillations in *Xenopus* extract. Similarly, the FADS motif presented in Chapter 2 describes a simple network structure employing just three major components to generate a bistable cell cycle switch, and demonstrates how it can be applied to multiple cell cycle transitions.

However, an inherent limitation of this reductionist approach to cell cycle regulation is that it misses the diversity of overlapping regulatory mechanisms which may be active at a single cell cycle transition. For example, the FADS SAC model presented in Chapter 2 (Section 2.3.2) and the 'full' SAC model presented in Chapter 3 (Section 3.2) both describe the SAC as a bistable switch dependent on a double-negative feedback loop between APC/C^{Cdc20}, Cdk1:CycB and MCC, but differ greatly in the level of detail surrounding this core network feature. Yet even the more detailed SAC model presented in Chapter 3 does not include all possible actors in this process. As discussed in Section 3.5.2, CDK phosphorylation also negatively affects APC/C activity via regulation of other pathways (for example error correction and inhibitory phosphorylation of Cdh1), which are not included in this model.

While it would be possible to extend the model by incorporating these additional pathways, we have not chosen to do so due to the additional complexity that this introduces, without necessarily providing additional clarity. While the model we propose is able to accurately reproduce the effects of experiments, it is a necessary approximation which does not cover details of parallel pathways which would not be so easily detected in the experimental data available. A full picture of M-phase regulation and the influence of overlapping double-negative feedback loops would require a more complete modelling approach.

6.3.2 Kinetic Schemes

In Chapter 2, we discuss some of the drawbacks of typical methods used in mathematical models of biochemical reaction networks to generate the necessary non-linearity in signal response to allow the emergence of more complex behaviours such as bistability (Section 2.1.2). While each of these methods uses assumptions about the properties of the species within the network which may be valid for particular known species (for

example the existence of multiple cooperative phosphorylation sites on a target protein), we caution that these specific requirements cannot be assumed to apply generically to all possible network components. We argue that the existence of a tight-binding stoichiometric inhibitor is a more reasonable starting assumption in the absence of any specific knowledge about reactant kinetics, since the necessary properties are intrinsic to the definition of a stoichiometric inhibitor.

Nevertheless, we have chosen to use some of these same methods in other models in this thesis, specifically the meiotic resumption model in Chapter 4, and the combined APC/C and Cdc20 phosphorylation model in Chapter 3 (Section 3.3) both make use of Goldbeter-Koshland kinetics. Indeed, we specifically explore the effects of non-linearity introduced by the Goldbeter-Koshland functions in this latter example.

The use of these highly non-linear kinetic schemes is a potential limitation of the conclusions drawn from the models in these chapters, since it is a necessary requirement for the bistable or oscillatory model behaviour captured in each case. Nevertheless, it is still instructive to approach the modelling in this way, since it provides a clearer view of the potential scope of system behaviour than if it were limited to purely linear mass-action kinetics. The exact source of non-linearity may or may not be due to Goldbeter-Koshland phosphorylation and dephosphorylation kinetics, but the existence of *any* source of non-linearity in the system would not be surprising.

6.3.3 Parameter Selection

The choice of parameter values for use in mathematical models of biochemical systems is an important consideration. As discussed in the introduction (Section 1.6.1), while experimental data can be used to place constraints on parameter values, in practice the large number of parameters required for a typical ODE model means that the model is unlikely to precisely capture the *in vivo* parameter regime.

However, this does not imply that the model has no validity when used for analysing the properties of these systems. As discussed above, the network structures themselves are by necessity only an approximation of the true system, in order to allow for a reasonable analysis of particular aspects of the system properties. Similarly, the parameters

selected may not precisely reflect the actual values of the underlying system, but the generalised behaviour of the model should nonetheless provide insight into the principles governing the system as a whole. The rationale behind this type of modelling and analysis is that if we can demonstrate the existence of complex behaviour in a simplified representation of the system, then this is likely to hold true as a core principle of system behaviour even if additional complexity is overlaid onto it.

The simplified FADS motif examples in Chapter 2 are an example of this type of approach. In these cases, the simple three-component model is bistable for a wide range of parameter values. The parameters selected did not correspond to any specific values from experimental data, but were chosen in order to fit the bistable range of the cell cycle transition so that it was consistent with the known function of the transition. The more complex SAC model in Chapter 3 required more precise fitting in order to correspond with the measured MS data, however its fundamental properties were unaffected, as seen by the similarities between the bifurcation diagrams in these two chapters (compare Figures 2.13B and 3.7A). The more constrained parameter set in the second model allows us to draw more precise conclusions about the exact timing of events such as reactivation, but the more general features of the model remain true across a wide range of parameter values.

6.3.4 Sources of Noise

An important limitation of ODE models is that they are purely deterministic in nature, i.e. that each simulation will only ever give the same results from a given set of parameter values and initial conditions. This is in stark contrast to experimental data produced from real biochemical systems, which can demonstrate significant variation in response to the same set of conditions (for example the population studies of mitotic exit time in Figure 3.5A). Biochemical systems are subject to both intrinsic noise (stochastic fluctuations within a single cell due to low molecule numbers of system components) and extrinsic noise (larger scale cell-to-cell variation). When considering experimental data the effects of measurement noise and experimental error also contribute.

In this thesis we have chosen not to model intrinsic noise. In some cases this is because

this is not suitable for the required purpose, for example when conducting a steady state analysis of the FADS models in Chapter 2. ODE models provide a robust framework for steady state analysis via phaseplanes and bifurcation diagrams which would not be possible for a stochastic model. In other cases, where we primarily deal with timecourse data which is averaged across a cell population, a deterministic ODE model provides a reasonable approximation to this average value. Examples of this include the meiotic resumption timecourses in Chapter 4, or the fit to the MS data in Chapter 3.

In other cases where cell-to-cell variation is captured in the data, for example the SAC reactivation timecourses in Chapter 3, it is not clear that the observed variation is on account of noise at the level of the components featured in our models. By definition, components with low molecule number are responsible for the majority of cellular noise. In the case of biochemical reaction networks, one of the major contributors to molecular noise is therefore the synthesis of low copy number mRNA molecules, which are vastly outnumbered by their protein products. A simple stochastic implementation of one of the ODE models using a Gillespie algorithm would underestimate the likely stochastic variation since we do not independently consider transcription and translation processes. While it would be possible to create an extended version of the models which did consider the effects of transcriptional regulation, the lack of detailed information on transcription rates or mRNA turnover for these components would add a large amount of additional unconstrained parameters. This would limit the confidence of any predictions about system behaviour made from such a stochastic model.

Instead, where appropriate we have modelled extrinsic noise within the framework of our deterministic ODE models by randomly sampling selected parameter and initial condition values from a lognormal distribution, as described in the introduction (Section 1.6.1). This is able to reproduce the effects of the variation in the population on mitotic exit timing, but this method is only an approximation for the true extent of extrinsic noise in the system, which could depend on variation in many more factors than used here.

6.4 Conclusion

In this thesis, mathematical modelling techniques have been used to investigate mechanisms and network motifs governing M-phase progression in mitosis and meiosis. Working in collaboration with experimental scientists, we have applied these techniques to resolving specific outstanding questions in the field, and generated models which provide insight into the underlying biochemical reaction networks governing these processes.

We propose a network motif (FADS) common to multiple cell cycle transitions, and discuss in more detail the mechanisms of control of M-phase in both mitosis and meiosis. We extend existing models of mitosis to take into account new experimental results, and use these models to argue for checkpoint progression governed by a series of molecular switches which contribute to driving orderly progression through mitosis. Looking at meiosis, we propose a model for meiotic resumption which elucidates important experimental data regarding the role of Cdh1 in this process. Finally, we perform model-driven data analysis of mouse oocytes to raise important questions regarding the regulation of APC/C activity during meiosis I.

Taken together, this work provides insight into the common regulatory themes and motifs which govern much of the eukaryotic cell cycle and related events. At the same time, we highlight some of the key differences which allow the cell to make context-specific alterations to the basic cell cycle program, particularly with regard to the highly specialised M-phases occurring in meiosis. This work raises important questions regarding the nature of M-phase regulation in eukaryotic cells, which could form the basis for useful further work as outlined above.

Bibliography

[1] D. O. Morgan, *The Cell Cycle: Principles of Control*. London: New Science Press Ltd. in association with Oxford University Press, 2007.

[2] Y. Budirahardja and P. Gonczy, "Coupling the cell cycle to development," *Development*, vol. 136, no. 17, pp. 2861–2872, 2009.

[3] P. Kaldis and H. E. Richardson, "When cell cycle meets development," *Development*, vol. 139, no. 2, pp. 225–230, 2012.

[4] D. Hanahan and R. A. Weinberg, "The Hallmarks of Cancer," *Cell*, vol. 100, no. 1, pp. 57–70, 2000.

[5] G. I. Evan and K. H. Vousden, "Proliferation, cell cycle and apoptosis in cancer," *Nature*, vol. 411, no. 6835, pp. 342–8, 2001.

[6] D. J. Gordon, B. Resio, and D. Pellman, "Causes and consequences of aneuploidy in cancer," *Nature Reviews Genetics*, vol. 13, no. 3, pp. 189–203, 2012.

[7] S. Sazer, M. Lynch, and D. Needleman, "Deciphering the evolutionary history of open and closed mitosis," *Current Biology*, vol. 24, no. 22, pp. R1099–R1103, 2014.

[8] D. O. Morgan, "Cyclin-dependent kinases: Engines, Clocks, and Microprocessors," *Annual Review of Cell and Developmental Biology*, vol. 13, no. 1, pp. 261–91, 1997.

[9] L. Hartwell and T. Weinert, "Checkpoints: controls that ensure the order of cell cycle events," *Science*, vol. 246, no. 4930, pp. 629–634, 1989.

[10] K. J. Barnum, "Cell Cycle Regulation by Checkpoints," in *Cell Cycle Control* (E. Noguchi and M. C. Gadaleta, eds.), vol. 1170 of *Methods in Molecular Biology*, New York, NY: Humana Press, 2014.

[11] P. Nurse, "Universal control mechanism regulating onset of M-phase," *Nature*, vol. 344, no. 6266, pp. 503–8, 1990.

[12] D. O. Morgan, "Regulation of the APC and the exit from mitosis.," *Nature cell biology*, vol. 1, no. 2, pp. E47–53, 1999.

[13] M. Malumbres and M. Barbacid, "Mammalian cyclin-dependent kinases," *Trends in Biochemical Sciences*, vol. 30, no. 11, pp. 630–641, 2005.

[14] M. Malumbres, "Cyclin-dependent kinases," *Genome Biology*, vol. 15, no. 6, p. 122, 2014.

[15] J. a. Ubersax, E. L. Woodbury, P. N. Quang, M. Paraz, J. D. Blethrow, K. Shah, K. M. Shokat, and D. O. Morgan, "Targets of the cyclin-dependent kinase Cdk1," *Nature*, vol. 425, no. 6960, pp. 859–64, 2003.

[16] T. Evans, E. T. Rosenthal, J. Youngblom, D. Distel, and T. Hunt, "Cyclin: a protein specified by maternal mRNA in sea urchin eggs that is destroyed at each cleavage division," *Cell*, vol. 33, no. 2, pp. 389–96, 1983.

[17] P. H. O'Farrell, "Triggering the all-or-nothing switch into mitosis," *Trends in Cell Biology*, vol. 11, no. 12, pp. 512–519, 2001.

[18] N. Hégarat, S. Rata, and H. Hochegger, "Bistability of mitotic entry and exit switches during open mitosis in mammalian cells," *BioEssays*, vol. 38, no. 7, pp. 627–643, 2016.

[19] J. A. Perry and S. Kornbluth, "Cdc25 and Wee1: Analogous opposites?," *Cell Division*, vol. 2, pp. 1–12, 2007.

[20] C. J. Sherr and J. M. Roberts, "CDK inhibitors: positive and negative regulators of G1-phase progression.," *Genes & Development*, vol. 13, no. 12, pp. 1501–12, 1999.

[21] A. De Clercq and D. Inzé, "Cyclin-dependent kinase inhibitors in yeast, animals, and plants: A functional comparison," *Critical Reviews in Biochemistry and Molecular Biology*, vol. 41, no. 5, pp. 293–313, 2006.

[22] E. Schwob, T. Bohm, M. D. Mendenhall, and K. Nasmyth, "The B-type cyclin kinase inhibitor $p40^{SIC1}$ controls the G1 to S transition in S. cerevisiae," *Cell*, vol. 79, no. 2, pp. 233–244, 1994.

[23] H. Ceulemans and M. Bollen, "Functional Diversity of Protein Phosphatase-1, a Cellular Economizer and Reset Button," *Physiological Reviews*, vol. 84, no. 1, pp. 1–39, 2004.

[24] I. Verbinnen, M. Ferreira, and M. Bollen, "Biogenesis and activity regulation of protein phosphatase 1," *Biochemical Society Transactions*, vol. 45, no. 1, pp. 89–99, 2017.

[25] M. Dohadwala, E. F. da Cruz e Silva, F. L. Hall, R. T. Williams, D. A. Carbonaro-Hall, A. C. Nairn, P. Greengard, and N. Berndt, "Phosphorylation and inactivation of protein phosphatase 1 by cyclin-dependent kinases," *Proceedings of the National Academy of Sciences*, vol. 91, no. 14, pp. 6408–6412, 1994.

[26] J. Q. Wu, J. Y. Guo, W. Tang, C. S. Yang, C. D. Freel, C. Chen, A. C. Nairn, and S. Kornbluth, "PP1-mediated dephosphorylation of phosphoproteins at mitotic exit is controlled by inhibitor-1 and PP1 phosphorylation," *Nature Cell Biology*, vol. 11, no. 5, pp. 644–651, 2009.

[27] N. Wlodarchak and Y. Xing, "PP2A as a master regulator of the cell cycle," *Critical Reviews in Biochemistry and Molecular Biology*, vol. 51, no. 3, pp. 162–184, 2016.

[28] A. D. Deana, F. Marchiori, F. Meggio, and L. A. Pinna, "Dephosphorylation of synthetic phosphopeptides by protein phosphatase-T, a phosphothreonyl protein phosphatase.," *The Journal of Bological Chemistry*, vol. 257, no. 15, pp. 8565–8, 1982.

[29] A. D. Deana and L. A. Pinna, "Identification of pseudo phosphothreonyl-specific' protein phosphatase T with a fraction of polycation-stimulated protein phosphatase 2A," *Biochimica et Biophysica Acta*, vol. 968, no. 2, pp. 179–185, 1988.

[30] J. B. Hein, E. P. T. Hertz, D. H. Garvanska, T. Kruse, and J. Nilsson, "Distinct kinetics of serine and threonine dephosphorylation are essential for mitosis," *Nature Cell Biology*, vol. 19, no. 12, pp. 1433–1440, 2017.

[31] I. Primorac and A. Musacchio, "Panta rhei: The APC/C at steady state," *Journal of Cell Biology*, vol. 201, no. 2, pp. 177–189, 2013.

[32] R. W. King, J. M. Peters, S. Tugendreich, M. Rolfe, P. Hieter, and M. W. Kirschner, "A 20s complex containing CDC27 and CDC16 catalyzes the mitosis-specific conjugation of ubiquitin to cyclin B," *Cell*, vol. 81, no. 2, pp. 279–288, 1995.

[33] A. Musacchio, "The molecular biology of spindle assembly checkpoint signaling dynamics," *Current Biology*, vol. 25, no. 20, pp. R1002–R1018, 2015.

[34] K. I. Nakayama and K. Nakayama, "Ubiquitin ligases: Cell-cycle control and cancer," *Nature Reviews Cancer*, vol. 6, no. 5, pp. 369–381, 2006.

[35] M. Min and C. Lindon, "Substrate targeting by the ubiquitin-proteasome system in mitosis," *Seminars in Cell and Developmental Biology*, vol. 23, no. 5, pp. 482–491, 2012.

[36] T. Inobe and A. Matouschek, "Paradigms of protein degradation by the proteasome," *Current Opinion in Structural Biology*, vol. 24, no. 1, pp. 156–164, 2014.

[37] R. J. Deshaies and C. A. Joazeiro, "RING Domain E3 Ubiquitin Ligases," *Annual Review of Biochemistry*, vol. 78, no. 1, pp. 399–434, 2009.

[38] H. Yu and A. Matouschek, "Recognition of client proteins by the proteasome," *Annual Review of Biophysics*, vol. 46, no. 1, pp. 149–173, 2017.

[39] F. E. Reyes-Turcu, K. H. Ventii, and K. D. Wilkinson, "Regulation and cellular roles of ubiquitin-specific deubiquitinating enzymes," *Annual Review of Biochemistry*, vol. 78, no. 1, pp. 363–397, 2009.

[40] V. Sudakin, D. Ganoth, A. Dahan, H. Heller, J. Hershko, F. C. Luca, J. V. Ruderman, and A. Hershko, "The cyclosome, a large complex containing cyclin-selective ubiquitin ligase activity, targets cyclins for destruction at the end of mitosis," *Molecular Biology of the Cell*, vol. 6, no. 2, pp. 185–197, 1995.

[41] A. W. Murray, M. J. Solomon, and M. W. Kirschner, "The role of cyclin synthesis and degradation in the control of maturation promoting factor activity," *Nature*, vol. 339, no. 6222, pp. 280–286, 1989.

[42] K. Nasmyth, "Segregating sister genomes: The molecular biology of chromosome separation," *Science*, vol. 297, no. 5581, pp. 559–565, 2002.

[43] M. Shirayama, A. Tóth, M. Gálová, and K. Nasmyth, "APC(Cdc20) promotes exit from mitosis by destroying the anaphase inhibitor Pds1 and cyclin Clb5," *Nature*, vol. 402, pp. 203–7, nov 1999.

[44] R. Wäsch and F. R. Cross, "APC-dependent proteolysis of the mitotic cyclin Clb2 is essential for mitotic exit.," *Nature*, vol. 418, pp. 556–62, aug 2002.

[45] M. Schwab, M. Neutzner, D. Möcker, and W. Seufert, "Yeast Hct1 recognizes the mitotic cyclin Clb2 and other substrates of the ubiquitin ligase APC," *The EMBO Journal*, vol. 20, no. 18, pp. 5165–5175, 2001.

[46] S. Sivakumar and G. J. Gorbsky, "Spatiotemporal regulation of the anaphase-promoting complex in mitosis," *Nature Reviews Molecular Cell Biology*, vol. 16, no. 2, pp. 82–94, 2015.

[47] C. M. Pfleger and M. W. Kirschner, "The KEN box: An APC recognition signal distinct from the D box targeted by Cdh1," *Genes and Development*, vol. 14, no. 6, pp. 655–665, 2000.

[48] M. Glotzer, A. W. Murray, and M. W. Kirschner, "Cyclin is degraded by the ubiquitin pathway," *Nature*, vol. 349, no. 6305, pp. 132–138, 1991.

[49] B. DiFiore, N. E. Davey, A. Hagting, D. Izawa, J. Mansfeld, T. J. Gibson, and J. Pines, "The ABBA Motif binds APC/C activators and is shared by APC/C substrates and regulators," *Developmental Cell*, vol. 32, no. 3, pp. 358–372, 2015.

[50] M. E. Matyskiela, M. C. Rodrigo-Brenni, and D. O. Morgan, "Mechanisms of ubiquitin transfer by the anaphase-promoting complex.," *Journal of biology*, vol. 8, no. 10, p. 92, 2009.

[51] S. Geley, E. Kramer, C. Gieffers, J. Gannon, J. M. Peters, and T. Hunt, "Anaphase-promoting complex/cyclosome-dependent proteolysis of human cyclin A starts at the beginning of mitosis and is not subject to the spindle assembly checkpoint," *Journal of Cell Biology*, vol. 153, no. 1, pp. 137–147, 2001.

[52] M. J. Hayes, Y. Kimata, S. L. Wattam, C. Lindon, G. Mao, H. Yamano, and A. M. Fry, "Early mitotic degradation of Nek2A depends on Cdc20-independent interaction with the APC/C," *Nature Cell Biology*, vol. 8, no. 6, pp. 607–614, 2006.

[53] B. R. Thornton and D. P. Toczyski, "Securin and B-cyclin/CDK are the only essential targets of the APC," *Nature Cell Biology*, vol. 5, no. 12, pp. 1090–1094, 2003.

[54] R. Wolthuis, L. Clay-Farrace, W. van Zon, M. Yekezare, L. Koop, J. Ogink, R. Medema, and J. Pines, "Cdc20 and Cks Direct the Spindle Checkpoint-Independent Destruction of Cyclin A," *Molecular Cell*, vol. 30, no. 3, pp. 290–302, 2008.

[55] B. Di Fiore and J. Pines, "How cyclin A destruction escapes the spindle assembly checkpoint," *Journal of Cell Biology*, vol. 190, no. 4, pp. 501–509, 2010.

[56] C. Alfieri, S. Zhang, and D. Barford, "Visualizing the complex functions and mechanisms of the anaphase promoting complex/cyclosome (APC/C)," *Open Biology*, vol. 7, no. 11, 2017.

[57] A. Zur and M. Brandeis, "Securin degradation is mediated by fzy and fzr, and is required for complete chromatid separation but not for cytokinesis," *EMBO Journal*, vol. 20, no. 4, pp. 792–801, 2001.

[58] J. W. Raff, K. Jeffers, and J. Y. Huang, "The roles of Fzy/Cdc20 and Fzr/Cdh1 in regulating the destruction of cyclin B in space and time," *Journal of Cell Biology*, vol. 157, no. 7, pp. 1139–1149, 2002.

[59] M. Shteinberg, Y. Protopopov, T. Listovsky, M. Brandeis, and A. Hershko, "Phosphorylation of the cyclosome is required for its stimulation by Fizzy/cdc20," *Biochemical and Biophysical Research Communications*, vol. 260, no. 1, pp. 193–198, 1999.

[60] E. R. Kramer, N. Scheuringer, A. V. Podtelejnikov, M. Mann, and J. M. Peters, "Mitotic regulation of the APC activator proteins CDC20 and CDH1.," *Molecular Biology of the Cell*, vol. 11, no. 5, pp. 1555–69, 2000.

[61] W. Zachariae, M. Schwab, K. Nasmyth, and W. Seufert, "Control of cyclin ubiquitination by CDK-regulated binding of Hct1 to the anaphase promoting complex," *Science*, vol. 282, no. 5394, pp. 1721–4, 1998.

[62] H. Labit, K. Fujimitsu, N. S. Bayin, T. Takaki, J. Gannon, and H. Yamano, "Dephosphorylation of Cdc20 is required for its C-box-dependent activation of the APC/C," *The EMBO Journal*, vol. 31, no. 15, pp. 3351–3362, 2012.

[63] C. Kraft, "Mitotic regulation of the human anaphase-promoting complex by phosphorylation," *The EMBO Journal*, vol. 22, no. 24, pp. 6598–6609, 2003.

[64] S. Zhang, L. Chang, C. Alfieri, Z. Zhang, J. Yang, S. Maslen, M. Skehel, and D. Barford, "Molecular mechanism of APC/C activation by mitotic phosphorylation," *Nature*, vol. 533, pp. 260–264, 2016.

[65] K. Fujimitsu, M. Grimaldi, and H. Yamano, "Cyclin-dependent kinase 1-dependent activation of APC/C ubiquitin ligase," *Science*, vol. 352, no. 6289, pp. 1121–1124, 2016.

[66] R. Qiao, F. Weissmann, M. Yamaguchi, N. G. Brown, R. VanderLinden, R. Imre, M. A. Jarvis, M. R. Brunner, I. F. Davidson, G. Litos, D. Haselbach, K. Mechtler, H. Stark, B. A. Schulman, and J.-M. Peters, "Mechanism of APC/C^{Cdc20} activation by mitotic phosphorylation," *Proceedings of the National Academy of Sciences*, vol. 113, no. 19, pp. E2570–E2578, 2016.

[67] Y. Yudkovsky, M. Shteinberg, T. Listovsky, M. Brandeis, and A. Hershko, "Phosphorylation of Cdc20/Fizzy negatively regulates the mammalian Cyclosome/APC in the mitotic checkpoint," *Biochemical and Biophysical Research Communications*, vol. 271, no. 2, pp. 299–304, 2000.

[68] J. Weinstein, "Cell Cycle-regulated Expression, Phosphorylation, and Degradation of p55Cdc," *Journal of Biological Chemistry*, vol. 272, no. 45, pp. 28501–28511, 1997.

[69] J. B. Hein and J. Nilsson, "Interphase APC/C-Cdc20 inhibition by cyclin A2-Cdk2 ensures efficient mitotic entry," *Nature Communications*, vol. 7, p. 10975, 2016.

[70] V. D'Angiolella, C. Mari, D. Nocera, L. Rametti, and D. Grieco, "The spindle checkpoint requires cyclin-dependent kinase activity," *Genes & Development*, vol. 17, no. 20, pp. 2520–5, 2003.

[71] E. Chung and R.-H. Chen, "Phosphorylation of Cdc20 is required for its inhibition by the spindle checkpoint," *Nature Cell Biology*, vol. 5, no. 8, pp. 748–753, 2003.

[72] A. Ciliberto, A. Lukács, A. Tóth, J. J. Tyson, and B. Novák, "Rewiring the exit from mitosis," *Cell Cycle*, vol. 4, no. 8, pp. 1107–1112, 2005.

[73] J. Y. Hsu, J. D. Reimann, C. S. Sørensen, J. Lukas, and P. K. Jackson, "E2F-dependent accumulation of hEmi1 regulates S phase entry by inhibiting APC^{Cdh1}," *Nature Cell Biology*, vol. 4, no. 5, pp. 358–366, 2002.

[74] S. D. Cappell, K. G. Mark, D. Garbett, L. R. Pack, M. Rape, and T. Meyer, "EMI1 switches from being a substrate to an inhibitor of APC/C^{CDH1} to start the cell cycle," *Nature*, vol. 558, no. 7709, pp. 313–317, 2018.

[75] U. Alon, "Network motifs: Theory and experimental approaches," *Nature Reviews Genetics*, vol. 8, no. 6, pp. 450–461, 2007.

[76] J. J. Tyson, K. C. Chen, and B. Novak, "Sniffers, buzzers, toggles and blinkers: Dynamics of regulatory and signaling pathways in the cell," *Current Opinion in Cell Biology*, vol. 15, no. 2, pp. 221–231, 2003.

[77] B. Novák and J. J. Tyson, "Numerical analysis of a comprehensive model of M-phase control in Xenopus oocyte extracts and intact embryos," *Journal of Cell Science*, vol. 106, pp. 1153–1168, 1993.

[78] J. E. Ferrell, T. Y. C. Tsai, and Q. Yang, "Modeling the cell cycle: Why do certain circuits oscillate?," *Cell*, vol. 144, no. 6, pp. 874–885, 2011.

[79] A. W. Murray and M. W. Kirschner, "Cyclin synthesis drives the early embryonic cell cycle," *Nature*, vol. 339, no. 6222, pp. 275–280, 1989.

[80] J. E. Ferrell, "Self-perpetuating states in signal transduction: Positive feedback, double-negative feedback and bistability," *Current Opinion in Cell Biology*, vol. 14, no. 2, pp. 140–148, 2002.

[81] A. Ciliberto and J. V. Shah, "A quantitative systems view of the spindle assembly checkpoint," *EMBO Journal*, vol. 28, no. 15, pp. 2162–2173, 2009.

[82] K. Nasmyth and C. H. Haering, "Cohesin: its roles and mechanisms," *Annual Review of Genetics*, vol. 43, no. 1, pp. 525–558, 2009.

[83] J. M. Peters, A. Tedeschi, and J. Schmitz, "The cohesin complex and its roles in chromosome biology," *Genes and Development*, vol. 22, no. 22, pp. 3089–3114, 2008.

[84] I. Litwin and R. Wysocki, "New insights into cohesin loading," *Current Genetics*, vol. 64, no. 1, pp. 53–61, 2018.

[85] I. C. Waizenegger, S. Hauf, A. Meinke, and J. M. Peters, "Two distinct pathways remove mammalian cohesin from chromosome arms in prophase and from centromeres in anaphase," *Cell*, vol. 103, no. 3, pp. 399–410, 2000.

[86] N. C. Hornig, P. P. Knowles, N. Q. McDonald, and F. Uhlmann, "The dual mechanism of separase regulation by securin," *Current Biology*, vol. 12, no. 12, pp. 973–982, 2002.

[87] S. Luo and L. Tong, "Structural biology of the separase-securin complex with crucial roles in chromosome segregation.," *Current Opinion in Structural Biology*, vol. 49, pp. 114–122, 2018.

[88] O. Cohen-Fix, J. M. Peters, M. W. Kirschner, and D. Koshland, "Anaphase initiation in *Saccharomyces cerevisiae* is controlled by the APC-dependent degradation of the anaphase inhibitor Pds1p," *Genes & Development*, vol. 10, no. 24, pp. 3081–3093, 1996.

[89] R. Ciosk, W. Zachariae, C. Michaelis, A. Shevchenko, M. Mann, and K. Nasmyth, "An ESP1/PDS1 complex regulates loss of sister chromatid cohesion at the metaphase to anaphase transition in yeast," *Cell*, vol. 93, no. 6, pp. 1067–1076, 1998.

[90] A. Musacchio and A. Desai, "A molecular view of kinetochore assembly and function," *Biology*, vol. 6, no. 1, p. 5, 2017.

[91] K. L. McKinley and I. M. Cheeseman, "The molecular basis for centromere identity and function," *Nature Reviews Molecular Cell Biology*, vol. 17, no. 1, pp. 16–29, 2016.

[92] M. E. Pesenti, J. R. Weir, and A. Musacchio, "Progress in the structural and functional characterization of kinetochores," *Current Opinion in Structural Biology*, vol. 37, pp. 152–163, 2016.

[93] I. M. Cheeseman, J. S. Chappie, E. M. Wilson-Kubalek, and A. Desai, "The conserved KMN network constitutes the core microtubule-binding site of the kinetochore," *Cell*, vol. 127, no. 5, pp. 983–997, 2006.

[94] J. G. DeLuca, W. E. Gall, C. Ciferri, D. Cimini, A. Musacchio, and E. D. Salmon, "Kinetochore microtubuledynamics and attachment stability Are regulated by Hec1," *Cell*, vol. 127, no. 5, pp. 969–982, 2006.

[95] S. Petry, "Mechanisms of mitotic spindle assembly," *Annual Review of Biochemistry*, vol. 85, no. 1, pp. 659–683, 2016.

[96] M. Bornens, "The centrosome in cells and organisms," *Science*, vol. 335, no. 6067, pp. 422–426, 2012.

[97] G. J. Brouhard and L. M. Rice, "The contribution of $\alpha\beta$-tubulin curvature to microtubule dynamics," *Journal of Cell Biology*, vol. 207, no. 3, pp. 323–334, 2014.

[98] S. Florian and T. J. Mitchison, "Anti-Microtubule Drugs," in *The Mitotic Spindle* (P. Chang and R. Ohi, eds.), pp. 403–421, New York, NY: Humana Press, 2016.

[99] T. M. Kapoor, T. U. Mayer, M. L. Coughlin, and T. J. Mitchison, "Probing spindle assembly mechanisms with monastrol, a small molecule inhibitor of the mitotic kinesin, Eg5," *Journal of Cell Biology*, vol. 150, no. 5, pp. 975–988, 2000.

[100] V. Sudakin, G. K. T. Chan, and T. J. Yen, "Checkpoint inhibition of the APC/C in HeLa cells is mediated by a complex of BUBR1, BUB3, CDC20, and MAD2," *Journal of Cell Biology*, vol. 154, no. 5, pp. 925–936, 2001.

[101] X. Luo, Z. Tang, G. Xia, K. Wassmann, T. Matsumoto, J. Rizo, and H. Yu, "The Mad2 spindle checkpoint protein has two distinct natively folded states," *Nature Structural and Molecular Biology*, vol. 11, no. 4, pp. 338–345, 2004.

[102] A. DeAntoni, V. Sala, A. Musacchio, M. Herbert, J. K. Heriche, and T. Mitchison, "Explaining the oligomerization properties of the spindle assembly checkpoint protein Mad2," *Philosophical Transactions of the Royal Society of London. Series B: Biological Sciences*, vol. 360, no. 1455, pp. 637–648, 2005.

[103] M. Mapelli, L. Massimiliano, S. Santaguida, and A. Musacchio, "The Mad2 Conformational Dimer: Structure and Implications for the Spindle Assembly Checkpoint," *Cell*, vol. 131, no. 4, pp. 730–743, 2007.

[104] M. Mapelli and A. Musacchio, "MAD contortions: conformational dimerization boosts spindle checkpoint signaling," *Current Opinion in Structural Biology*, vol. 17, no. 6, pp. 716–725, 2007.

[105] X. Luo and H. Yu, "Protein metamorphosis: The two-state behavior of Mad2," *Structure*, vol. 16, no. 11, pp. 1616–1625, 2008.

[106] M. Simonetta, R. Manzoni, R. Mosca, M. Mapelli, L. Massimiliano, M. Vink, B. Novak, A. Musacchio, and A. Ciliberto, "The influence of catalysis on Mad2 activation dynamics," *PLoS Biology*, vol. 7, no. 1, p. e10, 2009.

[107] L. Mariani, E. Chiroli, L. Nezi, H. Muller, S. Piatti, A. Musacchio, and A. Ciliberto, "Role of the Mad2 dimerization interface in the spindle assembly checkpoint independent of kinetochores," *Current Biology*, vol. 22, no. 20, pp. 1900–1908, 2012.

[108] Y. Hiruma, C. Sacristan, S. T. Pachis, A. Adamopoulos, T. Kuijt, M. Ubbink, E. von Castelmur, A. Perrakis, and G. J. P. L. Kops, "Competition between MPS1 and microtubules at kinetochores regulates spindle checkpoint signaling," *Science*, vol. 348, no. 6240, pp. 1264–1267, 2015.

[109] Z. Ji, H. Gao, and H. Yu, "Kinetochore attachment sensed by competitive Mps1 and microtubule binding to Ndc80C," *Science*, vol. 348, no. 6240, pp. 1260–1264, 2015.

[110] A. R. Schutz and M. Winey, "New alleles of the yeast MPS1 gene reveal multiple requirements in spindle pole body duplication," *Molecular Biology of the Cell*, vol. 9, no. 4, pp. 759–774, 1998.

[111] X. Liu and M. Winey, "The MPS1 family of protein kinases," *Annual Review of Biochemistry*, vol. 81, no. 1, pp. 561–585, 2012.

[112] A. N. Pike and H. A. Fisk, "Centriole assembly and the role of Mps1: Defensible or dispensable?," *Cell Division*, vol. 6, no. 1, p. 9, 2011.

[113] V. M. Stucke, H. H. W. Silljé, L. Arnaud, and E. A. Nigg, "Human Mps1 kinase is required for the spindle assembly checkpoint but not for centrosome duplication," *EMBO Journal*, vol. 21, no. 7, pp. 1723–1732, 2002.

[114] S.-T. Liu, G. K. Chan, J. C. Hittle, G. Fujii, E. Lees, and T. J. Yen, "Human MPS1 kinase is required for mitotic arrest induced by the loss of CENP-E from kinetochores," *Molecular Biology of the Cell*, vol. 14, no. 4, pp. 1638–1651, 2003.

[115] N. London, S. Ceto, J. A. Ranish, and S. Biggins, "Phosphoregulation of Spc105 by Mps1 and PP1 regulates Bub1 localization to kinetochores," *Current Biology*, vol. 22, no. 10, pp. 900–906, 2012.

[116] L. A. Shepperd, J. C. Meadows, A. M. Sochaj, T. C. Lancaster, J. Zou, G. J. Buttrick, J. Rappsilber, K. G. Hardwick, and J. B. A. Millar, "Phosphodependent recruitment of Bub1 and Bub3 to Spc7/KNL1 by Mph1 kinase maintains the spindle checkpoint," *Current Biology*, vol. 22, no. 10, pp. 891–899, 2012.

[117] Y. Yamagishi, C. H. Yang, Y. Tanno, and Y. Watanabe, "MPS1/Mph1 phosphorylates the kinetochore protein KNL1/Spc7 to recruit SAC components," *Nature Cell Biology*, vol. 14, no. 7, pp. 746–752, 2012.

[118] P. Lara-Gonzalez, F. G. Westhorpe, and S. S. Taylor, "The spindle assembly checkpoint," *Current Biology*, vol. 22, no. 22, pp. R966–R980, 2012.

[119] Z. Ji, H. Gao, L. Jia, B. Li, and H. Yu, "A sequential multi-target Mps1 phosphorylation cascade promotes spindle checkpoint signaling," *eLife*, vol. 6, pp. 1–23, 2017.

[120] A. C. Faesen, M. Thanasoula, S. Maffini, C. Breit, F. Müller, S. Van Gerwen, T. Bange, and A. Musacchio, "Basis of catalytic assembly of the mitotic checkpoint complex," *Nature*, vol. 542, no. 7642, pp. 498–502, 2017.

[121] A. Espert, P. Uluocak, R. N. Bastos, D. Mangat, P. Graab, and U. Gruneberg, "PP2A-B56 opposes Mps1 phosphorylation of Knl1 and thereby promotes spindle assembly checkpoint silencing," *Journal of Cell Biology*, vol. 206, no. 7, pp. 833–842, 2014.

[122] A. P. Joglekar and A. A. Kukreja, "How kinetochore architecture shapes the mechanisms of its function," *Current Biology*, vol. 27, no. 16, pp. R816–R824, 2017.

[123] D. Izawa and J. Pines, "The mitotic checkpoint complex binds a second CDC20 to inhibit active APC/C," *Nature*, vol. 517, no. 7536, pp. 631–634, 2015.

[124] C. Alfieri, L. Chang, Z. Zhang, J. Yang, S. Maslen, M. Skehel, and D. Barford, "Molecular basis of APC/C regulation by the spindle assembly checkpoint," *Nature*, vol. 536, no. 7617, pp. 431–436, 2016.

[125] M. Yamaguchi, R. VanderLinden, F. Weissmann, R. Qiao, P. Dube, N. G. Brown, D. Haselbach, W. Zhang, S. S. Sidhu, J. M. Peters, H. Stark, and B. A. Schulman, "Cryo-EM of mitotic checkpoint complex-bound APC/C reveals reciprocal and conformational regulation of ubiquitin ligation," *Molecular Cell*, vol. 63, no. 4, pp. 593–607, 2016.

[126] F. Herzog, I. Primorac, P. Dube, P. Lenart, B. Sander, K. Mechtler, H. Stark, and J.-M. Peters, "Structure of the anaphase-promoting complex/cyclosome interacting with a mitotic checkpoint complex," *Science*, vol. 323, no. 5920, pp. 1477–1481, 2009.

[127] K. Uzunova, B. T. Dye, H. Schutz, R. Ladurner, G. Petzold, Y. Toyoda, M. A. Jarvis, N. G. Brown, I. Poser, M. Novatchkova, K. Mechtler, A. A. Hyman, H. Stark, B. A. Schulman, and J.-M. Peters, "APC15 mediates CDC20 autoubiquitylation by APC/C^{MCC} and disassembly of the mitotic checkpoint complex," *Nature Structural & Molecular Biology*, vol. 19, no. 11, pp. 1116–1123, 2012.

[128] R. B. Nicklas and C. A. Koch, "Chromosome micromanipulation. 3. Spindle fiber tension and the reorientation of mal-oriented chromosomes.," *Journal of Cell Biology*, vol. 43, no. 1, pp. 40–50, 1969.

[129] S. Biggins and A. W. Murray, "The budding yeast protein kinase Ipl1/Aurora allows the absence of tension to activate the spindle checkpoint," *Genes & Development*, vol. 15, no. 23, pp. 3118–3129, 2001.

[130] T. U. Tanaka, N. Rachidi, C. Janke, G. Pereira, M. Galova, E. Schiebel, M. J. Stark, and K. Nasmyth, "Evidence that the Ipl1-Sli15 (Aurora Kinase-INCENP) complex promotes chromosome bi-orientation by altering kinetochore-spindle pole connections," *Cell*, vol. 108, no. 3, pp. 317–329, 2002.

[131] S. Hauf, R. W. Cole, S. LaTerra, C. Zimmer, G. Schnapp, R. Walter, A. Heckel, J. Van Meel, C. L. Rieder, and J. M. Peters, "The small molecule Hesperadin reveals a role for Aurora B in correcting kinetochore-microtubule attachment and in maintaining the spindle assembly checkpoint," *Journal of Cell Biology*, vol. 161, no. 2, pp. 281–294, 2003.

[132] M. Munoz-Barrera and F. Monje-Casas, "Increased Aurora B activity causes continuous disruption of kinetochore-microtubule attachments and spindle instability," *Proceedings of the National Academy of Sciences*, vol. 111, no. 38, pp. E3996–E4005, 2014.

[133] V. Krenn and A. Musacchio, "The Aurora B kinase in chromosome bi-orientation and spindle checkpoint signaling," *Frontiers in Oncology*, vol. 5, no. October, 2015.

[134] J. P. Welburn, M. Vleugel, D. Liu, J. R. Yates, M. A. Lampson, T. Fukagawa, and I. M. Cheeseman, "Aurora B phosphorylates spatially distinct targets to differentially regulate the kinetochore-microtubule interface," *Molecular Cell*, vol. 38, no. 3, pp. 383–392, 2010.

[135] D. Liu, O. Davydenko, and M. A. Lampson, "Polo-like kinase-1 regulates kinetochore-microtubule dynamics and spindle checkpoint silencing," *Journal of Cell Biology*, vol. 198, no. 4, pp. 491–499, 2012.

[136] D. Liu, G. Vader, M. J. M. Vromans, M. A. Lampson, and S. M. A. Lens, "Sensing chromosome bi-orientation by spatial separation of Aurora B kinase from kinetochore substrates," *Science*, vol. 323, no. 5919, pp. 1350–1353, 2009.

[137] A. Khodjakov and J. Pines, "Centromere tension: A divisive issue," *Nature Cell Biology*, vol. 12, no. 10, pp. 919–923, 2010.

[138] T. Zhang, R. A. Oliveira, B. Schmierer, and B. Novák, "Dynamical scenarios for chromosome bi-orientation," *Biophysical Journal*, vol. 104, no. 12, pp. 2595–2606, 2013.

[139] E. S. Tubman, S. Biggins, and D. J. Odde, "Stochastic modeling yields a mechanistic framework for spindle attachment error correction in budding yeast mitosis," *Cell Systems*, vol. 4, no. 6, pp. 645–650.e5, 2017.

[140] B. Etemad and G. J. P. L. Kops, "Attachment issues: Kinetochore transformations and spindle checkpoint silencing," *Current Opinion in Cell Biology*, vol. 39, pp. 101–108, 2016.

[141] B. Etemad, T. E. F. Kuijt, and G. J. P. L. Kops, "Kinetochore-microtubule attachment is sufficient to satisfy the human spindle assembly checkpoint," *Nature Communications*, vol. 6, p. 8987, 2015.

[142] E. C. Tauchman, F. J. Boehm, and J. G. DeLuca, "Stable kinetochore-microtubule attachment is sufficient to silence the spindle assembly checkpoint in human cells," *Nature Communications*, vol. 6, pp. 1–9, 2015.

[143] S. Santaguida, C. Vernieri, F. Villa, A. Ciliberto, and A. Musacchio, "Evidence that Aurora B is implicated in spindle checkpoint signalling independently of error correction," *EMBO Journal*, vol. 30, no. 8, pp. 1508–1519, 2011.

[144] A. T. Saurin, M. S. van der Waal, R. H. Medema, S. M. A. Lens, and G. J. P. L. Kops, "Aurora B potentiates Mps1 activation to ensure rapid checkpoint establishment at the onset of mitosis.," *Nature Communications*, vol. 2, no. 1, p. 316, 2011.

[145] A. T. Saurin, "Kinase and phosphatase cross-talk at the kinetochore," *Frontiers in Cell and Developmental Biology*, vol. 6, pp. 1–23, 2018.

[146] M. D. Vázquez-Novelle, L. Sansregret, A. E. Dick, C. A. Smith, A. D. Mcainsh, D. W. Gerlich, and M. Petronczki, "Cdk1 inactivation terminates mitotic checkpoint surveillance and stabilizes kinetochore attachments in anaphase," *Current Biology*, vol. 24, no. 6, pp. 638–645, 2014.

[147] A. Rattani, P. Vinod, J. Godwin, K. Tachibana-Konwalski, M. Wolna, M. Malumbres, B. Novák, and K. Nasmyth, "Dependency of the spindle assembly checkpoint on Cdk1 renders the anaphase transition irreversible," *Current Biology*, vol. 24, no. 6, pp. 630–637, 2014.

[148] A. E. Dick and D. W. Gerlich, "Kinetic framework of spindle assembly checkpoint signalling," *Nature Cell Biology*, vol. 15, no. 11, pp. 1370–1377, 2013.

[149] G. J. P. L. Kops, "Cell division: SACing the anaphase problem," *Current Biology*, vol. 24, no. 6, pp. R224–R226, 2014.

[150] M. D. Vázquez-Novelle, L. Mirchenko, F. Uhlmann, and M. Petronczki, "The 'anaphase problem': how to disable the mitotic checkpoint when sisters split," *Biochemical Society Transactions*, vol. 38, no. 6, pp. 1660–1666, 2010.

[151] U. Gruneberg, R. Neef, R. Honda, E. A. Nigg, and F. A. Barr, "Relocation of Aurora B from centromeres to the central spindle at the metaphase to anaphase transition requires MKlp2," *Journal of Cell Biology*, vol. 166, no. 2, pp. 167–172, 2004.

[152] M. D. Vázquez-Novelle and M. Petronczki, "Relocation of the chromosomal passenger complex prevents mitotic checkpoint engagement at

anaphase," *Current Biology*, vol. 20, no. 15, pp. 1402–1407, 2010.

[153] M. Mirkovic, L. H. Hutter, B. Novák, and R. A. Oliveira, "Premature sister chromatid separation is poorly detected by the spindle assembly checkpoint as a result of system-level feedback," *Cell Reports*, vol. 13, no. 3, pp. 469–478, 2015.

[154] J. Kamenz and S. Hauf, "Slow checkpoint activation kinetics as a safety device in anaphase," *Current Biology*, vol. 24, no. 6, pp. 646–651, 2014.

[155] G. Fang, Y. Hongtao, and M. W. Kirschner, "Direct binding of CDC20 protein family members activates the anaphase-promoting complex in mitosis and G1," *Molecular Cell*, vol. 2, no. 2, pp. 163–171, 1998.

[156] S. Prinz, E. S. Hwang, R. Visintin, and A. Amon, "The regulation of Cdc20 proteolysis reveals a role for the APC components Cdc23 and Cdc27 during S phase and early mitosis," *Current Biology*, vol. 8, no. 13, pp. 750–760, 1998.

[157] J. Nilsson, M. Yekezare, J. Minshull, and J. Pines, "The APC/C maintains the spindle assembly checkpoint by targeting Cdc20 for destruction," *Nature Cell Biology*, vol. 10, no. 12, pp. 1411–1420, 2008.

[158] S. K. Reddy, M. Rape, W. A. Margansky, and M. W. Kirschner, "Ubiquitination by the anaphase-promoting complex drives spindle checkpoint inactivation," *Nature*, vol. 446, no. 7138, pp. 921–925, 2007.

[159] S. Ge, J. R. Skaar, and M. Pagano, "APC/C- and Mad2-mediated degradation of Cdc20 during spindle checkpoint activation," *Cell Cycle*, vol. 8, no. 1, pp. 167–171, 2009.

[160] G. Varetti, C. Guida, S. Santaguida, E. Chiroli, and A. Musacchio, "Homeostatic control of mitotic arrest," *Molecular Cell*, vol. 44, no. 5, pp. 710–720, 2011.

[161] E. Eytan, K. Wang, S. Miniowitz-Shemtov, D. Sitry-Shevah, S. Kaisari, T. J. Yen, S.-T. Liu, and A. Hershko, "Disassembly of mitotic checkpoint complexes by the joint action of the AAA-ATPase TRIP13 and p31^{comet}," *Proceedings of the National Academy of Sciences*, vol. 111, no. 33, pp. 12019–12024, 2014.

[162] K. Wang, B. Sturt-Gillespie, J. C. Hittle, D. Macdonald, G. K. Chan, T. J. Yen, and S. T. Liu, "Thyroid hormone receptor interacting protein 13 (TRIP13) AAA-ATPase is a novel mitotic checkpoint-silencing protein," *Journal of Biological Chemistry*, vol. 289, no. 34, pp. 23928–23937, 2014.

[163] F. G. Westhorpe, A. Tighe, P. Lara-Gonzalez, and S. S. Taylor, "p31^{comet}-mediated extraction of Mad2 from the MCC promotes efficient mitotic exit," *Journal of Cell Science*, vol. 124, no. 22, pp. 3905–3916, 2011.

[164] Q. Ye, S. C. Rosenberg, A. Moeller, J. A. Speir, T. Y. Su, and K. D. Corbett, "TRIP13 is a protein-remodeling AAA+ ATPase that catalyzes MAD2 conformation switching," *eLife*, vol. 2015, no. 4, pp. 1–44, 2015.

[165] C. Alfieri, L. Chang, and D. Barford, "Mechanism for remodelling of the cell cycle checkpoint protein MAD2 by the ATPase TRIP13," *Nature*, vol. 559, no. 7713, pp. 274–278, 2018.

[166] J. S. Han, A. J. Holland, D. Fachinetti, A. Kulukian, B. Cetin, and D. W. Cleveland, "Catalytic assembly of the mitotic checkpoint inhibitor BubR1-Cdc20 by a Mad2-induced functional switch in Cdc20," *Molecular Cell*, vol. 51, no. 1, pp. 92–104, 2013.

[167] E. A. Foley, M. Maldonado, and T. M. Kapoor, "Formation of stable attachments between kinetochores and microtubules depends on the B56-PP2A phosphatase," *Nature Cell Biology*, vol. 13, no. 10, pp. 1265–1271, 2011.

[168] S. J. E. Suijkerbuijk, M. Vleugel, A. Teixeira, and G. J. P. L. Kops, "Integration of Kinase and Phosphatase Activities by BUBR1 Ensures Formation of Stable Kinetochore-Microtubule Attachments," *Developmental Cell*, vol. 23, no. 4, pp. 745–755, 2012.

[169] T. Kruse, G. Zhang, M. S. Y. Larsen, T. Lischetti, W. Streicher, T. Kragh Nielsen, S. P. Bjorn, and J. Nilsson, "Direct binding between BubR1 and B56-PP2A phosphatase complexes regulate mitotic progression," *Journal of Cell Science*, vol. 126, no. 5, pp. 1086–1092, 2013.

[170] W. Nijenhuis, G. Vallardi, A. Teixeira, G. J. P. L. Kops, and A. T. Saurin, "Negative feedback at kinetochores underlies a responsive spindle checkpoint signal," *Nature Cell Biology*, vol. 16, no. 12, pp. 1257–1264, 2014.

[171] D. Liu, M. Vleugel, C. B. Backer, T. Hori, T. Fukagawa, I. M. Cheeseman, and M. A. Lampson, "Regulated targeting of protein phosphatase 1 to the outer kinetochore by KNL1 opposes Aurora B kinase," *Journal of Cell Biology*, vol. 188, no. 6, pp. 809–820, 2010.

[172] A. Grallert, E. Boke, A. Hagting, B. Hodgson, Y. Connolly, J. R. Griffiths, D. L. Smith, J. Pines, and I. M. Hagan, "A PP1-PP2A phosphatase relay controls mitotic progression," *Nature*, vol. 517, no. 7532, pp. 94–98, 2014.

[173] M. J. Cundell, R. N. Bastos, T. Zhang, J. Holder, U. Gruneberg, B. Novak, and F. A. Barr, "The BEG (PP2A-B55/ENSA/Greatwall) pathway ensures cytokinesis follows chromosome separation," *Molecular Cell*, vol. 52, no. 3, pp. 393–405, 2013.

[174] A. Gharbi-Ayachi, J.-C. Labbe, A. Burgess, S. Vigneron, J.-M. Strub, E. Brioudes, A. Van-Dorsselaer, A. Castro, and T. Lorca, "The substrate of Greatwall kinase, Arpp19, controls mitosis by inhibiting protein phosphatase 2A," *Science*, vol. 330, no. 6011, pp. 1673–1677, 2010.

[175] S. Mochida, S. L. Maslen, M. Skehel, and T. Hunt, "Greatwall phosphorylates an inhibitor

of protein phosphatase 2A that is essential for mitosis," *Science*, vol. 330, no. 6011, pp. 1670–1673, 2010.

[176] B. C. Williams, J. J. Filter, K. A. Blake-Hodek, B. E. Wadzinski, N. J. Fuda, D. Shalloway, and M. L. Goldberg, "Greatwall-phosphorylated endosulfine is both an inhibitor and a substrate of PP2A-B55 heterotrimers," *eLife*, no. 3, p. e01695, 2014.

[177] K. A. Blake-Hodek, B. C. Williams, Y. Zhao, P. V. Castilho, W. Chen, Y. Mao, T. M. Yamamoto, and M. L. Goldberg, "Determinants for activation of the atypical AGC kinase greatwall during M Phase entry," *Molecular and Cellular Biology*, vol. 32, no. 8, pp. 1337–1353, 2012.

[178] N. Hégarat, C. Vesely, P. K. Vinod, C. Ocasio, N. Peter, J. Gannon, A. W. Oliver, B. Novák, and H. Hochegger, "PP2A/B55 and Fcp1 regulate Greatwall and Ensa dephosphorylation during mitotic exit," *PLoS Genetics*, vol. 10, no. 1, p. e1004004, 2014.

[179] P. K. Vinod and B. Novak, "Model scenarios for switch-like mitotic transitions," *FEBS Letters*, vol. 589, no. 6, pp. 667–671, 2015.

[180] A. Heim, A. Konietzny, and T. U. Mayer, "Protein phosphatase 1 is essential for Greatwall inactivation at mitotic exit," *EMBO reports*, vol. 16, no. 11, pp. 1501–1510, 2015.

[181] S. Rogers, D. Fey, R. A. McCloy, B. L. Parker, N. J. Mitchell, R. J. Payne, R. J. Daly, D. E. James, C. E. Caldon, D. N. Watkins, D. R. Croucher, and A. Burgess, "PP1 initiates the dephosphorylation of MASTL, triggering mitotic exit and bistability in human cells," *Journal of Cell Science*, vol. 129, no. 7, pp. 1340–1354, 2016.

[182] H. T. Ma and R. Y. C. Poon, "TRIP13 regulates both the activation and inactivation of the spindle-assembly checkpoint," *Cell Reports*, vol. 14, no. 5, pp. 1086–1099, 2016.

[183] N. Sagata, "Meiotic metaphase arrest in animal oocytes: Its mechanisms and biological significance," *Trends in Cell Biology*, vol. 6, no. 1, pp. 22–28, 1996.

[184] D. Adhikari and K. Liu, "The regulation of maturation promoting factor during prophase I arrest and meiotic entry in mammalian oocytes," *Molecular and Cellular Endocrinology*, vol. 382, no. 1, pp. 480–487, 2014.

[185] J. S. Richards, D. L. Russell, S. Ochsner, and L. L. Espey, "Ovulation: new dimensions and new regulators of the inflammatory-like response," *Annual Review of Physiology*, vol. 64, no. 1, pp. 69–92, 2002.

[186] D. Adhikari, W. Zheng, Y. Shen, N. Gorre, Y. Ning, G. Halet, P. Kaldis, and K. Liu, "Cdk1, but not Cdk2, is the sole Cdk that is essential and sufficient to drive resumption of meiosis in mouse oocytes," *Human Molecular Genetics*, vol. 21, no. 11, pp. 2476–2484, 2012.

[187] O. Davydenko, R. M. Schultz, and M. A. Lampson, "Increased CDK1 activity determines the timing of kinetochore-microtubule attachments in meiosis I," *Journal of Cell Biology*, vol. 202, no. 2, pp. 221–229, 2013.

[188] Z. Polanski, E. Ledan, S. Brunet, S. Louvet, M. H. Verlhac, J. Z. Kubiak, and B. Maro, "Cyclin synthesis controls the progression of meiotic maturation in mouse oocytes," *Development*, vol. 125, no. 24, pp. 4989–4997, 1998.

[189] S. J. Han, R. Chen, M. P. Paronetto, and M. Conti, "Wee1B is an oocyte-specific kinase involved in the control of meiotic arrest in the mouse," *Current Biology*, vol. 15, no. 18, pp. 1670–1676, 2005.

[190] A. J. Lincoln, D. Wickramasinghe, P. Stein, R. M. Schultz, M. E. Palko, M. P. De Miguel, L. Tessarollo, and P. J. Donovan, "Cdc25b phosphatase is required for resumption of meiosis during oocyte maturation," *Nat Genet*, vol. 30, no. 4, pp. 446–449, 2002.

[191] S. J. Han and M. Conti, "New pathways from PKA to the Cdc2/cyclin B complex in oocytes: Wee1B as a potential PKA substrate," *Cell Cycle*, vol. 5, no. 3, pp. 227–231, 2006.

[192] G. Pirino, M. P. Wesco, and P. J. Donovan, "Protein kinase A regulates resumption of meiosis by phosphorylation of Cdc25B in mammalian oocytes," *Cell Cycle*, vol. 8, no. 4, pp. 665–670, 2009.

[193] J. S. Oh, S. J. Han, and M. Conti, "Wee1B, Myt1, and Cdc25 function in distinct compartments of the mouse oocyte to control meiotic resumption," *Journal of Cell Biology*, vol. 188, no. 2, pp. 199–207, 2010.

[194] I. Hoffmann, P. R. Clarke, M. J. Marcote, E. Karsenti, and G. Draetta, "Phosphorylation and activation of human cdc25-C by cdc2-cyclin B and its involvement in the self-amplification of MPF at mitosis," *The EMBO Journal*, vol. 12, no. 1, pp. 53–63, 1993.

[195] T. Izumi and J. L. Maller, "Elimination of cdc2 phosphorylation sites in the cdc25 phosphatase blocks initiation of M-phase," *Molecular Biology of the Cell*, vol. 4, no. 12, pp. 1337–1350, 1993.

[196] A. Reis, H. Y. Chang, M. Levasseur, and K. T. Jones, "APCcdh1Activity in Mouse Oocytes Prevents Entry into the First Meiotic Division," *Nature Cell Biology*, vol. 8, no. 5, pp. 539–540, 2006.

[197] J. E. Holt, S. M. Tran, J. L. Stewart, K. Minahan, I. Garcia-Higuera, S. Moreno, and K. T. Jones, "The APC/C activator FZR1 coordinates the timing of meiotic resumption during prophase I arrest in mammalian oocytes," *Development*, vol. 138, no. 5, pp. 905–913, 2011.

[198] T. M. Yamamoto, M. Iwabuchi, K. Ohsumi, and T. Kishimoto, "APC/C-Cdc20-mediated degradation of cyclin B participates in CSF arrest in unfertilized *Xenopus* eggs," *Developmental Biology*, vol. 279, no. 2, pp. 345–355, 2005.

[199] J. J. Tung, D. V. Hansen, K. H. Ban, A. V. Loktev, M. K. Summers, J. R. Adler, and P. K. Jackson, "A role for the anaphase-promoting complex inhibitor Emi2/XErp1, a homolog of early mitotic inhibitor 1, in cytostatic factor arrest of Xenopus eggs.," *Proceedings of the National Academy of Sciences*, vol. 102, no. 12, pp. 4318–4323, 2005.

[200] K. Sako, K. Suzuki, M. Isoda, S. Yoshikai, C. Senoo, N. Nakajo, M. Ohe, and N. Sagata, "Emi2 mediates meiotic MII arrest by competitively inhibiting the binding of Ube2S to the APC/C," *Nature Communications*, vol. 5, p. 3667, 2014.

[201] Q. Wu, Y. Guo, A. Yamada, J. A. Perry, M. Z. Wang, M. Araki, C. D. Freel, J. J. Tung, W. Tang, S. S. Margolis, P. K. Jackson, H. Yamano, M. Asano, and S. Kornbluth, "A role for Cdc2- and PP2A-mediated regulation of Emi2 in the maintenance of CSF arrest," *Current Biology*, vol. 17, no. 3, pp. 213–224, 2007.

[202] M. Isoda, K. Sako, K. Suzuki, K. Nishino, N. Nakajo, M. Ohe, T. Ezaki, Y. Kanemori, D. Inoue, H. Ueno, and N. Sagata, "Dynamic regulation of Emi2 by Emi2-bound Cdk1/Plk1/CK1 and PP2A-B56 in meiotic arrest of *Xenopus* eggs," *Developmental Cell*, vol. 21, no. 3, pp. 506–519, 2011.

[203] A. J. Holland, F. Böttger, O. Stemmann, and S. S. Taylor, "Protein phosphatase 2A and separase form a complex regulated by separase autocleavage.," *The Journal of Biological Chemistry*, vol. 282, no. 34, pp. 24623–32, 2007.

[204] N. R. Rauh, A. Schmidt, J. Bormann, E. A. Nigg, and T. U. Mayer, "Calcium triggers exit from meiosis II by targeting the APC/C inhibitor XErp1 for degradation," *Nature*, vol. 437, no. 7061, pp. 1048–1052, 2005.

[205] A. Rattani, M. Wolna, M. Ploquin, W. Helmhart, S. Morrone, B. Mayer, J. Godwin, W. Xu, O. Stemmann, A. Pendas, and K. Nasmyth, "Sgol2 provides a regulatory platform that coordinates essential cell cycle processes during meiosis I in oocytes," *eLife*, vol. 2013, no. 2, p. e01133, 2013.

[206] E. Llano, R. Gómez, C. Gutiérrez-Caballero, Y. Herrán, M. Sánchez-Martín, L. Vázquez-Quiñones, T. Hernández, E. De Álava, A. Cuadrado, J. L. Barbero, J. A. Suja, and A. M. Pendás, "Shugoshin-2 is essential for the completion of meiosis but not for mitotic cell division in mice," *Genes and Development*, vol. 22, no. 17, pp. 2400–2413, 2008.

[207] L. M. Lister, A. Kouznetsova, L. A. Hyslop, D. Kalleas, S. L. Pace, J. C. Barel, A. Nathan, V. Floros, C. Adelfalk, Y. Watanabe, R. Jessberger, T. B. Kirkwood, C. Höög, and M. Herbert, "Age-related meiotic segregation errors in mammalian oocytes are preceded by depletion of cohesin and Sgo2," *Current Biology*, vol. 20, no. 17, pp. 1511–1521, 2010.

[208] A. L. Marston and K. Wassmann, "Multiple duties for spindle assembly checkpoint kinases in meiosis," *Frontiers in Cell and Developmental Biology*, vol. 5, p. 109, 2017.

[209] J. R. Sanders and K. T. Jones, "Regulation of the meiotic divisions of mammalian oocytes and eggs," *Biochemical Society Transactions*, vol. 46, no. 4, pp. 797–806, 2018.

[210] T. Hassold and P. Hunt, "To err (meiotically) is human: the genesis of human aneuploidy," *Nature Reviews Genetics*, vol. 2, no. 4, pp. 280–291, 2001.

[211] H. Shao, R. Li, C. Ma, E. Chen, and X. J. Liu, "Xenopus oocyte meiosis lacks spindle assembly checkpoint control," *Journal of Cell Biology*, vol. 201, no. 2, pp. 191–200, 2013.

[212] B. E. McGuinness, M. Anger, A. Kouznetsova, A. M. Gil-Bernabé, W. Helmhart, N. R. Kudo, A. Wuensche, S. Taylor, C. Hoog, B. Novak, and K. Nasmyth, "Regulation of APC/C activity in oocytes by a Bub1-dependent spindle assembly checkpoint," *Current Biology*, vol. 19, no. 5, pp. 369–380, 2009.

[213] K. Hached, S. Z. Xie, E. Buffin, D. Cladiere, C. Rachez, M. Sacras, P. K. Sorger, and K. Wassmann, "Mps1 at kinetochores is essential for female mouse meiosis I," *Development*, vol. 138, no. 11, pp. 2261–2271, 2011.

[214] J. Sebestova, A. Danylevska, L. Novakova, M. Kubelka, and M. Anger, "Lack of response to unaligned chromosomes in mammalian female gametes," *Cell Cycle*, vol. 11, no. 16, pp. 3011–3018, 2012.

[215] L. Gui and H. Homer, "Spindle assembly checkpoint signalling is uncoupled from chromosomal position in mouse oocytes," *Development*, vol. 139, no. 11, pp. 1941–1946, 2012.

[216] S. I. R. Lane, Y. Yun, and K. T. Jones, "Timing of anaphase-promoting complex activation in mouse oocytes is predicted by microtubule-kinetochore attachment but not by bivalent alignment or tension," *Journal of Cell Science*, vol. 125, no. 11, pp. e1–e1, 2012.

[217] S. A. Touati and K. Wassmann, "How oocytes try to get it right: spindle checkpoint control in meiosis," *Chromosoma*, vol. 125, no. 2, pp. 321–335, 2016.

[218] G. B. Ermentrout, "XPPAUT 8.0," 2016.

[219] The MathWorks Inc., "MATLAB R2017b (9.3.0)," 2017.

[220] M. Hopkins, J. J. Tyson, and B. Novák, "Cell-cycle transitions: a common role for stoichiometric inhibitors," *Molecular Biology of the Cell*, vol. 28, no. 23, pp. 3437–3446, 2017.

[221] J. E. Ferrell and S. H. Ha, "Ultrasensitivity part II: multisite phosphorylation, stoichiometric inhibitors, and positive feedback.," *Trends in Biochemical Sciences*, vol. 39, no. 11, pp. 556–69, 2014.

[222] J. Monod, J. Wyman, and J. P. Changeux, "On the nature of allosteric transitions: A plausible model," *Journal of Molecular Biology*, vol. 12, no. 1, pp. 88–118, 1965.

[223] D. E. Koshland, J. G. Nemethy, and D. Filmer, "Comparison of experimental binding data and theoretical models in proteins containing subunits," *Biochemistry*, vol. 5, no. 1, pp. 365–385, 1966.

[224] J. Gunawardena, "Multisite protein phosphorylation makes a good threshold but can be a poor switch," *Proceedings of the National Academy of Sciences*, vol. 102, no. 41, pp. 14617–14622, 2005.

[225] A. Verdugo, P. K. Vinod, J. J. Tyson, and B. Novak, "Molecular mechanisms creating bistable switches at cell cycle transitions," *Open Biology*, vol. 3, no. 3, p. 120179, 2013.

[226] A. Goldbeter and D. E. Koshland, "An amplified sensitivity arising from covalent modification in biological systems," *Proceedings of the National Academy of Sciences*, vol. 78, no. 11, pp. 6840–4, 1981.

[227] C. D. Thron, "Theoretical dynamics of the cyclin B-MPF system: a possible role for $p13^{suc1}$," *BioSystems*, vol. 32, no. 2, pp. 97–109, 1994.

[228] M. Sabouri-Ghomi, A. Ciliberto, S. Kar, B. Novak, and J. J. Tyson, "Antagonism and bistability in protein interaction networks," *Journal of Theoretical Biology*, vol. 250, no. 1, pp. 209–218, 2008.

[229] E. Schwob and K. Nasmyth, "CLB5 and CLB6, a new pair of B cyclins involved in DNA replication in Saccharomyces cerevisiae," *Genes & Development*, vol. 7, no. 7A, pp. 1160–75, 1993.

[230] J. Correa-Bordes and P. Nurse, "$p25^{rum1}$ orders S phase and mitosis by acting as an inhibitor of the $p34^{cdc2}$ mitotic kinase," *Cell*, vol. 83, no. 6, pp. 1001–9, 1995.

[231] J. Benito, C. Martín-Castellanos, and S. Moreno, "Regulation of the G1 phase of the cell cycle by periodic stabilization and degradation of the p25\textsupersciptrum1 CDK inhibitor," *The EMBO Journal*, vol. 17, no. 2, pp. 482–97, 1998.

[232] M. Kõivomägi, E. Valk, R. Venta, A. Iofik, M. Lepiku, E. R. M. Balog, S. M. Rubin, D. O. Morgan, and M. Loog, "Cascades of multisite phosphorylation control Sic1 destruction at the onset of S phase," *Nature*, vol. 480, no. 7375, pp. 128–131, 2011.

[233] T. T. Nugroho and M. D. Mendenhall, "An inhibitor of yeast cyclin-dependent protein kinase plays an important role in ensuring the genomic integrity of daughter cells," *Molecular and Cellular Biology*, vol. 14, no. 5, pp. 3320–3328, 1994.

[234] R. J. Sheaff and J. M. Roberts, "End of the line: proteolytic degradation of cyclin-dependent kinase inhibitors.," *Chemistry & Biology*, vol. 3, no. 11, pp. 869–73, 1996.

[235] B. L. Schneider, Q. H. Yang, and A. B. Futcher, "Linkage of replication to start by the Cdk inhibitor Sic1," *Science*, vol. 272, no. 5261, pp. 560–562, 1996.

[236] T. Moll, G. Tebb, U. Surana, H. Robitsch, and K. Nasmyth, "The role of phosphorylation and the CDC28 protein kinase in cell cycle-regulated nuclear import of the S. cerevisiae transcription factor SW15," *Cell*, vol. 66, no. 4, pp. 743–758, 1991.

[237] M. Costanzo, J. L. Nishikawa, X. Tang, J. S. Millman, O. Schub, K. Breitkreuz, D. Dewar, I. Rupes, B. Andrews, and M. Tyers, "CDK activity antagonizes Whi5, an inhibitor of G1/S transcription in yeast," *Cell*, vol. 117, no. 7, pp. 899–913, 2004.

[238] R. A. M. de Bruin, W. H. McDonald, T. I. Kalashnikova, J. Yates, and C. Wittenberg, "Cln3 activates G1-specific transcription via phosphorylation of the SBF bound repressor Whi5," *Cell*, vol. 117, no. 7, pp. 887–98, 2004.

[239] M. Feinberg, "CRNT Toolbox v.2.3."

[240] J. J. Filter, B. C. Williams, M. Eto, D. Shalloway, and M. L. Goldberg, "Unfair competition governs the interaction of pCPI-17 with myosin phosphatase (PP1-MYPT1)," *eLife*, vol. 6, pp. 1–27, 2017.

[241] D. Hayward, T. Alfonso-Perez, M. J. Cundell, M. Hopkins, J. Holder, J. Bancroft, L. H. Hutter, B. Novak, F. A. Barr, and U. Gruneberg, "CDK1-CCNB1 creates a spindle checkpoint-permissive state by enabling MPS1 kinetochore localization," *Journal of Cell Biology*, p. jcb.201808014, 2019.

[242] E. He, O. Kapuy, R. a. Oliveira, F. Uhlmann, J. J. Tyson, and B. Novák, "System-level feedbacks make the anaphase switch irreversible," *Proceedings of the National Academy of Sciences*, vol. 108, no. 24, pp. 10016–10021, 2011.

[243] D. Hayward, T. Alfonso-Perez, M. J. Cundell, M. Hopkins, J. Holder, J. Bancroft, L. H. Hutter, B. Novak, F. A. Barr, and U. Gruneberg, "Cdk1-CCNB1 and PP2A-B55 license the spindle checkpoint by regulating MPS1 kinetochore localisation." unpublished.

[244] A. Rattani, R. Ballesteros Mejia, K. Roberts, M. B. Roig, J. Godwin, M. Hopkins, M. Eguren, L. Sanchez-Pulido, E. Okaz, S. Ogushi, M. Wolna, J. Metson, A. M. Pendás, M. Malumbres, B. Novák, M. Herbert, and K. Nasmyth, "APC/C^{Cdh1} enables removal of Shugoshin-2 from the arms of bivalent chromosomes by moderating cyclin-dependent kinase activity," *Current Biology*, vol. 27, no. 10, pp. 1462–1476.e5, 2017.

[245] A. Reis, S. Madgwick, H.-Y. Chang, I. Nabti, M. Levasseur, and K. T. Jones, "Prometaphase APC^{cdh1} activity prevents non-disjunction in mammalian oocytes," *Nature Cell Biology*, vol. 9, no. 10, pp. 1192–1198, 2007.

[246] M. Lewandoski, K. M. Wassarman, and G. R. Martin, "Zp3-cre, a transgenic mouse line for the activation or inactivation of loxP-flanked target genes specifically in the female germ line," *Current Biology*, vol. 7, no. 2, pp. 148–51, 1997.

[247] S. Mochida, S. Rata, H. Hino, T. Nagai, and B. Novák, "Two bistable switches govern M phase entry," *Current Biology*, vol. 26, no. 24, pp. 3361–3367, 2016.

[248] S. Rata, M. F. Suarez Peredo Rodriguez, S. Joseph, N. Peter, F. Echegaray Iturra, F. Yang, A. Madzvamuse, J. G. Ruppert, K. Samejima, M. Platani, M. Alvarez-Fernandez, M. Malumbres, W. C. Earnshaw, B. Novak, and H. Hochegger, "Two interlinked bistable switches govern mitotic control in mammalian cells," *Current Biology*, vol. 28, no. 23, pp. 3824–3832.e6, 2018.

Appendix A

Model .ode files

In this Appendix are provided the .ode files for simulating the models presented in previous chapters. These files can be run using the free ODE solver **XPPAUT**, (available from `http://www.math.pitt.edu/~bard/xpp/xpp.html`) [218]. To simulate the models listed below, copy into a text editor and save as a .ode file, and then open using XPPAUT. Note that the backslash character (\) is used to continue an expression over a linebreak, and should be retained when copying across to a .ode file.

A.1 FADS models (Chapter 2)

Some of the models in this chapter are also published in the supplementary material of the associated paper [220].

A.1.1 Generic FADS motif

```
# ODEs
dIM/dt = kcat*AI - kdemi*R*IM
dR/dt = kdemr*W*(RT - R) - kmodr*(AT - AI)*R
# Definition of Michaelis constant
!Km = (kdis + kcat)/kass
# Algebraic equation for pseudo-steady state concentration of AI complex
AI = 0.5*(AT + IT - IM + Km - sqrt((AT + IT - IM + Km)^2 - 4*AT*(IT - IM)))
# Parameters
p AT=1
p kmodr=2, kdemr=1, W=0.05
p RT=1, IT=3
p kdemi=0.1
p kdis=0.01, kass=100, kcat=0.05
# XPP settings
@ xp=IM, yp=R, xlo=0, xhi=3, ylo=0, yhi=1.5
@ nmesh=400, meth=stiff, total=100, dt=0.1
done
```

A.1.2 G1/S (Sic1/Swi5)

```
# ODEs
dIT/dt = ksyn*R - kdeg*IT - kphosi*G*(IT-AI) - kcat*AI
dR/dt = kdephr*W*(RT - R) - kphosr*(AT - AI)*R
# Definition of Michaelis constant
!Km = (kdis + kcat)/kass
# Algebraic equation for pseudo-steady state concentration of AI complex
AI = 0.5*(AT + IT + Km - sqrt((AT + IT + Km)^2 - 4*AT*IT))
# Parameters
p G=0.5
p kphosr=0.3, kdephr=1, W=0.05
p AT=1, RT=1
p ksyn=0.15, kdeg=0.035, kphosi=0.15
p kdis=0.01, kass=10, kcat=0.05
# XPP settings
@ xp=IT, yp=R, xlo=0, xhi=3, ylo=0, yhi=1.2
@ nmesh=400, meth=stiff, total=500, dt=0.5
done
```

A.1.3 SAC

```
# ODEs
dMCCT/dt = kassemb*uKT* CycB*(LimCompT - MCCT) - kcat*APCMCC
dCycB/dt = ksyn - (k'deg + kdeg*(APCT - APCMCC))*CycB
# Definition of Michaelis constant
!Km = (kdis + kcat)/kass
# Algebraic equation for pseudo-steady state concentration of APC:MCC complex
APCMCC = 0.5*(APCT + MCCT + Km - sqrt((APCT + MCCT + Km)^2 - 4*APCT*MCCT))
# Parameters
p uKT=0.1
p kdeg=2, ksyn=0.01, k'deg=0.01
p APCT=1, LimCompT=3
p kassemb=1
p kdis=0.01, kass=100, kcat=0.05
# Initial Conditions
init CycB=1, MCCT=3
# XPP Settings
@ xp=MCCT, yp=CycB, xlo=0, xhi=3, ylo=0, yhi=1
@ nmesh=400, meth=stiff, total=500, dt=0.5
done
```

A.1.4 Mitotic Exit

```
# ODEs
dIM/dt = kphosi*R*(IT - IM) - kcat*AI
dR/dt = kphosr*W*(RT - R) - kdephr*(AT - AI)*R
```

```
# Definition of Michaelis constant
!Km = (kdis + kcat)/kass
# Algebraic equation for pseudo-steady state concentration of AI complex
AI = 0.5*(AT + IM + Km - sqrt((AT + IM + Km)^2 - 4*AT*IM))
# Parameters
p W=1
p kdephr=2, kphosr=0.05
p AT=1, RT=1, IT=3
p kphosi=0.1
p kdis=0.01, kass=10, kcat=0.05
# XPP Settings
@ xp=IM, yp=R, xlo=0, xhi=3, ylo=0, yhi=1.1
@ nmesh=400, meth=stiff, total=500, dt=0.5
done
```

A.1.5 G1/S (Emi1/Cdh1)

```
# ODEs
dEmi1T/dt = ksEmi - kdEmi*Emi1T - kd2Emi*Complex
dCycA/dt = ksCycA - (kdCycA + kd2CycA*(Cdh1unP - Complex))*CycA
# Algebraic equation for Cdh1 phosphorylation state
Cdh1unP = kdpCdh1*Cdh1T/(kdpCdh1 + kpCdh1 + kp2Cdh1*(CycE + CycA))
# Algebraic equation for pseudo-steady state concentration
# of Emi1:Cdh1 complex
CC = kdiComp + kd2Emi + kpCdh1 + kp2Cdh1*(CycE + CycA)
BB = Emi1T + Cdh1unP + CC/kasComp
Complex = 2*Emi1T*Cdh1unP/(BB+sqrt(BB^2-4*Emi1T*Cdh1unP))
# Parameters
p CycE=0
p ksEmi=0.01, kdEmi=0.01, kd2Emi=0.025
p ksCycA=0.01, kdCycA=0.01, kd2CycA=1
p kdpCdh1=0.02, kpCdh1=0, kp2Cdh1=0.2, Cdh1T=1
p kdiComp=0.01, kasComp=10
# XPP Settings
@ xp=Emi1T, yp=CycA, xlo=-0.1, xhi=1, ylo=0, yhi=1.5
@ nmesh=400, meth=stiff, t=100, dt=0.1
# AUTO settings
@ parmin=-1, parmax=5, autoxmin=0
@autoymin=-0.1, autoxmax=1, autoymax=1.5
@ ntst=50, ds=0.01, dsmax=0.02, nmax=200000000
@ npr=1000, EPSL=1e-7, EPSS=1E-7, EPSU=1E-7
done
```

A.2 Mitosis (Chapter 3)

The MPS1 phosphorylation model below is also included in the joint manuscript under submission to JCB [243].

A.2.1 MPS1 phosphorylation model

```
# Unified model for Greatwall pathway controlled SAC signalling
# Initial Conditions
init CycB=1.012, GwlP=0.793, ENSAPt=1.423, Mps1P=0.908
init Mad2at=0.968, MCCt=0.677, MCCAPC=0.0287, Cdc20T=0.712, uKT=0
# ODEs for the Greatwall pathway and SAC signalling
CycB' = kscyc' + kscyc*Cdk1 - (kdcyc' + kdcyc*Psome*Cdc20)*CycB
GwlP' = kagw*Cdk1*(GwlT - GwlP) - (kigw' + kigw*B55)*GwlP
ENSAPt' = kaensa*GwlP*(ENSAT - ENSAPt) - \
kiensa*ENSAB55 - kiensa'*(ENSAPt - ENSAB55)
Mps1P' = kamps1*Cdk1*(Mps1T-Mps1P)-kimps1*(B55+PP)*Mps1P
# Mad2at represents free and MCC incorporated Mad2a
Mad2at' = kamad*Mps1P*uKT*Mad2i - kimad*Psome*MCCAPC
# MCCt represent free and APC/C-Cdc20 bound MCC
MCCt' = kasmcc*Mad2a*Cdc20f \
- (kdimcc + kdcdc20)*MCCt - kimad*Psome*MCCAPC
MCCAPC' = kasapc*MCC*Cdc20 \
- (kdiapc + kdimcc + 2*kdcdc20 + kimad*Psome)*MCCAPC
Cdc20T' = kscdc20 - kdcdc20*Cdc20T - kimad*Psome*MCCAPC
uKT' = kauKT*(1 - uKT) - kiuKT*uKT
# Calculation of pENSA:B55 complex in pseudo-steady state BB = ENSAPt +
B55T + (kdi55ensa + kiensa)/kas55ensa
ENSAB55 = 2*ENSAPt*B55T/(BB + sqrt(BB^2 - 4*ENSAPt*B55T))
B55 = B55T - ENSAB55
# Calculation of other forms in the network
Mad2i = Mad2T - Mad2at
Mad2a = Mad2at - MCCt
MCC = MCCt - MCCAPC
Cdk1 = (CycB + eps)/(1 + flavo)
Cdc20f = Cdc20T - MCCt - MCCAPC
Cdc20 = Cdc20f/(1 + alpha*Cdk1)
# Calculation of auxiliary variables
aux relENSA = ENSAPt*delta
aux KTMps1P = Mps1P*uKT
aux B55 = B55T - ENSAB55
# Values of kinetic parameters
p kscyc'=0.0005, kscyc=0.0045, kdcyc'=0.005
p kdcyc=0.7, Psome=1, eps=0.01
p GwlT=1, kagw=8, kigw'=2, kigw=2
p ENSAT=2, kaensa=0.7, kiensa=0.25, kiensa'=0.175
p Mps1T=1, B55T=1, kas55ensa=10, kdi55ensa=0.01
p kamps1=0.5, kimps1=0.5, PP=0.05
p Mad2T=1, kamad=1, kimad=1
p kasmcc=100, kdimcc=0.1, kasapc=100, kdiapc=0.1
p kscdc20=0.1, kdcdc20=0.1, kauKT=0, kiuKT=0
p delta=0.5, alpha=8, flavo=0
# XPP Settings
@ total=70,dt=1
```

```
@ meth=STIFF,xlo=0,xhi=70,ylo=0,yhi=1.05
# Default lines for plotting
@ xp=time,nplot=7
@ yp=CycB,yp2=GwlP,yp3=relENSA,yp4=Mps1P,yp5=MCCt,yp6=KTMps1P,yp7=B55
done
```

A.2.2 Cdc20 and APC/C phosphorylation model

Three different model variants are included below, using different kinetic schemes (mass action or Goldbeter-Koshland) for APC/C and/or Cdc20 phosphorylation.

Mass action APC/C, Goldbeter-Koshland Cdc20

```
# ODEs CycB' = ksCycB - (kd1CycB + kd2CycB*APCpC20 + \
kd3CycB*APCC20 + kd4CycB*APCpC20p + kd5CycB*APCC20p)*CycB
APCpT' = kpAPC*Cdk1*APCdpT - kdpAPC*APCpT
# Expressions for pesudo-steady state Goldbeter-Koshland kinetics
GB(Va,Vi,J) = Vi-Va+(Vi+Va)*J
GK(Va,Vi,J) = 2*Va*J/(GB(Va,Vi,J) + sqrt(GB(Va,Vi,J)^2-4*(Vi-Va)*Va*J))
# Algebraic Equations for APC:Cdc20 complexes
APCdpT = Cdc20T - APCpT
APCC20 = APCdpT*GK(kdpC20, kpC20*Cdk1, JC20)
APCC20p = APCdpT - APCC20
APCpC20 = APCpT*GK(kdpC20, kpC20*Cdk1, JC20)
APCpC20p = APCpT - APCpC20
# Rate Constants
kd3CycB=kd2CycB*rdcycAPC
kd4CycB=kd2CycB*rdcycC20p
kd5CycB=kd2CycB*rdcycAPC*rdcycC20p
Cdk1=CycB/(1 + kicdk)
# Parameters
p Cdc20T=0
p kicdk=0
p ksCycB=0.01, kd1CycB=0.01, kd2CycB=0.1
p rdcycC20p=0.01, rdcycAPC=0.2
p kpC20=1, kdpC20=0.2, JC20=0.15
p kpAPC=0.5, kdpAPC=0.02
# XPP Settings
@ total=500, dt=0.5
@ xp=APCpT, yp=CycB, meth=stiff, xhi=1.5, ylo=0
@ yhi=1, bound=1000, nmesh=400
# AUTO settings
@ parmin=0, parmax=2, autoxmin=0
@ autoymin=0, autoxmax=2, autoymax=1
@ ntst=50, ds=0.01, dsmax=0.02, nmax=200000000
@ npr=10000,EPSL=1e-9,EPSS=1E-9,EPSU=1E-9
done
```

Goldbeter-Koshland APC/C and Cdc20

```
# ODEs
CycB' = ksCycB - (kd1CycB + kd2CycB*APCpC20 \
+ kd3CycB*APCC20 + kd4CycB*APCpC20p + kd5CycB*APCC20p)*CycB
APCpT' = kpAPC*Cdk1*APCdpT/(JAPC + APCdpT) - kdpAPC*APCpT/(JAPC + APCpT)
# Expressions for pesudo-steady state Goldbeter-Koshland kinetics
GB(Va,Vi,J) = Vi-Va+(Vi+Va)*J
GK(Va,Vi,J) = 2*Va*J/(GB(Va,Vi,J) + sqrt(GB(Va,Vi,J)^2-4*(Vi-Va)*Va*J))
# Algebraic Equations for APC:Cdc20 complexes
APCdpT = Cdc20T - APCpT
APCC20 = APCdpT*GK(kdpC20, kpC20*Cdk1, JC20)
APCC20p = APCdpT - APCC20
APCpC20 = APCpT*GK(kdpC20, kpC20*Cdk1, JC20)
APCpC20p = APCpT - APCpC20
# Rate Constants
kd3CycB=kd2CycB*rdcycAPC
kd4CycB=kd2CycB*rdcycC20p
kd5CycB=kd2CycB*rdcycAPC*rdcycC20p
Cdk1=CycB/(1 + kicdk)
# Parameters
p Cdc20T=1
p kicdk=0
p ksc20=0.01, kd1C20=0.03
p ksCycB=0.01, kd1CycB=0.01, kd2CycB=0.2
p rdcycC20p=0.01, rdcycAPC=0.15
p kpC20=1, kdpC20=0.2, JC20=0.1
p kpAPC=0.08, kdpAPC=0.02, JAPC=0.1
# XPP Settings
@ total=1000, dt=0.5
@ xp=APCpT, yp=CycB, meth=stiff, xhi=1
@ ylo=0, yhi=1, bound=1000, nmesh=400
done
```

Mass-action APC/C and Cdc20

```
# ODEs
CycB' = ksCycB - (kd1CycB + kd2CycB*APCpC20 \
+ kd3CycB*APCC20 + kd4CycB*APCpC20p + kd5CycB*APCC20p)*CycB
APCpT' = kpAPC*Cdk1*APCdpT - kdpAPC*APCpT
# Expressions for pesudo-steady state Goldbeter-Koshland kinetics
GB(Va,Vi,J) = Vi-Va+(Vi+Va)*J
GK(Va,Vi,J) = 2*Va*J/(GB(Va,Vi,J)+sqrt(GB(Va,Vi,J)^2-4*(Vi-Va)*Va*J))
# Algebraic Equations for APC:Cdc20 complexes
APCdpT = Cdc20T - APCpT
APCC20 = kdpC20*APCdpT/(kpC20*Cdk1 + kdpC20)
APCC20p = APCdpT - APCC20
APCpC20 = kdpC20*APCpT/(kpC20*Cdk1 + kdpC20)
APCpC20p = APCpT - APCpC20
```

```
# Rate Constants
kd3CycB=kd2CycB*rdcycAPC
kd4CycB=kd2CycB*rdcycC20p
kd5CycB=kd2CycB*rdcycAPC*rdcycC20p
Cdk1=CycB/(1 + kicdk)
# Parameters
p Cdc20T=1
p kicdk=0
p ksc20=0.01, kd1C20=0.03
p ksCycB=0.01, kd1CycB=0.01, kd2CycB=0.1
p rdcycC20p=0.01, rdcycAPC=0.2
p kpC20=1, kdpC20=0.2, JC20=0.15
p kpAPC=0.5, kdpAPC=0.02
# XPP Settings
@ total=500, dt=0.1
@ xp=APCpT, yp=CycB, meth=stiff, xhi=1.5
@ ylo=0, yhi=1, bound=1000, nmesh=400
# AUTO settings
@ parmin=0, parmax=2, autoxmin=0
@ autoymin=0, autoxmax=2, autoymax=1
@ ntst=50, ds=0.01, dsmax=0.02, nmax=200000000
@ npr=1000,EPSL=1e-7,EPSS=1E-7,EPSU=1E-7
done
```

A.3 Meiotic Resumption Models (Chapter 4)

The full model given below is also included in the supplement of the joint paper with Ahmed Rattani and colleagues [244].

A.3.1 Full model (timecourse simulations)

```
# ODEs
CycBT' = ksCycB - (kd1CycB + kd2CycB*Cdh1)*CycBT
Cdk1' = ksCycB - (kd1CycB + kd2CycB*Cdh1)*Cdk1 \
- (Vi2CDK*Wee1 + Vi1CDK*Wee1p)*Cdk1 \
+ (Va2CDK*Cdc25p + Va1CDK*Cdc25)*Cdk1p
Cdh1' = VaCdh1*Cdh1p/(JCdh1 + Cdh1p) - ViCdh1*Cdk1*Cdh1/(JCdh1 + Cdh1)
Cdc25T' = ksc25 - (kd1c25 + kd2c25*Cdh1)*Cdc25T
Cdc25p' = Va25*Cdk1*Cdc25/(J25 + Cdc25) - Vi25*Cdc25p/(J25 + Cdc25p) \
- (kd1c25 + kd2c25*Cdh1)*Cdc25p
Wee1' = VaWee*Wee1p/(JWee + Wee1p) - ViWee*Wee1*Cdk1/(JWee + Wee1)
# Algebraic mass conservation equations
Cdc25 = Cdc25T - Cdc25p
Wee1p = Wee1T - Wee1
Cdk1p = CycBT - Cdk1
Cdh1p = Cdh1T - Cdh1
# Parameters (for WT GV arrest)
```

```
p Va1CDK=0.015, Va2CDK=1.5, Vi1CDK=0.015, Vi2CDK=0.3
p VaCdh1=1.5, ViCdh1=6, JCdh1=0.15, Cdh1T=1
p VaWee=0.375, ViWee=1.5, Jwee=0.01, Wee1T=1
p Va25=1.5, Vi25=0.375, J25=0.01
p ksc25=0.015, kd1c25=0.015, kd2c25=0.15
p ksCycB=0.015, kd1CycB=0.015, kd2CycB=0.075
# Initial Conditions (WT GV arrest)
init CycBT=0.1701, Cdk1=0.04000, Cdh1=0.9759
init Cdc25p=0.001675, Wee1=0.9981, Cdc25T=0.09295
# XPP settings
@ XP=t, YP=Cdk1, TOTAL=480, METH=stiff, XHI=480
@ YLO=0, YHI=1, BOUND=1000, dt=0.1
# Default lines for plotting
@ NPLOT=5
@ yp1=CycBT, yp2=Cdk1, yp3=Cdh1, yp4=Cdc25p, yp5=Wee1
done
```

A.3.2 Reduced model (phaseplane analysis)

```
# ODEs
Cdk1' = ksCycB - VdCycB*Cdk1 - kwee*Cdk1 + k25*Cdk1p
Cdh1' = VaCdh1*Cdh1p/(JCdh1 + Cdh1p) - ViCdh1*Cdk1*Cdh1/(JCdh1 + Cdh1)
# Expressions for pesudo-steady state Goldbeter-Koshland kinetics
GB(arg1,arg2,arg3,arg4) = arg2-arg1+arg2*arg3+arg1*arg4
GK(arg1,arg2,arg3,arg4) = 2*arg1*arg4/(GB(arg1,arg2,arg3,arg4) \
+sqrt(GB(arg1,arg2,arg3,arg4)^2-4*(arg2-arg1)*arg1*arg4))
# Algebraic equation for pseudo-steady state concentration of Cyclin B
VdCycB = kd1CycB+kd2CycB*Cdh1
CycBT = ksCycB/Vdcycb
aux CycBT = ksCycB/Vdcycb
# Algebraic equations for psuedo-steady state activities of Wee1 and Cdc25
Cdc25T = ksc25/(kd1c25 + kd2c25*Cdh1)
aux Cdc25T = Cdc25T
kwee = Vi1CDK + (Vi2CDK-Vi1CDK)*GK(Vawee, Viwee*Cdk1, Jwee, Jwee)
k25 = Cdc25T*(Va1CDK + (Va2CDK-Va1CDK)*GK(Va25*Cdk1,Vi25,J25/Cdc25T,J25/Cdc25T))
# Algebraic mass conservation equations
Cdc25 = Cdc25T - Cdc25p
Wee1p = Wee1T - Wee1
Cdk1p = CycBT - Cdk1
Cdh1p = Cdh1T - Cdh1
# Parameters (for WT GV arrest)
p Va1CDK=0.015, Va2CDK=1.5, Vi1CDK=0.015, Vi2CDK=0.3
p VaCdh1=1.5, ViCdh1=6, JCdh1=0.15, Cdh1T=1
p VaWee=0.375, ViWee=1.5, Jwee=0.01, Wee1T=1
p Va25=1.5, Vi25=0.375, J25=0.01
p ksc25=0.015, kd1c25=0.015, kd2c25=0.15
p ksCycB=0.015, kd1CycB=0.015, kd2CycB=0.075
# Initial Conditions
init Cdk1=1
```

```
# XPP settings
@ XP=Cdk1, YP=Cdh1, TOTAL=150, METH=stiff, XHI=1.1
@ YLO=-0.1, YHI=1.1, XLO=-0.1, BOUND=1000, nmesh=400
# AUTO settings
@ parmin=0, parmax=10, autoxmin=0
@ autoymin=0, autoxmax=1, autoymax=1
@ ntst=50, ds=-0.01, dsmax=0.02, nmax=200000000
@ npr=1000, EPSL=1e-7, EPSS=1E-7, EPSU=1E-7
done
```

Appendix B

GK() function for pseudo–steady-state Goldbeter-Koshland kinetics

The pseudo–steady-state solution to describe the state of a substrate subject to modification and demodification by Goldbeter-Koshland kinetics is a quadratic involving combinations of four different rate constants. For simplicity we define a pair of functions which perform this operation.

We consider a species A which can exist in one of two modification states A_1 and A_2. A_1 is converted to A_2 by enzyme E_1, and A_2 converted back to A_1 by enzyme E_2. Both enzymes obey Michaelis-Menten kinetics.

To calculate the pseudo–steady-state fraction of A in the A_2 state, we require the V_{max} and K_M of the reactions catalysed by E_1 and E_2, which we denote v_1 and v_2, and K_1 and K_2 respectively. We then define the function $\mathrm{GK}(v_1, v_2, K_1, K_2)$ as follows:

$$\frac{[\mathrm{A}_2]}{[\mathrm{A}_1] + [\mathrm{A}_2]} = \mathrm{GK}(v_1, v_2, K_1, K_2) = \frac{2v_1K_2}{G_B + \sqrt{{G_B}^2 - 4(v_2 - v_1)v_1K_2}} \tag{B.1}$$

Where:

$$\mathrm{G_B} = v_2 - v_1 + v_2K_1 + v_1K_2 \tag{B.2}$$

Note that either A_1 or A_2 can be defined as the modified form, depending on whether the fraction of modified or unmodified substrate is the desired output.

Appendix C

Meiotic resumption phaseplanes

C.1 Explaining the [Cdk1]' vector field

In this Appendix we provide a more detailed intuitive explanation of the shaded vector fields overlaid on the meiotic resumption phaseplanes in Figure 4.5. This is intended as an aid to understanding the analysis in Section 4.4.3, but does not of itself introduce any new results. We therefore include it here to avoid introducing unnecessary complication to the main text.

Shading is used to indicate the magnitude of the [Cdk1]' component of the underlying vector field. Darker shading indicates a region of the phaseplane where [Cdk1] is increasing quickly relative to lighter shaded areas, where [Cdk1] is changing very slowly or is decreasing. This shading is defined over all regions of the phaseplane according to Equation (4.1). Three major factors affect the magnitude of [Cdk1]'. These are the rate of CycB synthesis, the rate of CycB degradation by Cdh1, and the level of inhibitory phosphorylation determined by the relative activities of Wee1 and Cdc25. Of these factors, CycB is synthesised at a constant rate, so this is unaffected by the position in the phaseplane. CycB degradation depends on the level of Cdh1, so [Cdk1]' increases towards the bottom of the phaseplane, where [Cdh1] is lowest. Wee1 and Cdc25 activities are highly switch-like in response to Cdk1 activity. As a result, they divide the phaseplane into distinct regions where inhibitory Cdk1 phosphorylation is 'on' or 'off', but do not have a large impact on the magnitude of [Cdk1]' within those regions.

Where Cdk1 phosphorylation is 'off', the [Cdk1] nullcline represents the steady state reached by balancing the constant rate of CycB synthesis with the rate of CycB degradation as determined by Cdh1. This is most clearly seen in panels C and D of Figure 4.5, where inhibitory phosphorylation of Cdk1 is largely inactivated due to loss of PKA,

and the [Cdk1] nullcline is a simple decreasing function of [Cdh1]. Since the rate of degradation also depends on the concentration of Cdk1, [Cdk1]' increases to the left of the nullcline, and decreases to the right. [Cdk1]' is therefore highest in the bottom left hand corner of the phaseplane where both [Cdk1] and [Cdh1] are low.

This trend of increasing [Cdk1]' with decreased [Cdk1] does not extend completely to the y-axis due to the requirement for Cdk1 activity to maintain Wee1 inhibition and Cdc25 activation. Once [Cdk1] falls below a threshold where inhibitory phosphorylation increases, [Cdk1]' falls rapidly, since it is now necessary to overcome this additional inhibition before Cdk1 can become active. In the meiotic resumption phaseplanes, this only represents a slowing down of Cdk1 activation, as there is no starting point on the phaseplane which will lead to the system adopting a low-[Cdk1] steady state. In the GV arrest phaseplanes (panels A and B), this is not the case and multiple [Cdk1] steady states exist for certain values of [Cdh1]. The leftmost branch of the [Cdk1]' curve in these panels corresponds to the steady state reached between CycB synthesis and Wee1-dependent inactivation of Cdk1. The limited role of Cdh1-dependent degradation of CycB in this case can be seen since the curve is almost vertical with little change as [Cdh1] is lowered. This is consistent with the observed ability of *Cdh1*Δ cells to maintain a GV arrest. The middle branch of the [Cdk1] nullcline is the unstable steady state separating regions of the phaseplane where [Cdk1] is increasing towards the upper steady state from those where [Cdk1] is decreasing towards the lower steady state.